AN ABSTRACT OF THE DISSERTATION OF

Christopher C. Thornburg for the degree of Doctor of Philosophy in Pharmacy presented on March 25, 2013.

Title: Investigation of Unique Marine Environments for Microbial Natural Products

Abstract approved:

Kerry L. McPhail

Metagenomics has revealed that the marine microbial biosphere is immensely more diverse than originally considered, and is an almost untapped reservoir for the potential discovery of microbial natural products. Despite numerous advances in culturing, biosynthetic engineering and genomic-based screening efforts to uncover much of this diversity in relatively accessible environments, a high rediscovery rate has resulted in the investigation of unique, relatively unexplored ecosystems harboring phylogenetically diverse communities of marine organisms. The focus of this research was to establish a culture repository of microorganisms collected from the Red Sea and from deep-sea hydrothermal vents, and to assess their biosynthetic potential for the production of new chemical scaffolds. Cultivation of marine cyanobacteria from the Red Sea has led to the identification of five new cyclic depsipeptides, apratoxin H, grassypeptolides D and E, Ibu-epidemethoxylyngbyastin 3 and leptochelin, the latter possessing a unique chemical scaffold capable of binding metals. A collection of deep-sea hydrothermal vent sediment and microbial mat samples led to the isolation of 64 unique bacterial strains, with eight assigned as members of the order Actinomycetales. Importantly, these isolates, along with a collection of deep-vent invertebrates and microbes, have led to the development of methods for the collection, culturing and biological screening of organisms from this extreme environment for future natural products research.

Investigation of Unique Marine Environments for Microbial Natural Products

by
Christopher C. Thornburg

A DISSERTATION
submitted to
Oregon State University

in partial fulfillment of
the requirements for the
degree of

Doctor of Philosophy

Presented March 25, 2013
Commencement June 2013

Doctor of Philosophy dissertation of Christopher C. Thornburg presented on March 25, 2013.

APPROVED:

Major Professor, representing Pharmacy

Dean of the College of Pharmacy

Dean of the Graduate School

I understand that my dissertation will become part of the permanent collection of Oregon State University libraries. My signature below authorizes release of my dissertation to any reader upon request.

Christopher C. Thornburg, Author

ACKNOWLEDGEMENTS

First, I would like to thank Dr. Kerry McPhail, my research advisor, for providing me with the exciting opportunity to pursue a career in natural products research. For this, as well as your guidance, enthusiastic encouragement and valuable critiques of my work, I am forever grateful. I would like to express my very great appreciation to Dr. Mark Zabriskie for your kindness, support and advice throughout my graduate career.

I also wish to acknowledge Dr. Taifo Mahmud and Dr. Philip Proteau for challenging me in the classroom and supporting my work along the way. A special thanks is owed to my external committee members, Dr. Martin Schuster and Dr. Daniel Rockey for your time and assistance during this process.

I wish to acknowledge Jeff Morré and Rodger Kohnert for assisting me with many of the technical applications applied throughout this dissertation, as well as Dr. Jane Ishmael and her lab members for their assistance with biological testing. I am particularly grateful to all of my friends and colleagues, past and present, from the McPhail, Zabriskie, Mahmud and Proteau groups. Thank you all for making my graduate experience a memorable one.

To my wife Theresa: Thank you for allowing me to pursue my dream! Your incredible patience, unconditional love, and belief in me gave me the strength to carry on when I needed it most. I am also deeply thankful to my parents and my wife's family for their incredible support and encouragement throughout this incredible journey. Finally, I would like to thank my wonderful son, Matthew, for filling my heart with an immeasurable warmth. I am blessed to have you as my son, and I cannot imagine what my life would be like without you.

CONTRIBUTION OF AUTHORS

The collection of cyanobacteria from the Red Sea was performed in collaboration with Prof. Diaa T.A. Youssef from King Abdulaziz University, Saudi Arabia, while Dr. Lamiaa A. Shaala prepared the organic extracts from these collections. Dr. Muralidhara Thimmaiah synthesized chemical standards that were used in the assignment of absolute configuration of Ibu-epidemethoxylygbyastatin 3. Elise S. Cowley assisted with the development of fractionation and purification schemes for the isolation of apratoxin A and analogues. Acquisition of NMR data for unbound leptochelin was performed by Florina A. Vulpanovici, and pure samples for biological testing and further data acquisition were kindly provided by Dr. William H. Gerwick from Scripps Institution of Oceanography, University of California, San Diego. Biological testing for cancer cell cytotoxicity was performed by Andrew M. Hau, Jeffrey D. Serrill, Jay M. Malmo, and Justyna Sikorska under the guidance of Dr. Jane Ishmael. Edward A. Mitchell performed the RNA polymerase gamma subunit (*rpoC1*) gene analysis described in Chapter Four. Dr. Kerry L. McPhail contributed to research design, data analysis, writing and editing.

Collections of deep-sea hydrothermal vent organisms were performed in collaboration with Dr. William W. Chadwick Jr. of the NOAA Vents program at Oregon State University and Dr. David A. Butterfield of the Pacific Marine Environmental Laboratory (PMEL) and Joint Institute for the Study of Atmosphere and Ocean, University of Washington. Oliver B. Vining and Edward A. Mitchell assisted with the development of collection and culturing methods. In addition, Edward A. Mitchell performed the 16S rRNA gene sequencing and 454 pyrosequencing analysis described in Chapter Five. Dr. Kerry L. McPhail and Dr. Mark Zabriskie contributed to research design, data analysis, writing and editing.

TABLE OF CONTENTS

	Page
Chapter One: General Introduction	1
Microbial Natural Products	2
Marine Bacterial Natural Products	2
Marine Cyanobacterial Natural Products	5
Thesis Overview	9
References	12
Chapter Two: Cyclic Depsipeptides, Grassypeptolides D and E and Ibu-epidemethoxylyngbyastatin 3, from a Red Sea *Leptolyngbya* Cyanobacterium	19
Abstract	20
Introduction	21
Results and Discussion	24
Experimental	36
Acknowledgement	47
Supporting Information	48
References	73
Chapter Three: Apratoxin H, a Cytotoxic Cyclic Depsipeptide from a Red Sea *Moorea producens* Cyanobacterium	76
Abstract	77
Introduction	78
Results and Discussion	81
Experimental	99
Acknowledgement	104
Supporting Information	105
References	126

TABLE OF CONTENTS (Continued)

Page

Chapter Four: Leptochelin, a Cytotoxic Metal Ion Chelator from a *Leptolyngbya* Cyanobacterium 130

Abstract 131

Introduction 132

Results and Discussion 138

Experimental 151

Acknowledgement 155

Supporting Information 156

References 176

Chapter Five: Method Development and Sample Screening for Natural Products from Deep-Sea Hydrothermal Vent Organisms 181

Abstract 182

Introduction 183

Geology and Distribution of Deep-Sea Hydrothermal Vents 185

Biogeography and Diversity of Deep-Sea Vent Eukaryotes 188

Chemosynthesis and the Biogeography and Diversity of Archaea and Bacteria 194

Natural Products from Deep-Sea Vent Environments 202

Results and Discussion 207

Method Development 207

Collection of Deep-Sea Vent Organisms 207

Cultivation of Deep-Sea Vent Actinobacteria 218

Biological Screening of Deep-Sea Vent Organisms 220

Extract Library Preparation and Bioassay Development 220

TABLE OF CONTENTS (Continued)

Page

Screening of Deep-Sea Vent Invertebrates and Microbial Mats 223

Screening of Deep-Sea Vent Actinobacteria from Culture 233

Conclusion 238

Experimental 240

Acknowledgement 247

Supporting Information 248

References 253

Chapter Six: General Conclusions 266

References 272

Appendix 274

LIST OF FIGURES

Figure — Page

Figure 1.1 Structures of seminal natural products from marine actinomycetes with the producing organism, antimicrobial / cytotoxicity data, therapeutic class, or stage of clinical trial listed below each name. 4

Figure 1.2 Marine natural products of putative microbial/symbiont biogenetic origin approved by the U.S. Food and Drug Administration (FDA), European Commission (EC) or in various stages of clinical trial. 6

Figure 1.3. Examples of natural products from marine cyanobacteria that showcase their enormous structural diversity, potent cytotoxicity and profound selectivity. For each structure the producing organism, cytotoxicity data, molecular target or mechanism of action is listed. 8

Figure 2.1. Phylogenetic relationship of Red Sea filamentous cyanobacteria with other cyanobacterial groups based on SSU (16S) rRNA gene sequences 34

Figure S-2.1. ^{1}H NMR spectrum for grassypeptolide D (1) in CDCl3 (700 MHz) 56

Figure S-2.2. ^{13}C NMR spectrum for grassypeptolide D (1) in $CDCl_3$ (100 MHz) 57

Figure S-2.3. DQF COSY spectrum for grassypeptolide D (1) in $CDCl_3$ (400 MHz) 58

Figure S-2.4. Multiplicity-edited HSQC spectrum for grassypeptolide D (1) in $CDCl_3$ (400 MHz). 59

Figure S-2.5. HMBC spectrum for grassypeptolide D (1) in $CDCl_3$ (400 MHz) 60

Figure A-2.6. ROESY spectrum for grassypeptolide D (1) in $CDCl_3$ (400 MHz) 61

LIST OF FIGURES (Continued)

Figure	Page
Figure S-2.7. HSQC-TOCSY spectrum for grassypeptolide D (1) in $CDCl_3$ (400 MHz).....	62
Figure S-2.8. ^{1}H NMR spectrum for grassypeptolide E (2) in $CDCl_3$ (700 MHz).....	63
Figure S-2.9. ^{13}C NMR spectrum for grassypeptolide E (2) in $CDCl_3$ (175 MHz).....	64
Figure S-2.10. COSY spectrum for grassypeptolide E (2) in $CDCl_3$ (700 MHz).....	65
Figure S-2.11. Multiplicity-edited HSQC spectrum for grassypeptolide E (2) in $CDCl_3$ (700 MHz).	66
Figure S-2.12. HMBC spectrum for grassypeptolide E (2) in $CDCl_3$ (700 MHz).....	67
Figure S-2.13. ROESY spectrum for grassypeptolide E (2) in $CDCl_3$ (700 MHz).....	68
Figure S-2.14. ^{1}H NMR spectrum for Ibu-epidemethoxylyngbyastatin 3 (3) in $CDCl_3$ (700 MHz).	69
Figure S-2.15. ^{13}C NMR spectrum for Ibu-epidemethoxylyngbyastatin 3 (3) in $CDCl_3$ (175 MHz).	70
Figure S-2.16. ^{1}H NMR spectrum for dolastatin 12 in $CDCl_3$ (700 MHz).....	71
Figure S-2.17. ^{13}C NMR spectrum for dolastatin 12 in $CDCl_3$ (175 MHz).....	72
Figure 3.1. Apratoxins A–G.	82

LIST OF FIGURES (Continued)

Figure — Page

Figure 3.2. Schematic showing the fragmentation pattern of compounds 1 and 2 relative to the major MS^3 fragmentation pattern observed for apratoxin A. 86

Figure 3.3. Assignment of MS^3 fragmentation data for compound apratoxin A sulfoxide (2). 87

Figure 3.4. Marine natural products of putative biosynthetic origin containing oxidized sulfur atoms. 88

Figure 3.5. Oxidation of apratoxin A. 89

Figure 3.6. Semisynthetic apratoxin analogue *E*-dehydroapratoxin A (Luesch et al., 2002) along with the synthetic analogues of apratoxin A, apratoxin A/E hybrid (Chen et al., 2011) and oxoapratoxin A (Ma et al., 2006). 90

Figure 3.7. Differential ^{13}C NMR chemical shifts of the polyketide moiety in apratoxin A versus compounds 1 (A) and 2 (B). 91

Figure 3.8. CD spectra of apratoxin A, H (1) and apratoxin A sulfoxide (2). 92

Figure 3.9. Structure-activity relationships (SAR) profile of the apratoxins modified from Tidgewell et al. (2010) to include cytotoxicity data for 1 and 2 relative to apratoxin A, and the reported analogues. 94

Figure 3.10. Phylogenetic relationship of the apratoxin-producing cyanobacteria with other marine filamentous cyanobacteria based on SSU (16S) rRNA gene sequences. 97

Figure S-3.1. Dose-response curves of apratoxin A, apratoxin H (1) and the oxidized apratoxin A analogue (2) in the human NCI-H460 lung cancer cell line (n = 3). 106

LIST OF FIGURES (Continued)

Figure	Page
Figure S-3.2. ^{1}H NMR spectrum for apratoxin H (1) in $CDCl_3$ (700 MHz).	109
Figure S-3.3. ^{13}C NMR spectrum for apratoxin H (1) in $CDCl_3$ (125 MHz).	110
Figure S-3.4. DQF COSY spectrum for apratoxin H (1) in $CDCl_3$ (500 MHz).	111
Figure S-3.5. Multiplicity-edited HSQC spectrum for apratoxin H (1) in $CDCl_3$ (500 MHz).	112
Figure S-3.6. HMBC spectrum for apratoxin H (1) in $CDCl_3$ (500 MHz).	113
Figure S-3.7. ROESY spectrum for apratoxin H (1) in $CDCl_3$ (500 MHz).	114
Figure S-3.8. ^{1}H NMR spectrum for apratoxin A sulfoxide (2) in $CDCl_3$ (700 MHz).	115
Figure S-3.9. ^{13}C NMR spectrum for apratoxin A sulfoxide (2) in $CDCl_3$ (175 MHz).	116
Figure S-3.10. COSY spectrum for apratoxin A sulfoxide (2) in $CDCl_3$ (700 MHz).	117
Figure S-3.11. Multiplicity-edited HSQC spectrum for apratoxin A sulfoxide (2) in $CDCl_3$ (700 MHz).	118
Figure S-3.12. HMBC spectrum for apratoxin A sulfoxide (2) in $CDCl_3$ (700 MHz).	119
Figure S-3.13. ROESY spectrum for apratoxin A sulfoxide (2) in $CDCl_3$ (700 MHz).	120
Figure S-3.14. ^{1}H NMR spectrum for apratoxin A in $CDCl_3$ (700 MHz).	121

LIST OF FIGURES (Continued)

Figure	Page
Figure S-3.15. ^{13}C NMR spectrum for apratoxin A in $CDCl_3$ (175 MHz).	122
Figure S-3.16. Annotated MS/MS spectrum of apratoxin A [collision energy (CE), 25; declustering potential (DP), 33; entrance potential (EP), 10; T = 400 °C].	123
Figure S-3.17. Annotated MS/MS spectrum of apratoxin H (2) [collision energy (CE), 25; declustering potential (DP), 33; entrance potential (EP), 10; T = 400 °C].	124
Figure S-3.18. Annotated MS/MS spectrum of apratoxin A sulfoxide [collision energy (CE), 25; declustering potential (DP), 33; entrance potential (EP), 10; T = 400 °C].	125
Figure 4.1. Structures of patellamides A and C with the thiazole (T), amine (A) and oxazole (O) nitrogens or TAO metal binding domains shown in red.	134
Figure 4.2. Structure of bleomycins (6) and derivates that comprise Bleonoxane®.	135
Figure 4.3. Structures of the potent HDAC inhibitors largazole (7) and romidepsin (8, Istodax®).	136
Figure 4.4. HRTOFMS spectra showing the distinct isotope patterns observed for unbound/free leptochelin (9) and the Zn(II) adduct.	139
Figure 4.5. Selected ^{13}C-^{13}C (INADEQUATE) and ^{1}H-^{15}N HMBC correlations establishing key fragments containing the 2,4-diamino-3-hydroxy-2-methylpentanoic acid unit (A) and the 4-methyl thiazoline/2-methyloxirane-containing fragment (B) in leptochelin (9).	142
Figure 4.6. Selected 2D NMR correlations connecting the macrocyclic backbone of leptochelin (9).	143

LIST OF FIGURES (Continued)

Figure — Page

Figure 4.7. Differential ^{13}C NMR chemical shifts for leptochelin (9) and Zn-leptochelin ($\Delta = \delta_C$ 9 – δ_C Zn-9). 144

Figure 4.8. Phylogenetic relationship of the leptochelin-producing cyanobacteria with other marine filamentous cyanobacteria based on SSU (16S) rRNA gene sequences. 147

Figure A-4.1. The dose response curves for leptochelin (9) and Zn-leptochelin in human NCI-H460 (n = 3) and HeLa cervical carcinoma cell lines (n = 3). 157

Figure S-4.2. CD (A) and UV (B) spectra for leptochelin (9, blue) and Zn-leptochelin (red). 158

Figure S-4.3. ^{1}H NMR spectrum for leptochelin (9) in $CDCl_3$ (600 MHz). 161

Figure S-4.4. ^{13}C NMR spectrum for leptochelin (9) in $CDCl_3$ (150 MHz). 162

Figure S-4.5. COSY spectrum for leptochelin (9) in $CDCl_3$ (600 MHz). 163

Figure S-4.6. Multiplicity-edited HSQC spectrum for leptochelin (9) in $CDCl_3$ (600 MHz). 164

Figure S-4.7. HSQC-TOCSY spectrum for leptochelin (9) in $CDCl_3$ (600 MHz). 165

Figure S-4.8. HMBC spectrum for leptochelin (9) in $CDCl_3$ (600 MHz). 166

Figure S-4.9. ^{13}C INADEQUATE NMR spectrum for ^{13}C-labeled leptochelin (9) in $CDCl_3$ (400 MHz). 167

Figure S-4.10. ^{1}H-^{15}N multiplicity-edited HSQC spectrum for leptochelin (9) in $CDCl_3$ (600 MHz). 168

LIST OF FIGURES (Continued)

Figure	Page
Figure S-4.11. ^{1}H-^{15}N gHMBC spectrum for leptochelin (9) in $CDCl_3$ (500 MHz).	169
Figure S-4.12. ^{1}H NMR spectrum for Zn-leptochelin in $CDCl_3$ (700 MHz).	170
Figure S-4.13. ^{13}C NMR spectrum for Zn-leptochelin in $CDCl_3$ (175 MHz).	171
Figure S-4.14. COSY spectrum for Zn-leptochelin in $CDCl_3$ (500 MHz).	172
Figure S-4.15. Multiplicity edited HSQC spectrum for Zn-leptochelin in $CDCl_3$ (700 MHz)..	173
Figure S-4.16. HMBC spectrum for Zn-leptochelin in $CDCl_3$ (500 MHz).	174
Figure S-4.17. ROESY spectrum for Zn-leptochelin in $CDCl_3$ (500 MHz).	175
Figure 5.1. Map showing the major mid-ocean ridges and known deep-sea hydrothermal vent biogeographic provinces: Pink, western Pacific; green, northeast Pacific; blue, East Pacific Rise; yellow, Azores; red, Mid-Atlantic Ridge; orange, Indian Ocean.	186
Figure 5.2. Relative abundances of bacterial phyla (including classes of Proteobacteria) found in the deep-sea as determined by 16S rRNA gene sequence analysis and reported in the Ribosomal Database Project (RDP, http://rdp.cme.msu.edu/): (a) hydrothermal vent samples and (b) non-thermal water column and sediment samples (Cole et al., 2007; Cole et al., 2009).	200
Figure 5.3. Relative abundances of phyla and component classes of archaea found in the deep-sea as determined by 16S rRNA gene sequence analysis and reported in the Ribosomal Database Project (RDP, http://rdp.cme.msu.edu/): (a) hydrothermal vent samples and (b) non-thermal water column and sediment samples (Cole et al., 2007; Cole et al., 2009).	202

LIST OF FIGURES (Continued)

Figure	Page
Figure 5.4. Bathymetry map of the Axial Volcano (Seamount) caldera located along the Juan de Fuca Ridge in the Pacific Ocean approximately 480 km (300 mi) west of Cannon Beach, Oregon.	211
Figure 5.5. (A) Modified Sharpvet nylon syringe (100 mL, small syringe) used to collect isolated pockets of microbial mats and/or sediment.	212
Figure 5.6. (A) Picture of a large syringe (400 mL) made from materials purchased from a local hardware store.	213
Figure 5.7. (A) Blue carpet-like mats of the marine ciliate *Folliculinopsis* sp. in close proximity to limpets and scale worms covered in white filamentous microbial mats.	214
Figure 5.8. (A, B) Orange microbial mat growing on a tubeworm assemblage located near the Marker 113 vent site (1523 m) at Axial Seamount.	215
Figure 5.9. General bioassay-guided fractionation scheme for organic extracts showing the typical number of fractions collected at each chromatographic separation step and their corresponding eluting solvent.	221
Figure 5.10. (A) ^{1}H (700 MHz) and (B) ^{13}C (175 MHz) NMR spectra for cholesterol (15) obtained from a white filamentous microbial mat (DSV-09-14E/F).	227
Figure 5.11. (A) ^{1}H (700 MHz) NMR spectrum of DSV-09-16F2/G2 with key integrals labeled to show a 2:3 ratio of 16 to 17.	229
Figure 5.12. Phylogenetic tree showing the relationship between the cultured Axial Seamount actinomycetes and nearest type strains (^{T}) based on Maximum-likelihood (PhyML) analysis of SSU (16S) rRNA gene sequences. .	235

LIST OF FIGURES (Continued)

Figure	Page
Figure 5.13. Rarefaction analysis for the number of OTUs present at 3%, 5% and 10% divergent levels within the ribosomal RNA dataset obtained from an orange microbial mat (J2-520 T07) collected from Axial Seamount at Marker 113.	237
Figure A-1. Laboratory cultures and their corresponding photomicrographs (x400 and x1000, respectively) for filamentous marine cyanobacteria isolated from the Red Sea.	275
Figure A-2. Laboratory cultures and their corresponding photomicrographs (x400 and x1000, respectively) for filamentous marine cyanobacteria isolated from the Red Sea.	276

LIST OF TABLES

Table	Page
Table 2.1. ^{1}H (700 MHz) and ^{13}C (175 MHz) NMR Spectroscopic Data for Grassypeptolides D (1) and E (2) in $CDCl_3$.	25
Table S-2.1. List of and growth mediums used to culture Red Sea cyanobacteria.	49
Table S-2.2. NMR Spectroscopic Data for Grassypeptolide D (1) in $CDCl_3$ (400 MHz).	50
Table S-2.3. NMR Spectroscopic Data for Grassypeptolide E (2) in $CDCl_3$ (700 MHz).	52
Table S-2.4. NMR Spectroscopic Data for Ibu-epidemethoxylyngbyastatin 3 (3) in $CDCl_3$ (400 MHz).	54
Table 3.1. NMR Spectroscopic Data for Apratoxin H (1) in $CDCl_3$ (500 MHz).	84
Table S-3.1. NMR Spectroscopic Data for Apratoxin A sulfoxide in $CDCl_3$ (700 MHz).	107
Table 4.1. NMR Spectroscopic Data for Leptochelin (9) and Zn-Leptochelin in $CDCl_3$.	140
Table S-4.1. NMR Spectroscopic Data for Leptochelin (9) in $CDCl_3$.	159
Table S-4.2. NMR Spectroscopic Data for Zn-Leptochelin Complex in $CDCl_3$.	160
Table 5.1. Representative bacterial counts and phylogenetic diversity reported from different hydrothermal vent niches.	193
Table 5.2. Scientific Institutions that Operate Deep-Sea Submersibles.	209

LIST OF TABLES (Continued)

Table	Page
Table 5.3. Summary of June 2009 Axial Seamount collections of deep vent invertebrates for natural product investigations.	216
Table 5.4. List of August 2010 Axial Seamount collections of deep-vent microbial samples for natural product investigations.	217
Table 5.5. Antimicrobial activity of organic extracts and VLC fractions from deep-sea hydrothermal vent invertebrates and microbial mat collections.	224
Table S-5.1. Information on the deep-sea hydrothermal vent bacterial isolates including collection site, depth, isolation medium, colony morphology and nearest strain ID determined by BLAST analysis of representative 16S rRNA gene sequences.	249
Table S-5.2. List of isolation and growth mediums used to culture deep-sea hydrothermal vent microorganisms.	252

DEDICATION

To Theresa, Matthew

&

Mom

Chapter One

General Introduction

Christopher C. Thornburg

Microbial Natural Products

The biochemical molecules and receptors involved in the many pathways required for cellular function have enormous structural diversity, suggesting the need for a complementary level of diversity among small molecule ligands to modulate each of these processes, both selectively and efficaciously (Dobson, 2004; Lipinski & Hopkins, 2004). In this regard, it is well recognized that natural product-based drugs provide a foundation of chemotherapy (Newman & Cragg, 2012) and trace back to the use of terrestrial plants and intertidal marine algae as traditional medicines thousands of years ago (Schmidt et al., 2008). More recently, terrestrial microorganisms (fungi and bacteria) have had a major impact on the development of antimicrobial and antitumor compounds since the original discovery of penicillin in 1929 (Drews, 2000). In fact, actinomycete soil bacteria (order Actinomycetales) are the source of nearly 45% of all biologically active microbial metabolites and are responsible for over 50% of the microbial antibiotics discovered to date, most of which originate from the *Streptomyces* and *Micromonospora* genera (Berdy, 2005). In the last 65 years, and as technologies have advanced, the search for new natural product sources of biologically active compounds has expanded from terrestrial plants and microbes, to shallow water reef marine algae and invertebrates with their associated symbionts and ocean sediment-derived marine microbes (Cragg & Newman, 2006; Kingston, 2010; Newman & Hill, 2006).

Marine Bacterial Natural Products

When marine actinomycetes taxonomically related to known terrestrial genera were first isolated from shallow coastal sediments, they were largely believed to originate from dormant spores deposited in marine sediments from terrestrial run-off (Fenical & Jensen, 2006; Lam, 2006). However, since the first description of an

autochthonous marine actinomycete species, *Rhodococcus marinononascens* (Helmke & Weyland, 1984), many obligate halophiles have been characterized, including many new taxa. Over the last 15 years, seminal research by Fenical and Jensen (2006) has firmly established actinobacteria from shallow and deep-sea marine sediments as a valuable source of drug discovery leads (Figure 1.1). More recently, deep-sea invertebrates and microorganisms have emerged as a rich source of natural products (Skropeta, 2008), at a time when there is a dire need for new drug templates to combat the escalating problem of drug resistance, especially in infectious diseases and cancer. Considering the largely unexplored natural product potential of deep-sea hydrothermal vent environments, of specific interest is that new actinomycetes have been isolated from hydrothermal vent fluids in the Mariana Trough (ca. 2850 m) and Suiyo Seamount (ca. 1390 m; Naganuma et al., 2007), and from hydrothermally active sediments of the Guaymas Basin (ca. 2005 m; Teske et al., 2002). Furthermore, filamentous bacteria (possibly Actinobacteria) have been observed in the guts of vent invertebrates (Baross & Deming, 1985). However, of the few reports of natural products from deep-sea vent organisms, none are from actinomycetes. Chapter Five of this dissertation will review the microbial diversity at deep-sea hydrothermal vents in more detail, as well as discuss the methods employed to screen for bioactive natural products from hydrothermal vent invertebrates and cultured actinomycetes.

To date, more than 22,000 marine-derived natural products (MNPs) have been discovered (Blunt et al., 2013). However, somewhat concerning is that the rate of discovery of new natural products from marine invertebrates and microorganisms appeared to have peaked in the late 1990's and to be declining at the turn of the century. However, increasing numbers of new, biologically active marine natural products are once again being reported: 961 new compounds were reported in 2007 versus 779 new compounds in 2006 (Blunt et al., 2009), and 2008 marked the first year that the number of new MNPs (1065) reported exceeded 1000 (Blunt et al., 2010). Remarkably, subsequent to 2008 the number of new compounds reported from

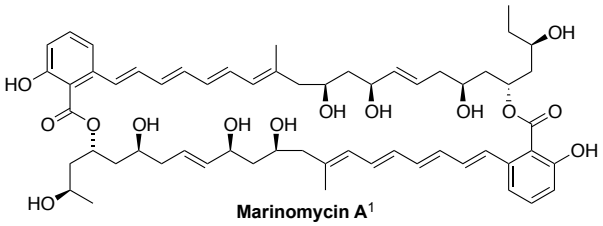

Marinomycin A[1]
Marinospora sp.
antimicrobial
methicillin-resistant *Staphylococcus aureus*
vancomycin-resistant *Enterococcus faceium*
MIC_{90} = 0.13 μM

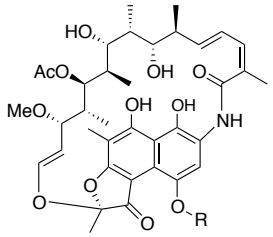

Rifamycin B (R = CH_2COOH)
Amycolatopsis rifamycinica (terrestrial)[2]
Salinospora spp. (marine)[3]
Rifamycin SV (R = H) precursor to clinically used antibiotic derivatives: Rifampicin, Rifabutin, Rifapentine[4]

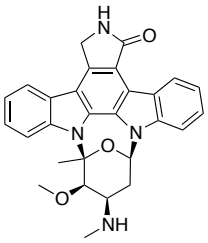

Staurosporine[5]
(Natural Product)

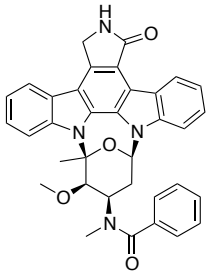

PKC412 (Midostaurin)[6]
Streptomyces staurosporeus
Protein Kinase Inhibitor, Phase II / III (Cancer)[7]

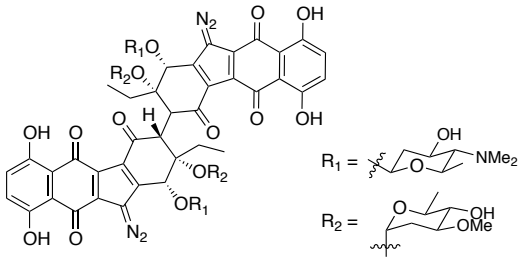

Lomaiviticin A[8]
Micromonospora lomaivitiensis
24-cancer cell line panel: IC_{50} = 0.01 to 0.98 ng/mL

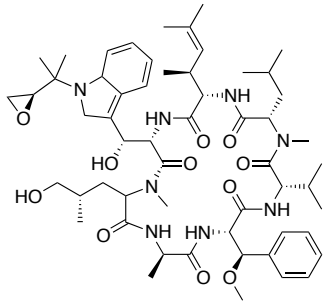

Cyclomarin A
Streptomyces sp.[9], *Salinispora arenicola*[10]
anti-inflammatory
(92% edema inhibition in PMA-induced mouse ear edema assay)

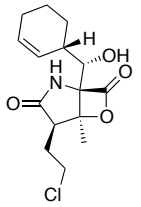

Salinosporamide A (Marizomib, NPI-0052)[11]
Salinospora tropica
Proteasome Inhibitor, Phase I (Cancer)[12]

Figure 1.1. Structures of seminal natural products from marine actinomycetes with the producing organism, antimicrobial / cytotoxicity data, therapeutic class, or stage of clinical trial listed below each name. References: **1**, (Kwon et al., 2006); **2**, (Bala et al., 2004; Sensi et al., 1959); **3**, (Kim et al., 2006); **4**, (Floss & Yu, 2005); **5**, (Funato et al., 1994; Omura et al., 1977); **6**, **7** ("Novartis Oncology US," 2013); **8**, (He et al., 2001); **9**, (Renner et al., 1999); **10**, (Schultz et al., 2008); **11**, (Fenical et al., 2009); **12**, ("Nereus Pharmaceuticals, Inc.," 2013).

marine organisms has averaged over 1000 per year (Blunt et al., 2012, 2013; Blunt, Copp et al., 2011). This dramatic increase is attributable primarily to an increased focus on marine microorganisms. Furthermore, the continued dominance of marine invertebrates (sponges, tunicates, soft corals, gorgonians) as a source of new compounds is consistent with the diverse assemblages of microbial symbionts associated with these relatively collectable organisms, many compounds from which are of putative or proven microbial origin (Dunlap et al., 2007; Simmons et al., 2008). Perhaps the most acclaimed of the microbial-derived marine natural products are the dolastatins from the sea hare *Dolabella auricularia*. The low yields of dolastatins (typically 10^{-6} to 10^{-8} % wet wt.) suggested that these compounds were actually produced microbially and or sequestered through the sea hare's diet (Luesch et al., 2002; Pettit et al., 1989; Pettit et al., 1987). The cyanobacterial origin of dolastatin 10 and several closely related peptides was subsequently confirmed by their direct isolation from the marine cyanobacterium *Symploca* (Harrigan et al., 1998; Taori et al., 2009). These and examples of other clinically relevant marine natural products of putative microbial/symbiont biogenetic origin are highlighted in Figure 1.2, together with their FDA-approved derivatives.

Marine Cyanobacterial Natural Products

Marine cyanobacteria are among the oldest life forms on earth, with the oldest fossils discovered dating back ~2.15 billion years ago (Rasmussen et al., 2008). Since this time, eons of evolution have optimized their arsenal of chemical weapons to defend against a diverse army of grazers (Nagle & Paul, 1999), resulting in highly specific natural products with sub-nanomolar potency. However, the emergence of marine cyanobacteria as a valuable source of natural products was only realized through the pioneering work of Richard E. Moore at the University of Hawaii in the 1970s to early 2000s (Cardellina & Moore, 2010). Currently there are over 800

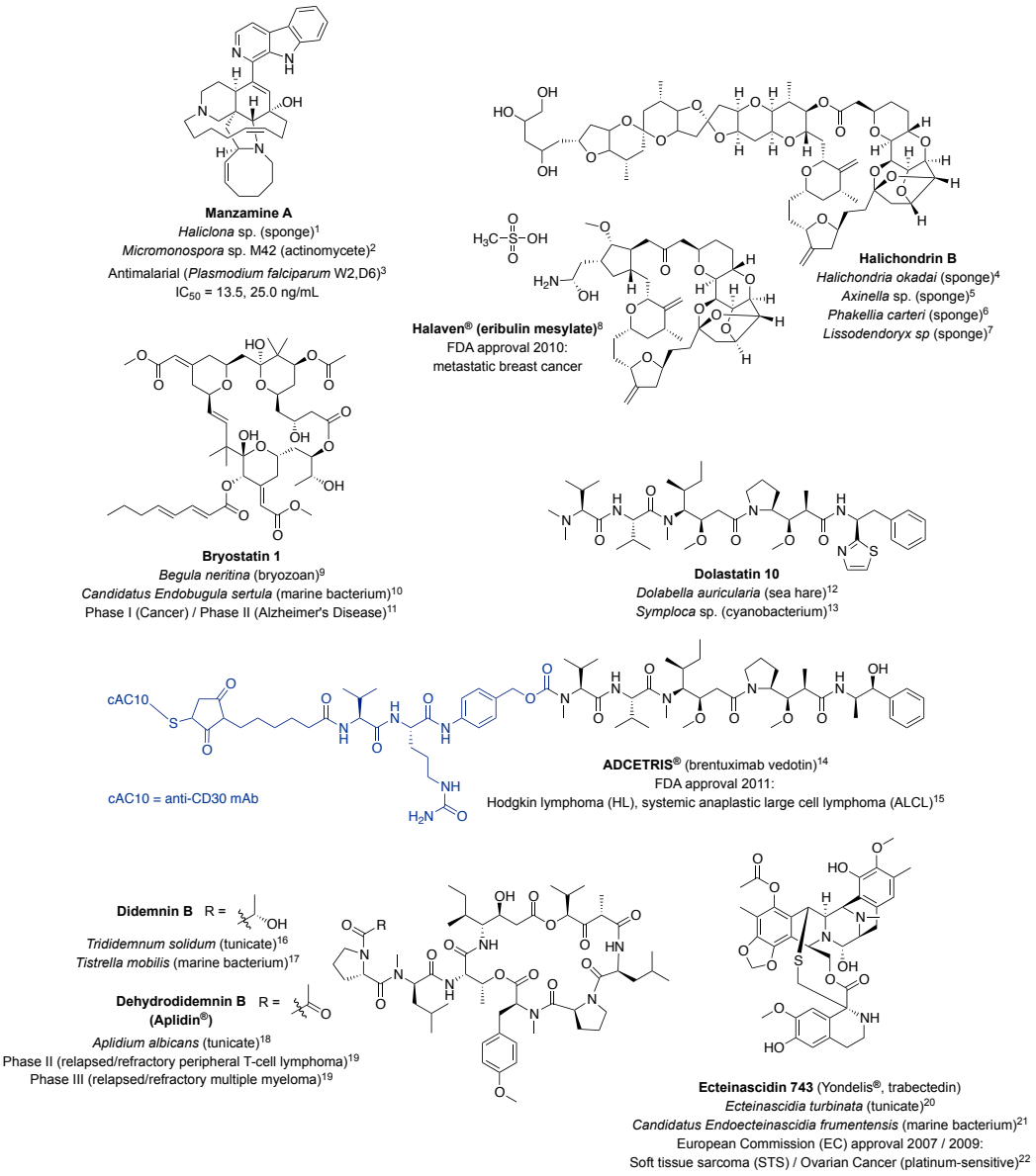

Figure 1.2. Marine natural products of putative microbial/symbiont biogenetic origin approved by the U.S. Food and Drug Administration (FDA), European Commission (EC) or in various stages of clinical trial. References: **1**, (Sakai et al., 1986); **2**, (Hill et al., 2005); **3**, (Winkler et al., 2006); **4**, (Uemura et al., 1985); **5**, (Pettit et al., 1991); **6**, (Pettit et al., 1993); **7**, (Litaudon et al., 1994); **8**, ("Eisai Oncology," 2013); **9**, (Pettit et al., 1982); **10**, (Sudek et al., 2006); **11**, ("NIH ClinicalTrials," 2013); **12**, (Pettit et al., 1987); **13**, (Luesch et al., 2001); **14**, (Francisco et al., 2003); **15**, ("Seattle Genetics," 2013); **16**, (Rinehart et al., 1981); **17**, (Tsukimoto et al., 2011); **18**, (Sakai et al., 1996); **19**, ("PharmaMar," 2013a); **20**, (Rinehart et al., 1990; Wright et al., 1990); **21**, (Moss et al., 2003; Rath et al., 2011); **22**, ("PharmaMar," 2013b).

bioactive metabolites that have been reported from marine cyanobacteria, the majority of which result from the integration of two biosynthetic classes, nonribosomal peptide synthetases (NRPSs) and polyketide synthases (PKSs; Choi et al., 2012). There are more than 500 non-proteinogenic amino acid building blocks reported for NRPSs, coupled with an array of tailoring enzymes that further diversify these amino acids and PKS building blocks with unusual oxidations, methylations and halogenations (Walsh & Fischbach, 2010). It is clear that the immense structural diversity and complexity of cyanobacterial metabolites has only begun to be realized (Figure 1.3). Incredibly, a majority of cyanobacterial metabolites (> 330) reported to date have been ascribed to the genus *Lyngbya*, with nearly 75% assigned to the species *Lyngbya majuscula* (Choi et al., 2012; Tidgewell et al., 2010). However, recent molecular-based phylogenetics (16S rRNA), coupled with traditional morphology-based methods for the identification of cyanobacteria, has shown that several genera of morphologically similar cyanobacteria are polyphyletic, which may account for the perceived chemical richness of the 'morpho-species' *Lyngbya* (Castenholz, 2001; Engene et al., 2011; Sharp et al., 2009; Thacker & Paul, 2004). In fact, one of the phylogenetically distant lineages identified in the genus *Lyngbya* has recently been proposed as a new cyanobacterial genus, *Moorea*, which includes the incorrectly classified species *Lyngbya majuscula* (N. Engene et al., 2012). The importance of including molecular tools in the identification of marine cyanobacteria is further exemplified in Chapter Two of this dissertation, where analogues of the grassypeptolides originally isolated from *Lyngbya confervoides* (Kwan et al., 2010) were identified from a phylogenetically distant Red Sea cyanobacterium of the genus *Leptolyngbya*.

Over the last 65 years, the marine environment has proven to be a rich resource for discovering biologically relevant natural products with the potential to aid our fight against infectious diseases and cancer (Molinski et al., 2009; Newman & Cragg, 2012), and with over two-thirds of the Earth covered by oceans, many unexplored repositories remain. Accordingly, screening of phylogenetically diverse and unique

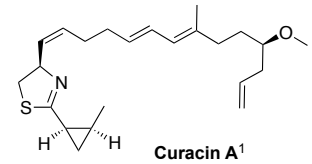

Curacin A[1]
Lyngbya majuscula (now *Moorea producens*)
tubulin polymerization inhibition (IC_{50} = 0.72 μM)
NCI-60 cancer cell line panel (IC_{50} = 1 – 100 nM)

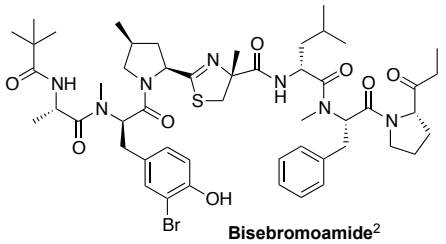

Bisebromoamide[2]
Lyngbya sp.
JFCR-39 cancer cell line panel (Mean GI_{50} = 40 nM)

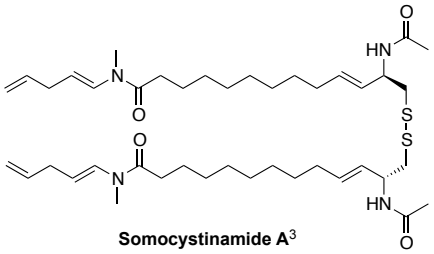

Somocystinamide A[3]
Lyngbya majuscula (now *Moorea producens*)/*Schizothrix* sp.
caspase-8-dependent apoptosis (100 pmol)[4]

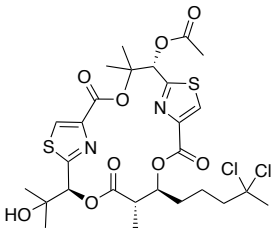

Hectochlorin[5]
Lyngbya majuscula (now *Moorea producens*)
actin polymerization induction (EC_{50} = 20 μM)

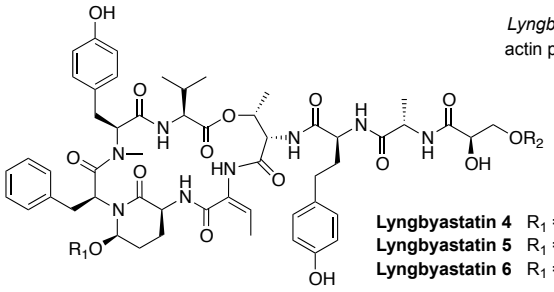

Lyngbyastatin 4 R_1 = H, R_2 = SO_3H
Lyngbyastatin 5 R_1 = H, R_2 = H
Lyngbyastatin 6 R_1 = CH_3, R_2 = SO_3Na

Lyngbya confervoides
serine protease inhibitor (elastase: IC_{50} = 3 – 14 nM)[6]

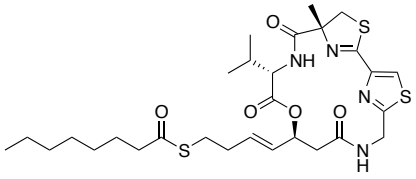

Largazole[7]
Symploca sp.
MDA-MB-231 breast cancer cells (GI_{50} = 7.7 nM)
histone deacetylase (HDAC) inhibitior (class I): 0.4 – 0.9 nM[8]

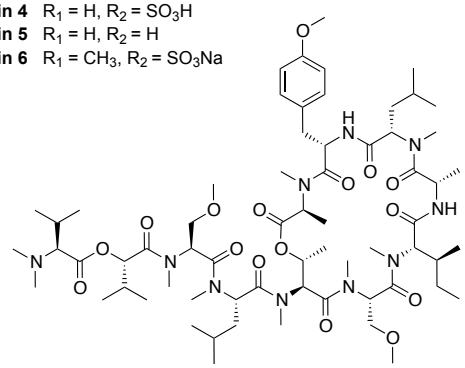

Coibamide A[9]
Symploca coibensis
MDA-MB-231 breast cancer cells (GI_{50} = 2.8 nM)
NCI-60 cancer cell line panel (Mean GI_{50} = 6.4 nM)

Figure 1.3. Examples of natural products from marine cyanobacteria that showcase their enormous structural diversity, potent cytotoxicity and profound selectivity. For each structure the producing organism, cytotoxicity data, molecular target or mechanism of action is listed. References: **1**, (Gerwick et al., 1994); **2**, (Gao et al., 2010; Teruya et al., 2009); **3**, (Nogle & Gerwick, 2002); **4**, (Wrasidlo et al., 2008); **5**, (Marquez et al., 2002); **6**, (Matthew et al., 2007; Taori et al., 2007); **7**, (Taori et al., 2008); **8**, (Hong & Luesch, 2012); **9**, (Medina et al., 2008).

organisms from rare or extreme ecosystems is a rational approach to discover novel chemotypes with medicinally relevant biological activities (Cragg & Newman, 2002). Furthermore, advances in analytical tools for molecular structure elucidation have progressed to permit routine characterization of microgram quantities of pure, unprecedented natural products. However, the characterization of new chemotypes from complex extract mixtures that also comprise a substantial mass of inorganic contaminants still requires significant biomass of source organisms. Thus, field collections of cyanobacteria, deep-sea vent invertebrates and collectable microbial mats may need to be several liters in volume, which is often not possible given the paucity of many marine organisms. Laboratory cultivation of microorganisms of interest is therefore highly desirable, and can facilitate further investigation of the pharmacology, biosynthesis and genetics of the bioactive compounds produced. As such, this dissertation focuses on the isolation and structure elucidation of bioactive natural products from cultured microorganisms inhabiting unique environments.

Thesis Overview

Chapters 2–4 describe five new bioactive natural products from cultured marine cyanobacteria collected from the Red Sea, one of the most saline and pristine water bodies in the world. The text of Chapter Two is included as it appears in: Thornburg, C. C., Thimmaiah, M., Shaala, L. A., Hau, A. M., Malmo, J. M., Ishmael, J. E., Youssef, D. T. A., & McPhail, K. L. (2011). Cyclic Depsipeptides, Grassypeptolides D and E and Ibu-epidemethoxylyngbyastatin 3, from a Red Sea *Leptolyngbya* Cyanobacterium. *J. Nat. Prod., 74*(8), 1677-1685. The dissertation author is the primary author of this manuscript. It is important to note that Figure 1, as it appears in the manuscript, has been updated to include the currently accepted nomenclature and additional SSU (16S) rRNA gene sequences obtained for each of the Red Sea cyanobacterial isolates included in this dissertation.

Chapter Three presents a new apratoxin A analogue from a Red Sea *Moorea* sp. with equipotent nanomolar activity against NCI-H460 human lung cancer cells, and thus provides further insight into the structure–activity relationships of the apratoxin family. In addition, the phylogenetic relationships of the apratoxin-producing cyanobacterial strains collected pantropically reveal a method for predicting the biosynthetic capacity of closely related marine cyanobacteria. The text of Chapter Three is included in the manuscript format for submission to the *Journal of Natural Products* in March, 2013.

In Chapter Four, a highly modified and previously unresolved metabolite from an Indonesian *Leptolyngbya* sp. is revisited as we have re-isolated it from a Red Sea *Leptolyngbya* sp. and assigned its planar structure. This unique structure further reveals the capacity of marine cyanobacteria to produce structurally diverse and complex natural products. Furthermore, the ability of this compound to chelate metal ions, for which it has been termed leptochelin, aided in the assignment of its planar structure and significantly increased its potency against human NCI-H460 human lung cancer and HeLa cervical carcinoma cells. Importantly, between these two cell lines, the metal free compound shows selectivity to human NCI-H460 lung cancer cells, which may indicate a cancer specific cellular target for this natural product.

Chapter Five describes the method development for the collection, culturing and screening of deep-sea hydrothermal vent organisms for bioactive natural products. In particular, the isolation and chemical screening of several marine actinomycetes (*Dietzia* and *Rhodococcus* spp.) and a bright blue carpet-like mat identified as a folliculinid ciliate (*Folliculinopsis* sp.) collected during the 2009 and 2010 New Millennium Observatory (NeMO) expeditions will be discussed. Finally, the diversity of cultured microbes as wells as pyrosequencing results obtained on a tubeworm associated hydrothermal vent mat will be presented. Given that deep-sea hydrothermal vents are a newly explored environment for natural products research, the introductory text of this chapter is included as it appears in an extensive review of deep-sea

hydrothermal vents: Thornburg, C. C., Zabriskie, T. M., & McPhail, K. L. (2010). Deep-Sea Hydrothermal Vents: Potential Hot Spots for Natural Products Discovery? *J. Nat. Prod., 73*(3), 489-499. The dissertation author is the primary author of this manuscript.

Chapter Six concludes the dissertation with a general discussion of the results obtained in the preceding chapters, and presents future research that should follow these discoveries.

References

Bala, S., Khanna, R., Dadhwal, M., Prabagaran, S. R., Shivaji, S., Cullum, J., & Lal, R. (2004). Reclassification of *Amycolatopsis mediterranei* DSM 46095 as *Amycolatopsis rifamycinica* sp. nov. *Int. J. Syst. Evol. Microbiol., 54*(Pt 4), 1145-1149.

Baross, J. A., & Deming, J. D. (1985). The role of bacteria in the ecology of black smoker environments. In M. L. Jones (Ed.), *The Hydrothermal Vents of the Eastern Pacific-an Overview.* (Vol. 6, pp. 355-371): Biol. Soc. Wash. Bull.

Berdy, J. (2005). Bioactive Microbial Metabolites. *J. Antibiot., 58*(1), 1-26.

Blunt, J. W., Copp, B. R., Hu, W. P., Munro, M. H., Northcote, P. T., & Prinsep, M. R. (2009). Marine natural products. *Nat. Prod. Rep., 26*, 170-244.

Blunt, J. W., Copp, B. R., Keyzers, R. A., Munro, M. H., & Prinsep, M. R. (2012). Marine natural products. *Nat. Prod. Rep., 29*(2), 144-222.

Blunt, J. W., Copp, B. R., Keyzers, R. A., Munro, M. H., & Prinsep, M. R. (2013). Marine natural products. *Nat. Prod. Rep., 30*(2), 237-323.

Blunt, J. W., Copp, B. R., Munro, M. H., Northcote, P. T., & Prinsep, M. R. (2010). Marine natural products. *Nat. Prod. Rep., 27*(2), 165-237.

Blunt, J. W., Copp, B. R., Munro, M. H., Northcote, P. T., & Prinsep, M. R. (2011). Marine natural products. *Nat. Prod. Rep., 28*(2), 196-268.

Cardellina, J. H., & Moore, B. S. (2010). Richard E. Moore (1933−2007). *J. Nat. Prod., 73*(3), 301-302.

Castenholz, R. W. (2001). Phylum BX. Cyanobacteria oxygenic photosynthetic bacteria. *Bergey's Manual of Systematic Bacteriology* (Vol. 1, pp. 473-553).

Choi, H., Pereira, A., & Gerwick, W. (2012). The Chemistry of Marine Algae and Cyanobacteria. In E. Fattorusso, W. H. Gerwick & O. Taglialatela-Scafati (Eds.), Handbook of Marine Natural Products (pp. 55-152): Springer Netherlands.

Cragg, G. M., & Newman, D. J. (2002). Chemical diversity: a function of biodiversity. *Trends Pharmacol. Sci., 23*(404-405).

Cragg, G. M., & Newman, D. J. (2006). Natural product sources of drugs: plants, microbes, marine organisms, and animals. *Comprehensive Medicinal Chemistry II, 1*, 355-403.

Dobson, C. M. (2004). Chemical space and biology. *Nature, 432*(7019), 824-828.

Drews, J. (2000). Drug Discovery: A Historical Perspective. *Science, 287*(5460), 1960-1964.

Dunlap, W. C., Battershill, C. N., Liptrot, C. H., Cobb, R. E., Bourne, D. G., Jaspars, M., Long, P. F., & Newman, D. J. (2007). Biomedicinals from the

phytosymbionts of marine invertebrates: a molecular approach. *Methods, 42*(4), 358-376.

Eisai Oncology. (2013). Retrieved February 24, 2013, from www.halaven.com

Engene, N., Choi, H., Esquenazi, E., Rottacker, E. C., Ellisman, M. H., Dorrestein, P. C., & Gerwick, W. H. (2011). Underestimated biodiversity as a major explanation for the perceived rich secondary metabolite capacity of the cyanobacterial genus *Lyngbya*. *Environ. Microbiol., 13*(6), 1601-1610.

Engene, N., Rottacker, E. C., Kaštovský, J., Byrum, T., Choi, H., Ellisman, M. H., Komárek, J., & Gerwick, W. H. (2012). *Moorea producens* gen. nov., sp. nov. and *Moorea bouillonii* comb. nov., tropical marine cyanobacteria rich in bioactive secondary metabolites. *Int. J. Syst. Evol. Microbiol., 62*(Pt 5), 1171-1178.

Fenical, W., & Jensen, P. R. (2006). Developing a new resource for drug discovery: marine actinomycete bacteria. *Nat. Chem. Biol., 2*(12), 666-673.

Fenical, W., Jensen, P. R., Palladino, M. A., Lam, K. S., Lloyd, G. K., & Potts, B. C. (2009). Discovery and development of the anticancer agent salinosporamide A (NPI-0052). *Biorg. Med. Chem., 17*(6), 2175-2180.

Floss, H. G., & Yu, T. W. (2005). Rifamycin-mode of action, resistance, and biosynthesis. *Chem. Rev., 105*(2), 621-632.

Francisco, J. A., Cerveny, C. G., Meyer, D. L., Mixan, B. J., Klussman, K., Chace, D. F., Rejniak, S. X., Gordon, K. A., DeBlanc, R., Toki, B. E., Law, C. L., Doronina, S. O., Siegall, C. B., Senter, P. D., & Wahl, A. F. (2003). cAC10-vcMMAE, an anti-CD30-monomethyl auristatin E conjugate with potent and selective antitumor activity. *Blood, 102*(4), 1458-1465.

Funato, N., Takayanagi, H., Konda, Y., Toda, Y., Harigaya, Y., Iwai, Y., & Ōmura, S. (1994). Absolute Configuration of Staurosporine By X-Ray Analysis. *Tetrahedron Lett., 35*(8), 1251-1254.

Gao, X., Liu, Y., Kwong, S., Xu, Z., & Ye, T. (2010). Total Synthesis and Stereochemical Reassignment of Bisebromoamide. *Org. Lett., 12*(13), 3018-3021.

Gerwick, W. H., Proteau, P. J., Nagle, D. G., Hamel, E., Blokhin, A., & Slate, D. L. (1994). Structure of Curacin A, a Novel Antimitotic, Antiproliferative and Brine Shrimp Toxic Natural Product from the Marine Cyanobacterium *Lyngbya majuscula*. *J. Org. Chem., 59*(6), 1243-1245.

Harrigan, G. G., Luesch, H., Yoshida, W. Y., Moore, R. E., Nagle, D. G., Paul, V. J., Mooberry, S. L., Corbett, T. H., & Valeriote, F. A. (1998). Symplostatin 1: A Dolastatin 10 Analogue from the Marine Cyanobacterium *Symploca* hydnoides. *J. Nat. Prod., 61*(9), 1075-1077.

He, H., Ding, W.-D., Bernan, V. S., Richardson, A. D., Ireland, C. M., Greenstein, M., Ellestad, G. A., & Carter, G. T. (2001). Lomaiviticins A and B, Potent

Antitumor Antibiotics from *Micromonospora lomaivitiensis*. *J. Am. Chem. Soc., 123*(22), 5362-5363.

Helmke, E., & Weyland, H. (1984). *Rhodococcus marinonascens* sp. nov., an actinomycete from the sea. *Int. J. Syst. Bacteriol., 34*, 127-138.

Hill, R. T., Peraud, O., Hamann, M. T., & Kasanah, N. (2005). US Patent No. 2005/0244938. U.S.P.T. Office.

Hong, J., & Luesch, H. (2012). Largazole: From discovery to broad-spectrum therapy. *Nat. Prod. Rep., 29*(4), 449-456.

Kim, T. K., Hewavitharana, A. K., Shaw, P. N., & Fuerst, J. A. (2006). Discovery of a New Source of Rifamycin Antibiotics in Marine Sponge Actinobacteria by Phylogenetic Prediction. *Appl. Environ. Microbiol., 72*(3), 2118-2125.

Kingston, D. G. I. (2010). Modern Natural Products Drug Discovery and Its Relevance to Biodiversity Conservation. *J. Nat. Prod., 74*(3), 496-511.

Kwan, J. C., Ratnayake, R., Abboud, K. A., Paul, V. J., & Luesch, H. (2010). Grassypeptolides A-C, Cytotoxic Bis-thiazoline Containing Marine Cyclodepsipeptides. *J. Org. Chem., 75*(23), 8012-8023.

Kwon, H. C., Kauffman, C. A., Jensen, P. R., & Fenical, W. (2006). Marinomycins A −D, Antitumor-Antibiotics of a New Structure Class from a Marine Actinomycete of the Recently Discovered Genus “Marinispora”. *J. Am. Chem. Soc., 128*(5), 1622-1632.

Lam, K. S. (2006). Discovery of novel metabolites from marine actinomycetes. *Curr. Opin. Microbiol., 9*(245-251).

Lipinski, C., & Hopkins, A. (2004). Navigating chemical space for biology and medicine. *Nature, 432*(7019), 855-861.

Litaudon, M., Hart, J. B., Blunt, J. W., Lake, R. J., & Munro, M. h. (1994). Isohomohalichondrin B, a new antitumour polyether macrolide from the New Zealand deep-water sponge *Lissodendoryx* sp. *Tetrahedron Lett., 35*(50), 9435-9438.

Luesch, H., Harrigan, G. G., Goetz, G., & Horgen, F. D. (2002). The Cyanobacterial Origin of Potent Anticancer Agents Originally Isolated from Sea Hares. *Curr. Med. Chem., 9*(20), 1791.

Luesch, H., Moore, R. E., Paul, V. J., Mooberry, S. L., & Corbett, T. H. (2001). Isolation of Dolastatin 10 from the Marine Cyanobacterium *Symploca* Species VP642 and Total Stereochemistry and Biological Evaluation of Its Analogue Symplostatin 1. *J. Nat. Prod., 64*(7), 907-910.

Marquez, B. L., Watts, K. S., Yokochi, A., Roberts, M. A., Verdier-Pinard, P., Jimenez, J. I., Hamel, E., Scheuer, P. J., & Gerwick, W. H. (2002). Structure and Absolute Stereochemistry of Hectochlorin, a Potent Stimulator of Actin Assembly. *J. Nat. Prod., 65*(6), 866-871.

Matthew, S., Ross, C., Rocca, J. R., Paul, V. J., & Luesch, H. (2007). Lyngbyastatin 4, a Dolastatin 13 Analogue with Elastase and Chymotrypsin Inhibitory Activity from the Marine Cyanobacterium *Lyngbya confervoides*. *J. Nat. Prod., 70*(1), 124-127.

Medina, R. A., Goeger, D. E., Hills, P., Mooberry, S. L., Huang, N., Romero, L. I., Ortega-Barria, E., Gerwick, W. H., & McPhail, K. L. (2008). Coibamide A, a potent antiproliferative cyclic depsipeptide from the Panamanian marine cyanobacterium *Leptolyngbya* sp. *J. Am. Chem. Soc., 130*(20), 6324-6325.

Molinski, T. F., Dalisay, D. S., Lievens, S. L., & Saludes, J. P. (2009). Drug development from marine natural products. *Nat. Rev. Drug Discov., 8*, 69-85.

Moss, C., Green, D. H., Pérez, B., Velasco, A., Henríquez, R., & McKenzie, J. D. (2003). Intracellular bacteria associated with the ascidian *Ecteinascidia turbinata*: phylogenetic and *in situ* hybridisation analysis. *Mar. Biol., 143*(1), 99-110.

Naganuma, T., Miyoshi, T., & Kimura, H. (2007). Phylotype diversity of deep-sea hydrothermal vent prokaryotes trapped by 0.2- and 0.1-μm-pore-size filters. *Extremophiles, 11*(4), 637-646.

Nagle, D. G., & Paul, V. J. (1999). Production of secondary metabolites by filamentous tropical marine cyanobacteria: ecological functions of the compounds. *J. Phycol., 35*(6), 1412-1421.

Nereus Pharmaceuticals, Inc. (2013). Retrieved February 22, 2013, from http://www.nereuspharm.com/ClinicalTrialsNPI-0052.shtml

Newman, D. J., & Cragg, G. M. (2012). Natural products as sources of new drugs over the 30 years from 1981 to 2010. *J. Nat. Prod., 75*(3), 311-335.

Newman, D. J., & Hill, R. (2006). New drugs from marine microbes: the tide is turning. *J. Ind. Microbiol. Biotechnol., 33*(7), 539-544.

NIH ClinicalTrials. (2013). Retrieved February 24, 2013, from www.clinicaltrials.gov

Nogle, L. M., & Gerwick, W. H. (2002). Somocystinamide A, a Novel Cytotoxic Disulfide Dimer from a Fijian Marine Cyanobacterial Mixed Assemblage. *Org. Lett., 4*(7), 1095-1098.

Novartis Oncology US. (2013). Retrieved February 22, 2013, from http://www.novartisoncology.us/research/pipeline/midostaurin.jsp

Omura, S., Iwai, Y., Hirano, A., Nakagawa, A., Awaya, J., Tsuchya, H., Takahashi, Y., & Masuma, R. (1977). A new alkaloid AM-2282 OF Streptomyces origin. Taxonomy, fermentation, isolation and preliminary characterization. *J. Antibiot., 30*(4), 275-282.

Pettit, G. R., Herald, C. L., Boyd, M. R., Leet, J. E., Dufresne, C., Doubek, D. L., Schmidt, J. M., Cerny, R. L., Hooper, J. N. A., & Rutzler, K. C. (1991). Isolation and structure of the cell growth inhibitory constituents from the western Pacific marine sponge *Axinella* sp. *J. Med. Chem., 34*(11), 3339-3340.

Pettit, G. R., Herald, C. L., Doubek, D. L., Herald, D. L., Arnold, E., & Clardy, J. (1982). Isolation and structure of bryostatin 1. *J. Am. Chem. Soc., 104*(24), 6846-6848.

Pettit, G. R., Kamano, Y., Dufresne, C., Cerny, R. L., Herald, C. L., & Schmidt, J. M. (1989). Isolation and structure of the cytostatic linear depsipeptide dolastatin 15. *J. Org. Chem., 54*(26), 6005-6006.

Pettit, G. R., Kamano, Y., Herald, C. L., Tuinman, A. A., Boettner, F. E., Kizu, H., Schmidt, J. M., Baczynskyj, L., Tomer, K. B., & Bontems, R. J. (1987). The isolation and structure of a remarkable marine animal antineoplastic constituent: dolastatin 10. *J. Am. Chem. Soc., 109*(22), 6883-6885.

Pettit, G. R., Tan, R., Gao, F., Williams, M. D., Doubek, D. L., Boyd, M. R., Schmidt, J. M., Chapuis, J. C., Hamel, E., & et al. (1993). Isolation and structure of halistatin 1 from the eastern Indian Ocean marine sponge *Phakellia carteri*. *J. Org. Chem., 58*(9), 2538-2543.

PharmaMar. (2013a). *PharmaMar, Zeltia Group. Aplidin®.* Retrieved February 24, 2013, from http://www.pharmamar.com/aplidin.aspx

PharmaMar. (2013b). *PharmaMar, Zeltia Group. Yondelis® (trabectedin).* Retrieved February 24, 2013, from http://www.pharmamar.com/yondelis.aspx

Rasmussen, B., Fletcher, I. R., Brocks, J. J., & Kilburn, M. R. (2008). Reassessing the first appearance of eukaryotes and cyanobacteria. *Nature, 455*(7216), 1101-1104.

Rath, C. M., Janto, B., Earl, J., Ahmed, A., Hu, F. Z., Hiller, L., Dahlgren, M., Kreft, R., Yu, F., Wolff, J. J., Kweon, H. K., Christiansen, M. A., Hakansson, K., Williams, R. M., Ehrlich, G. D., & Sherman, D. H. (2011). Meta-omic characterization of the marine invertebrate microbial consortium that produces the chemotherapeutic natural product ET-743. *ACS Chem Biol, 6*(11), 1244-1256.

Renner, M. K., Shen, Y.-C., Cheng, X.-C., Jensen, P. R., Frankmoelle, W., Kauffman, C. A., Fenical, W., Lobkovsky, E., & Clardy, J. (1999). Cyclomarins A−C, New Antiinflammatory Cyclic Peptides Produced by a Marine Bacterium (*Streptomyces sp*.). *J. Am. Chem. Soc., 121*(49), 11273-11276.

Rinehart, K. L., Gloer, J. B., Cook, J. C., Mizsak, S. A., & Scahill, T. A. (1981). Structures of the didemnins, antiviral and cytotoxic depsipeptides from a Caribbean tunicate. *J. Am. Chem. Soc., 103*(7), 1857-1859.

Rinehart, K. L., Holt, T. G., Fregeau, N. L., Stroh, J. G., Keifer, P. A., Sun, F., Li, L. H., & Martin, D. G. (1990). Ecteinascidins 729, 743, 745, 759A, 759B, and 770: potent antitumor agents from the Caribbean tunicate *Ecteinascidia turbinata*. *J. Org. Chem., 55*(15), 4512-4515.

Sakai, R., Higa, T., Jefford, C. W., & Bernardinelli, G. (1986). Manzamine A, a novel antitumor alkaloid from a sponge. *J. Am. Chem. Soc., 108*(20), 6404-6405.

Sakai, R., Rinehart, K. L., Kishore, V., Kundu, B., Faircloth, G., Gloer, J. B., Carney, J. R., Namikoshi, M., Sun, F., Hughes, R. G., Grávalos, D. G., de Quesada, T. G., Wilson, G. R., & Heid, R. M. (1996). Structure−Activity Relationships of the Didemnins1,2. *J. Med. Chem., 39*(14), 2819-2834.

Schmidt, B., Ribnicky, D. M., Poulev, A., Logendra, S., Cefalu, W. T., & Raskin, I. (2008). A natural history of botanical therapeutics. *Metabolism, Clinical and Experimental 57*, S3-S9.

Schultz, A. W., Oh, D.-C., Carney, J. R., Williamson, R. T., Udwary, D. W., Jensen, P. R., Gould, S. J., Fenical, W., & Moore, B. S. (2008). Biosynthesis and Structures of Cyclomarins and Cyclomarazines, Prenylated Cyclic Peptides of Marine Actinobacterial Origin. *J. Am. Chem. Soc., 130*(13), 4507-4516.

Seattle Genetics. (2013). *CD30-Directed Adcetris® (brentuximab vedotin)*. Retrieved January 21, 2013, from www.seattlegenetics.com/adcetris

Sensi, P., Margalith, P., & Timbal, M. T. (1959). Rifomycin, a new antibiotic; preliminary report. *Il Farmaco; edizione scientifica, 14*(2), 146-147.

Sharp, K., Arthur, K. E., Gu, L., Ross, C., Harrison, G., Gunasekera, S. P., Meickle, T., Matthew, S., Luesch, H., Thacker, R. W., Sherman, D. H., & Paul, V. J. (2009). Phylogenetic and Chemical Diversity of Three Chemotypes of Bloom-Forming *Lyngbya* Species (Cyanobacteria: Oscillatoriales) from Reefs of Southeastern Florida. *Appl. Environ. Microbiol., 75*(9), 2879-2888.

Simmons, T. L., Coates, R. C., Clark, B. R., Engene, N., Gonzalez, D., Esquenazi, E., Dorrestein, P. C., & Gerwick, W. H. (2008). Chemical Ecology Special Feature: Biosynthetic origin of natural products isolated from marine microorganism-invertebrate assemblages. *Proc. Natl. Acad. Sci., 105*(12), 4587-4594.

Skropeta, D. (2008). Deep-Sea natural products. *Nat. Prod. Rep, 25*(6), 1131-1166.

Sudek, S., Lopanik, N. B., Waggoner, L. E., Hildebrand, M., Anderson, C., Liu, H., Patel, A., Sherman, D. H., & Haygood, M. G. (2006). Identification of the Putative Bryostatin Polyketide Synthase Gene Cluster from "Candidatus *Endobugula sertula*", the Uncultivated Microbial Symbiont of the Marine Bryozoan *Bugula neritina*. *J. Nat. Prod., 70*(1), 67-74.

Taori, K., Liu, Y., Paul, V. J., & Luesch, H. (2009). Combinatorial Strategies by Marine Cyanobacteria: Symplostatin 4, an Antimitotic Natural Dolastatin 10/15 Hybrid that Synergizes with the Coproduced HDAC Inhibitor Largazole. *ChemBioChem, 10*(10), 1634-1639.

Taori, K., Matthew, S., Rocca, J. R., Paul, V. J., & Luesch, H. (2007). Lyngbyastatins 5-7, Potent Elastase Inhibitors from Floridian Marine Cyanobacteria, *Lyngbya* spp. *J. Nat. Prod., 70*(10), 1593-1600.

Taori, K., Paul, V. J., & Luesch, H. (2008). Structure and Activity of Largazole, a Potent Antiproliferative Agent from the Floridian Marine Cyanobacterium *Symploca* sp. *J. Am. Chem. Soc., 130*(6), 1806-1807.

Teruya, T., Sasaki, H., Fukazawa, H., & Suenaga, K. (2009). Bisebromoamide, a Potent Cytotoxic Peptide from the Marine Cyanobacterium *Lyngbya sp*.: Isolation, Stereostructure, and Biological Activity. *Org. Lett., 11*(21), 5062-5065.

Teske, A., Hinrichs, K.-U., Edgcomb, V., de Vera Gomez, A., Kysela, D., Sylva, S. P., Sogin, M. L., & Jannasch, H. W. (2002). Microbial Diversity of Hydrothermal Sediments in the Guaymas Basin: Evidence for Anaerobic Methanotrophic Communities. *Appl. Environ. Microbiol., 68*(4), 1994-2007.

Thacker, R. W., & Paul, V. J. (2004). Morphological, Chemical, and Genetic Diversity of Tropical Marine Cyanobacteria Lyngbya spp. and Symploca spp. (Oscillatoriales). *Appl. Environ. Microbiol., 70*(6), 3305-3312.

Tidgewell, K., Clark, B. R., & Gerwick, W. H. (2010). 2.06 - The Natural Products Chemistry of Cyanobacteria. In M. Editors-in-Chief: Lew & L. Hung-Wen (Eds.), *Comprehensive Natural Products II* (pp. 141-188). Oxford: Elsevier.

Tsukimoto, M., Nagaoka, M., Shishido, Y., Fujimoto, J., Nishisaka, F., Matsumoto, S., Harunari, E., Imada, C., & Matsuzaki, T. (2011). Bacterial production of the tunicate-derived antitumor cyclic depsipeptide didemnin B. *J. Nat. Prod., 74*(11), 2329-2331.

Uemura, D., Takahashi, K., Yamamoto, T., Katayama, C., Tanaka, J., Okumura, Y., & Hirata, Y. (1985). Norhalichondrin A: an antitumor polyether macrolide from a marine sponge. *J. Am. Chem. Soc., 107*(16), 4796-4798.

Walsh, C. T., & Fischbach, M. A. (2010). Natural Products Version 2.0: Connecting Genes to Molecules. *J. Am. Chem. Soc., 132*(8), 2469-2493.

Winkler, J. D., Londregan, A. T., & Hamann, M. T. (2006). Antimalarial Activity of a New Family of Analogues of Manzamine A. *Org. Lett., 8*(12), 2591-2594.

Wrasidlo, W., Mielgo, A., Torres, V. A., Barbero, S., Stoletov, K., Suyama, T. L., Klemke, R. L., Gerwick, W. H., Carson, D. A., & Stupack, D. G. (2008). The marine lipopeptide somocystinamide A triggers apoptosis via caspase 8. *Proc. Natl. Acad. Sci., 105*(7), 2313-2318.

Wright, A. E., Forleo, D. A., Gunawardana, G. P., Gunasekera, S. P., Koehn, F. E., & McConnell, O. J. (1990). Antitumor tetrahydroisoquinoline alkaloids from the colonial ascidian *Ecteinascidia turbinata*. *J. Org. Chem., 55*(15), 4508-4512.

Chapter Two

Cyclic Depsipeptides, Grassypeptolides D and E and Ibu-epidemethoxylyngbyastatin 3, from a Red Sea *Leptolyngbya* Cyanobacterium

Christopher C. Thornburg, Muralidhara Thimmaiah, Lamiaa A. Shaala,
Andrew M. Hau, Jay M. Malmo, Jane E. Ishmael, Diaa T.A. Youssef,
and Kerry L. McPhail

Journal of Natural Products
2011, 74(8), pp 1677-1685
DOI: 10.1021/np200270d

Abstract

Two new grassypeptolides and a lyngbyastatin analogue, together with the known dolastatin 12, have been isolated from field collections and laboratory cultures of the marine cyanobacterium *Leptolyngbya* sp. collected from the *SS Thistlegorm* shipwreck in the Red Sea. The overall stereostructures of grassypeptolides D (**1**) and E (**2**) and Ibu-epidemethoxylyngbyastatin 3 (**3**) were determined by a combination of 1D and 2D NMR experiments, mass spectrometric analysis, Marfey's methodology and HPLC-MS. Compounds **1** and **2** contain 2-methyl-3-aminobutyric acid (Maba) and 2-aminobutyric acid (Aba), while biosynthetically distinct **3** contains 3-amino-2-methylhexanoic acid (Amha) and the β-keto amino acid 4-amino-2,2-dimethyl-3-oxopentanoic acid (Ibu). Grassypeptolides D (**1**) and E (**2**) showed significant cytotoxicity to HeLa (IC_{50} = 335 and 192 nM, respectively) and mouse neuro-2a blastoma cells (IC_{50} = 599 and 407 nM, respectively), in contrast to Ibu-epidemethoxylyngbyastatin 3 (neuro-2a cells, IC_{50} > 10 μM) and dolastatin 12 (neuro-2a cells, IC_{50} > 1 μM).

Introduction

Microbial metabolites appear to be characteristic of certain biotopes, both on an environmental and a species level, which has provided a diversity of chemical structures unparalleled by even the largest combinatorial libraries (Clardy & Walsh, 2004). Our research has recently focused on the isolation and structure elucidation of biologically active natural products from microorganisms inhabiting unique environments. The Red Sea represents an unexplored repository of diverse cyanobacteria, although in low abundance. This may result from the low annual rainfall, minimal freshwater input and high evaporation rate that make the Red Sea one of the most saline and pristine water bodies in the world (Fenton et al., 2000). Despite these conditions, we have collected specimens from a range of cyanobacterial genera including *Moorea*, *Phormidium*, *Symploca,* and the *Leptolyngbya* that is the subject of this report. Thus, we are interested to compare the biosynthetic capabilities of these Red Sea organisms with those collected pantropically. As is the case for natural products in general, cyanobacterial metabolites often occur as sets of related analogues that possess varying biological selectivity, putatively for optimal adaptation to a range of environments (Tan, 2010). In addition, the capacity of any one cyanobacterium to produce several biosynthetically distinct metabolites (Harrigan et al., 1998), as well as the production of the same or biosynthetically related natural products by different genera of cyanobacteria is the subject of intense investigation (Niclas Engene et al., 2010). One proposal is that common heterotrophic bacteria associated with cyanobacteria may be the biosynthetic origin of the isolated products. Alternatively, horizontal gene transfer between different cyanobacteria or between heterotrophic bacteria may account for the presence of multiple biosynthetic gene clusters in cyanobacterial genomes (Hess, 2008). Remarkably, a Floridian *Lyngbya confervoides* has afforded lyngbyastatins 4-6 (Matthew et al., 2007; Taori et al., 2007), pompanopeptins A and B (Matthew et al., 2008), largamides A–H (Matthew et al.,

2009a), tiglicamides A–C (Matthew et al., 2009b), and grassypeptolides A-C (Kwan et al., 2010). Here we report the isolation of grassypeptolides D (**1**) and E (**2**) and Ibu-epidemethoxylyngbyastatin 3 (**3**), as well as the known dolastatin 12 (Pettit et al., 1989), from a marine *Leptolyngbya* cyanobacterium collected from the Red Sea shipwreck *SS Thistlegorm* (46 – 98 ft). All four macrocyclic depsipeptides are also produced by the laboratory-cultured (monoclonal) Red Sea *Leptolyngbya*. While grassypeptolide D (**1**) is ~1.5-fold less cytotoxic to HeLa cervical carcinoma and neuro-2a mouse blastoma cells than grassypeptolide E (**2**), these threonine/*N*-methylleucine diastereomers do not show the dramatic natural structure-activity relationship observed between the *N*-methyl phenylalanine epimers grassypeptolides A and C (Kwan et al., 2010). Ibu-epidemethoxylyngbyastatin 3 (**3**, IC_{50} > 10 μM) was significantly less cytotoxic to neuro-2a cells than the grassypeptolides and related dolastatin 12 (IC_{50} > 1 μM).

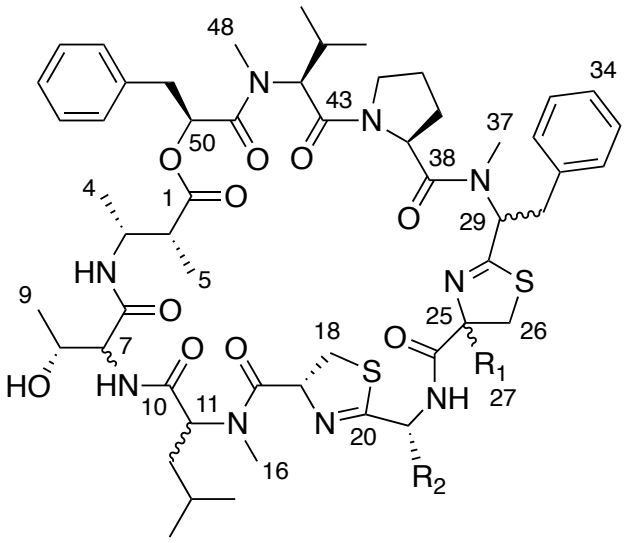

					R_1	R_2
Grassypeptolide D (**1**)	7*R*,	11*R*,	25*S*,	29*S*	Me	Et
Grassypeptolide E (**2**)	7*S*,	11*S*,	25*S*,	29*S*	Me	Et
Grassypeptolide A	7*R*,	11*R*,	25*R*,	*29*R*	H	Et
Grassypeptolide B	7*R*,	11*R*,	25*R*,	*29*R*	H	Me
Grassypeptolide C	7*R*,	11*R*,	25*R*,	*29*S*	H	Et

* This is position 28 in the original report of grassypeptolides A-C

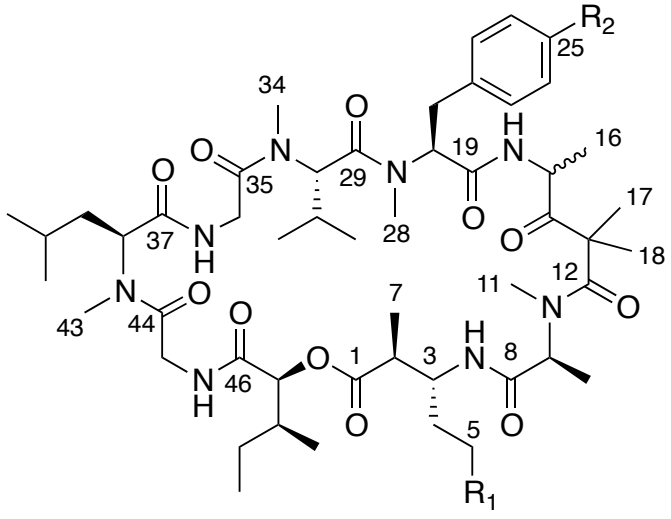

		R_1	R_2
Ibu-epidemethoxylyngbyastatin (**3**)	15*S*	Me	H
Dolastatin 12	15*S*	H	H
Lyngbyastatin 3	15*R*	Me	OMe

Results and Discussion

A crude organic extract of the Red Sea *Leptolyngbya* was subjected to bioassay-guided fractionation via normal phase vacuum liquid chromatography (NP VLC) using a stepped gradient of hexanes to EtOAC to MeOH. The fraction eluting with 25% MeOH-EtOAC was highly cytotoxic to mouse neuro-2a neurobastoma cells (30 mg/ mL reduced cell viability by 99.6%). This VLC fraction was separated by C_{18} reversed-phase (RP_{18}) solid phase extraction (SPE) and exhaustive RP-HPLC to yield three minor cytotoxic metabolites (**1**, 1.5 mg; **2**, 0.5 mg and **3**, 2.9 mg) and the known depsipeptide dolastatin 12 (5.0 mg) as the major component.

A molecular formula of $C_{57}H_{81}N_9O_{10}S_2$ for both grassypeptolides D (**1**) and E (**2**) was provided by HRMS ($[M + Na]^+$ *m/z* 1138.5515 and 1138.5413, respectively) and supported by NMR spectroscopic (Table 2.1) data. The ^1H and ^{13}C NMR spectra for each compound were very similar, and indicated peptidic metabolites due to the presence of three NH doublets (δ_H 6.45–7.50), three *N*-methyl substituents (δ_H 3.1–3.5), nine α-H multiplets (δ_H 3.4–5.9), numerous overlapped methyl doublets (δ_H 0.74–0.99) and ten putative ester/amide carbonyl ^{13}C signals (δ_C 168–175 ppm) in each case. These data suggested that **1** and **2** were structurally related to the Floridian *Lyngbya confervoides* metabolites grassypeptolides A-C, and very similar to grassypeptolide C in particular (Kwan et al., 2010). However, the 1D NMR spectra for both **1** and **2** contain a 3H singlet ($\delta_{H\text{-}27}$ 1.35 and 1.38, respectively) and a quaternary carbon ($\delta_{C\text{-}25}$ 84.0) not present in the spectra for grassypeptolide C. In addition, comparison of the α-CH chemical shifts for **1**, **2** and grassypeptolide C revealed significant differences between compounds **1** and **2** (Table 2.1), whereas the α-CH chemical shifts for **1** more closely matched those for grassypeptolide C. These differences led us to investigate the structures of **1** and **2** more closely.

Table 2.1. ^{1}H (700 MHz) and ^{13}C (175 MHz) NMR Spectroscopic Data for Grassypeptolides D (**1**) and E (**2**) in $CDCl_3$.

		Grassypeptolide D (**1**)		Grassypeptolide E (**2**)	
unit	position	δ_H, mult. (*J* in Hz)	δ_C, mult.	δ_H, mult. (*J* in Hz)	δ_C, mult.
Maba	1		172.4, C		172.9, C
	2	2.50, dq (7.0, 6.8)	45.6, CH	2.51, dq (7.0, 4.5)	45.5, CH
	3	4.22, m	48.5, CH	4.23, m	47.0, CH
	4	1.19, d (6.7)	19.9, CH_3	1.10, d (7.0)	19.3, CH_3
	5	1.12, d (7.0)	14.4, CH_3	1.16, d (7.0)	14.4, CH_3
	NH	7.70, br		6.45, d (9.9)	
Thr	6		169.3, C		170.5, C
	7	4.45, dd (6.8, 6.1)	59.1, CH	3.36, dd (6.9, 3.3)	57.0, CH
	8	4.02, m	69.1, CH	3.30, m	67.9, CH
	9	1.22, d (6.4)	19.7, CH_3	0.87, d (6.5)	19.4, CH_3
	OH	4.00, br			
	NH	6.90, d (7.3)		6.90, d (6.9)	
N-Me-Leu	10		170.3, C		170.0, C
	11	4.70, br	57.5, CH	5.15, t (7.7)	54.6, CH
	12a	1.97, m	37.2, CH_2	1.78, m	37.1, CH_2
	12b	1.67, m			
	13	1.58, m	25.3, CH	1.52, m	25.3, CH
	14	0.98, d (6.4)	23.2, CH_3	0.98, d (6.6)	23.2, CH_3
	15	0.94, d (6.5)	22.8, CH_3	0.93, d (6.7)	22.4, CH_3
	16	3.20, s	33.2, CH_3	3.49, s	30.7, CH_3
Aba-thn-ca	17		170.4, C		169.3, C
	18	5.29, m	78.1, CH	5.07, m	75.9, CH
	19a	3.60, m	33.3, CH_2	4.15, br dd	35.5, CH_2
	19b	3.26, m		3.44, dd (-11.2, 8.5)	
	20		178.0, C		175.0, C
	21	4.55, m	54.2, CH	4.71, ddd (9.0, 4.0, 2.7)	53.2, CH
	22a	2.11, m	25.2, CH_2	1.95, dqd (-11.5, 7.4, 4.0)	28.5, CH_2
	22b	1.86, m		1.48, m	
	23	0.96, t (6.9)	11.6, CH_3	0.74, t (7.4)	10.0, CH_3
	NH	7.10, d (7.7)		7.50, d (9.0)	
N-Me-Phe-thn-ca	24		173.7, C		168.9, C
	25		84.0, C		84.0, C
	26a	3.74, d (-11.5)	43.1, CH_2	3.29, d (-11.6)	41.5, CH_2
	26b	3.17, d (-11.3)		3.18, d (-11.7)	
	27	1.35, s	24.3, CH_3	1.38, s	23.9, CH_3

Table 2.1 (continued). ^{1}H (700 MHz) and ^{13}C (175 MHz) NMR Spectroscopic Data for Grassypeptolides D (**1**) and E (**2**) in $CDCl_3$.

		Grassypeptolide D (**1**)		Grassypeptolide E (**2**)	
unit	position	δ_H, mult. (*J* in Hz)	δ_C, mult.	δ_H, mult. (*J* in Hz)	δ_C, mult.
N-Me-Phe-thn-ca	28		173.9, C		173.9, C
	29	5.39, dd (10.7, 6.4)	58.9, CH	5.87, dd (12.2, 3.0)	55.8, CH
	30a	3.24, m	36.0, CH_2	3.55, br	36.1, CH_2
	30b	3.16, m		3.28, m	
	31		135.5, C		137.7, C
	32/36	7.33, m	129.2, CH	7.18, m	129.6, CH
	33/35	7.22, m	128.5, CH	7.03, br	129.3, CH
	34	7.20, m	127.6, CH	7.08, m	127.3, CH
	37	3.21, s	30.7, CH_3	3.17, s	30.2, CH_3
Pro	38		172.7, C		171.2, C
	39	4.84, dd (8.8,5.1)	57.5, CH	5.10, br	58.8, CH
	40a	2.22, m	27.5, CH_2	2.30, m	31.2, CH_2
	40b	1.93, m		2.10, m	
	41a	1.99, m	24.9, CH_2	2.01, m	21.7, CH_2
	41b	1.63, m			
	42a	3.97, m	47.8, CH_2	3.80, m	46.9, CH_2
	42b	3.53, m		3.69, m	
N-Me-Val	43		168.6, C		168.5, C
	44	4.98, d (11.0)	60.0, CH	5.01, d (10.8)	58.1, CH
	45	2.32, m	27.4, CH	2.35, m	28.1, CH
	46	0.98, d (6.4)	19.6, CH_3	0.95, d (6.7)	19.5, CH_3
	47	0.88, d (6.6)	18.0, CH_3	0.85, d (6.7)	18.6, CH_3
	48	3.12, s	30.0, CH_3	3.20, s	30.3, CH_3
Pla	49		170.2, C		171.4, C
	50	5.33, dd (9.9, 3.2)	72.4, CH	5.33, dd (9.7, 3.8)	72.4, CH
	51a	3.09, dd (-14.5, 9.9)	36.9, CH_2	3.16, m	36.9, CH_2
	51b	3.04, dd (-14.4, 3.2)		3.01, m	
	52		134.9, C		136.1, C
	53/57	7.22, m	129.1, CH	7.12, m	129.1, CH
	54/56	7.24, m	129.5, CH	7.31, m	129.5, CH
	55	7.27, m	127.6, CH	7.24, m	127.4, CH

Analysis of the 2D NMR spectra in $CDCl_3$ for **1** and **2** (HSQC, HSQC-TOCSY, HMBC, COSY, ROESY) confirmed that grassypeptolides D (**1**) and E (**2**) had the same connectivity of planar structure as grassypeptolide C. An HSQC-TOCSY experiment for **1** identified spin systems for Thr, Leu, Pro and Val amino acid side chains, and key HMBC (supported by COSY and ROESY) correlations established that Leu and Val were *N*-methylated as in grassypeptolide C. A pair of doublet methyl signals ($\delta_{H\text{-}4}$ 1.19 and $\delta_{H\text{-}5}$ 1.12) correlated to two vicinally coupled methine multiplets ($\delta_{H\text{-}2}$ 2.50 and $\delta_{H\text{-}3}$ 4.22) distinguished the β-amino acid residue 2-methyl-3-aminobutyric acid (Maba). COSY correlations from an upfield methyl doublet ($\delta_{H\text{-}23}$ 0.96) to a relatively shielded methylene ($\delta_{H\text{-}22}$ 2.11/1.86), in turn coupled to a methine ($\delta_{H\text{-}21}$ 4.55), supported a 2-aminobutyric acid (Aba) residue. An HMBC correlation to the putative carbonyl ^{13}C of Aba from a relatively deshielded methylene ($\delta_{H\text{-}19}$ 3.60/3.26), which also correlated to a second deshielded quaternary ^{13}C ($\delta_{C\text{-}17}$ 170.4), was consistent with an Aba-derived thiazoline carboxylic acid (Aba-thn-ca). Chemical shift comparison with grassypeptolide C and HMBC analysis (see Supporting Information, Table 2.2) also confirmed the presence of two aromatic residues, phenyllactic acid (Pla) and *N*-methylphenylalanine (*N*-Me-Phe). The latter residue is incorporated into a thiazoline carboxylic acid in grassypeptolide C. However, no –$CHCH_2$– motif consistent with this remaining thiazoline ring was apparent in the spectra for grassypeptolide D (**1**). Instead, an AB spin system of a fifth isolated methylene ($\delta_{H\text{-}26}$ 3.74/3.17) showed HMBC correlations to a methyl ($\delta_{C\text{-}27}$ 24.3), a midfield quaternary ($\delta_{C\text{-}25}$ 84.0) and two deshielded quaternary ($\delta_{C\text{-}28}$ 173.9 and $\delta_{C\text{-}24}$ 173.7) carbons. This indicated the presence of a 2-methylthiazoline carboxylic acid derived from *N*-methylphenylalanine (*N*-Me-Phe-4-Me-thn-ca). Although none of the previously reported grassypeptolides A–C contain a methylated thiazoline carboxylic acid, this unit has been reported in largazole (Taori et al., 2008) and the hoiamides (Choi et al., 2010) from marine cyanobacteria, as well as several terrestrial bacteria.

Analysis of the 2D NMR data for **2** revealed the same sequence of units as found in **1**. However, the α-CH chemical shifts for Thr ($\delta_H/\delta_{C\text{-}7}$ 3.36/ 57.0) and *N*-Me-Leu ($\delta_H/\delta_{C\text{-}11}$ 5.15/54.6) in **2** were substantially different from those observed for **1** (Thr, $\delta_H/\delta_{C\text{-}7}$ 4.45/59.1; *N*-Me-Leu, $\delta_H/\delta_{C\text{-}11}$ 4.70/57.5) and grassypeptolide C (Thr, $\delta_H/\delta_{C\text{-}7}$ 4.44/59.2; *N*-Me-Leu, $\delta_H/\delta_{C\text{-}11}$ 4.70/57.6). Furthermore, the *N*-CH_3-16 singlet (δ_H 3.49) for **2** was shifted slightly downfield compared to those for **1** and grassypeptolide C (δ_H 3.20 and 3.17, respectively). Overall, these chemical shift differences suggested different configurations for both Thr and *N*-Me-Leu in **2** relative to **1** and grassypeptolide C.

The absolute configurations of grassypeptolides D (**1**) and E (**2**) were determined by a combination of acid hydrolysis and oxidative ozonolysis followed by chiral LC-MS or Marfey's analysis. Chiral LC-MS of the acid hydrolysates of **1** and **2** established the presence of L-Pla, while analysis by RP_{18} HPLC of the ozonolysis and acid hydrolysate products of **1** and **2** derivatized with *N*-α-(5-fluoro-2,4-dinitrophenyl-)-L-leucinamide (Marfey's reagent) indicated the presence of *N*-Me-L-Val, L-Pro, *N*-Me-L-Phe, (2*S*)-MeCysA, D-Aba, L-Cya and (2*R*, 3*R*)-Maba. Consistent with the observed differences in the α-CH chemical shifts of Thr and *N*-Me-Leu described above, Marfey's analysis of the grassypeptolide D (**1**) ozonolysis and hydrolysis product matched the configurations observed for grassypeptolide C (D-*allo*-Thr and *N*-Me-D-Leu), while grassypeptolide E (**2**) hydrolysate retention times indicated the presence of L-Thr and *N*-Me-L-Leu.

Ibu-epidemethoxylyngbyastatin 3 (**3**) was isolated from the same first tier RP-HPLC fraction as the grassypeptolides. The molecular composition of **3** was established as $C_{51}H_{82}N_8O_{11}$ from HRFTMS data ($[M + Na]^+$ *m/z* 1005.5983). While the ^1H NMR spectrum for compound **3** also exhibited resonances typical of a peptide, it was significantly different to those for grassypeptolides **1** and **2**. In addition, inspection of the ^{13}C NMR spectrum for compound **3** revealed the absence of a midfield quaternary (δ_C 84.0 ppm) and the presence of a downfield quaternary carbon

(δ_C 208.4 ppm), which in combination with the reduced molecular mass, suggested a different planar structure for **3** relative to compounds **1** and **2**. Instead, the 1D spectra for **3** were very similar to those for dolastatin 12, isolated as the major component from the preceding first tier HPLC fraction. Examination of the 2D NMR data for **3** confirmed that an additional methyl triplet (δ_H 0.86 ppm) in the ^{1}H NMR spectrum for **3** and increase of 14 mass units relative to dolastatin 12 were attributable to the presence of 3-amino-2-methylhexanoic acid (Amha) in **3**, rather than the 3-amino-2-methylpentanoic acid (Ampa) in dolastatin 12. Thus, the planar structure of **3** could best be designated as demethoxylyngbyastatin 3, indicating replacement of the *N*,*O*-dimethylTyr in lyngbyastatin 3 (Williams et al., 2003) with *N*-methylPhe in **3**. The configurational assignment of the Ibu unit in the lyngbyastatin/dolastatin series has proven arduous given the propensity of this unit to decarboxylate and epimerize during acid hydrolysis to yield (2*R/S*)-2-amino-4-methylpentan-3-one (Amp; Carter et al., 1984; Harrigan et al., 1998). The analysis and comparison of this series of depsipeptides containing Ibu is further confounded by whether or not the neighboring Ala unit is *N*-methylated. Williams and coworkers (2003) deduced that their cyanobacterial samples of dolastatin 12 and lyngbyastatins 1 and 3 each comprised Ibu epimeric mixtures following $NaBH_4$ reduction of the natural products, acid hydrolysis and comparisons with the reduced Ibu standards, (3*R/S*, 4*S*)-4-amino-2,2-dimethyl-3-hydroxy-pentanoic acid (Adhpa). It was shown that very little enolization occurs during the $NaBH_4$ reduction itself, which is performed to avoid extensive enolization of the β-keto moiety in Ibu during subsequent acid hydrolysis. To investigate further the timing of epimerization at C-15 in **3** and dolastatin 12 during acid hydrolysis, we first undertook an alternate strategy. Compound **3** and dolastatin 12 were subjected to Marfey's analysis following acid hydrolysis under two different conditions: (A) hydrolysis with 6N HCl for 50 seconds using a microwave and Ace high-pressure tube; and (B) treatment with 6N HCl at 110 °C for 18 h. Analysis of the reaction products of **3** by RP_{18}-HPLC revealed the presence of both enantiomers of Amp in the

S/*R* ratio of 4.1:1 and 1:2.2 for treatments A and B, respectively. A similar result was obtained in the analysis of dolastatin 12 under these conditions, suggesting that racemization of the Ibu unit likely occurs more slowly than peptide hydrolysis; a rapid acid hydrolysis reaction results in less enolization of the Ibu substrate. In tandem with the lack of extremely broad peaks (characteristic of the *R*-Ibu epimer lyngbyastatin 1; Bai et al., 2002) in the ^{1}H NMR spectra for **3** and dolastatin 12, these data suggest that both compounds contain *S*-Ibu. Given the relatively sharp ^{1}H NMR signals for the natural products, it is unlikely that epimerization from an *R*-Ibu to *S*-Ibu occurred prior to amide hydrolysis, despite that the *S*-Ibu configuration is thermodynamically favored (Bai et al., 2002). Noteworthy also is that the analysis of the *S*-Amp standard derivatized with Marfey's reagent under standard reaction conditions (40 °C, 1 h) showed the presence of both enantiomers in the *S/R* ratio of 6.7:1, whereas Marfey's derivatization for 24 h resulted in the ratio of 1.8:1. Thus, further enolization of the Amp unit in the natural product hydrolysate may occur during the derivatization process.

To corroborate our assignment of *S*-Ibu following the method of Williams et al. (2003) compound **3** was reduced with $NaBH_4$, subjected to microwave hydrolysis, and the Marfey's derivatives compared to synthetically prepared Adhpa standards. Analysis of the reaction products of **3** by RP_{18} HPLC-MS revealed the presence of enantiomers of Adhpa in the *S*/*R* ratio 13.8:1. The absolute configurations of the remaining chiral centers in Ibu-epidemethoxylyngbyastatin **3** were assigned by a combination of chiral LC-MS and Marfey's analysis using commercially available or synthetic (Amha) standards. Following acid hydrolysis of **3**, chiral LC-MS analysis revealed the presence of (2*S*, 3*S*)-HMPA. Derivatization of the acid hydrolysate of **3** with Marfey's reagent, followed by RP_{18} HPLC or LC-MS established the presence of *N*-Me-L-Ala, *N*-Me-L-Val, *N*-Me-L-Phe and *N*-Me-L-Leu, and (2*S*, 3*R*)-Amha.

Diastereomeric grassypeptolides D (**1**) and E (**2**) both showed significant cytotoxicity to HeLa (IC_{50} 335 and 192 nM, respectively) and neuro-2a (IC_{50} 599 and

407 nM, respectively) cells. The small (~1.5-fold) difference in cytotoxicity between **1** and **2** indicates that the chirality of the *N*-Me-Leu and Thr α position is not critical for activity and that this region is not central to the pharmacophore of these structures. In contrast, Kwan et al. (2010) conclude that the *N*-Me-Phe region of grassypeptolides A-C is critical for their cytotoxicity given that grassypeptolide C (*N*-Me-L-Phe) showed 16-23- and 65-fold greater potency, respectively, than grassypeptolides A and B (both *N*-Me-D-Phe) against colorectal adenocarcinoma HT29 and cervical carcinoma HeLa cells. In addition the ethyl sidechain of the Aba-thn-ca in grassypeptolides A and C is associated with enhanced activity over the methyl of the Ala unit in grassypeptolide B (Kwan et al., 2010). Like grassypeptolide C, grassypeptolides D (**1**) and E (**2**) also contain Aba and *N*-Me-L-Phe thiazoline carboxylic acid units. The only structural difference between **1** (IC_{50} 335 nM, HeLa cells) and grassypeptolide C (IC_{50} 45 nM, HeLa cells) is a methylated thiazoline of opposite chirality (25*S*). The apparent ~7.5-fold difference in cytotoxicity between grassypeptolides D (**1**) and C supports the hypothesis that the *N*-Me-Phe-thn-ca-Aba-thn-ca motif is central to the pharmacophore of the grassypeptolides. While lyngbyastatin 3 was reported previously to be potently cytotoxic to KB (epithelial carcinoma, subline of HeLa) and LoVo (colon carcinoma) cell lines (IC_{50} = 32 and 400 nM, respectively; Williams et al., 2003), we observed little effect of Ibu-epidemethoxylyngbyastatin 3 (**3**) on neuro-2a cells (IC_{50} > 10 μM). Similarly dolastatin 12 was only slightly more cytotoxic to these cells than **3** (IC_{50} > 1 μM).

A majority of the more than 300 known marine cyanobacterial metabolites have been reported from the genus formerly known as *Lyngbya* (Tan, 2010). However, metabolites closely related to these "*Lyngbya* compounds" have also been reported from non-*Lyngbya* species, as in the case of the four compounds reported here. This has lead to an inability to define strong chemotaxonomic trends for cyanobacterial genera. The taxonomic description of cyanobacteria has transitioned from the traditional phycological system to the modern bacteriological system, supported by

use of the 16S rRNA gene for phylogenetic determinations. Phylogenetic revision of cyanobacterial taxonomy is in progress for several genera, including the newly proposed cyanobacterial genus *Moorea* gen. nov. for the pan-tropical group incorrectly classified as the genus *Lyngbya* (Niclas Engene et al., 2010; N. Engene et al., 2012). In tandem with confirmation of the biogenetic source of compounds isolated from mixed field collections, this may clarify chemotaxonomic relationships. Although it belongs to a less commonly reported genus and is collected from a unique habitat, the Red Sea *Leptolyngbya* sp. RS03 reported here shows biosynthetic capabilities comparable to cyanobacteria collected pantropically. Bis-thiazoline-containing grassypeptolides D (**1**) and E (**2**) are closely related to grassypeptolide C, one of three structural analogues reported from a Florida Keys collection of *Lyngbya confervoides* (Kwan et al., 2010), while Ibu-epidemethoxylyngbyastatin 3 (**3**) and dolastatin 12 are additional congeners of the large family of lyngbyastatins and micropeptins. A systematic classification of the cultured Red Sea *Leptolyngbya* sp. RS03 indicates that this organism is *Leptolyngbya ectocarpi* (Gomont) Anagnostidis et Komárek 1988, according to Komárek and Anagnostidis (2005). A phylogenetic analysis of the partial 16S rRNA sequences from *Leptolyngbya* sp. RS03 (GenBank Acc. No. JF518829) and the marine *Leptolyngbya* reference strain *Leptolyngbya ectocarpi* ATCC 29409 revealed a distinct cluster of *Leptolyngbya* spp. from various marine habitats (Figure 2.1), with the exception of *Phormidium persicinium* SAG 80.79. However, the latter shares ~99.7% 16S rRNA gene sequence identity with the *Leptolyngbya* reference strains included in this analysis and may represent the same organism that has been maintained in different culture collections (Marquardt & Palinska, 2007). Noteworthy is that the Floridian *Lyngbya* cf. *confervoides* VP0401 clusters with members of the *Phormidium* subgenus *Geitlerinema* Anagnostidis et Komárek 1988, which seemingly supports the notion that horizontal gene transfer plays an important role in the evolution of cyanobacteria (Komárek & Anagnostidis, 2005). Also included in this analysis, is a separate cultured Red Sea *Leptolyngbya* sp. (RS02) that produces the brominated

macrolide phormidolide (Williamson et al., 2003), which was previously isolated from an Indonesian *Phormidium* sp. Further chemical and biological characterization of this second Red Sea *Leptolyngbya* is in progress. While it is well recognized that organisms isolated from their native environment may not produce the same secondary metabolites in laboratory culture (Scherlach & Hertweck, 2009), LC-MS analysis of extracts of monoclonal cultures of the Red Sea *Leptolyngbya* sp. RS03 confirmed its production of the four metabolites reported here. The stereoisomerism and natural SAR within the grassypeptolide series presents an intriguing example of the biosynthetic flexibility of cyanobacteria. Characterization and manipulation of the biosynthetic pathways for these natural products may provide exciting opportunities to produce new biologically active metabolites.

Figure 2.1. Phylogenetic relationship of Red Sea filamentous cyanobacteria with other cyanobacterial groups based on SSU (16S) rRNA gene sequences. The tree topology was constructed using a maximum-likelihood (PhyML) algorithm with the support values at important nodes indicated as bootstrap and posterior probability (bayesian inference; MrBayes). Labels on the terminal nodes indicate the taxa, strain, GenBank accession numbers in parenthesis and collection sites for relevant strains. Reference (^{R}) or type strains (^{T}) are included within each cyanobacterial group. Strains with SSU (16S) rRNA gene sequences determined in this study are indicated in blue. Support values < 60 are not indicated (* = bootstrap of > 95% and a posterior probability of 1.0). The scale bar indicates 0.03 expected nucleotide substitutions per site. Note that this figure is modified from the published manuscript to include the currently accepted nomenclature and the additional SSU (16S) rRNA gene sequences from each of the Red Sea cyanobacterial isolates included in this thesis.

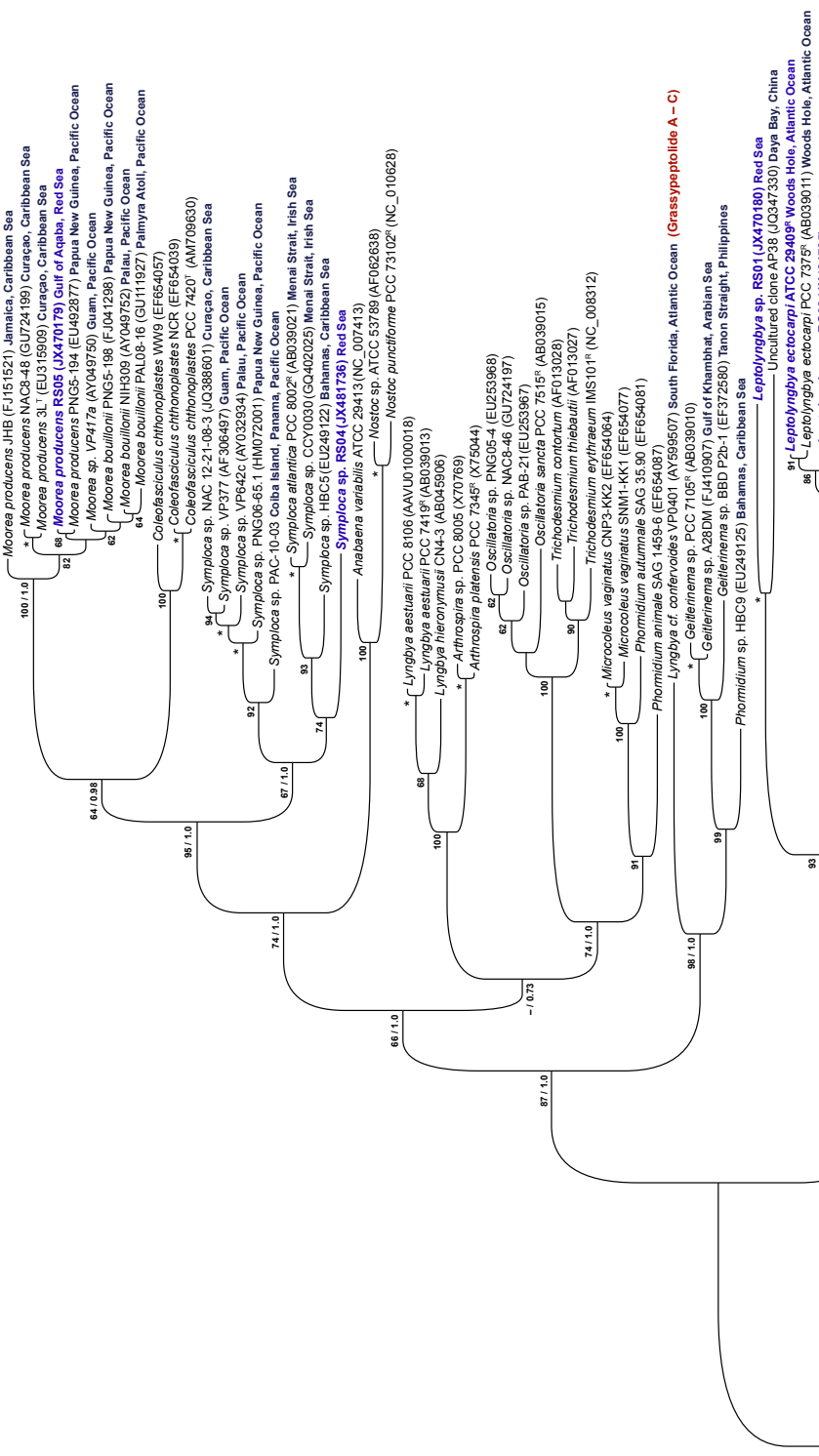
Moorea producens JHB (FJ151521) Jamaica, Caribbean Sea
Moorea producens NAC8-48 (GU724199) Curaçao, Caribbean Sea
Moorea producens 3L T (EU315909) Curaçao, Caribbean Sea
Moorea producens RS05 (JX470179) Gulf of Aqaba, Red Sea
Moorea producens PNG5-194 (EU492877) Papua New Guinea, Pacific Ocean
Moorea sp. VP417a (AY049750) Guam, Pacific Ocean
Moorea bouillonii PNG5-198 (FJ041298) Papua New Guinea, Pacific Ocean
Moorea bouillonii NIH309 (AY049752) Palau, Pacific Ocean
Moorea bouillonii PAL08-16 (GU111927) Palmyra Atoll, Pacific Ocean
Coleofasciculus chthonoplastes WW9 (EF654057)
Coleofasciculus chthonoplastes NCR (EF654039)
Coleofasciculus chthonoplastes PCC 7420T (AM709630)
Symploca sp. NAC 12-21-08-3 (JQ388601) Curaçao, Caribbean Sea
Symploca sp. VP377 (AF306497) Guam, Pacific Ocean
Symploca sp. VP642c (AY032934) Palau, Pacific Ocean
Symploca sp. PNG06-65.1 (HM072001) Papua New Guinea, Pacific Ocean
Symploca sp. PAC-10-03 Colba Island, Panama, Pacific Ocean
Symploca atlantica PCC 8002R (AB039021) Menai Strait, Irish Sea
Symploca sp. CCY0030 (GQ402025) Menai Strait, Irish Sea
Symploca sp. HBC5 (EU249122) Bahamas, Caribbean Sea
Symploca sp. RS04 (JX481736) Red Sea
Anabaena variabilis ATCC 29413 (NC_007413)
Nostoc sp. ATCC 53789 (AF062638)
Nostoc punctiforme PCC 73102R (NC_010628)
Lyngbya aestuarii PCC 8106 (AAVU01000018)
Lyngbya aestuarii PCC 7419R (AB039013)
Lyngbya hieronymusii CN4-3 (AB045906)
Arthrospira sp. PCC 8005 (X70769)
Arthrospira platensis PCC 7345R (X75044)
Oscillatoria sp. PNG05-4 (EU253968)
Oscillatoria sp. NAC8-46 (GU724197)
Oscillatoria sp. PAB-21(EU253967)
Oscillatoria sancta PCC 7515R (AB039015)
Trichodesmium contortum (AF013028)
Trichodesmium thiebautii (AF013027)
Trichodesmium erythraeum IMS101R (NC_008312)
Microcoleus vaginatus CNP3-KK2 (EF654064)
Microcoleus vaginatus SNM1-KK1 (EF654077)
Phormidium autumnale SAG 35.90 (EF654081)
Phormidium animale SAG 1459-6 (EF654087)
Lyngbya cf. confervoides VP0401 (AY599507) South Florida, Atlantic Ocean (Grassypeptolide A – C)
Geitlerinema sp. PCC 7105R (AB039010)
Geitlerinema sp. A28DM (FJ410907) Gulf of Khambhat, Arabian Sea
Geitlerinema sp. BBD P2b-1 (EF372580) Tanon Straight, Philippines
Phormidium sp. HBC9 (EU249125) Bahamas, Caribbean Sea
Leptolyngbya sp. RS01 (JX470180) Red Sea
Uncultured clone AP38 (JQ347330) Daya Bay, China
Leptolyngbya ectocarpi ATCC 29409R Woods Hole, Atlantic Ocean
Leptolyngbya ectocarpi PCC 7375R (AB039011) Woods Hole, Atlantic Ocean
Leptolyngbya sp. RS02 (JX481735) Red Sea
Leptolyngbya sp. HB_3/1/21 Sulawesi, Indonesia
Leptolyngbya sp. FLKBBD1 (EF110975) Bahamas, Caribbean Sea
Leptolyngbya sp. P2b-2 (EF372581) Tanon Strait, Philippines
Leptolyngbya sp. HBC2 (EU249128) Bahamas, Caribbean Sea
Leptolyngbya sp. RS03 (JF518829) Red Sea (Grassypeptolide D, E)
Synechococcus elongatus PCC 6301T (NC_006576)
Synechococcus elongatus PCC 7942 (NC_007604)
Synechococcus sp. CC9605 (NC_007516)
Synechococcus sp. WH8102 (NC_005070)
Gloeobacter violaceus PCC 7421T (NC_005125)
0.03

Figure 2.1.

Experimental

General Experimental Procedures. Optical rotations were measured on a Jasco P-1010 polarimeter. UV spectra were measured on a SpectraMax190 (Molecular Devices). NMR data were acquired in $CDCl_3$ referenced to residual $CHCl_3$ chemical shifts (δ_C 77.2, δ_H 7.26) on a Bruker Avance III 700 MHz spectrometer equipped with a 5mm ^{13}C cryogenic probe for compound **2**. NMR data for **1** and **3** were acquired in $CDCl_3$ on a Bruker DPX 400 MHz spectrometer equipped with a 5mm BBI probe and also in CD_3OD (residual CH_3OH, δ_C 49.2, δ_H 3.31) on a Bruker DRX 600 MHz spectrometer equipped with a 5 mm TXI probe. High-resolution mass spectrometry was performed in positive ion mode on Thermo Scientific LTQ FT Ultra Hybrid and AB SCIEX Triple TOF 5600 mass spectrometers. LC-ESIMS data were obtained on an AB SCIEX 3200 Q TRAP mass spectrometer. HPLC was performed using a Shimadzu dual LC-20AD solvent delivery system with a Shimadzu SPD-M20A UV/ VIS photodiode array detector.

Collection, Isolation and Culture of the Red Sea *Leptolyngbya*. An apparent mixed assemblage of cyanobacteria was collected by hand using SCUBA from the *SS Thistlegorm* shipwreck (46 – 98 ft) in the Red Sea (N 27° 48.849' E 33° 55.222') on May 27, 2007. Morphological characterization was performed using a Zeiss phase contrast microscope (×100 objective) and the specimen was identified systematically according to Komárek and Anagnostidis (2005). Live cyanobacteria were isolated microscopically (Olympus SZ40 stereomicroscope) and grown in triplicate in 24-well culture plates at 27 °C with a 12 hour light-dark cycle (~5 μmol photons s^{-1} m^{-2} provided by 40W cool-white fluorescent lights). Four different enrichment mediums were used to investigate optimal conditions for survival in laboratory culture. These included 0.2 μm-filtered seawater from the Red Sea (RSW); RSW amended with soil extract; BG-11 medium containing DN vitamin mix (Castenholz, 1988), which had been modified to closely resemble conditions of the cyanobacterium's natural

environment (RSM; pH 8.4 and salinity 41 ‰); and RSM + RSW (1:1). Monoclonal cultures of *Leptolyngbya* were isolated microscopically from serial dilutions of enrichment cultures in which exceptional growth was present (RSM:RSW) and maintained in RSM (see Supporting Information Figure S-2.1).

DNA Extraction and Amplification of Cyanobacterial 16S rRNA. Prior to DNA extraction, heterotrophic bacteria within the cyanobacterial cultures were reduced by sequential treatment through sonication, washing and addition of antibiotics as previously described (Han et al.). Genomic DNA was then extracted from approximately 40 mg of freeze-dried cyanobacterial tissue using the Wizard® Genomic DNA purification kit (Promega Inc., A1120) following the manufacturer's protocol. The isolated genomic DNA was subjected to further purification using an anion exchange column (Qiagen, Genomic-tip 20/G). DNA concentration and purity was measured on a Bio-Rad SmartSpec™ 3000 spectrophotometer. Approximately 650 bp of the upstream cyanobacterial 16S rRNA sequence was amplified from these genomic extracts using the cyanobacteria-specific primers, CYA106F and CYA781Ra/b (Nubel et al., 1997), while the cyanobacteria-specific primer (CYA359F) and general bacterial primer (1509R) were used to amplify 1,150 bp downstream(Martínez-Murcia et al., 1995). Sequences were amplified from approximately 50 ng of DNA using GoTaq Hot Start polymerase (0.5 μL, Promega) according to manufacturer's specifications. Polymerase chain reactions (PCR) were performed in an Eppendorf Mastercycler gradient thermal cycler (Eppendorf, Hauppauge, NY, USA) as follows: initial denaturation at 95 °C for 3 min; 15 cycles of Touch Down PCR: 95 °C for 30 sec, 65 °C for 45 sec (decreased by 1 °C per cycle), and 72 °C for 1 min; 15 additional cycles of amplification: 95 °C for 20 sec, 50 °C for 20 sec, and 72 °C for 1.5 min; and final elongation at 72 °C for 3 min. PCR products were gel-purified, cleaned with the QIAquick® Gel Extraction kit (cat. no. 28704, Promega) and directly sequenced on an ABI 3730 capillary sequencer by the Oregon State University Center for Genome Research and Biocomputing DNA Sequencing Core Facility. The amplification

primers described above were used as sequencing primers with the addition of reverse complement primers CYA359R and CYA781Fa/b for additional sequence coverage at the end regions of the 16S rRNA gene amplification product. The 16S rRNA partial gene sequences were inspected visually and assembled using CAP3 (Huang & Madan, 1999). The resulting contig was analyzed for chimeric sequences using Pintail (Ashelford et al., 2005) and compared to sequences in the Ribosomal Database Project database (http://rdp.cme.msu.edu) and GenBank (http://www.ncbi.nlm.nih.gov). The consensus sequence was deposited in GenBank under accession number JF518829.

Phylogenetic Analysis. A 16S rRNA gene library of 60 marine and freshwater cyanobacteria was produced from in house SSU (16S) rRNA sequence data for Red Sea cyanobacterial isolates and from sequences collected from the GenBank sequence database. The library was screened for chimeric sequences using the computer program Mallard (Ashelford et al., 2006), aligned using ClustalW in Geneious 5.6 (Drummond et al., 2010), and the resulting alignment edited to exclude gaps and missing data, for a total of 1275 positions (90.3 % identity) in the final dataset covering the V2 to V8 hypervariable regions within the 16S rRNA gene. Prior to phylogenetic predictions, a statistical selection of best-fit models of nucleotide substitutions for the SSU (16S) rRNA data set was selected using Akaike and Bayesian information criteria (AIC and BIC) in jModelTest 0.1.1 (Posada, 2008). Phylogenetic trees were calculated using the Bayesian (MrBayes; Huelsenbeck & Ronquist, 2001) and phylogenetic maximum likelihood (PhyML v3.0; Guindon & Gascuel, 2003) algorithms in Geneious 5.6 (Drummond et al., 2010). The PhyML analysis was performed with 500 bootstrap replicates using the GTR+I+G model (selected by AIC and BIC in jModelTest; proportion of invariable sites (pINV) = 0.450, shape parameter (α) = 0.387, number of rate categories = 4). Bayesian analysis was performed with the GTR substitution model (number of rate categories = 4). The Markov chain length (three heated) was set to 3 million with sampling performed every 100 generations (25% burn-in).

Extraction and Isolation of Compounds 1-3 and Dolastatin 12. The field collection of *Leptolyngbya* (500 mL, collection code EHu5-27-07-1) for chemical extraction was stored in 2-propanol at -20 °C until extraction to yield 1.26 g organic extract (CH_2Cl_2-MeOH, 2:1). The organic extract was subjected to bioassay-guided fractionation via NP VLC using a stepped gradient of hexanes to EtOAc to MeOH. The fraction eluting with 25% MeOH-EtOAc was further separated by RP_{18} SPE using a stepped gradient of MeOH-H_2O from 50% MeOH-H_2O to 100% MeOH, followed by 100% CH_2Cl_2. Isocratic RP-HPLC (column: Synergi Fusion-RP, 10 x 250 mm, 70% MeCN-H_2O, 3 mL/min) of the SPE fraction C eluting in 70% MeOH-H_2O yielded two impure HPLC peaks targeted for further purification. RP-HPLC (Chirobiotic TAG, 4.6 x 250 mm, 98% EtOH-H_2O, 0.5 mL/min) of the less polar of these fractions yielded Ibu-epidemethoxylyngbyastatin 3 (**3**, 2.9 mg) and a mixture of grassypeptolides D (**1**, 1.5 mg) and E (**2**, 0.5 mg), which were finally separated on the Chirobiotic TAG column using 75% MeOH-H_2O (0.5 mL/min). Dolastatin 12 was also isolated from the 25% MeOH-EtOAc NP VLC fraction H. Repeated isocratic RP-HPLC (column: Synergi Fusion-RP, 10 x 250 mm, 70% MeCN-H_2O, 3 mL/min) of the SPE fraction (H2) eluting in 70% MeOH-H_2O fraction yielded dolastatin 12 as the major component. Subsequent LC-MS profiling (Synergi Fusion-RP, 2 x 100 mm, 0.2 mL/min, linear gradient of 65 to 100% MeCN in 0.1% [v/v] aqueous TFA) of extracts from monoclonal *Leptolyngbya* cultures (2 x 1.5 L) yielded *m/z* 1138.6 (**1** and **2**, $[M+Na]^+$), 1005 (**3**, $[M+Na]^+$) at the same retention times as **1**, **2** and **3** purified from the original field collection.

Grassypeptolide D (1): colorless, amorphous solid; $[\alpha]^{21}_D$ +25.9 (*c* 0.15, CH_2Cl_2); UV (MeOH) λ_{max} (log ε) 212 (3.82), 260 (3.56); ^1H and ^{13}C NMR data, see Table 2.1 and Supporting Information (Table S-2.2); HRFTMS *m/z* 1138.5515 $[M + Na]^+$ (calcd for $C_{57}H_{81}N_9O_{10}S_2Na$, 1138.5445), *m/z* 1116.5458 $[M + H]^+$ (calcd for $C_{57}H_{82}N_9O_{10}S_2$, 1116.5620).

Grassypeptolide E (2): colorless, amorphous solid; $[\alpha]^{21}_{D}$ +13.2 (*c* 0.15, CH_2Cl_2); UV (MeOH) λ_{max} (log ε) 212 (3.73), 256 (3.48); ^{1}H and ^{13}C NMR data, see Table 2.1 and Supporting Information (Table S-2.3); HRTOFMS *m/z* 1138.5413 $[M + Na]^+$(calcd for $C_{57}H_{81}N_9O_{10}S_2Na$, 1138.5445), *m/z* 1116.5603 $[M + H]^+$ (calcd for $C_{57}H_{82}N_9O_{10}S_2$, 1116.5620).

Ibu-epidemethoxylyngbyastatin 3 (3): white, amorphous solid; $[\alpha]^{21}_{D}$ –48.6 (*c* 0.5, $CHCl_3$); UV (MeOH) λ_{max} (log ε) 212 (3.98), 256 (3.81); ^{1}H and ^{13}C NMR data, see Supporting Information (Table S-2.4); HRFTMS *m/z* 1005.5983 $[M + Na]^+$ (calcd for $C_{51}H_{82}N_8O_{11}Na$, 1005.6001), *m/z* 983.6162 $[M + H]^+$ (calcd for $C_{51}H_{83}N_8O_{11}$, 983.6175).

Dolastatin 12: white, amorphous solid; $[\alpha]^{21}_{D}$ -79.8 (*c* 0.5, $CHCl_3$); UV (MeOH) λ_{max} (log ε) 212 (3.71), 256 (3.57); ^{1}H and ^{13}C NMR data, see Supporting Information (Figures A-2.16 and 2.17) and (Pettit et al., 1989) HRTOFMS *m/z* 969.6035 $[M + H]^+$ (calcd for $C_{50}H_{81}N_8O_{11}$, 969.6019).

Absolute Configuration of Grassypeptolides D (1) and E (2). The amino acid standards relevant to compounds **1** and **2** were obtained commercially or as gifts and prepared as 50 mM solutions in H_2O. Standards for (2*R*)- and (2*S*)-methylcysteine were kindly provided by Dr. W.H. Gerwick, Scripps Institution of Oceanography, University of California, San Diego. A portion of each standard (5.0 mg) was dissolved in 720 μL HCO_2H at 0 °C. Next, 80 μL of H_2O_2 (30%) was added dropwise with continuous stirring and the reaction was carried out at 0 °C for 2 h to yield either (2*R*)- or (2*S*)-methylcysteic acid (MeCysA). The product mixture was dried under a steady stream of N_2 gas and resuspended in H_2O (50 mM). The *N*-benzoyl *O*-methyl ester of (2*R*,3*S*)-2-methyl-3-aminobutyric acid (Maba) was gratefully received from Dr. Hendrik Luesch, Department of Medicinal Chemistry, University of Florida. Approximately 0.4 mg was deprotected with 500 μL 6 N HCl at 110 °C for 24 h, evaporated to dryness and resuspended in H_2O (50 mM). Each standard was then derivatized for Marfey's analysis by adding 10 μL of 1 M $NaHCO_3$ and 50 μL of *N*-α-

(5-fluoro-2,4-dinitrophenyl-)-L-leucinamide (L-FDLA or D-FDLA, 1% w/v in acetone) to 25 μL of each standard solution. The mixture was heated at 40 °C for 1 h with continuous stirring, cooled to room temperature, acidified with 5 μL 2N HCl, evaporated to dryness and resuspended in 250 μL MeCN-H_2O (1:1).

Approximately 0.1 mg of **1** and 0.2 mg of **2** were dissolved separately in 3 mL CH_2Cl_2 (-78 °C). Ozone was then bubbled through each solution for 15 min. The solution was dried under a stream of N_2 gas, followed by an oxidative workup of the residue (0.6 mL of H_2O_2-HCOOH 1:2 at 70 °C for 20 min). The oxidation product was concentrated under vacuum and hydrolyzed with 1 mL of 6 N HCl at 110 °C for 18 h. The hydrolyzed products were resuspended in 25 μL H_2O and derivatized for Marfey's analysis in a similar manner to the derivatized chromatographic standards. The Marfey's products of **1** and **2** were resuspended in 50 μL MeCN-H_2O (1:1) and analyzed by reversed-phase HPLC (Gemini C_{18} 110 A, 4.6 x 150 mm, 5 µm, 1.0 mL/ min, UV detection at 340 nm) using a linear gradient of 30 to 70% MeCN in 0.1% (v/ v) aqueous TFA over 50 min. The retention time (t_R min) of the residues in the hydrolysate of **1** matched standards for D-Aba (21.9; L-Aba, 17.1), L-Cya (7.1; D-Cya, 6.5), (2*S*)-MeCysA [6.2; (2*R*)-MeCysA, 7.8], *N*-Me-D-Leu (27.8; *N*-Me-L-Leu, 24.5), (2*R,* 3*R*)-Maba L-FDLA [18.8; (2*R,*3*R*)-Maba D-FDLA, 25.6; (2*R,*3*S*)-Maba L-FDLA, 18.6; (2*R,*3*S*)-Maba D-FDLA, 20.8], L-Pro (14.1; D-Pro, 17.0), *N*-Me-L-Phe (22.7; *N*-Me-D-Phe, 24.6), *N*-Me-L-Val (21.2; *N*-Me-D-Val, 25.6), D-*allo*-Thr (12.6; L-Thr, 10.2; L-*allo*-Thr, 11.1; D-Thr, 14.4). The retention times for the residues in the hydrolysate of **2** were consistent with the results for **1**, with the exception of *N*-Me-L-Leu (24.5) and L-Thr (10.2) standards matching the corresponding residues in the hydrolysate of **2**. The configuration of the Pla residue in the hydrolysates of both **1** and **2** was determined by chiral LC-MS. The retention time [Chirobiotic TAG, 4.6 x 250 mm; MeOH-10 mM NH_4OAc (3:2, pH 5.50); flow rate, 0.4 mL/min; detection by ESIMS in negative ion mode] of the natural product hydrolysate matched that for L-Pla (7.4 min; D-Pla, 8.5).

Absolute Configuration of Ibu-epidemethoxylyngbyastatin (3).

Approximately 0.4 mg of **3** in 0.2 mL anhydrous MeOH was added to a solution of $NaBH_4$ (2 mg) in anhydrous MeOH at 0 °C. After stirring for 30 min, the solution was acidified with 1N HCl until pH 6. The solution was then partitioned between EtOAc and H_2O, and the organic layer concentrated to dryness for analysis by reversed-phase HPLC (Synergi Fusion-RP, 10 x 250 mm, 62% MeCN-H_2O, 3.5 mL/ min). A single product consistent with the dihydro-form of **3** (t_R 18.9 min) was present, while unreduced compound **3** (t_R 21.3 min) was not detected. This reduction product and an additional ~0.4 mg of **3** were separately hydrolyzed with 6N HCl (method A: Ace high-pressure tube, 1200W microwave for 50 s and immediately cooled to 0 °C; or method B: 110 °C for 18 h), evaporated to dryness and resuspended in H_2O (50 mM). Standards for the 3-amino-2-methylhexanoic acid (Amha) unit were kindly provided by Dr. David Horgen, College of Natural Sciences, Hawaii Pacific University. The other amino acid standards relevant to compound **3** were available commercially or from synthesis (Amp and Adhpa, see Experimental) and also prepared as 50 mM solutions in H_2O. Marfey's derivatization was performed by adding 10 μL of 1M $NaHCO_3$ and 50 μL of *N*-α -(5-fluoro-2,4-dinitrophenyl)-L-leucinamide (L-FDLA, 1% w/v in acetone) to 25 μL of each 50 mM solution. The mixture was heated at 40 °C for 1 h with stirring, cooled to room temperature, acidified with 5 μL 2N HCl and evaporated to dryness. The derivatized product was resuspended in 250 μL MeCN-H_2O (1:1) for each standard or 100 μL for the hydrolysate of **3** and analyzed by reversed-phase HPLC (Gemini C_{18} 110A, 4.6 x 150 mm, 5 μm, 1.0 mL/min, UV detection at 340 nm) using a linear gradient of 30 to 70% MeCN in 0.1% (v/v) aqueous TFA over 50 min. The retention times (t_R min) of the derivatized residues in the hydrolysate of **3** matched *N*-Me-L-Ala (16.2; *N*-Me-D-Ala, 16.8), (2*S*,3*R*)-Amha [28.6; (2*S*,3*S*)-Amha, 23.2; (2*R*,3*R*)-Amha; (2*R*,3*S*)-Amha, 22.5] and *N*-Me-L-Val (21.2; *N*-Me-D-Val, 25.5). The retention times of *N*-Me-L-Phe (23.2) and *N*-Me-D-Phe (24.5) standards overlapped with (2*S*,3*S*)-Amha (23.2) and *N*-Me-L-

Leu (24.5) standards. Thus, the derivatized hydrolysate was subjected to LC-MS analysis (Gemini C_{18}, 2.0 x 150 mm, 3 μm, 0.2 mL/min, UV and ESIMS detection, 340 nm and negative ion mode, respectively) using a linear gradient of 30 to 70% of 0.1% (v/v) formic acid in MeCN and 0.1% (v/v) formic acid in H_2O over 50 min. The retention times (t_R min, base peak *m/z*) of the derivatized residues in the hydrolysate matched *N*-Me-L-Phe (23.1, 472.1) and *N*-Me-L-Leu (24.9, 439.1). For the assignment of the Ibu unit, both the decarboxylated product, (2*S*)-amino-4-methylpentan-3-one (Amp), and the reduced Ibu unit, (3*R/S*, 4*S*)-4-amino-2,2-dimethyl-3-hydroxy-pentanoic acid (Adhpa) were prepared. Portions were then separately derivatized with L-FDLA and D-FDLA reagents and analyzed by reversed-phase HPLC (Kinetex XB-C_{18} 110A, 4.6 x 100 mm, 2.6 μm, 1.8 mL/min, UV detection at 340 nm) using a linear gradient of 30 to 70% MeCN in 0.1% (v/v) aqueous TFA over 15 min or LC-MS (Gemini C_{18}, 2.0 x 150 mm, 3 μm, 0.2 mL/min, UV and ESIMS detection, 340 nm and negative ion mode, respectively) using a linear gradient of 30 to 70% of 0.1% (v/v) formic acid in MeCN and 0.1% (v/v) formic acid in H_2O over 50 min. For the hydrolysate of **3** for method A, both *S*- and *R*-Amp were detected by reversed-phase HPLC at t_R = 9.8 and 10.0 min, respectively, in the ratio of 4.1:1. For the hydrolysate of **3** for method B, both *S*- and *R*-Amp were detected by reversed-phase HPLC at t_R = 9.8 and 10.0 min, respectively, in the ratio of 1:2.2. The retention times (t_R min; *S*/*R* ratio) of the Amp derivatized standards were as follows: L-FDLA-*S*-Amp (9.8, 6.7:1) and D-FDLA-*S*-Amp (10.0, 1:5.9). For the hydrolysate of the reduction product of **3** (method A), the assignment of the reduced Ibu unit was determined by LC-MS analysis due to overlap in the HPLC trace. The retention time (t_R min, 4*S* to 4*R* ratio, base peak *m/z*) of the reduced natural product hydrolysate matched L-FDLA-(3*RS*, 4*S*)-Adhpa (19.7, 13.8:1, 454.1), while D-FDLA-(3*RS*, 4*S*)-Adhpa eluted at 20.6 min.

Synthesis of (2*S*)-2-amino-4-methylpentan-3-one (Amp) and (3*R*/*S*, 4*S*)-4-amino-2,2-dimethyl-3-hydroxy-pentanoic acid (Adhpa) for assignment of desmethoxylyngbyastatin 3 (3). According to a procedure modified from Theberge

and Zercher (2003), carbonyl diimidazole (CDI, 981 mg, 5.87 mmol, 1.02 eq.) dissolved in 20 mL anhydrous THF was added to a stirred, room temperature solution of 1.09 g (5.75 mmol, 1 eq.) Boc-L-Ala in 10 mL anhydrous THF, contained in a 100 mL round-bottom flask. To a separate 250 mL round-bottom flask containing a solution of monobenzyl malonate (1.41 g, 6.9 mmol, 1.2 eq.) in 20 mL of anhydrous THF was added 3.45 mL (3.45 mmol) of a 1 M hexanes solution of dibutylmagnesium at 0 ºC. The acyl imidazole solution was transferred to this 250 mL flask containing the magnesium salt and the combined solutions were allowed to stir for 2 h in the ice-bath before being left to stir for 24 h at room temperature. The reaction was quenched by the addition of 40 mL sat. aq. NH_4Cl and extracted three times with 20 mL EtOAc. The combined organic layers were dried with Na_2SO_4, filtered, and concentrated. The crude residue was chromatographed on silica with 20% EtOAc in hexanes to yield 1.11 g (60 %) of (4*S*)-*N*-Boc-4-amino-3-oxo-pentanoic benzyl ester as a colorless oil, confirmed by ESIMS+ (*m/z* 344 $[M + Na]^+$) and comparison of ^1H NMR data with the literature (Williams et al., 2003). The latter product (1.00 g, 3.11 mmol, 1 eq.) was dissolved in anhydrous THF (10 mL) in a 100 mL round-bottom flask before CH_3I (1.76 mL, 28.0 mmol, 9 eq.) was added, followed immediately by NaH (dry, 95%, 79 mg, 3.11 mmol, 1 eq.). After stirring at room temperature for 1 h, additional CH_3I (9 eq.) and NaH (1 eq.) were added and the solution was stirred for 24 h. The concentrated reaction mixture was partitioned between EtOAc/H_2O and dried over Na_2SO_4 to give 730 mg crude (4*S*)-*N*-Boc-4-amino-2,2-dimethyl-3-oxopentanoic benzyl ester, as established by ESIMS+ ($[M+Na]^+$ *m/z* 371.9) and ^1H NMR.

A solution of the latter crude product (50 mg, 0.143 mmol) in 2.5 mL anhydrous MeOH was added dropwise to $NaBH_4$ (21.6 mg, 0.572 mmol, 4 eq.) in 2.5 mL anhydrous MeOH at 0 °C. After stirring for 30 min, the solution was acidified with 1N HCl until pH 6. The solution was then partitioned between EtOAc and brine, and the organic layer concentrated to dryness to yield 27 mg (0.078 mmol, 55%) of (3*R*/*S*, 4*S*)-*N*-Boc-4-amino-2,2-dimethyl-3-hydroxy-pentanoic benzyl ester. The benzyl protecting

group was removed by hydrogenation over 5% Pd/C in 2 mL anhydrous EtOH at room temperature for 18 h. The mixture was filtered, concentrated *in vacuo*, and resuspended in 1 mL CH_2Cl_2-TFA (1:1) with stirring for 2 h. The acid was removed under a stream of nitrogen to afford 10.5 mg (0.065 mmol, 83%) of (3*R*/*S*, 4*S*)-4-amino-2,2-dimethyl-3-hydroxy-pentanoic acid (Adhpa). Alternatively, 20 mg (0.057 mmol) of (4*S*)-*N*-Boc-4-amino-2,2-dimethyl-3-oxopentanoic benzyl ester was deprotected as described above to afford 4.2 mg (0.037 mmol, 65%) of the decarboxylated product (2*S*)-2-amino-4-methylpentan-3-one (Amp).

Preparation and Chiral LC-MS of 2-hydroxy-3-methylpentanoic acid (HMPA) for (3). Diazotization of L-Ile (100 mg, 0.75 mmol) dissolved in 50 mL of 0.2 N perchloric acid (0 °C) was carried out by the dropwise addition of a cold (0 °C) 20 mL solution of sodium nitrite (1.4 g, 20 mmol) with rapid stirring. The solution was stirred at room temperature until the evolution of N_2 subsided (~60 min). The solution was then brought to boiling for 3 min, cooled to room temperature, saturated with NaCl, and extracted with 20 mL EtOAc. The extract was dried with anhydrous Na_2SO_4 and concentrated under vacuum to afford (2*S*, 3*S*)-HMPA as an oil. The three other stereoisomers (2*S*,3*R*)-HMPA, (2*R*,3*R*)-HMPA and (2*R*,2*S*)-HMPA were synthesized in a similar manner from L-*allo*-Ile, D-Ile and D-*allo*-Ile, respectively. A portion of each standard was analyzed using chiral LC-MS. The retention time of the natural product hydrolysate matched that for (2*S*,3*S*)-HMPA (7.5 min; Chirobiotic TAG, 4.6 x 250 mm; MeOH-10 mM NH_4OAc 3:2 at pH 5.50; flow rate, 0.4 mL/min; detection by ESIMS in negative ion mode). The retention times of the remaining HMPA standards were as follows: (2*S*, 3*R*)-HMPA (6.5 min), (2*R*,3*R*)-HMPA (9.2 min), (2*R*,2*S*)-HMPA (8.1 min).

Cell Viability Assays. Mouse neuroblastoma neuro-2a or HeLa cells (ATCC, Manassas, VA) were cultured in RPMI-1640 media with 2 mM L-glutamine, pH 7.4 (Mediatech Inc., Manassas, VA) supplemented with 10% fetal bovine serum (HyClone, Logan, UT), 1 mM sodium pyruvate (Mediatech), and 1% penicillin/

streptomycin (Mediatech) at 37 ºC in a humidified chamber containing 5% CO_2. Cells were seeded into 96-well plates (neuro-2a: 20,000 cells per well; HeLa: 3,000 cells per well) in 90 μL of medium 4 h before treatment. Purified compounds were added to cells at final concentrations ranging from 10 nM to 10 μM (neuro-2a cells) or 2 μM (HeLa cells), each added in a 10 μL aliquot generated by serial dilution in serum-free medium on the day of the experiment, from stock solutions of 200 μM (**1** and **2**, both cell lines) or 2 mM (**3** and dolastatin 12, neuro-2a cells only) compound in 100% DMSO (neuro-2a cells) or 100% EtOH (HeLa cells). Each 96-well plate also contained untreated and vehicle-treated control cells. Neuro-2a cells were also treated with 30 μg/mL of the parent 25% MeOH-EtOAC fraction as a positive control. Cell viability was determined after 48 h treatment using a standard 3-(4,5-dimethylthiazol-2-yl)-2,5,diphenyly tetrazolium bromide (MTT) assay. Briefly, MTT reagent (0.5 mg/mL in PBS; Sigma, St. Louis, MO) was added to each well and incubated for 2 h at 37°C. The medium was then aspirated from all wells and the purple formazan product solubilized with DMSO. The optical density of each well was determined at 550 nm using a BioTek Synergy HT microplate reader with Gen5 software (Bio-Tek, Winooski, VT). The cytotoxicity of each purified compound was assessed in at least three independent cultures with the viability of vehicle-treated control cells defined as 100% in all experiments.

Acknowledgement

We thank the Red Sea Protectorate for permission to make collections of Red Sea cyanobacteria, and Brian Arbogast and Jeff Morre of the Environmental Health Sciences Center at OSU for mass spectrometric data acquisition (NIEHS P30 ES00210). The National Science Foundation (CHE-0722319) and the Murdock Charitable Trust (2005265) are acknowledged for their support of the OSU Natural Products and Small Molecule Nuclear Magnetic Resonance. Funding was provided by the OSU College of Pharmacy and an undergraduate scholarship from the OSU Research Office (to J.M.M.).

Supporting Information

Table S-2.1. List of and growth mediums used to culture Red Sea cyanobacteria.

Media	Constituents
RSM	1.5 g $NaNO_3$, 75 mg $MgSO_4$, 40 mg $K_2HPO_4 \cdot 3H_2O$, 20 mg $Na_2CO_3 \cdot H_2O$, 6 mg citric acid, 6 mg ferric ammonium citrate, 1 mg Na_2-EDTA, 1 mL Trace Metals, 1 mL DN Vitamin Mix and 998 mL Instant Ocean (41 g/L), pH 8.4
DN Vitamin Mix	0.2 g thiamine HCl, 0.1 g biotin, 0.1 g calcium pantothenate, 10 mg *para*-aminobenzoic acid, 1 mg cyanocobalamin, 1 mg folic acid, 1 mg myo-inositol, 1 mg nicotinic acid and 1 liter DI water
Soil Extract	5.0 g dry soil loam (mix of sand, silt and clay particles) and 200 mL DI water. Pasteurize over two consecutive days for 3 hours at 98 °C. Alternatively, autoclave for 1 hour at 121 °C, 15 psi., and filter particulates.
Trace Metals	520 mg Na_2-EDTA, 178 mg $FeSO_4 \cdot 7H_2O$, 23.2 mg $Co(NO_3)_2 \cdot 6H_2O$, 14.8 mg $ZnSO_4 \cdot 7H_2O$, 10 mg $MnCl_2$, 6.2 mg H_3BO_3, 3.6 mg $NaMoO_4 \cdot 2H_2O$, 2.7 mg $NiSO_4 \cdot 6H_2O$, 1.7 mg $CuCl_2 \cdot 2H_2O$ and 100 mL DI water

Table S-2.2. NMR Spectroscopic Data for Grassypeptolide D (**1**) in $CDCl_3$ (400 MHz).

unit	position	δ_C, mult.	δ_H, mult. (*J* in Hz)	COSY	HMBC	ROESY
Maba	1	172.4, C				
	2	45.6, CH	2.50, dq (7.0, 6.8)	H-3, H_3-5	3, 5	H-3, H_3-4, H_3-5
	3	48.5, CH	4.22, m	H-2, H_3-4, NH (A)		H-2, H_3-4, H_3-5
	4	19.9, CH_3	1.19, d (6.7)	H-3	1, 2, 3	H-2, H-3, H_3-5
	5	14.4, CH_3	1.12, d (7.0)	H-2	2, 3	H-3, H_3-4, H-55
	NH		7.70, br	H-3	6	
Thr	6	169.3, C				
	7	59.1, CH	4.45, dd (6.8, 6.1)	H-8, NH (B)	10	H_3-9, NH (B)
	8	69.1, CH	4.02, m	H-7, H_3-9		H_3-9, NH (B)
	9	19.7, CH_3	1.22, d (6.4)	H-8	7, 8	H-7, H-8
	OH		4.00, br			
	NH		6.9, d (7.3)	H-7	10	H-7, H-8, H-11, H-12b
N-Me-Leu	10	170.3, C				
	11	57.5, CH	4.70, br	H-12a/b		H-12a, H-12b, H_3-15, H-18, NH (B)
	12a	37.2, CH_2	1.97, m	H-11, H-12b, H-13		H-11, H_3-14
	12b		1.67, m	H-12a, H-13		H-11, H_3-15, NH (B)
	13	25.3, CH	1.58, m	H-12a, H-12b, H_3-14, H_3-15		
	14	23.2, CH_3	0.98, d (6.4)	H-13	12, 13, 15	H-12a, H-19b
	15	22.8, CH_3	0.94, d (6.5)	H-13	12, 14	H-11, H-12b, H_3-16
	16	33.2, CH_3	3.20, s		11, 17	H_3-15, H-18
Aba-thn-ca	17	170.4, C				
	18	78.1, CH	5.29, m	H-19a, H-19b	17, 20	H-11, H_3-16, H-19a
	19a	33.3, CH_2	3.60, m	H-18	17, 18	H-18
	19b		3.26, m	H-18	20	H_3-14
	20	178.0, C				
	21	54.2, CH	4.55, m	H-22b, NH (D)	20	H-22a
	22a	25.2, CH_2	2.11, m	H_3-23		H-21, H_3-23
	22b		1.86, m	H-21		H_3-23, NH (D)
	23	11.6, CH_3	0.96, t (6.9)	H-22a	21	H-21, H-22a, H-22b, NH (D)
	NH		7.10, d (7.7)	H-21	24	H-22b, H_3-23
N-Me-Phe-thn-ca	24	173.7, C				
	25	84.0, C				
	26a	43.1, CH_2	3.74, d (-11.5)	H-26b	24, 28	H-26b, H_3-27
	26b		3.17 d (-11.3)	H-26a	24, 25, 27	H-26a, H_3-27
	27	24.3, CH_3	1.35, s		24, 25, 26	H-26a, H-26b, H-33/35

Table S-2.2 (continued). NMR Spectroscopic Data for Grassypeptolide D (**1**) in $CDCl_3$ (400 MHz).

unit	position	δ_C, mult.	δ_H, mult. (*J* in Hz)	COSY	HMBC	ROESY
N-Me-Phe-thn-ca	28	173.9, C				
	29	58.9, CH	5.39, dd (10.7, 6.4)	H-30a, H-30b	28	H-30a, H-33/35
	30a	36.0, CH_2	3.24, m	H-29	29, 31, 32/36	
	30b		3.16, m	H-29	31, 32/36	H-32/36
	31	135.5, C				
	32/36	129.2, CH	7.33, m		31, 33/35	H-30b
	33/35	128.5, CH	7.22, m		34	H_3-27, H-29
	34	127.6, CH	7.20, m			
	37	30.7, CH_3	3.21, s		29, 38	H-39, H-41a, H-41b
Pro	38	172.7, C				
	39	57.5, CH	4.84, dd (8.8,5.1)	H-40a, H-40b		H_3-37, H-41a, H-42b
	40a	27.5, CH_2	2.22, m	H-39		
	40b		1.93, m	H-39		
	41a	24.9, CH_2	1.99, m			H_3-37, H-39, H-42a
	41b		1.63, m		40	H_3-37
	42a	47.8, CH_2	3.97, m	H-42a		H-41a, H-44
	42b		3.53, m	H-42b	43	H-40b, H-44
N-Me-Val	43	168.6, C				
	44	60.0, CH	4.98, d (11.0)	H-45	43, 45	H-42a, H-42b, H_3-46, H_3-47
	45	27.4, CH	2.32, m	H-44, H_3-46, H_3-47		H_3-48
	46	19.6, CH_3	0.98, d (6.4)	H-45	44, 45, 47	H-44, H-45
	47	18.0, CH_3	0.88, d (6.6)	H-45	44, 45, 46	H-44, H_3-48
	48	30.0, CH_3	3.12, s		44, 49	H-45, H_3-47, H-50, H-55
Pla	49	170.2, C				
	50	72.4, CH	5.33, dd (9.9, 3.2)	H-51a		H_3-48
	51a	36.9, CH_2	3.09, dd (-14.5, 9.9)	H-50	52, 53/57	
	51b		3.04, dd (-14.4, 3.2)		53/57	
	52	134.9, C				
	53/57	129.1, CH	7.22, m		55	
	54/56	129.5, CH	7.24, m		53/57	
	55	127.6, CH	7.27, m		54/56	H_3-5, H_3-48

Table S-2.3. NMR Spectroscopic Data for Grassypeptolide E (**2**) in $CDCl_3$ (700 MHz).

unit	position	δ_C, mult.	δ_H, mult. (*J* in Hz)	COSY	HMBC	ROESY
Maba	1	172.9, C				
	2	45.5, CH	2.51, qd (7.0, 4.5)	H-3, H_3-5	1, 5	H-3, H_3-4, H_3-5, H-14
	3	47.0, CH	4.23, m	H-2, H_3-4, NH (A)		H-2, H_3-4, NH (A)
	4	19.3, CH_3	1.10, d (7.0)	H-3	2, 3	H-3, H-5
	5	14.4, CH_3	1.16, d (7.0)	H-2	1, 2, 3	H-4
	NH		6.45, d (9.9)	H-3	6	H-7
Thr	6	170.5, C				
	7	57.0, CH	3.36, dd (6.9, 3.3)	NH (B)		H-11, NH (A)
	8	67.9, CH	3.30, m	H_3-9	6	H-9, NH (A), NH (B)
	9	19.4, CH_3	0.87, d (6.5)	H-8	7, 8	H-8
	OH					
	NH		6.9, d (6.9)	H-7	10	H-8, H-11
N-Me-Leu	10	170.0, C				
	11	54.6, CH	5.15, t (7.7)	H-12a/b	10, 12, 13, 16	H-7, H-12a/b, NH (B)
	12a/b	37.1, CH_2	1.78, m	H-11, H-13	10, 11, 13, 14, 15	H-11, H_3-14, H_3-15, H_3-16
	13	25.3, CH	1.52, m	H_3-14, H_3-15	11, 12, 14, 15	H_3-14, H_3-15, H_3-16
	14	23.2, CH_3	0.98, d (6.6)	H-13	12, 13, 15	H-2, H-12a/b, H-13
	15	22.4, CH_3	0.93, d (6.7)	H-13	12, 13, 14	H-12a.b, H-13
	16	30.7, CH_3	3.49, s		11, 17	H-12a/b, H-13
Aba-thn-ca	17	169.3, C				
	18	75.9, CH	5.07, m	H-19a, H-19b	17, 20	H-19a, H-19b
	19a	35.5, CH_2	4.15, br dd	H-18, H-19b	17, 18	H-18, H-19a, H-42a
	19b		3.44, dd (-11.2, 8.5)	H-18, H-19a	20	H-18, H-19b
	20	175.0, C				
	21	53.2, CH	4.71, ddd (9.0, 4.0, 2.7)	H-22a, H-22b, NH (D)		H-22a, H-22b, NH (D)
	22a	28.5, CH_2	1.95, dqd (-11.5, 7.4, 4.0)	H-21, H-22b, H_3-23	20, 21, 23	H-21, H-22b, H_3-23
	22b		1.48, m	H-21, H-22a, H_3-23	20, 21, 23	H-21, H-22a, H_3-23
	23	10.0, CH_3	0.74, t (7.4)	H-22a, H-22b	21, 22	H-22a, H-22b
	NH		7.5, d (9.0)	H-21	20	H-21
N-Me-Phe-thn-ca	24	168.9, C				
	25	84.0, C				
	26a	41.5, CH_2	3.29, d (-11.6)	H-26b	24, 25, 27, 28	
	26b		3.18, d (-11.7)	H-26a	24, 25, 27	H_3-27
	27	23.9, CH_3	1.38, s		25, 26, 28	H-26b

Table S-2.3 (continued). NMR Spectroscopic Data for Grassypeptolide E (**2**) in $CDCl_3$ (700 MHz).

unit	position	δ_C, mult.	δ_H, mult. (*J* in Hz)	COSY	HMBC	ROESY
N-Me-Phe-thn-ca	28	173.9, C				
	29	55.8, CH	5.87, dd (12.2, 3.0)	H-30a, H-30b	30, 37, 38	H-30b, H-32/36, H-33/35, H-34
	30a	36.1, CH_2	3.55, br	H-29, H-30b	29, 31, 32/36	H-30b, H_3-37
	30b		3.28, m	H-29, H-30a	28, 31, 32/36	H-29, H-30a, H_3-37
	31	137.7, C				
	32/36	129.6, CH	7.18, m	H-33/35	33/35, 34	H-29
	33/35	129.3, CH	7.03, br	H-32/36, H-34	31, 32/36	H-29
	34	127.3, CH	7.08, m	H-33/35	32/36	H-29
	37	30.2, CH_3	3.17, s		29, 38	H-30a, H-30b, H-39, H-40b, H-41a/b
Pro	38	171.2, C				
	39	58.8, CH	5.10, br	H-40a, H-40b	40, 41, 42, 43	H_3-37, H-40a, H-44
	40a	31.2, CH_2	2.30, m	H-39, H-40b, H-41a/b	39	H-39, H-40b
	40b		2.10, m	H-39, H-40a, H-41a/b	38, 39	H_3-37, H-40a, H-42a, H-42b
	41a/b	21.7, CH_2	2.01, m	H-40a, H-40b, H-42a, H-42b		H_3-37, H-42a, H-42b, H_3-46
	42a	46.9, CH_2	3.80, m	H-41a/b, H-42b	40	H-19, H-40b, H-41a/b
	42b		3.69, m	H-41a/b, H-42a	41	H-40a, H-40b, H-41a/b, H_3-48
N-Me-Val	43	168.5, C				
	44	58.1, CH	5.01, d (10.8)	H-45	43, 45, 47, 48, 49	H-39, H-45, H_3-46, H_3-47
	45	28.1, CH	2.35, m	H-44, H_3-46, H_3-47	44, 46, 47	H-44, H_3-46, H_3-47, H_3-48
	46	19.5, CH_3	0.95, d (6.7)	H-45	44, 45, 47	H-41a/b, H-44, H-45
	47	18.6, CH_3	0.85, d (6.7)	H-45	44, 45, 46	H-44, H-45
	48	30.3, CH_3	3.20, s		44, 49	H-45, H-42b
Pla	49	171.4, C				
	50	72.4, CH	5.33, dd (9.7, 3.8)	H-51a, H-51b	1, 51, 52	H-51a, H-51b
	51a	36.9, CH_2	3.16, m	H-50, H-51b	52, 53/57	H-50, H-51b
	51b		3.01, m	H-50, H-51a	49, 50, 52, 53/57	H-50, H-51a
	52	136.1, C				
	53/57	129.1, CH	7.12, m	H-54/56	54/56, 55	
	54/56	129.5, CH	7.31, m	H-53/57, H-55	52, 53/57	
	55	127.4, CH	7.24, m	H-54/56	54/56	

Table S-2.4. NMR Spectroscopic Data for Ibu-epidesmethoxylyngbyastatin 3 (**3**) in $CDCl_3$ (400 MHz).

unit	position	δ_C, mult.	δ_H, mult. (*J* in Hz)	COSY	HMBC	ROESY	HSQC-TOCSY
Amha	1	173.2, C					
	2	43.4, CH	2.89, ob	H-3, H_3-7	1	H_3-7	7
	3	52.8, CH	3.96, br	H-2, H-4b, NH (A)		H_3-7	
	4a	24.4, CH_2	1.53, m			H_3-7	
	4b		1.27, ob	H-3		H_3-7, NH (A)	3, 4
	5a	20.0, CH_2	1.44, m	H_3-6			3, 4, 6
	5b		1.32, m				
	6	13.9, CH_3	0.86, t (7.0)	H-5a	4, 5		3, 4, 5
	7	13.4, CH_3	1.21, d (6.9)	H-2	1, 2, 3	H-2, H-3, H-4a/b, H-47	2, 3
	NH		7.84, br	H-3		H-4b	
N-Me-Ala	8	169.6, C					
	9	53.3, CH	5.10,m	H_3-10	8	H-10	10
	10	14.0, CH_3	1.37, d (6.9)	H-9	8, 9	H-9	9
	11	31.1, CH_3	2.76, s		12	H_3-17, H_3-18	
Ibu	12	173.6, C					
	13	54.4, C					
	14	208.4, C					
	15	51.2, CH	4.83, br	H_3-16, NH (B)	16, 19	H_3-16, H_3-18	
	16	19.3, CH_3	1.18, d (6.8)	H-15		H-15	15
	17	23.5, CH_3	1.33, s		12, 13, 14, 18	H_3-11, H-23/27	
	18	21.6, CH_3	1.26, s		12, 13, 14, 17	H_3-11, H-15	
	NH		6.86, br	H-15	19		
N-Me-Phe	19	170.5, C					
	20	61.2, CH	4.98, br	H-21a, H-21b	19	H-23/27, H-30	21
	21a	35.9, CH_2	3.32, m	H-20, H-21b	20	H-23/27, H-30	20
	21b		2.92, br m	H-20, H-21a	19	H-23/27, H-30	20
	22	136.5, C					
	23/27	128.7, CH	7.23, m		25	H_3-17, H-20, H-21a, H-21b, H_3-28, H_3-33	24/26, 25
	24/26	129.0, CH	7.29, m		22, 23/27		23/27, 25
	25	127.3. CH	7.21, m				
	28	30.5, CH_3	2.98, s		20	H-23/27	

Table S-2.4 (continued). NMR Spectroscopic Data for Ibu-epidemethoxy-lyngbyastatin 3 (**3**) in $CDCl_3$ (400 MHz).

unit	position	δ_C, mult.	δ_H, mult. (*J* in Hz)	COSY	HMBC	ROESY	HSQC-TOCSY
N-Me-Val	29	169.9, C					
	30	58.0, CH	4.77, d (10.7)	H-31	29, 31, 33	H-20, H-21a, H-21b, H_3-32, H_3-33	31, 32, 33
	31	27.0, CH	2.22, br	H-30, H_3-32, H_3-33		H_3-32, H_3-33, H_3-34	30, 32, 33
	32	18.6, CH_3	0.69, br	H-31	30, 31, 33	H-30, H-31, H_3-33, H_3-34	30, 31, 33
	33	18.5, CH_3	0.36, br	H-31	30, 31, 32	H-23/27, H-30, H-31, H_3-32, H_3-34	30, 31, 32
	34	29.3, CH_3	2.97, s		30, 35	H-31, H_3-32, H_3-33, H-36a, H-36b	
Gly	35	169.2, C					
	36a	41.0, CH_2	4.45, br m	H-36b, NH (C)	35	H_3-34, H-36b	
	36b		3.72, br m	H-36a		H_3-34, H-36a	
	NH		7.10, ob	H-36a		H-38	
N-Me-Leu	37	170.5, C					
	38	55.0, CH	5.26, br dd (7.6, 6.7)	H-39a, H-39b	37, 39	H-39a, H_3-41, NH (C)	
	39a	37.3, CH_2	1.77, m	H-38, H-39b, H-40	40	H-38, H_3-41	38, 42
	39b		1.56, ob	H-38, H-39a	38, 40	H-38, H_3-43	38, 42
	40	24.7, CH	1.45, br m	H-39a, H_3-41, H_3-42	39, 42		39
	41	23.0, CH_3	0.93, d (6.6)	H-40	39, 40, 42	H-39a, H-39b	38, 42
	42	22.1, CH_3	0.87, d (7.0)	H-40			38
	43	29.6, CH_3	2.84, s			H-39b, H-45a, H-45b	
Gly	44	169.7, C					
	45a	42.0, CH_2	4.38, br m	H-45b, NH (D)			
	45b		3.75, br m	H-45a			
	NH		6.96, br	H-45a			
Hmpa	46	170.2, C					
	47	77.5, CH	5.28, br d (5.6)	H-48	1, 46, 48	H_3-7, H-48, H_3-50	48, 49, 50, 51
	48	37.2, CH	2.03, br m	H-47, H_3-51		H-47, H_3-50	
	49a	24.4, CH_2	1.59, ob	H-49b, H_3-50		H_3-50	
	49b		1.49, m	H-49a, H_3-50		H_3-51	48
	50	11.5, CH_3	0.88, t (5.6)	H-49a, H-49b	48, 49	H-47, H-48, H-49a	48, 49
	51	15.0, CH_3	0.90, d (7.7)	H-48	47, 48	H-49b	47, 48

ob = obscured

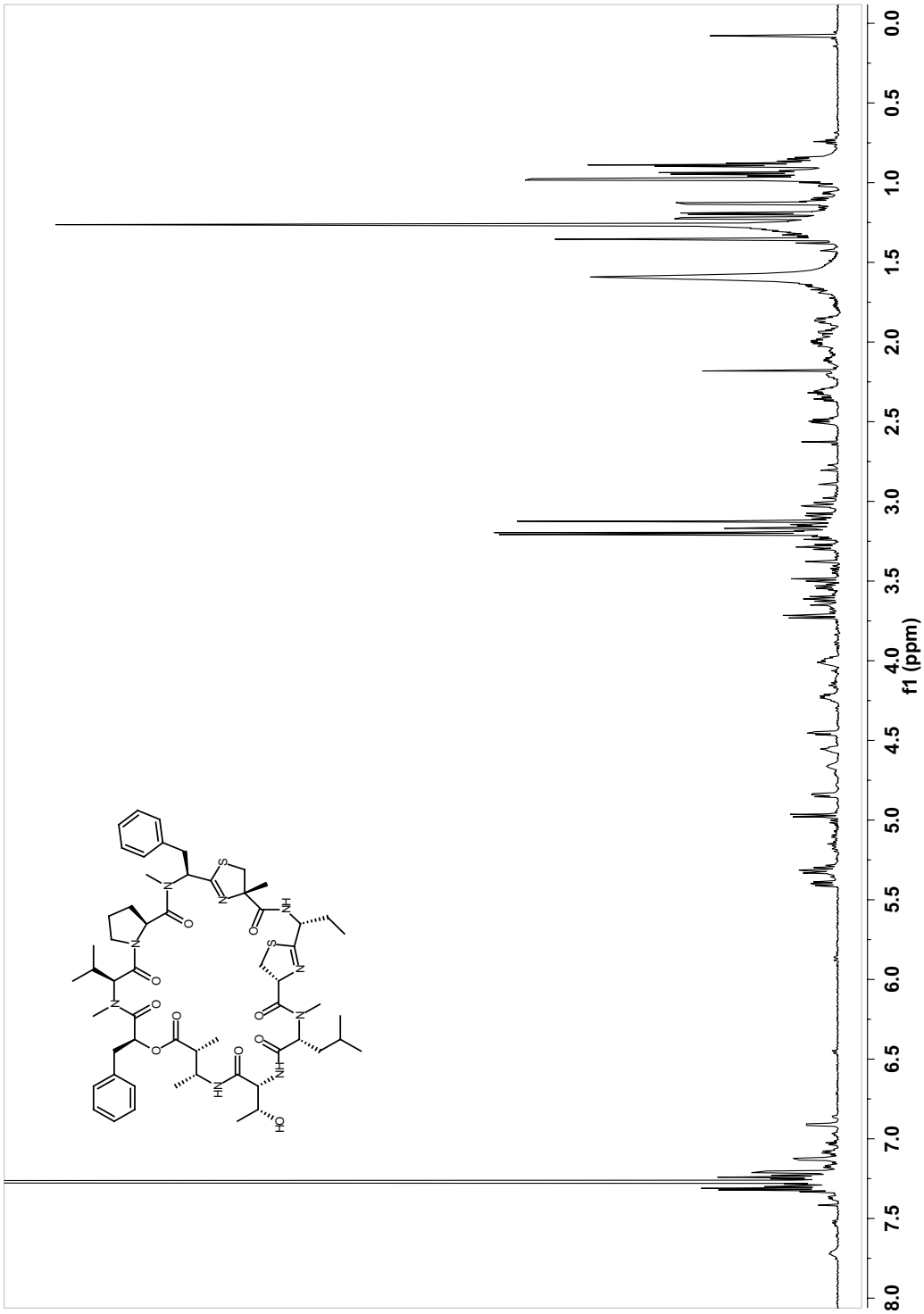

Figure S-2.1. ^{1}H NMR spectrum for grassypeptolide D (**1**) in $CDCl_3$ (700 MHz).

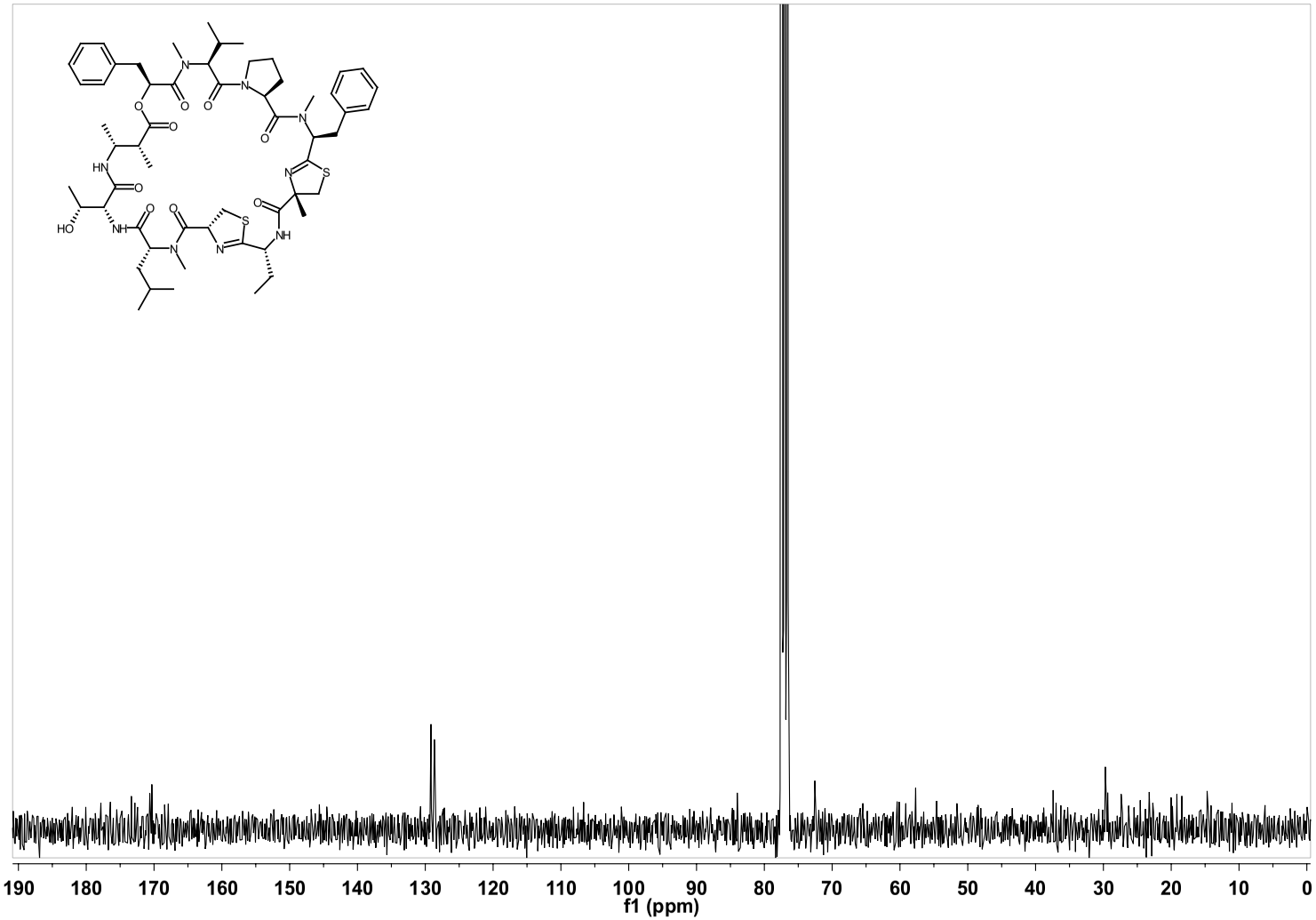

Figure S-2.2. ^{13}C NMR spectrum for grassypeptolide D (**1**) in $CDCl_3$ (100 MHz).

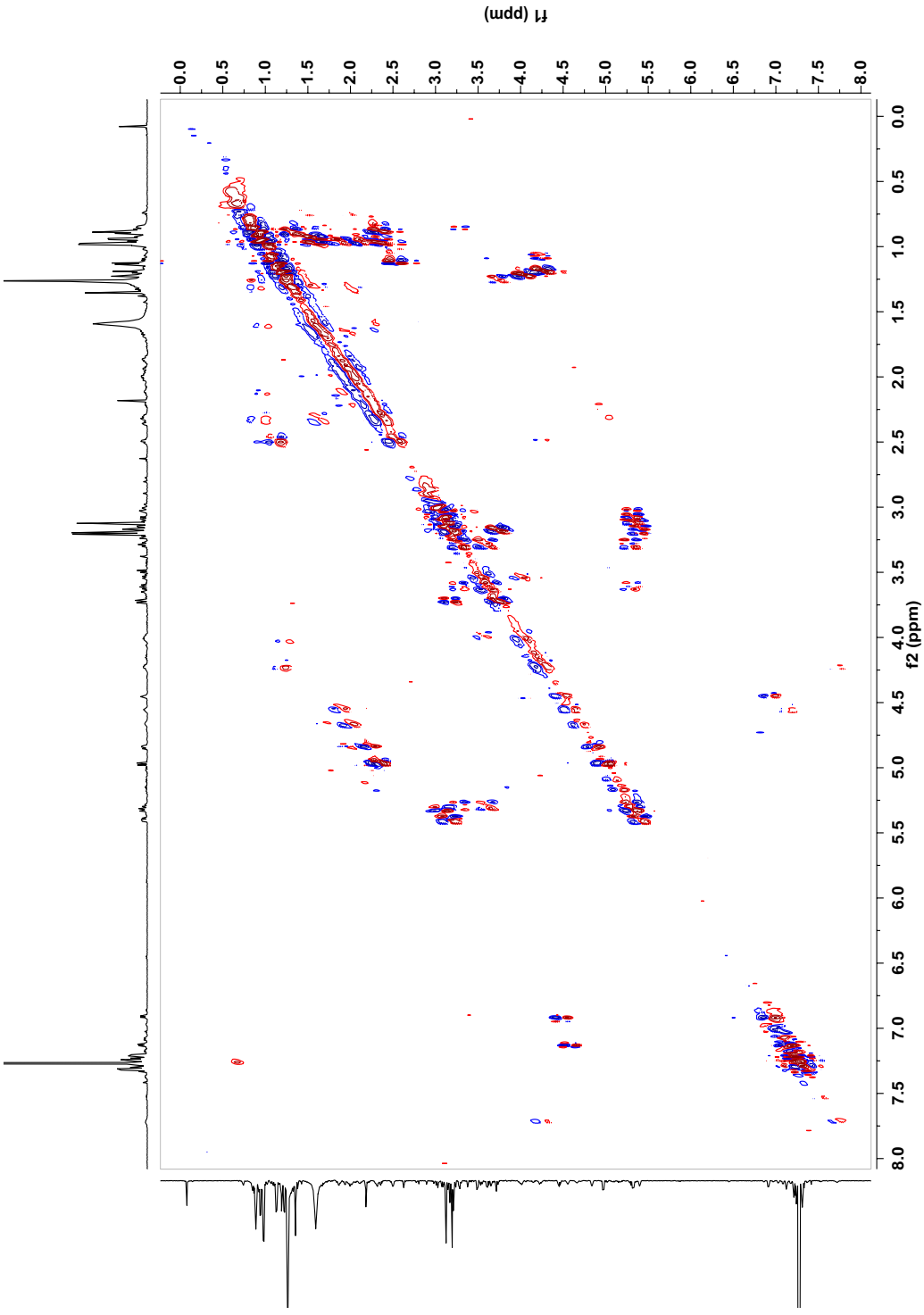

Figure S-2.3. DQF COSY spectrum for grassypeptolide D (**1**) in $CDCl_3$ (400 MHz).

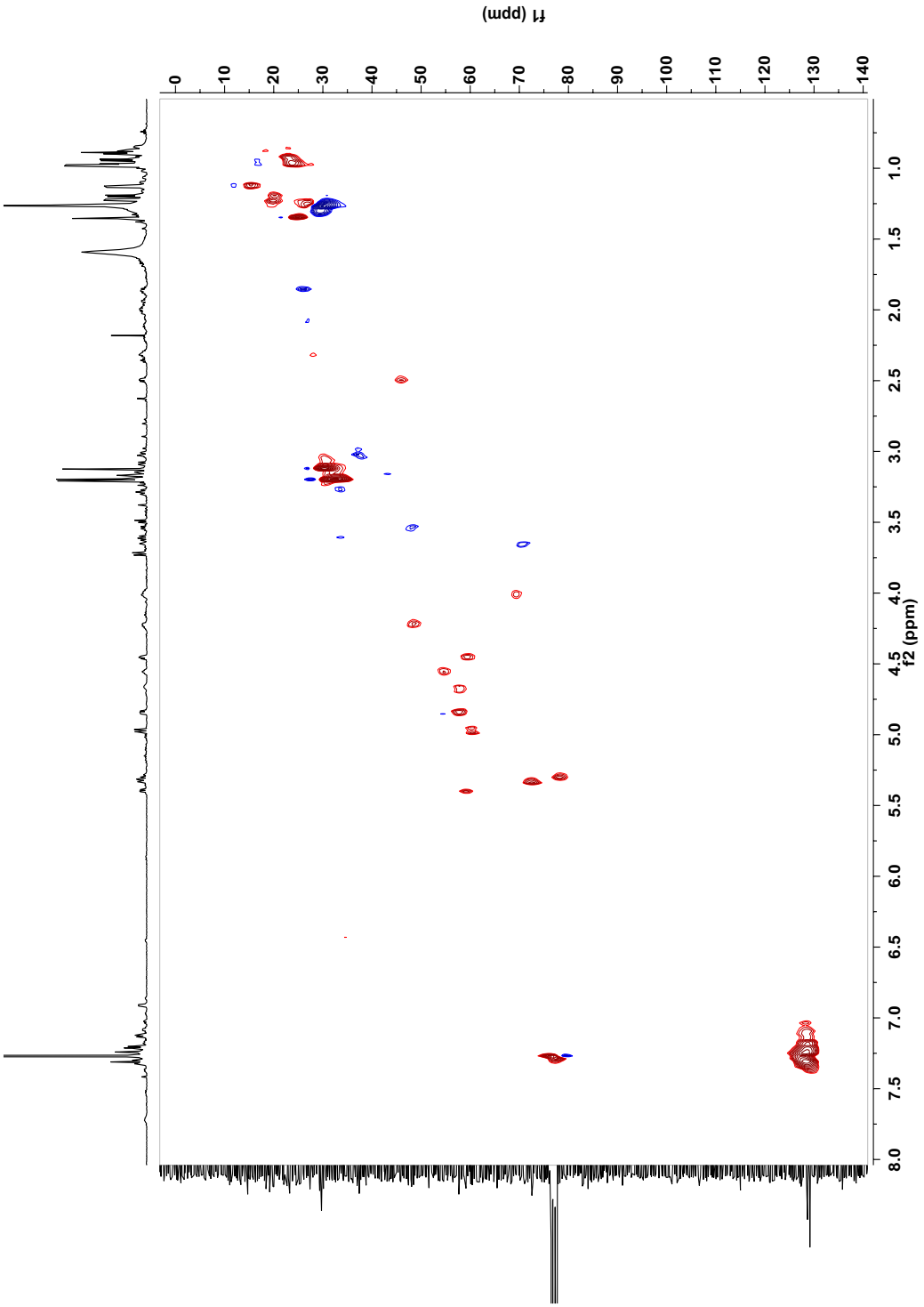

Figure S-2.4. Multiplicity-edited HSQC spectrum for grassypeptolide D (**1**) in $CDCl_3$ (400 MHz).

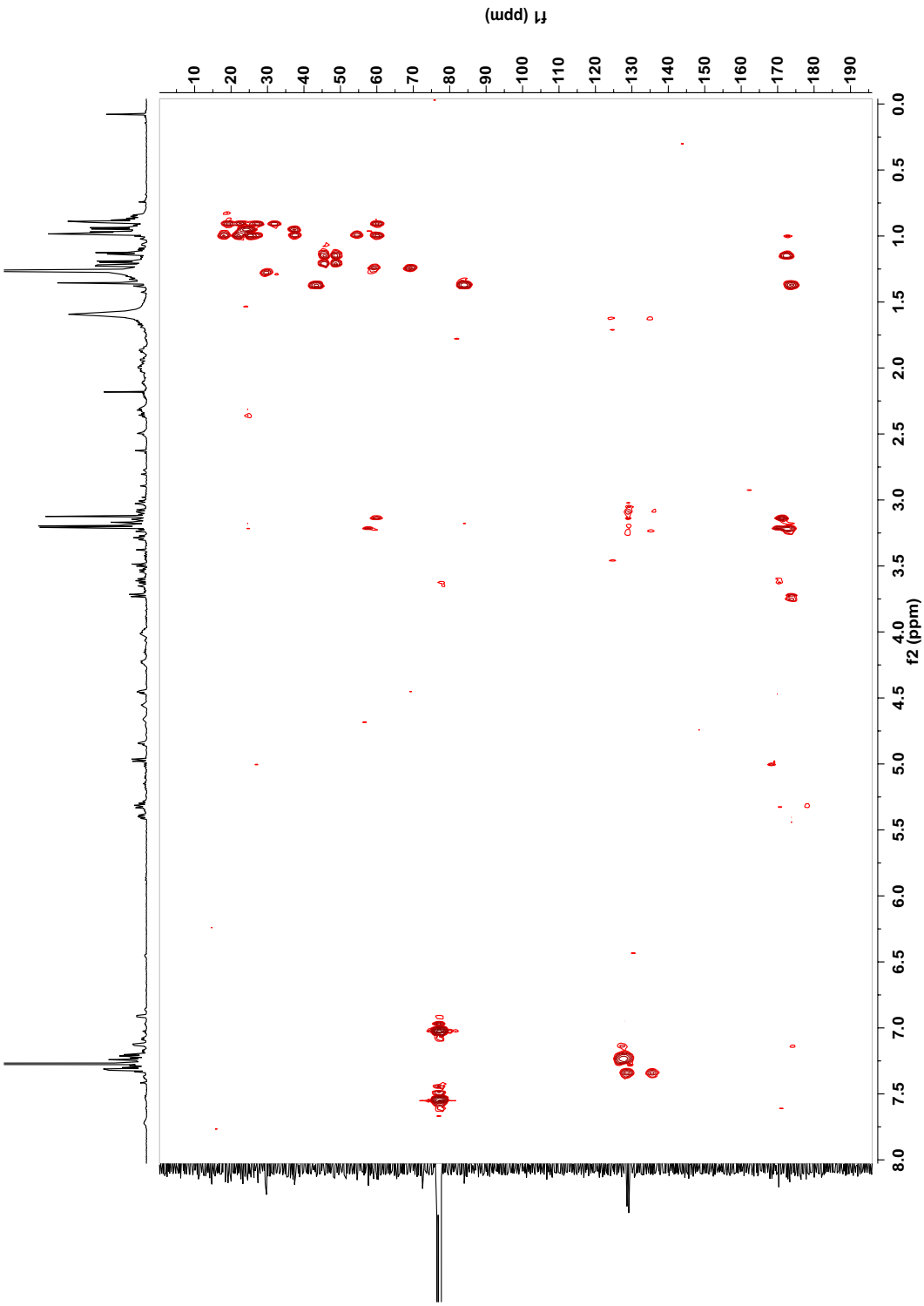

Figure S-2.5. HMBC spectrum for grassypeptolide D (**1**) in $CDCl_3$ (400 MHz).

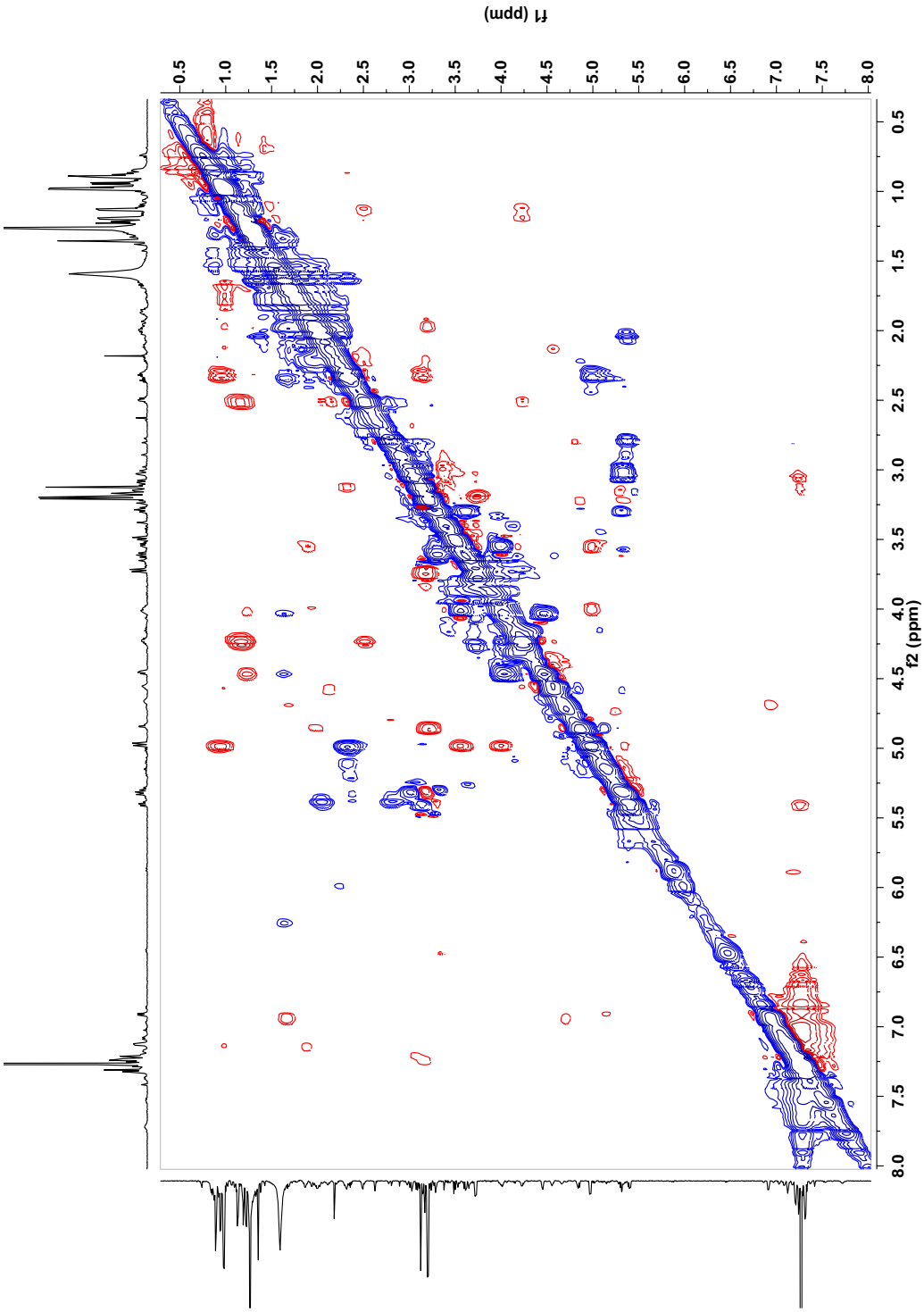

Figure S-2.6. ROESY spectrum for grassypeptolide D (**1**) in $CDCl_3$ (400 MHz).

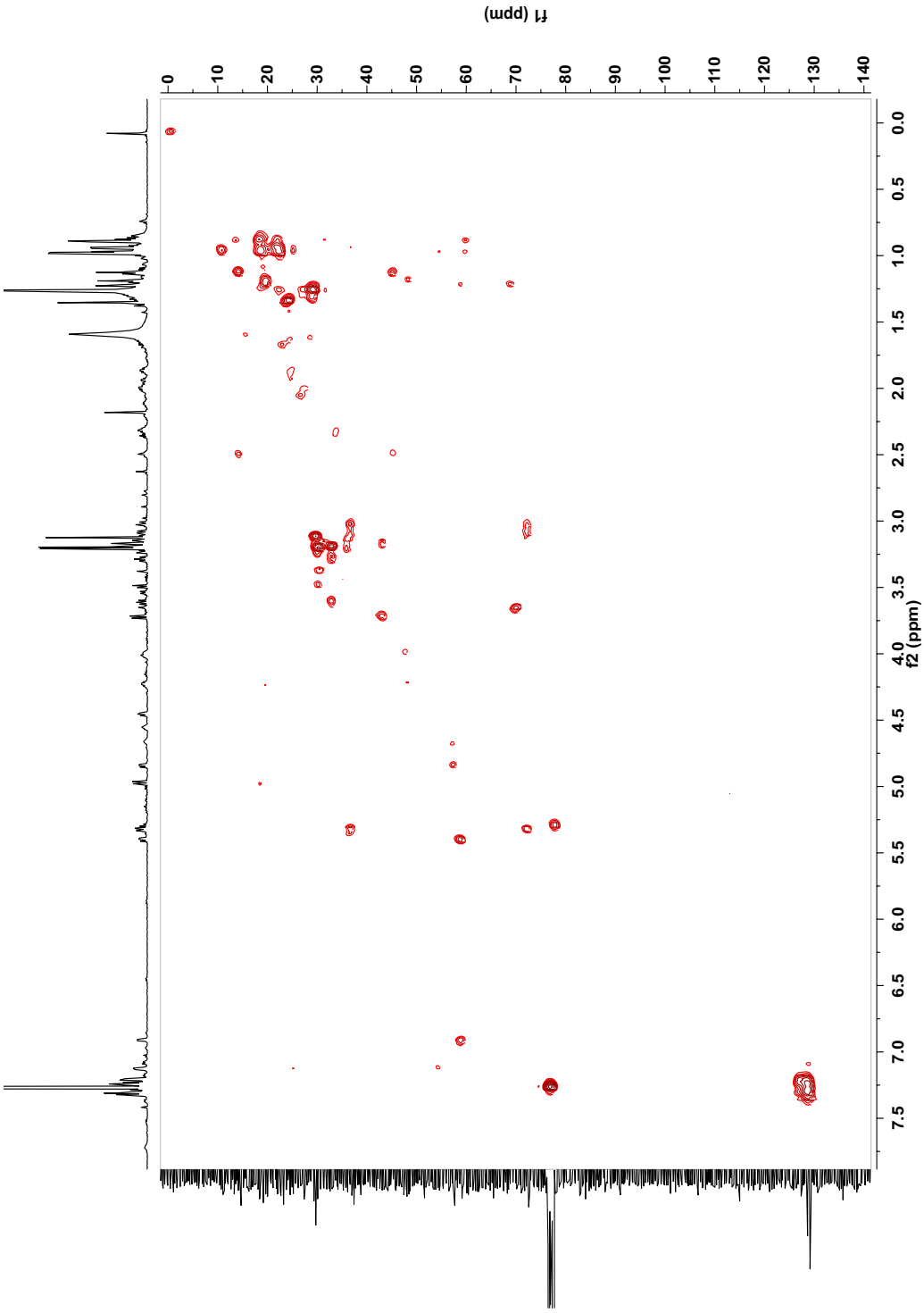

Figure S-2.7. HSQC-TOCSY spectrum for grassypeptolide D (**1**) in $CDCl_3$ (400 MHz).

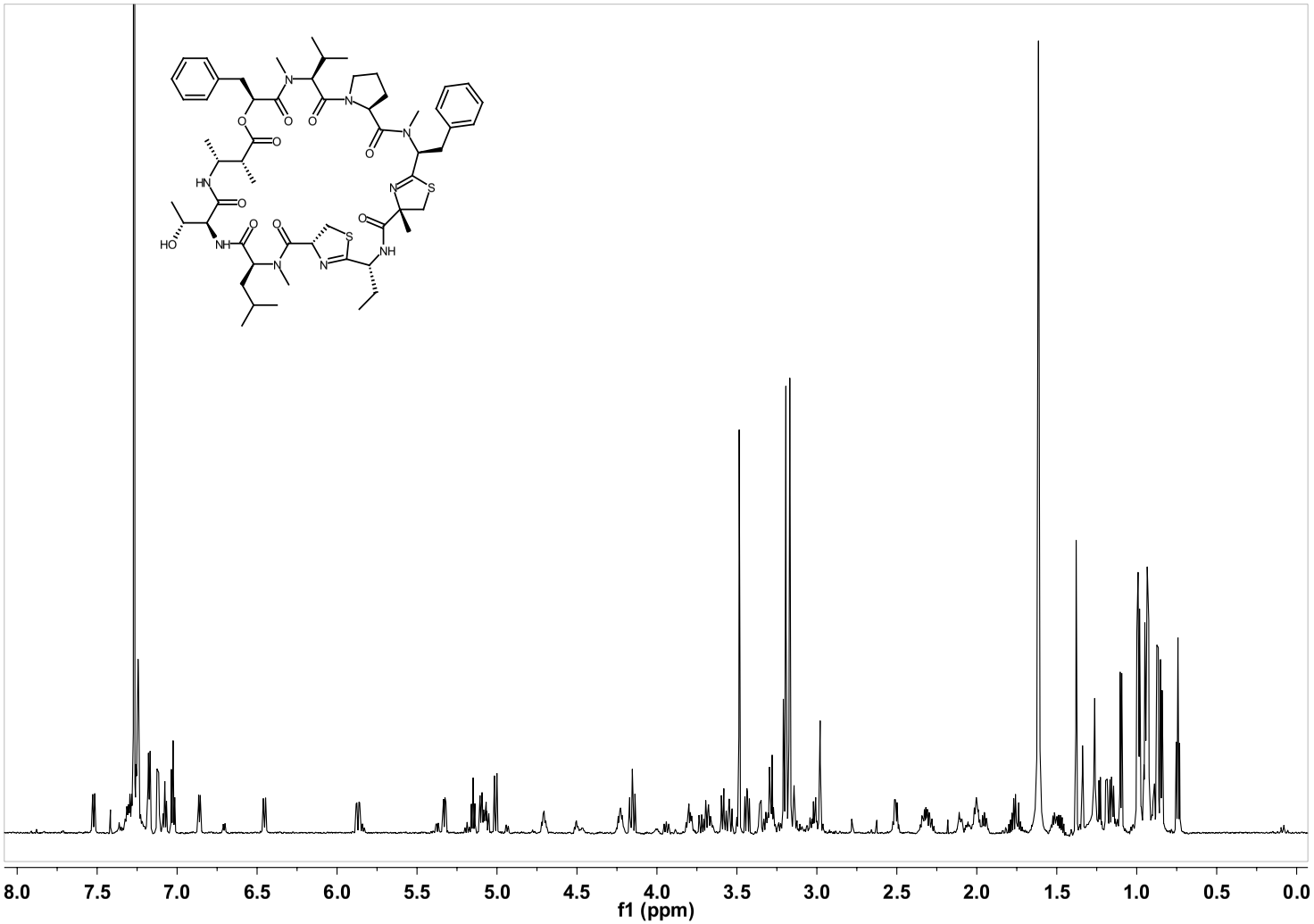

Figure S-2.8. ^{1}H NMR spectrum for grassypeptolide E (**2**) in $CDCl_3$ (700 MHz).

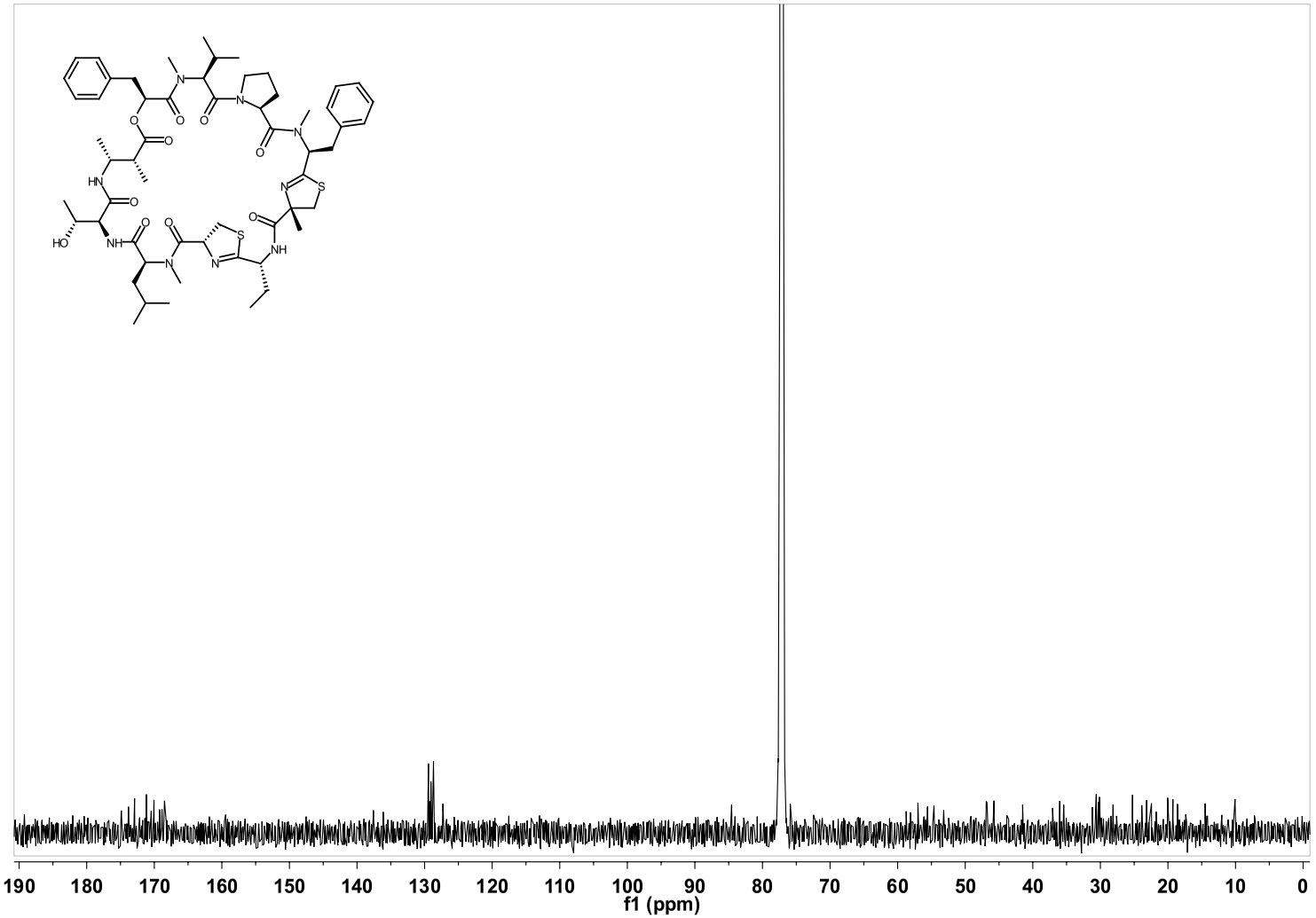

Figure S-2.9. ^{13}C NMR spectrum for grassypeptolide E (**2**) in $CDCl_3$ (175 MHz).

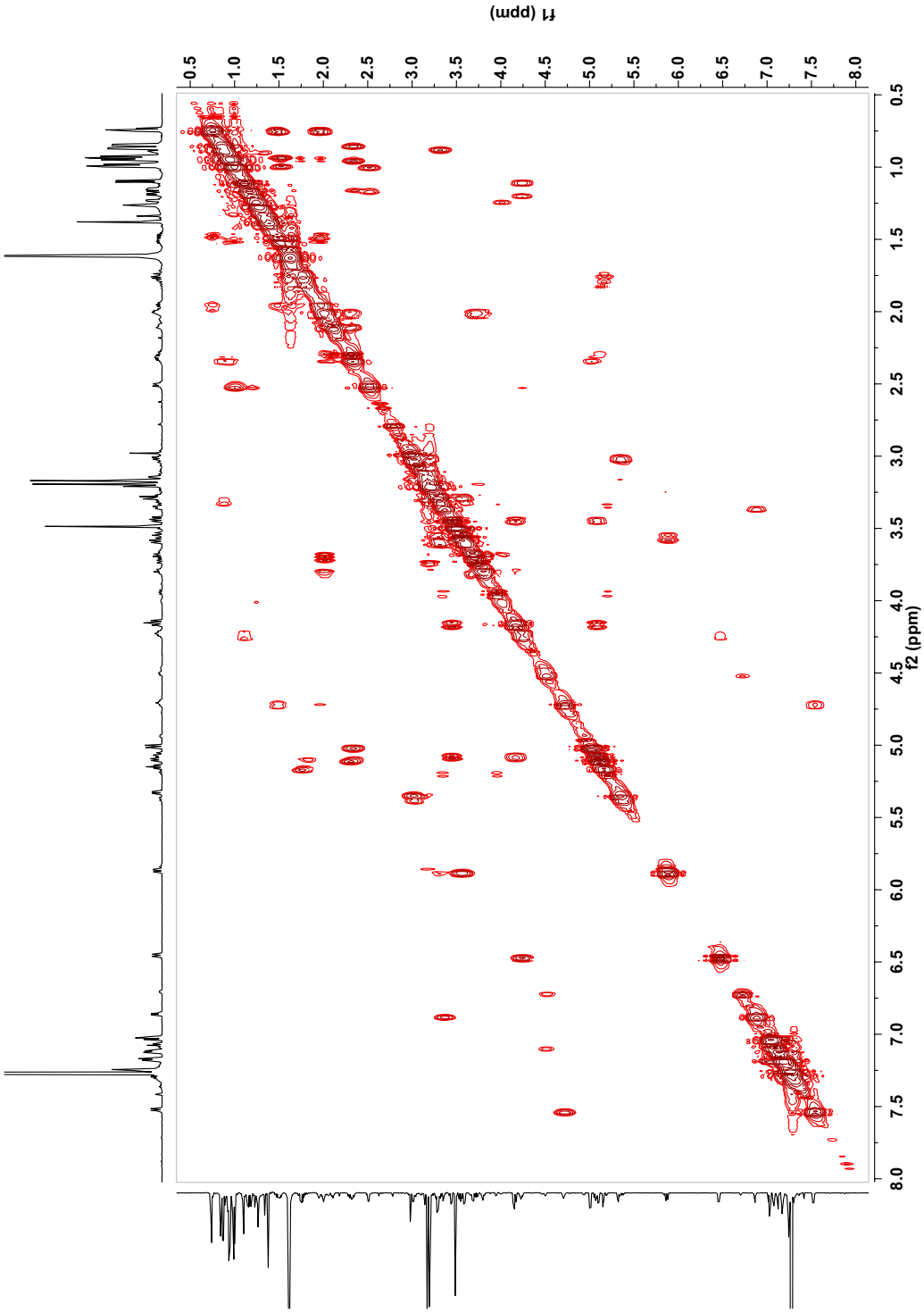

Figure S-2.10. COSY spectrum for grassypeptolide E (**2**) in $CDCl_3$ (700 MHz).

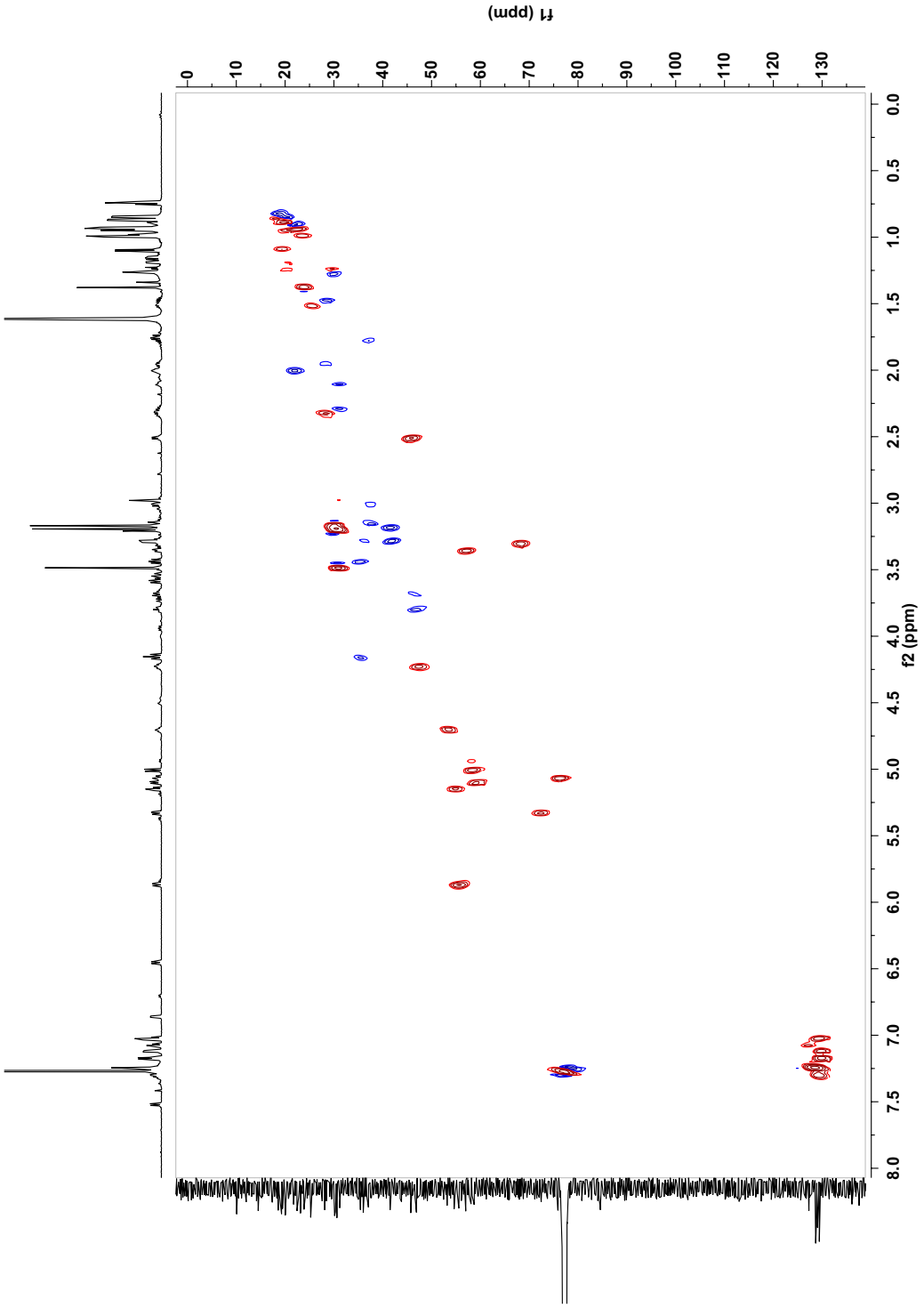

Figure S-2.11. Multiplicity-edited HSQC spectrum for grassypeptolide E (**2**) in $CDCl_3$ (700 MHz).

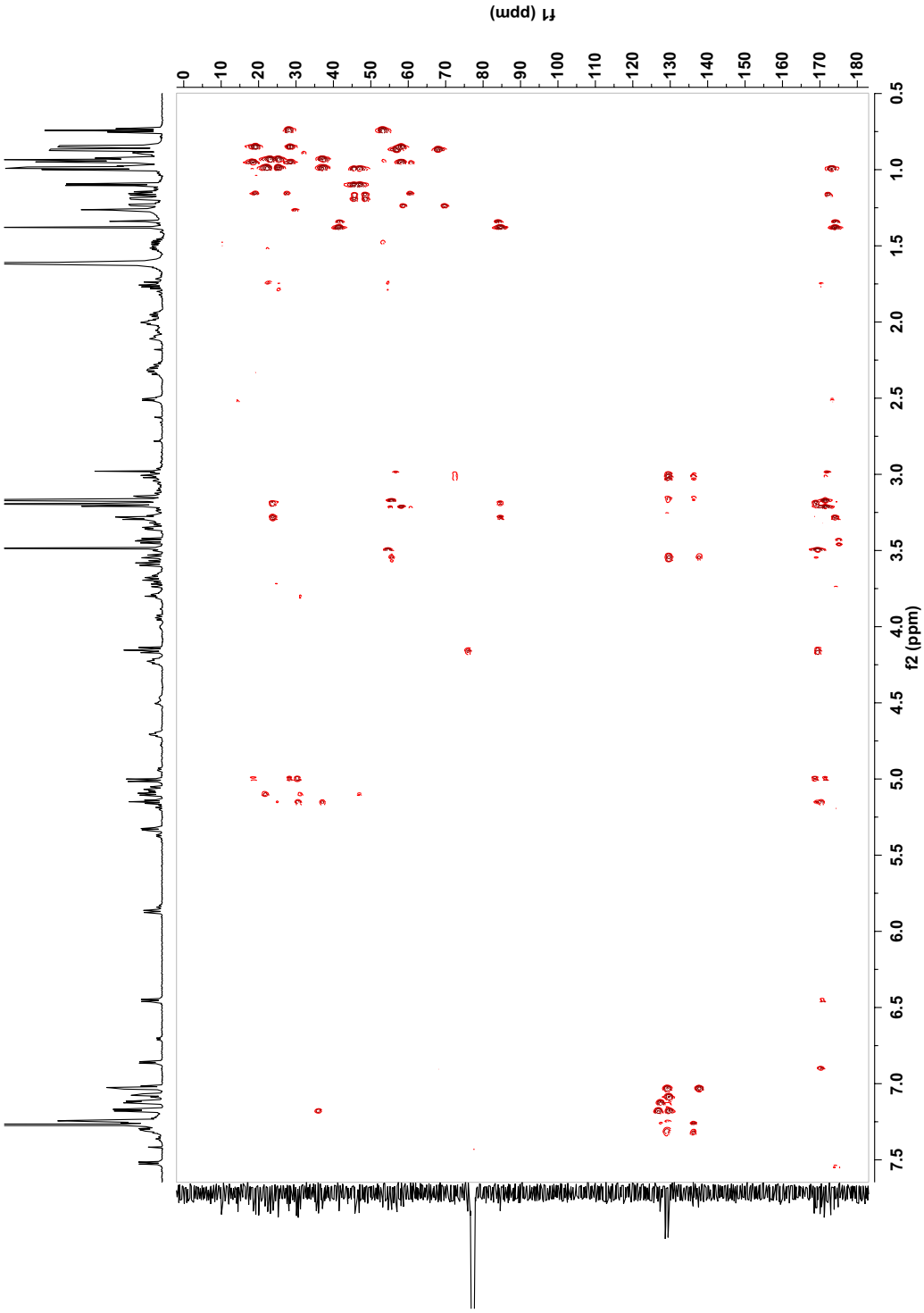

Figure S-2.12. HMBC spectrum for grassypeptolide E (**2**) in $CDCl_3$ (700 MHz).

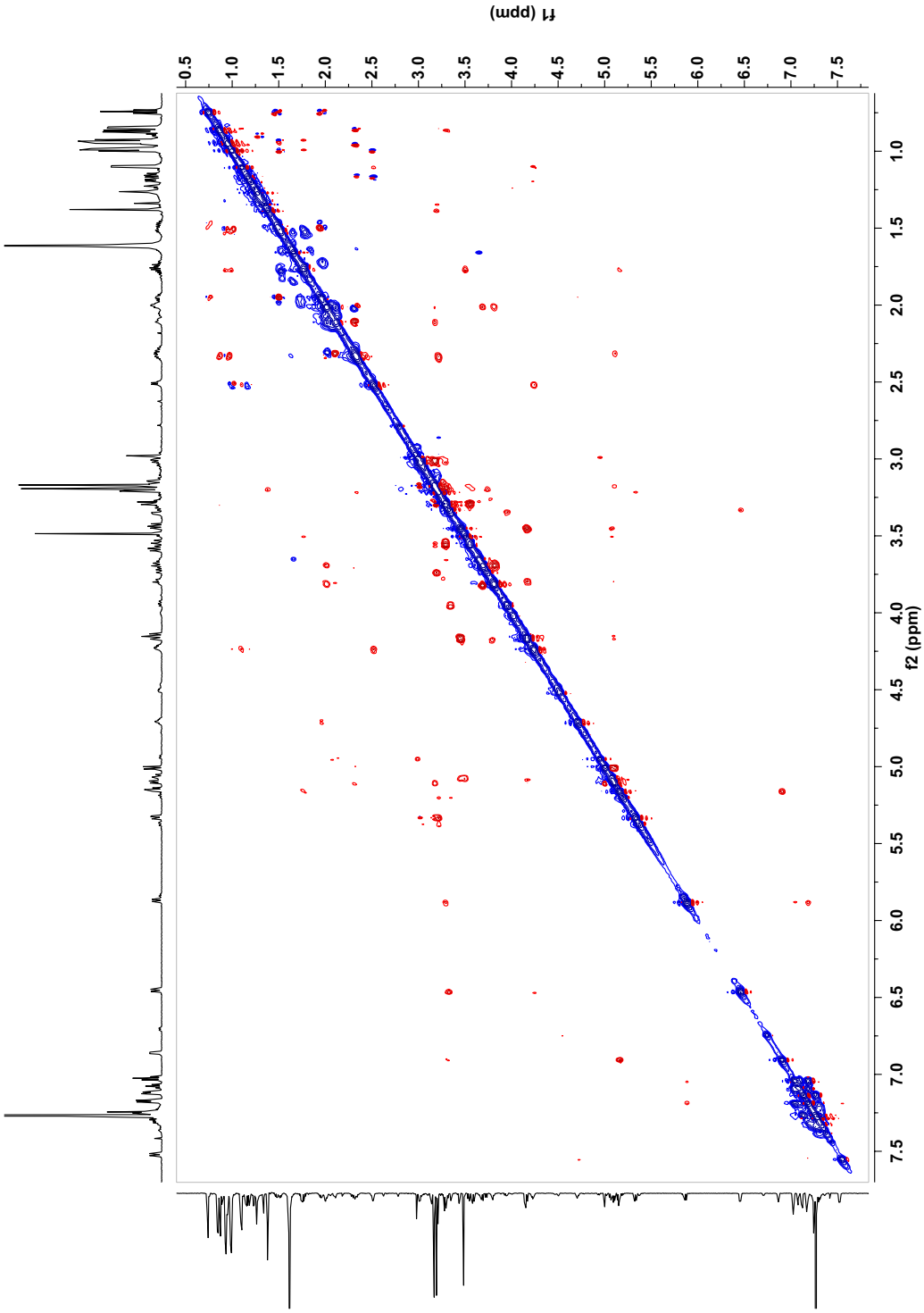

Figure S-2.13. ROESY spectrum for grassypeptolide E (**2**) in $CDCl_3$ (700 MHz).

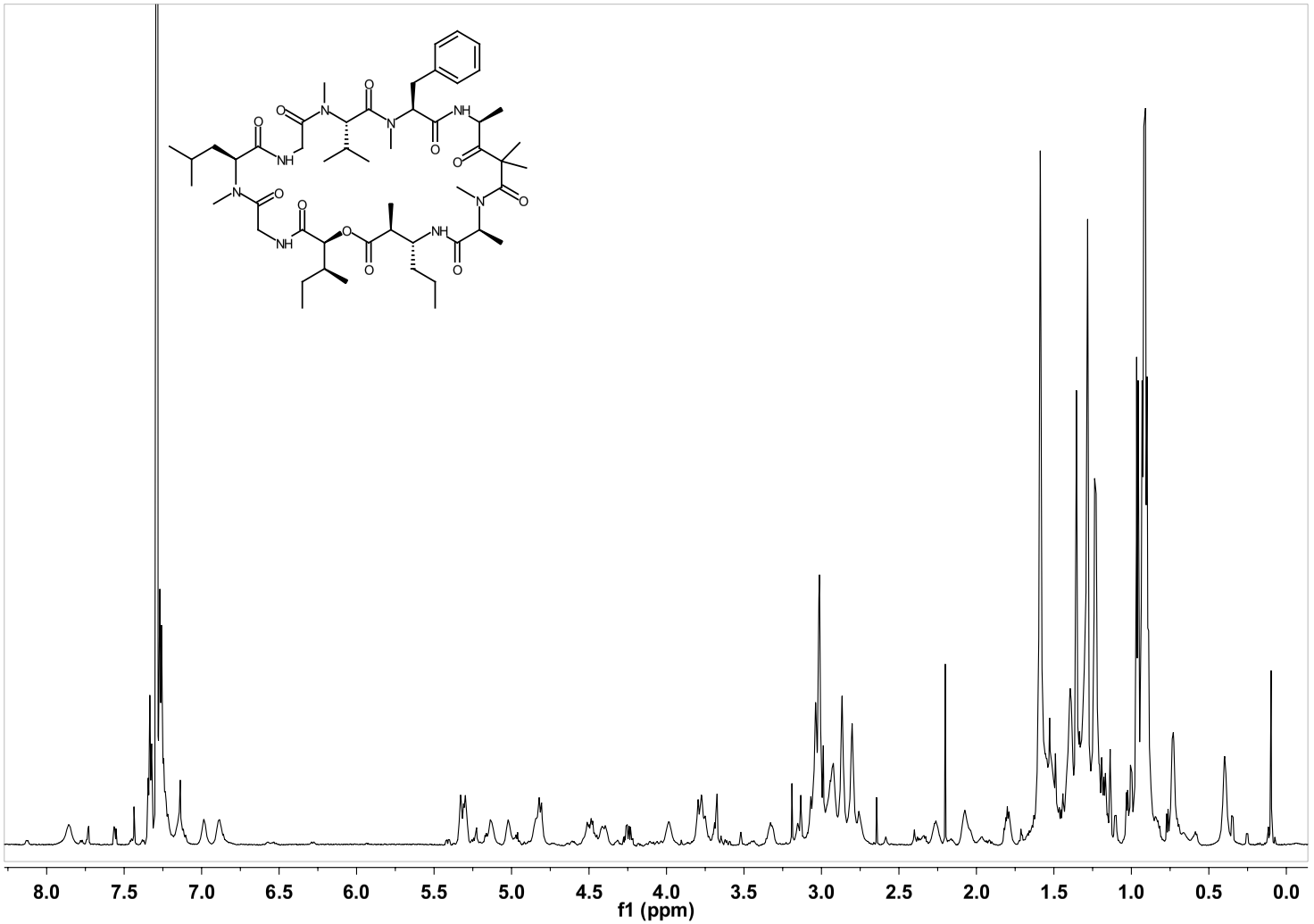

Figure S-2.14. ^{1}H NMR spectrum for Ibu-epidemethoxylyngbyastatin 3 (**3**) in $CDCl_3$ (700 MHz).

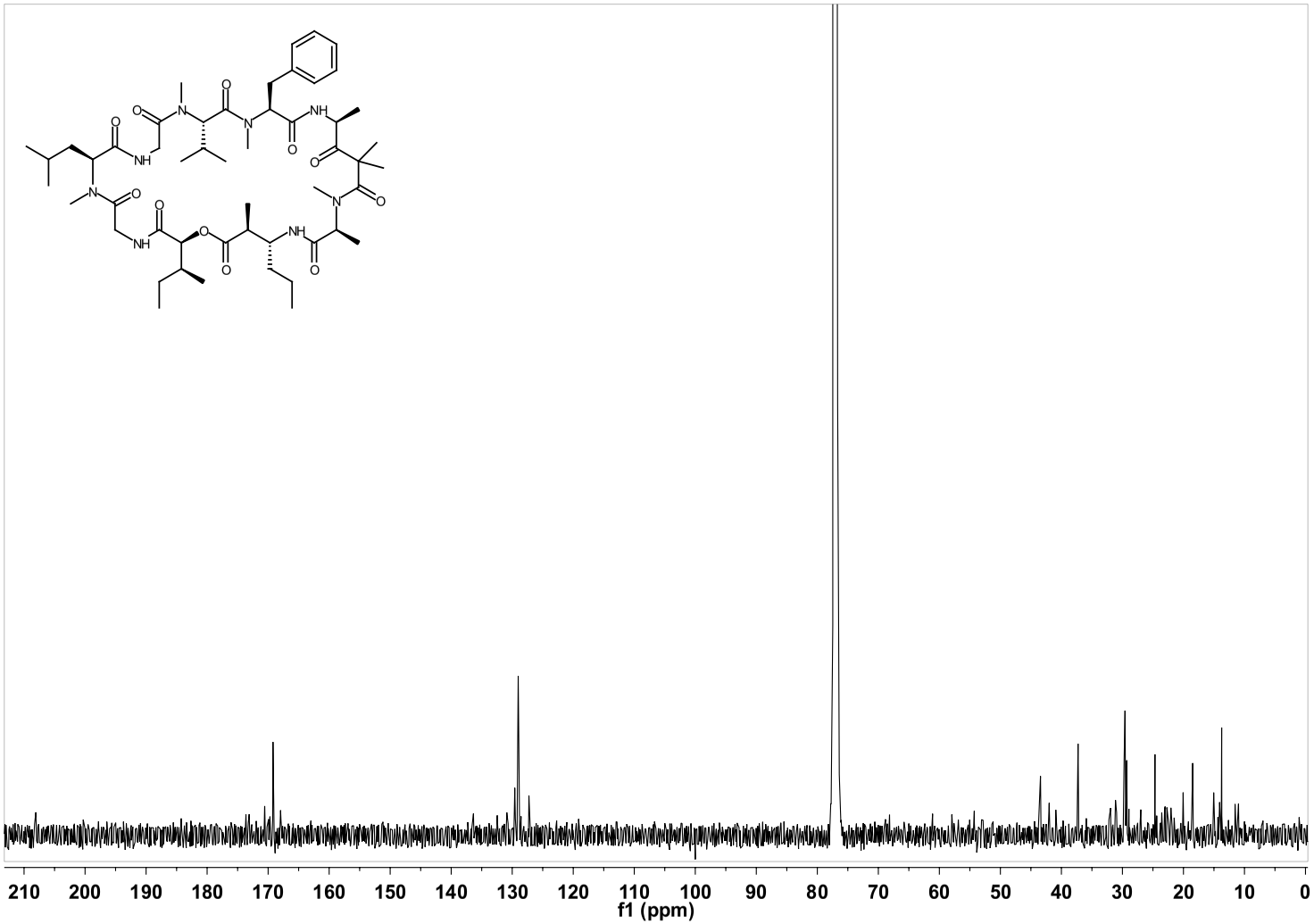

Figure S-2.15. ^{13}C NMR spectrum for Ibu-epidemethoxylyngbyastatin 3 (**3**) in $CDCl_3$ (175 MHz).

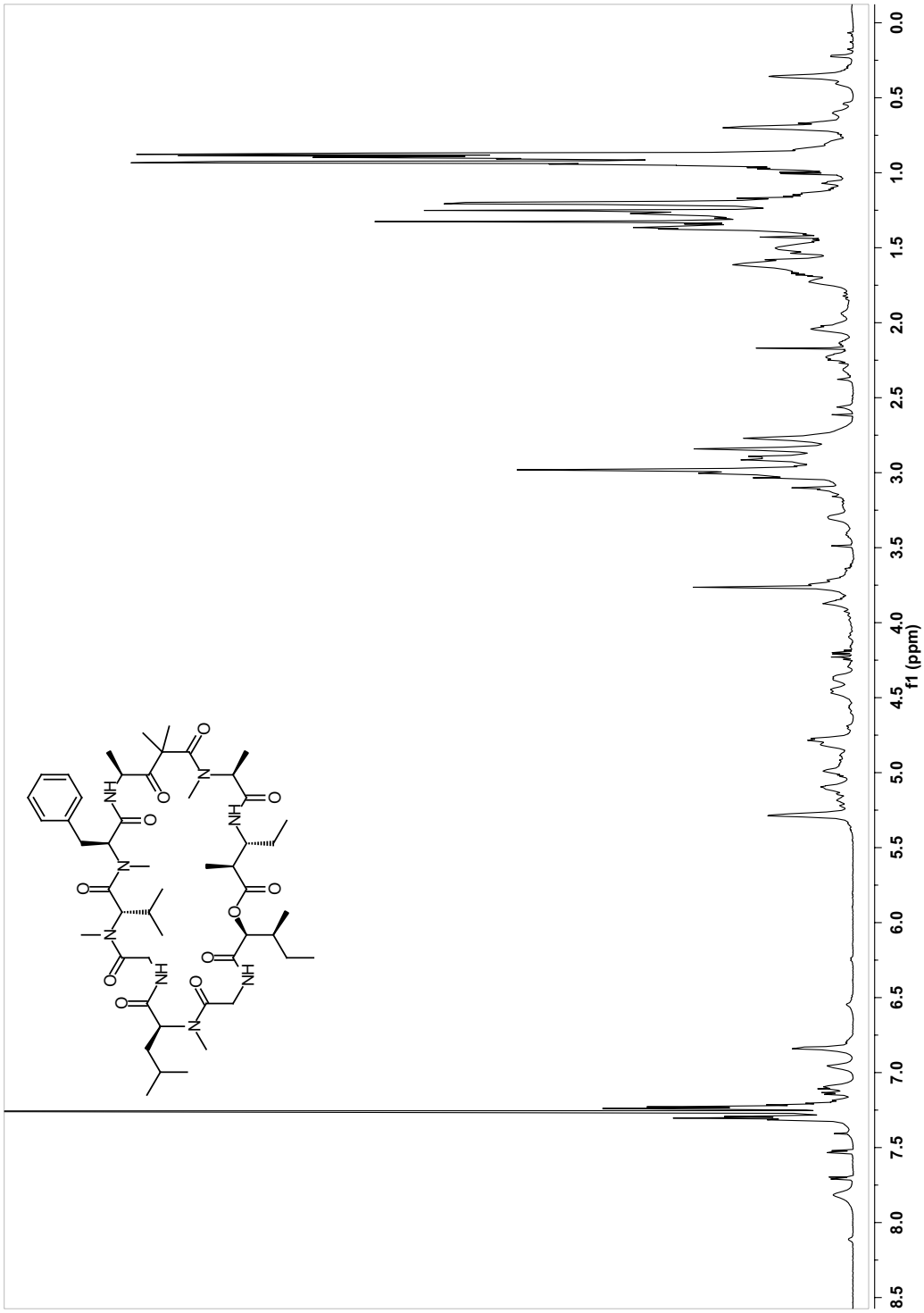

Figure S-2.16. ^{1}H NMR spectrum for dolastatin 12 in $CDCl_3$ (700 MHz).

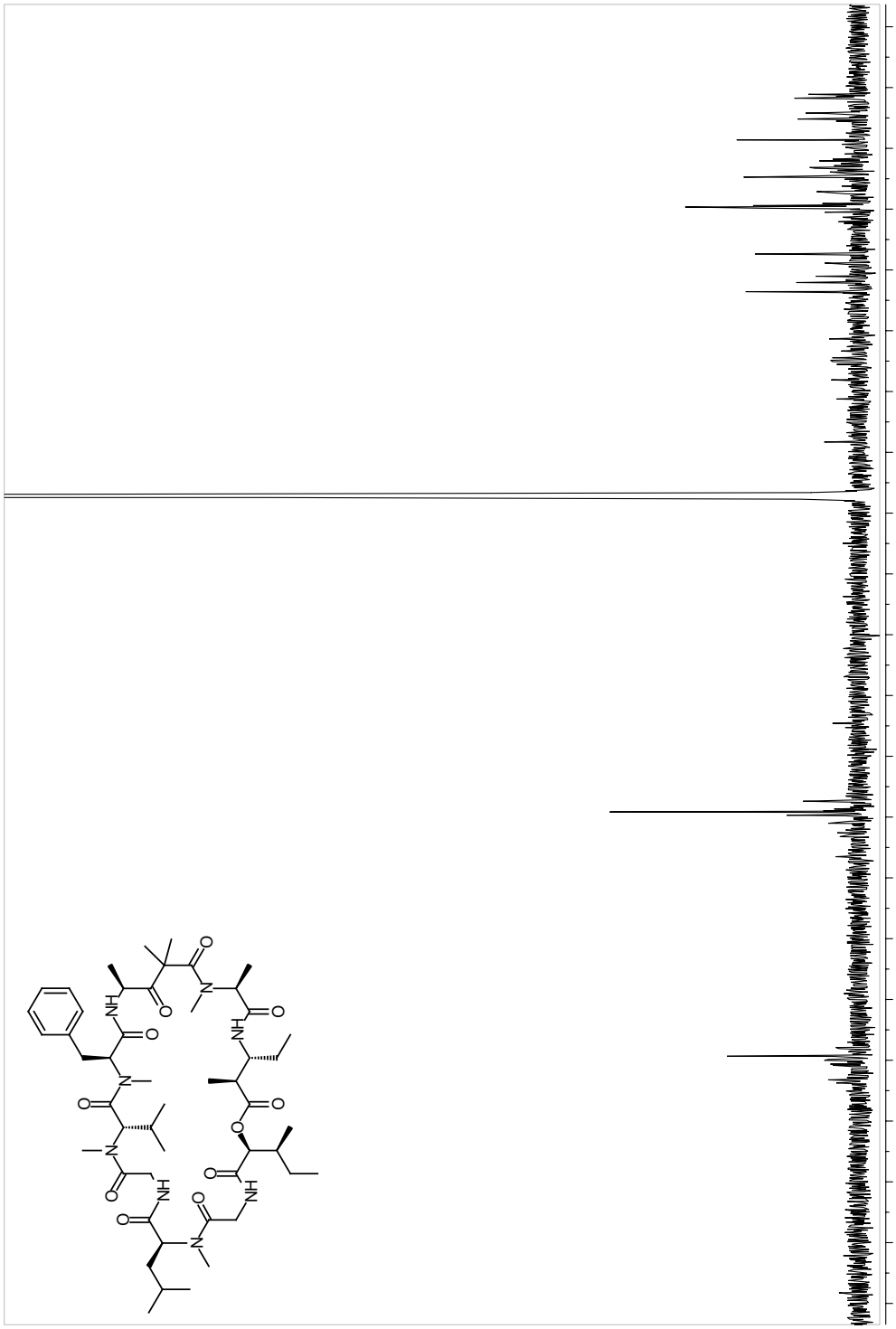

Figure S-2.17. ^{13}C NMR spectrum for dolastatin 12 in $CDCl_3$ (175 MHz).

References

Ashelford, K. E., Chuzhanova, N. A., Fry, J. C., Jones, A. J., & Weightman, A. J. (2005). At Least 1 in 20 16S rRNA Sequence Records Currently Held in Public Repositories Is Estimated To Contain Substantial Anomalies. *Appl. Environ. Microbiol., 71*(12), 7724-7736.

Ashelford, K. E., Chuzhanova, N. A., Fry, J. C., Jones, A. J., & Weightman, A. J. (2006). New Screening Software Shows that Most Recent Large 16S rRNA Gene Clone Libraries Contain Chimeras. *Appl. Environ. Microbiol., 72*(9), 5734-5741.

Bai, R., Bates, R. B., Hamel, E., Moore, R. E., Nakkiew, P., Pettit, G. R., & Sufi, B. A. (2002). Lyngbyastatin 1 and Ibu-epilyngbyastatin 1: Synthesis, Stereochemistry, and NMR Line Broadening. *J. Nat. Prod., 65*(12), 1824-1829.

Carter, D. C., Moore, R. E., Mynderse, J. S., Niemczura, W. P., & Todd, J. S. (1984). Structure of majusculamide C, a cyclic depsipeptide from *Lyngbya majuscula*. *J. Org. Chem., 49*(2), 236-241.

Castenholz, R. W. (1988). [3] Culturing methods for cyanobacteria. In A. N. G. Lester Packer (Ed.), *Methods in Enzymology* (Vol. Volume 167, pp. 68-93): Academic Press.

Choi, H., Pereira, A. R., Cao, Z., Shuman, C. F., Engene, N., Byrum, T., Matainaho, T., Murray, T. F., Mangoni, A., & Gerwick, W. H. (2010). The Hoiamides, Structurally Intriguing Neurotoxic Lipopeptides from Papua New Guinea Marine Cyanobacteria. *J. Nat. Prod., 73*(8), 1411-1421.

Clardy, J., & Walsh, C. (2004). Lessons from natural molecules. *Nature, 432*(7019), 829-837.

Drummond, A., Ashton, B., Buxton, S., Cheung, M., Cooper, A., Duran, C., Field, M., Heled , J., Kearse, M., Markowitz, S., Moir, R., Stones-Havas, S., Sturrock, S., Thierer, T., & Wilson, A. (2010). Geneious v5.3. from http://www.geneious.com

Engene, N., Coates, C. R., & Gerwick, W. H. (2010). 16S rRNA gene heterogeneity in the filamentous marine cyanobacterial genus *Lyngbya*. *J. Phycol., 46*(3), 591-601.

Engene, N., Rottacker, E. C., Kaštovský, J., Byrum, T., Choi, H., Ellisman, M. H., Komárek, J., & Gerwick, W. H. (2012). *Moorea producens* gen. nov., sp. nov. and *Moorea bouillonii* comb. nov., tropical marine cyanobacteria rich in bioactive secondary metabolites. *Int. J. Syst. Evol. Microbiol., 62*(Pt 5), 1171-1178.

Fenton, M., Geiselhart, S., Rohling, E. J., & Hemleben, C. (2000). Aplanktonic zones in the Red Sea. *Mar. Micropaleontol., 40*(3), 277-294.

Guindon, S., & Gascuel, O. (2003). A Simple, Fast, and Accurate Algorithm to Estimate Large Phylogenies by Maximum Likelihood. *Syst. Biol., 52*(5), 696-704.

Han, A. W., Oh, K. H., Jheong, W. H., & Cho, Y. C. Establishment of an Axenic Culture of Microcystin-Producing *Microcystis aeruginosa* Isolated from a Korean Reservoir. *J. Microbiol. Biotechnol., 20*(7), 1152-1155.

Harrigan, G. G., Yoshida, W. Y., Moore, R. E., Nagle, D. G., Park, P. U., Biggs, J., Paul, V. J., Mooberry, S. L., Corbett, T. H., & Valeriote, F. A. (1998). Isolation, Structure Determination, and Biological Activity of Dolastatin 12 and Lyngbyastatin 1 from *Lyngbya majuscula*/*Schizothrix calcicola* Cyanobacterial Assemblages. *J. Nat. Prod., 61*(10), 1221-1225.

Hess, W. R. (2008). Comparative genomics of marine cyanobacteria and their phages. In A. Herrero & E. Flores (Eds.), *Cyanobacteria*. Norwich, UK: Caister Academic Press.

Huang, X., & Madan, A. (1999). CAP3: A DNA Sequence Assembly Program. *Genome Res., 9*(9), 868-877.

Huelsenbeck, J. P., & Ronquist, F. (2001). MRBAYES: Bayesian inference of phylogenetic trees. *Bioinformatics, 17*(8), 754-755.

Komárek, J., & Anagnostidis, K. (2005). Cyanoprokaryota 2. Teil/ 2nd Part: Oscillatoriales. In B. Büdel, L. Krienitz, G. Gärtner & M. Schagerl (Eds.), *Süßwasserflora von Mitteleuropa 19/2* (pp. 759). Heidelberg: Elsevier/ Spektrum.

Kwan, J. C., Ratnayake, R., Abboud, K. A., Paul, V. J., & Luesch, H. (2010). Grassypeptolides A-C, Cytotoxic Bis-thiazoline Containing Marine Cyclodepsipeptides. *J. Org. Chem., 75*(23), 8012-8023.

Marquardt, J., & Palinska, K. A. (2007). Genotypic and phenotypic diversity of cyanobacteria assigned to the genus *Phormidium* (Oscillatoriales) from different habitats and geographical sites. *Arch. Microbiol., 187*(5), 397-413.

Martínez-Murcia, A. J., Acinas, S. G., & Rodriguez-Valera, F. (1995). Evaluation of prokaryotic diversity by restrictase digestion of 16S rDNA directly amplified from hypersaline environments. *FEMS Microbiol. Ecol., 17*(4), 247-255.

Matthew, S., Paul, V. J., & Luesch, H. (2009a). Largamides A-C, Tiglic Acid-Containing Cyclodepsipeptides with Elastase-Inhibitory Activity from the Marine Cyanobacterium *Lyngbya confervoides*. *Planta Med., 75*(05), 528,533.

Matthew, S., Paul, V. J., & Luesch, H. (2009b). Tiglicamides A-C, cyclodepsipeptides from the marine cyanobacterium *Lyngbya confervoides*. *Phytochemistry, 70*(17-18), 2058-2063.

Matthew, S., Ross, C., Paul, V. J., & Luesch, H. (2008). Pompanopeptins A and B, new cyclic peptides from the marine cyanobacterium *Lyngbya confervoides*. *Tetrahedron, 64*(18), 4081-4089.

Matthew, S., Ross, C., Rocca, J. R., Paul, V. J., & Luesch, H. (2007). Lyngbyastatin 4, a Dolastatin 13 Analogue with Elastase and Chymotrypsin Inhibitory Activity from the Marine Cyanobacterium *Lyngbya confervoides*. *J. Nat. Prod., 70*(1), 124-127.

Nubel, U., Garcia-Pichel, F., & Muyzer, G. (1997). PCR primers to amplify 16S rRNA genes from cyanobacteria. *Appl. Environ. Microbiol., 63*(8), 3327-3332.

Pettit, G. R., Kamano, Y., Kizu, H., Dufresne, C., Herald, C. L., Bontems, R. J., Schmidt, J. M., Boettner, F. E., & Nieman, R. A. (1989). Isolation and structure of the cell growth inhibitory depsipeptides dolastatins 11 and 12. *Heterocycles, 28*(2), 553-558.

Posada, D. (2008). jModelTest: Phylogenetic Model Averaging. *Mol. Biol. Evol., 25*(7), 1253-1256.

Scherlach, K., & Hertweck, C. (2009). Triggering cryptic natural product biosynthesis in microorganisms. *Org. Biomol. Chem., 7*(9), 1753-1760.

Tan, L. (2010). Filamentous tropical marine cyanobacteria: a rich source of natural products for anticancer drug discovery. *J. Appl. Phycol., 22*(5), 659-676.

Taori, K., Matthew, S., Rocca, J. R., Paul, V. J., & Luesch, H. (2007). Lyngbyastatins 5-7, Potent Elastase Inhibitors from Floridian Marine Cyanobacteria, *Lyngbya* spp. *J. Nat. Prod., 70*(10), 1593-1600.

Taori, K., Paul, V. J., & Luesch, H. (2008). Structure and Activity of Largazole, a Potent Antiproliferative Agent from the Floridian Marine Cyanobacterium *Symploca* sp. *J. Am. Chem. Soc., 130*(6), 1806-1807.

Theberge, C. R., & Zercher, C. K. (2003). Chain extension of amino acid skeletons: preparation of ketomethylene isosteres. *Tetrahedron, 59*(9), 1521-1527.

Williams, P. G., Moore, R. E., & Paul, V. J. (2003). Isolation and Structure Determination of Lyngbyastatin 3, a Lyngbyastatin 1 Homologue from the Marine Cyanobacterium *Lyngbya majuscula*. Determination of the Configuration of the 4-Amino-2,2-dimethyl-3-oxopentanoic Acid Unit in Majusculamide C, Dolastatin 12, Lyngbyastatin 1, and Lyngbyastatin 3 from Cyanobacteria. *J. Nat. Prod., 66*(10), 1356-1363.

Williamson, R. T., Boulanger, A., Vulpanovici, A., Roberts, M. A., & Gerwick, W. H. (2003). Structure and Absolute Stereochemistry of Phormidolide, a New Toxic Metabolite from the Marine Cyanobacterium *Phormidium* sp. *J. Org. Chem., 68*(5), 2060-2060.

Chapter Three

Apratoxin H, a Cytotoxic Cyclic Depsipeptide from a Red Sea *Moorea producens* Cyanobacterium

Christopher C. Thornburg, Elise S. Cowley, Justyna Sikorska, Lamiaa A. Shaala, Jane E. Ishmael, Diaa T.A. Youssef, and Kerry L. McPhail

Abstract

Cultivation of the marine cyanobacterium *Moorea producens*, collected from the Nabq Mangroves in the northern tip of the Red Sea (Gulf of Aqaba), led to the isolation of the potent cytotoxins apratoxin A and lyngbyabellin B. Furthermore, meticulous examination of the cytotoxic fractions revealed a new naturally occurring apratoxin analogue, apratoxin H (**1**), and a oxidized analogue, apratoxin A sulfoxide (**2**). The three-dimensional structures of compounds **1** and **2** were determined by chemical degradation, MS, NMR, and CD spectroscopy. Apratoxin H (**1**) contains pipecolic acid in place of the proline residue present in apratoxin A, expanding the naturally occurring analogues that display amino acid substitutions within the final module of the apratoxin biosynthetic pathway. Apratoxin A sulfoxide (**2**) was considered as a possible isolation artifact, however experimental oxidations of apratoxin A did not generate apratoxin A sulfoxide. Although the structural differences between compounds **1** and **2** relative to the previously reported apratoxins are minimal, their cytotoxicity to human NCI-H460 lung cancer cells (IC_{50} = 3.4 and 89.9 nM, respectively) provides further insight into the structure–activity relationships of the apratoxin family. Finally, phylogenetic analysis of the apratoxin-producing cyanobacterial strains belonging to the genus *Moorea*, coupled with the recently annotated apratoxin biosynthetic pathway, reveals that apratoxin production and structural diversity may be regulated by key environmental factors specific to their geographical niche.

Introduction

Marine cyanobacteria are capable of producing series of closely related and highly bioactive secondary metabolites, often of mixed biosynthetic origin, with unique cancer cell toxicity profiles. A number of these compounds have served as therapeutic lead compounds in cancer clinical trials (Simmons et al., 2005). Notably, Adcetris® (SGN-35, brentuximab vedotin), a synthetic dolastatin 10 analogue (monomethyl auristatin E) conjugated to an anti-CD30 monoclonal antibody (Francisco et al., 2003), has been granted accelerated approval by the U.S. Food and Drug Administration for treatment of Hodgkin lymphoma (HL) and systemic anaplastic large cell lymphoma (ALCL; "Seattle Genetics," 2013).

Recently, the depsipeptide scaffold of the apratoxin series of secondary metabolites, produced by several tropical marine cyanobacterial species of the *Moorea* genus (formerly classified as *Lyngbya bouillonii*, *L. majuscula* and *L. sordida*), has become an attractive platform for synthetic efforts aimed at developing more potent and selective analogues, given their subnanomolar activity to several cancer cell lines and unique mechanism of action (Chen et al., 2011; Y. Liu et al., 2009; Ma et al., 2006). Importantly, apratoxin A is the first antitumor agent identified to inhibit the cellular secretory pathway by preventing the *N*-glycosylation and subsequent cotranslational translocation of several cancer-associated receptors (including receptor tyrosine kinases, RTKs) and secreted proteins (e.g. growth factors and cytokines) from the cytoplasm to the endoplasmic reticulum (ER), leading to their rapid proteasomal degradation (Y. Liu et al., 2009). In agreement with this proposed mechanism of action, Luesch and colleagues (2011) subsequently synthesized an apratoxin A/E hybrid analogue with greater potency and efficacy. This synthetic hybrid not only depleted cellular levels of the tyrosine kinase receptors VEGFR-2 (vascular endothelial growth factor receptor) and PDGFR-β (platelet-derived growth factor receptor, β polypeptide) in mouse colorectal carcinomas (HCT116 xenograft), but also

displayed a marked reduction in toxicity compared to apratoxin A. Apratoxin A suppression of cotranslational translocation is somewhat specific in that it downregulates a relatively small subset of associated cell-surface proteins (66 of 476 identified) and RTKs in U2OS osteosarcoma cells (Liu et al., 2009). However, its selectivity may be further enhanced through the identification of additional apratoxin analogues and medicinal chemistry studies.

Our focus on microorganisms from unique marine environments lead to the identification of a new *Moorea producens* strain (RS05) that shares 98.9% sequence homology (SSU 16S rRNA gene) with the reported apratoxin-producing strains from Guam and Palau. Furthermore, preliminary data showed that this Red Sea *Moorea producens* RS05 strain produced several compounds within the apratoxin family. Thus, monophyletic cultures of *Moorea producens* RS05 were established and grown over the span of two years, which yielded a new apratoxin analogue along with the known compounds apratoxin A and lyngbyabellin B. Here we report the isolation, structure determination and biological activity of apratoxin H (**1**), and apratoxin A sulfoxide (**2**).

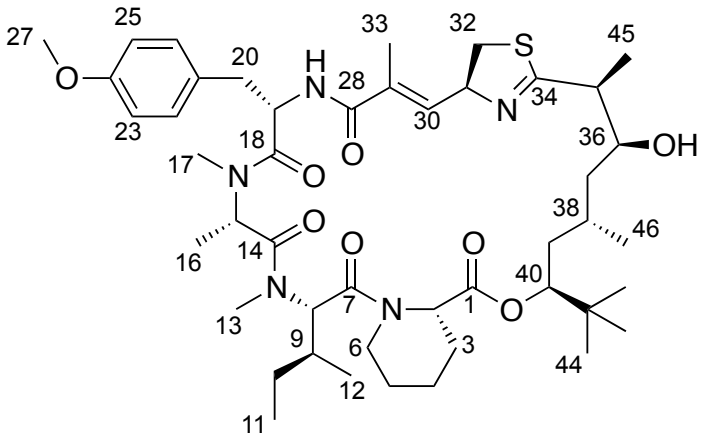

Apratoxin H (**1**)

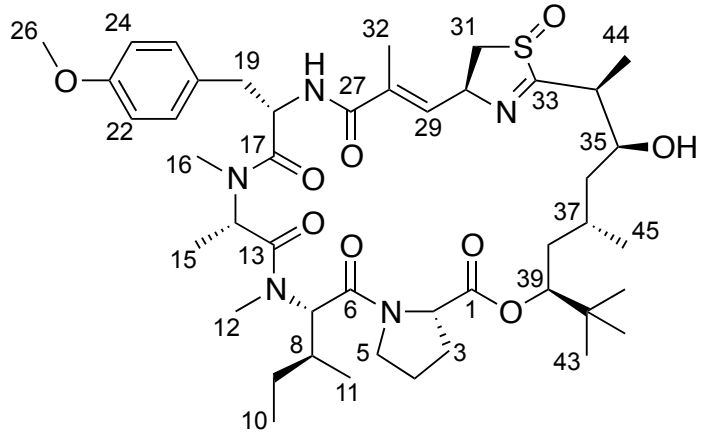

Apratoxin A sulfoxide (**2**)

Results and Discussion

In 2007, A dark brown filamentous "*Lyngbya*" cyanobacterium was collected by hand from the shallows of the Nabq Mangrove in the Gulf of Aqaba near Sharm el-Sheikh, Egypt. Microscopically, this cyanobacterium contained long, unbranched filaments with wide discoid cells that were contained within thick polysaccharide sheaths, which is consistent with the description of *Moorea producens* sp. nov. (N. Engene et al., 2012). A unialgal culture, established through repetitive isolation and subculturing of individual trichomes, as previously described (Thornburg et al., 2011), was maintained in laboratory culture and used to propagate multiple large cultures (30 × 1.5 L) over the span of two years. A crude organic extract of the Red Sea *Moorea producens* RS05 was subjected to bioassay-guided fractionation via normal phase vacuum liquid chromatography (NP-VLC) using a stepped solvent gradient of hexanes to EtOAc to MeOH. The fractions eluting with 100% EtOAc and 25% EtOAc–hexanes were highly toxic to brine shrimp (0.1 μg/mL resulted in 100% kill) and yielded two minor components (**1**, 3.5 mg and **2**, 0.9 mg), as well as the known cytotoxic macrolide lyngbyabellin B (4.6 mg) and the highly cytotoxic lipopeptide apratoxin A (41.0 mg) as the major component, following C_{18} solid-phase extraction and exhaustive RP-HPLC.

The ^{1}H and ^{13}C NMR spectra for **1** and **2** were very similar to apratoxin A (Hendrik Luesch et al., 2001) from a *Moorea* sp. (previously reported as *Lyngbya majuscula* and *Lyngbya bouillonii*) collected from Apra Harbor, Guam. In particular, the ^{1}H NMR spectrum showed two mutually coupled aromatic proton doublets (δ_H 7.17, 6.82), indicating the presence of a para-disubstituted benzene, one NH doublet (δ_H 6.05), a putative methoxy group (δ_H 3.79), two *N*-methyl substituents (δ_H 2.71, 2.79) and a 9H methyl singlet (δ_H 0.89) characteristic of a *tert*-butyl group. However, HRTOFMS data suggested a molecular formula of $C_{46}H_{71}N_5O_8S$ ($[M + H]^+$ *m/z* 854.5074) for **1** and $C_{45}H_{69}N_5O_9S$ ($[M + H]^+$ *m/z* 856.4897) for **2**, which putatively

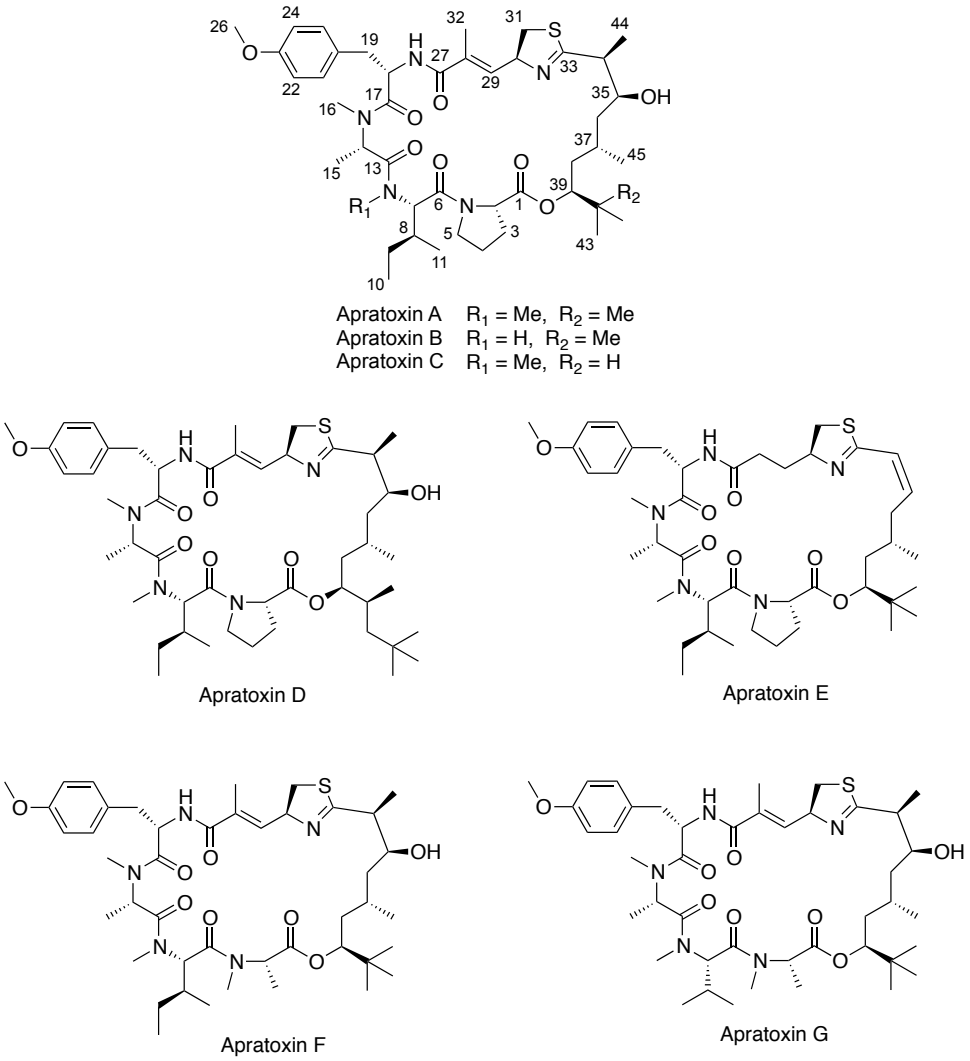

Figure 3.1. Apratoxins A–G.

differed from apratoxin A by a methylene and an oxygen atom, respectively. Furthermore, the HRMS data did not correspond to any of the known apratoxins (A–G; Figure 3.1), suggesting the isolation of two new apratoxin A analogues from the Red Sea *Moorea producens* strain. Analysis of the 2D NMR spectra (HSQC, HMBC, COSY, ROESY) for compounds **1** and **2** showed that **2** shared the same sequence of subunits as apratoxin A, while **1** possessed identical spin systems and planar

connectivities for the PKS moiety and four out of the five amino acid units of apratoxin A: *N*-Me-alanine (*N*-Me-Ala), modified cysteine (moCys), *N*-Me-isoleucine (*N*-Me-Ile) and *O*-methyl tyrosine (*O*-Me-Tyr). The HMBC and COSY experiments identified four contiguous methylene units within the final spin system of **1** (Table 3.1), attributable to the replacement of the proline residue in apratoxin A by pipecolic acid (Pip) in this new analogue designated apratoxin H (**1**).

Although compound **2** shares the planar connectivity of apratoxin A, examination of the 1D and 2D NMR data for **2** (Supporting Information, Table S-3.1) showed a significant downfield shift for the ^{13}C resonance of the methylene in the thiazoline (δ 57.0, C-31) relative to both **1** (δ 37.6, C-32) and apratoxin A (δ 37.6, C-31; Luesch et al., 2001), suggesting a heteroatom substitution or modification of the neighboring sulfur atom. The chemical shift of the equivalent C-2 carbon in an oxazoline is typically between 72.6 and 74.1 ppm (Ireland et al., 1982; Portmann et al., 2008). Thus, it is more likely that **2** contains an oxidized sulfur atom within the modified cysteine / thiazoline group, which is consistent with an increase of 16 mass units relative to apratoxin A. Therefore, we have assigned **2** as apratoxin A sulfoxide.

To further examine these closely related apratoxin analogues ESIMS^3 studies were performed. Analysis of the fragmentation patterns observed for compounds **1** and **2** relative to apratoxin A (Figure 3.2) shows that a pseudo c ion (*m*/*z* 725), resulting from ring opening at the ester linkage and loss of Pip/Pro, is present in compound **1** and apratoxin A. The subsequent loss of the polyketide subunit to leave a fragment of *m/*z 571 in compound **1** and apratoxin A, is followed by detection of a series of b ions due to loss of *N*-Me-Ile (*m*/*z* 444) and *N*-Me-Ala (*m*/*z* 359), which is consistent with previously reported cyclic peptide fragmentations that exhibit mostly b ions (W. Liu et al., 2009). Compound **2** yielded a minor fragmentation pattern that was identical to that of both **1** and apratoxin A, suggesting that compound **2** may share the same sequence as compound **1** and apratoxin A. However, the pseudo c ion in apratoxin A and **1** (Figure 3.2) was not observed for compound **2**. Instead, two major

Table 3.1. NMR Spectroscopic Data for Apratoxin H (**1**) in $CDCl_3$ (500 MHz).

unit	position	δ_C, mult.	δ_H, mult. (*J* in Hz)[a]	COSY	HMBC	ROESY
Pip	1	172.2, C	_			
	2	54.4, CH	4.60, dd (7.0, 3.6)	H-3a, H-3b	1, 3, 4, 6	H-3a, H-3b
	3a	25.7, CH_2	1.82, m	H-2, H-3b		H-2
	3b		2.03, m	H-2, H-3a	1, 5	H-2, H_3-42/43/44
	4a	19.2, CH_2	1.36, m	H-4b		H-4b
	4b		1.62, m	H-4a	1, 5	H-4a
	5a	24.3, CH_2	1.56, m	H-5a, H-6b		H-5b
	5b		1.82, m	H-5b, H-6b	6 (w)[c]	H-5a, H-6a
	6a	43.1, CH_2	3.50, m	H-5a, H-5b, H-6b	4 (w)[c], 5 (w)[c]	H-5b
	6b		4.35, m	H-6a	4, 5	H-8
N-Me-Ile	7	169.7, C	_			
	8	54.4, CH	5.48, d (11.5)	H-9	7, 9	H-6a, H_3-12, H_3-13
	9	31.8, CH	2.29, m	H-8, H-10b, H_3-12	11	H-10b, H_3-12, H_3-13
	10a	24.6, CH_2	0.99, m	H-9, H_3-11	8, 11, 12	H-10b, H-9
	10b		1.33, m	H-9, H_3-11		H-10a, H_3-13
	11	9.0, CH_3	0.91, ob	H-10b		
	12	14.5, CH_3	0.92, ob	H-9	8	H-8, H-9
	13	30.4, CH_3	2.71, s		8, 14	H-8, H-9, H-10b, H-15, H-19, OH
N-Me-Ala	14	169.6[b], C	_			
	15	60.8, CH	3.31, br m	H_3-16		H_3-13, H_3-17
	16	14.0, CH_3	1.25, d (6.7)	H-15	14, 15	H_3-17
	17	36.7, CH_3	2.79, s		15, 18	H-15, H_3-16, H-19, H-22/26
O-Me-Tyr	18	170.5, C	_			
	19	50.6, CH	5.06, ddd (10.9, 9.5, 4.8)	H-20a, H-20b, NH	18, 20, 21	H_3-17, H-20a, NH
	20a	37.3, CH_2	2.88, dd (-12.4, 4.8)	H-19, H-20b	18, 19, 21, 22/26	H-20b, H-22/26
	20b		3.14, dd (-12.4, 4.8)	H-19, H-20a	18, 19, 21, 22/26	H-20a, H-22/26
	21	128.3, C	_			
	22/26	130.6, CH	7.17, d (8.5)	H-23/25	22/26, 23/25, 24	H_3-17, H-19, H-20a, H-20b, H-23/25
	23/25	113.9, CH	6.82, d (8.6)	H-22/26	21, 23/25, 24	H-22/26, H_3-27
	24	158.7, C	_			
	27	55.3, CH_3	3.79, s		24	H-23/25
	NH		6.05, d (9.4)	H-19	28	H-19, H_3-33

Table 3.1 (continued). NMR Spectroscopic Data for Apratoxin H (**1**) in $CDCl_3$ (500 MHz).

unit	position	δ_C, mult.	δ_H, mult. (*J* in Hz)[a]	COSY	HMBC	ROESY
moCys	28	169.6[b], C	_			
	29	130.5, C	_			
	30	136.4, CH	6.36, br d (9.6)	H-31, H_3-33	28, 32, 33	H-31, H-32a, H-35
	31	72.6, CH	5.23, ddd (9.4, 9.1, 4.5)	H-30, H-32a, H-32b	29, 30	H-30, H-32b, H_3-33
	32a	37.6, CH_2	3.13, dd (-10.9, 4.7)	H-31, H-32b	29, 31, 34	H-30, H-32b
	32b		3.47, dd (-10.9, 8.7)	H-31, H-32a	30, 31, 34	H-31, H-32a
	33	13.4, CH_3	1.97, s	H-30	28, 29, 30, 31[d], 32	H-31, NH
polyketide	34	177.1, C	_			
	35	48.8, CH	2.65, ob	H-36, H_3-45	34, 36, 45	H-30, H-36, H-37b, H_3-45
	36	71.7, CH	3.56, dddd (10.9, 10.6, 10.4, 3.0)	H-35, H-37a, H-37b, OH		H-35, H_3-45, H_3-46
	37a	38.5, CH_2	1.11, ddd (-13.8, 10.9, 3.0)	H-36, H-37b, H-38	38	H-37b, H-38
	37b		1.46, ddd (-13.7, 11.1, 4.0)	H-36, H-37a	35, 36, 38, 46	H-35, H-37a, H-38, H-40
	38	24.5, CH	2.11, br m	H-37a, H-39a, H_3-46		H-37a, H-37b, H-39b, H_3-46, OH
	39a	37.8, CH_2	1.26, ob	H-38, H-39b, H-40	38	H-39b, H-40, H_3-42/43/44
	39b		1.79, m	H-39a, H-40	37, 38, 40	H-38, H-39a, H-40, H_3-42/43/44
	40	77.4, CH	4.90, dd (12.7, 2.2)	H-39a, H-39b	1, 39, 42/43/44	H-37b, H-39a, H-39b, H_3-42/43/44
	41	34.9, C	_			
	42/43/44	3 × 26.1, CH_3	3 × 0.89, s		40, 41, 42/43/44	H-3b, H-39a, H-39b, H-40
	45	16.7, CH_3	1.06, d (6.9)	H-35	34, 35, 36	H-35, H-36
	46	19.9, CH_3	1.01, d (6.7)	H-38	36[d], 37, 38, 39	H-36, H-38
	OH	_	4.40, d (10.9)	H-36	36	H_3-13, H-38

[a] *J* values obtained from ^1H spectrum recorded at 700 MHz. [b] These carbons have the same chemical shift. [c](w) indicates a weak correlation. [d] Four-bond HMBC correlation. ob = obscured.

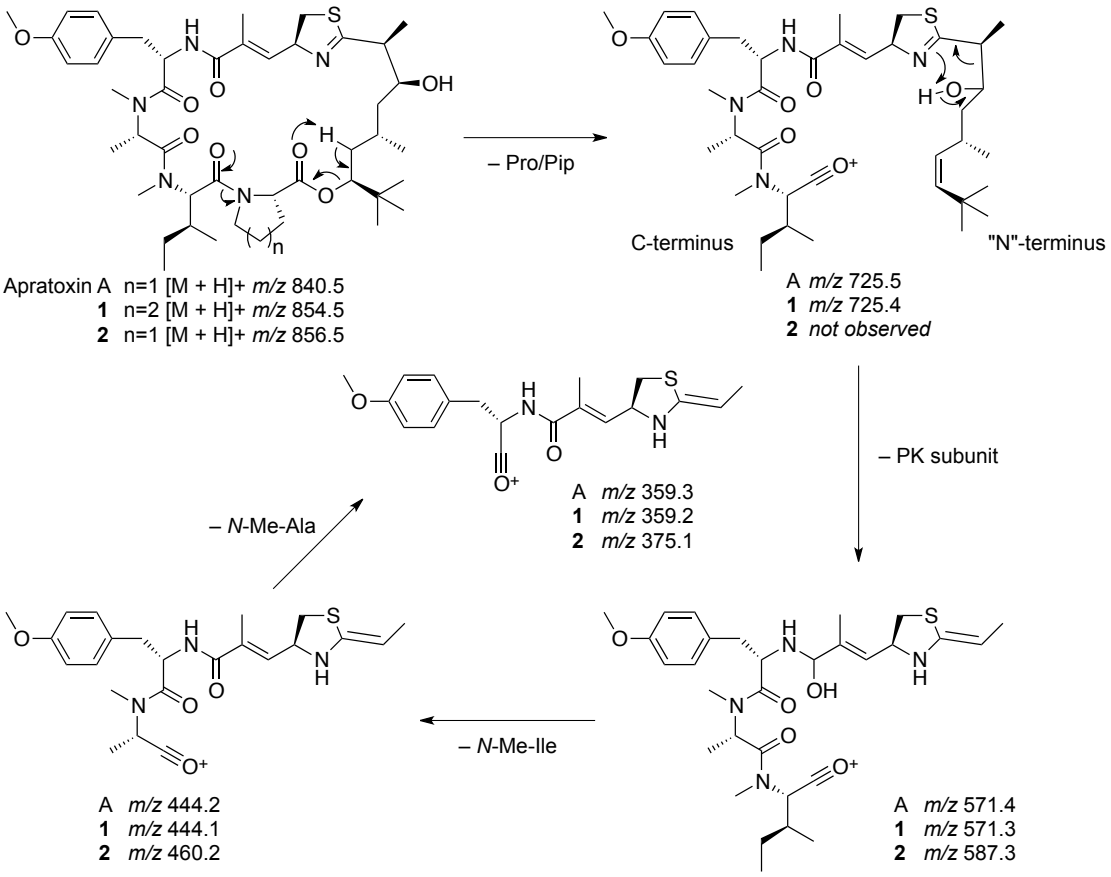

Figure 3.2. Schematic showing the fragmentation pattern of compounds **1** and **2** relative to the major MS^3 fragmentation pattern observed for apratoxin A.

fragmentation pathways were observed, resulting from ring opening and fragmentation of the thiazoline (Figure 3.3 A and B; Supporting Information, Figure S-3.18). A difference of 48 mass units (SO) between the two b ion series, coupled with an IR absorption at 1031 cm^{-1} (S=O stretching vibration), confirmed the presence of a sulfoxide group in **2**. For most cyclic peptides, fragmentation occurs following protonation of a peptide bond to open the macrocycle and give a linear form of the molecule with an acylium ion representing the C-terminus (Ngoka & Gross, 1999). However, in compound **2** it appears that oxidation of the thiazoline sulfur atom may

lead to an increase in ring strain and weakening of the carbon sulfur bond at C-33 due to the electron withdrawing properties of the oxygen atom.

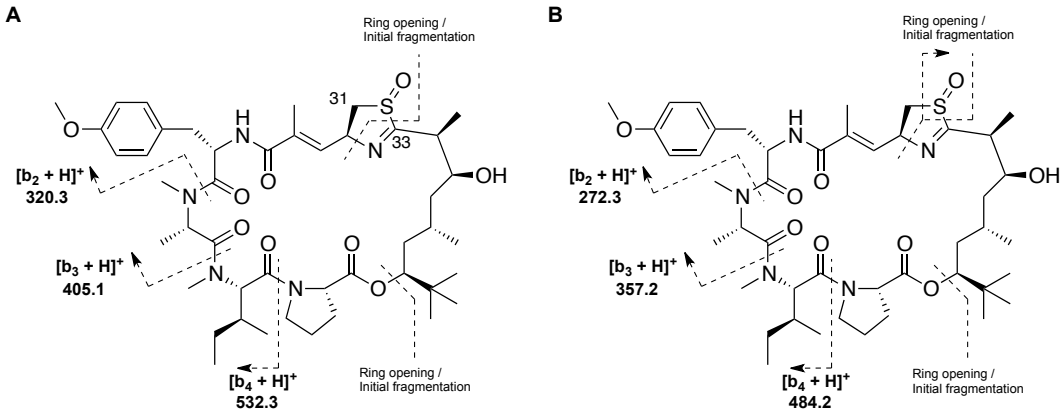

Figure 3.3. Assignment of MS^3 fragmentation data for compound apratoxin A sulfoxide (**2**).

The presence of a thiazoline sulfoxide moiety in a natural product is unprecedented in the literature. However, several prenylated quinones containing a rare 1,1-dioxo-1,4-thiazine ring (Figure 3.4, Ascidiathiazone A and B) have been reported from marine ascidians (Pearce et al., 2007). Additionally, there are numerous reports of methionine sulfoxide or sulfone residues of putative biosynthetic origin in natural products such as leinamycin from a *Streptomyces* sp. (Hara et al., 1989), dendroamide C from the epilithic cyanobacterium *Stigonema dendroideum* Fremy (Ogino et al., 1996), tenuecyclamide D isolated from a terrestrial cyanobacterium *Nostoc spongiaeforme* var. *tenue* (Banker & Carmeli, 1998), waiakeamide from the Indonesian sponge *Ircinia dendroides* (Mau et al., 1996), haligramide B from a *Haliclona nigra* sponge collected in Papua New Guinea (Rashid et al., 2000) and carriebowmide from the marine cyanobacterium "*Lyngbya*" *polychroa* (Figure 3.4; Gunasekera et al., 2008). Interestingly, Rashid et al. (2000) performed the oxidative conversion of haligramide A to waiakeamide in order to compare the overall stereostructures of the two compounds, which suggests that waiakeamide may in fact

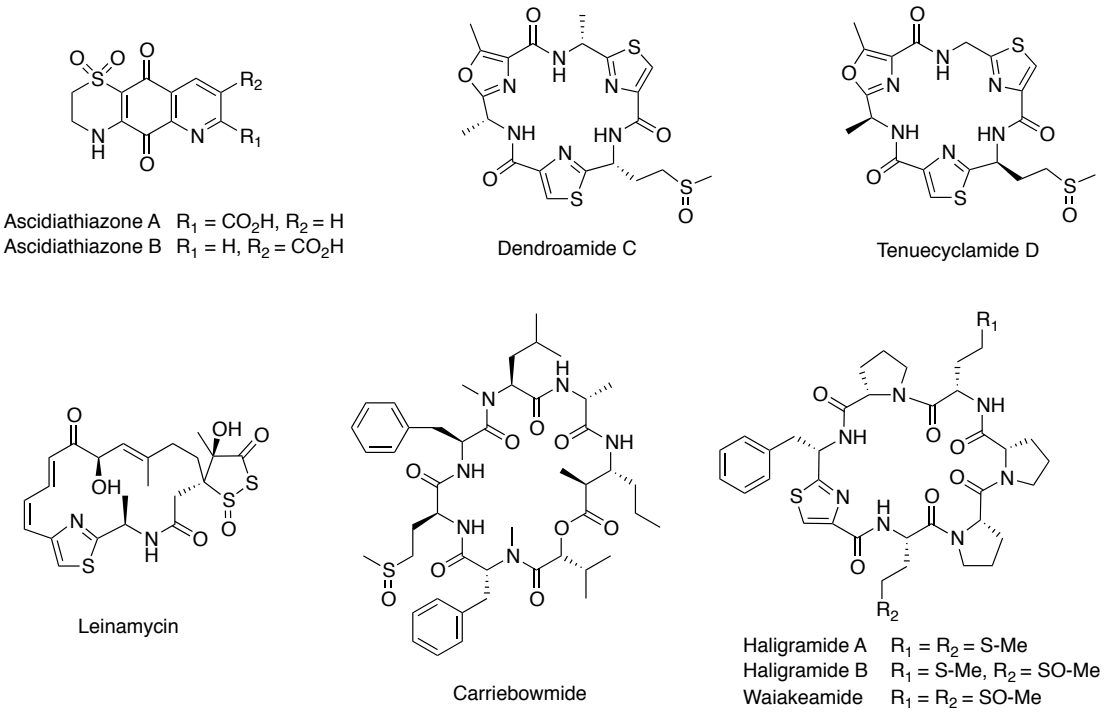

Figure 3.4. Marine natural products of putative biosynthetic origin containing oxidized sulfur atoms.

be an artifact rather than a natural product. However, Sera et al. (2003) later reported the isolation of a waiakeamide derivative containing a methionine-sulfoxide moiety along with a methionine-sulfone unit. Notably, the selective oxidation of the two methionine units within the haligramides was not observed by Rashid et al. (2000), suggesting that the waiakeamide sulfone analogue is not an artifact. In contrast, Baumann and colleagues (2007) report that the cyclic octapeptide planktocyclin undergoes oxidation of its methionine residue upon acidification of the HPLC eluents and during long term storage under atmospheric oxygen. Thus, it is possible that the sulfur atom of methionine-containing natural products undergoes oxidation under normal isolation and storage conditions.

To examine the possibility that apratoxin A was oxidized to compound **2** during the isolation process, apratoxin A was treated with 30% aqueous hydrogen peroxide

with and without acetic acid according to the methods of Rashid et al. (2000; Figure 3.5). Analysis of the reaction products of apratoxin A by RP_{18} HPLC-MS revealed the presence of apratoxin A and **3** (*m/z* $[M + H]^+$ 906.4; $[M + Na]^+$ 928.4; $[M – H + 2Na]^+$ 950.4; 1:1:1) in the ratio of 2.9:1 and 1.7:1 for treatments with and without acetic acid, respectively. A 1,1-dioxo- or 1-oxo thiazoline (**2**) was not detected in any of the HPLC-MS profiles, suggesting that the sulfur atom within the thiazoline is fully oxidized to cysteic acid under these reaction conditions. Noteworthy is that the haligramides contain a thiazole ring within their core structure that does not appear to undergo oxidation following treatment with acetic acid and 30% aqueous hydrogen peroxide for 6 h (Rashid et al., 2000). Although apratoxin A was unable to be oxidized to compound **2** under these reaction conditions, it is still possible that **2** was formed during the isolation process given that chlorinated solvents (CH_2Cl_2–MeOH, 2:1) become weakly acidic over time. In fact, *E*-dehydroapratoxin A (Figure 3.6) is a derivative that is presumed to form from the acid-catalyzed decomposition of apratoxin A in $CDCl_3$ (Luesch et al., 2002). However, *E*-dehydroapratoxin A was not detected within the fraction containing compound **2**. Alternatively, apratoxin A could undergo posttranslational modification within the cyanobacterium or through the actions of associated heterotrophic bacteria. The selective oxidation of a thiazoline moiety is intriguing and there is no evidence that **2** is an isolation artifact, particularly

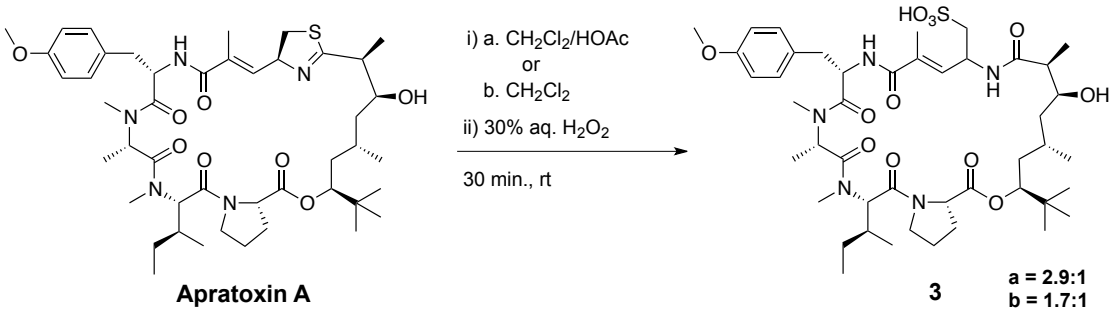

Figure 3.5. Oxidation of apratoxin A.

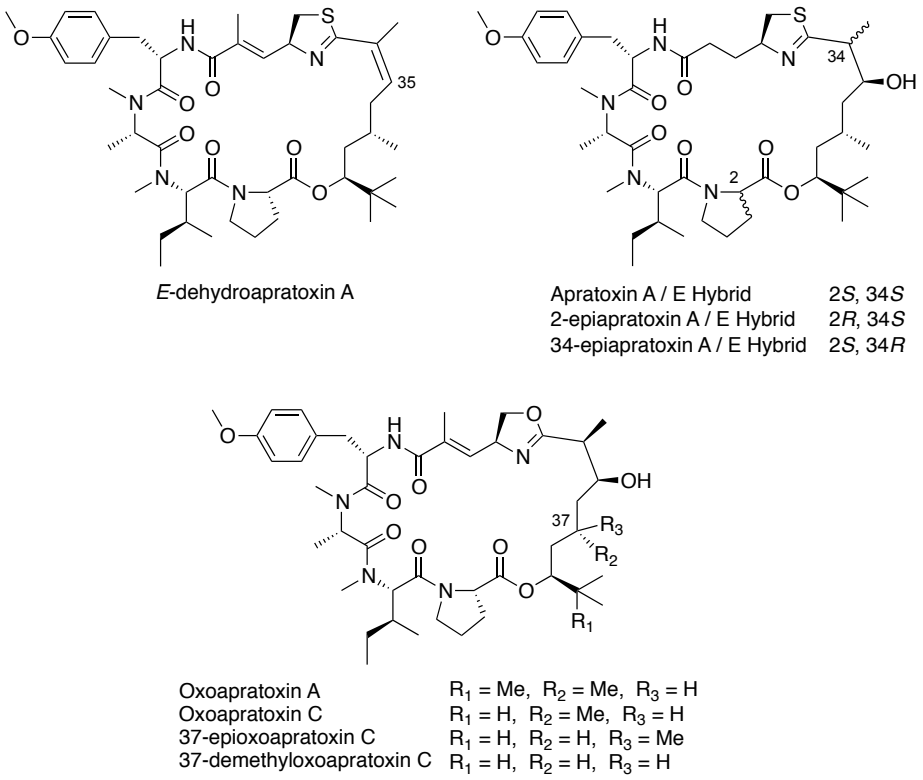

Figure 3.6. Semisynthetic apratoxin analogue *E*-dehydroapratoxin A (Luesch et al., 2002) along with the synthetic analogues of apratoxin A, apratoxin A/E hybrid (Chen et al., 2011) and oxoapratoxin A (Ma et al., 2006).

in the absence of any doubling of NMR chemical shifts that would suggest the presence of diastereomers generated by non-enzymatic oxidation. Further investigation of the function of some of the uncharacterized proteins within biosynthetic pathway of the apratoxins (Grindberg et al., 2011) may shed light onto their function and the possible biosynthetic origin of compound **2**.

The absolute configuration of the amino acid units within apratoxin H (**1**) and the sulfoxide analogue (**2**) were determined by RP_{18} HPLC-MS of the ozonolysis and acid hydrolysis products of **1** and **2** derivatized with *N*-α-(5-fluoro-2,4-dinitrophenyl-)-L-leucinamide (Marfey's reagent). Marfey's analysis indicated the presence of *N*-Me-L-Ala, D-Cya for an *S* configuration at the α-carbon, *N*-Me-L-Ile, *O*-Me-L-Tyr for **1** and

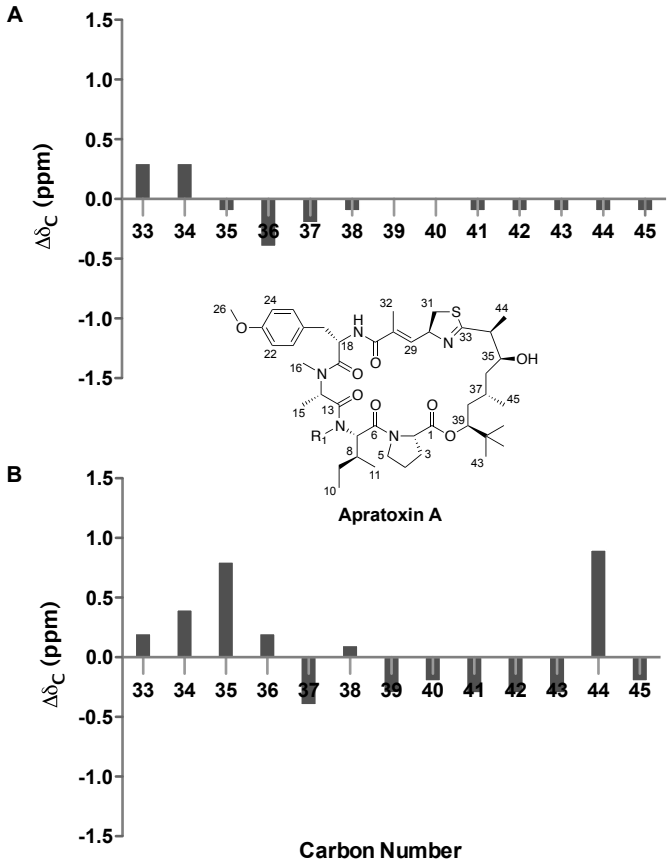

Figure 3.7. Differential ^{13}C NMR chemical shifts of the polyketide moiety in apratoxin A versus compounds **1** (**A**) and **2** (**B**).

2. Additionally, L-Pip was present in the hydrolysate of **1**, while **2** contained a corresponding L-Pro residue. The relative configuration of the polyketide moiety (C33–C45) of apratoxin H (**1**) was determined to be the same as in apratoxin A based on little to no variation in the ^{13}C NMR chemical shifts (Figure 3.7 A), which is consistent with the closely matching ^{1}H NMR shifts and coupling constants [Table 3.1 and (Luesch et al., 2001)]. Interestingly, the oxidized analogue (**2**) showed minor ^{13}C chemical shift variations (< 1 ppm) relative to apratoxin A for the C35 chiral center and CH_3-44 within the polyketide portion of the molecule (Figure 3.7 B), suggesting that oxidation of the sulfur atom alters the conformation of the thiazoline and adjacent carbon skeleton relative to apratoxin A. However, these chemical shift differences,

coupled with similar proton-proton coupling constants [Supporting Information, Table S-3.1 and (Luesch et al., 2001)] do not suggest a change in configuration at the C-34 and C-35 chiral centers. The overall stereostructure of apratoxin H (**1**) and apratoxin A were further compared by circular dichroism (CD), which produced nearly identical negative and positive Cotton effects (CEs) near 236 and 210 nm, respectively (Figure 3.8). However, the oxidized analogue (**2**) displayed a negative CE (ca. 236 nm) nearly 3–fold smaller than apratoxin A and H (**1**). This effect is likely caused by a slight change in the overall conformation of the structure due to the oxidation of the sulfur atom within the thiazoline moiety.

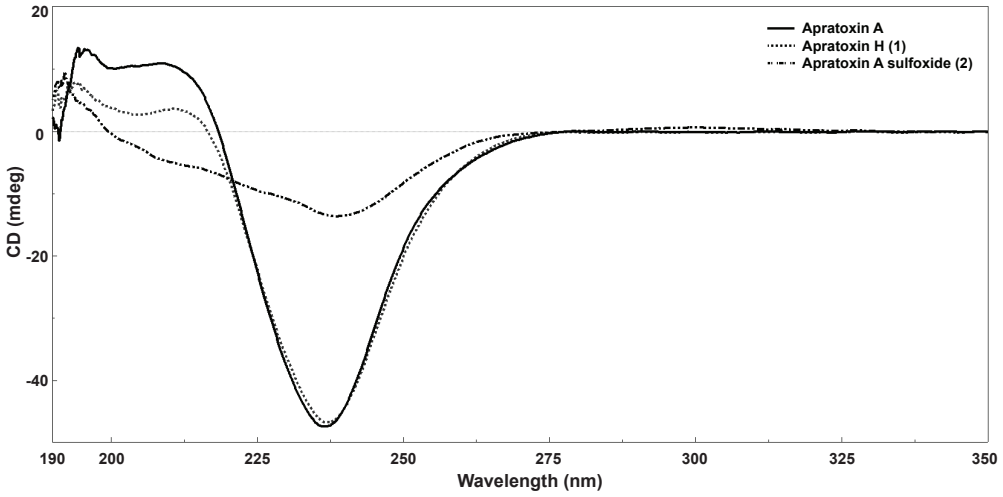

Figure 3.8. CD spectra of apratoxin A, H (**1**) and apratoxin A sulfoxide (**2**).

Apratoxin H (**1**) showed significant cytotoxicity to human NCI-H460 lung cancer cells (IC_{50} 3.4 nM), which is comparable to the results obtained for apratoxin A in this study (IC_{50} 2.5 nM; Supporting Information, Figure S-3.1). The small difference (~1.4-fold) in cytotoxicity between **1** and apratoxin A is consistent with the results obtained for the Pro to *N*-Me-Ala substitution present in apratoxin F (Tidgewell et al., 2010), indicating that this region of the molecule is not critical for activity (Figure

3.9). However, a Pro to *N*-Me-Ala substitution in combination with an *N*-Me-Ile to *N*-Me-Val exchange (apratoxin G) at the neighboring position results in a 7–fold reduction in activity (Tidgewell et al., 2010). Interestingly, a subsequent medicinal chemistry study focused on substitutions within the peptide portion of the apratoxin A scaffold reports a 62–fold decrease in activity against HCT116 colorectal carcinoma cells for an *N*-Me-Ile to *N*-Me-Ala substitution (AA4, Figure 3.9). In contrast, incorporation of *N*-Me-Val at AA4 does not affect cytotoxicity (Chen et al., 2011), suggesting that a more bulky hydrophobic group (i.e. Ile or Val) is required at this position (Figure 3.9).

The thiazoline S-oxidation product (**2**) showed a nearly 36–fold reduction in cytotoxicity against human NCI-H460 lung cancer cells (IC_{50} 89.9 nM), while a synthetic oxazoline analogue of apratoxin A (Figure 3.6) was only 4.4–fold less cytotoxic to HeLa cervical carcinoma cells than apratoxin A (Ma et al., 2006). Together, these results suggest that apratoxin cytotoxicity is sensitive to certain modifications of the moCys thiazoline unit (C27–C32). Remarkably, the synthetic apratoxin A/E hybrid (Figure 3.6), which lacks the allylic methyl group (C-32) and *α,β*-unsaturation (Δ 28), shows a 5.2–fold increase in potency against HCT116 colorectal carcinoma cells and less nonspecific, off-target effects. The latter is evidenced by greater *in vivo* tumor selectivity and a significant reduction of toxicity, which may stem from the inability to form conjugates with cellular nucleophiles following reduction of the Δ 28 double bond (Chen et al., 2011). Interestingly, the C-34 epimer of the apratoxin A/E hybrid (Figure 3.6) was equipotent (Chen et al., 2011), which suggests that the conformational flexibility observed in the upper portion of the polyketide moiety in compound **2** does not affect the activity. Thus, it is likely that a loss of pi bond characteristics in the thiazoline ring through resonance between the imino unsaturation and the sulfoxide group may play a more critical role in the loss of activity for this analogue. Similarly, replacement of the proline residue (AA5) in apratoxin A with the less rigid amino acid substituents present in apratoxin F and

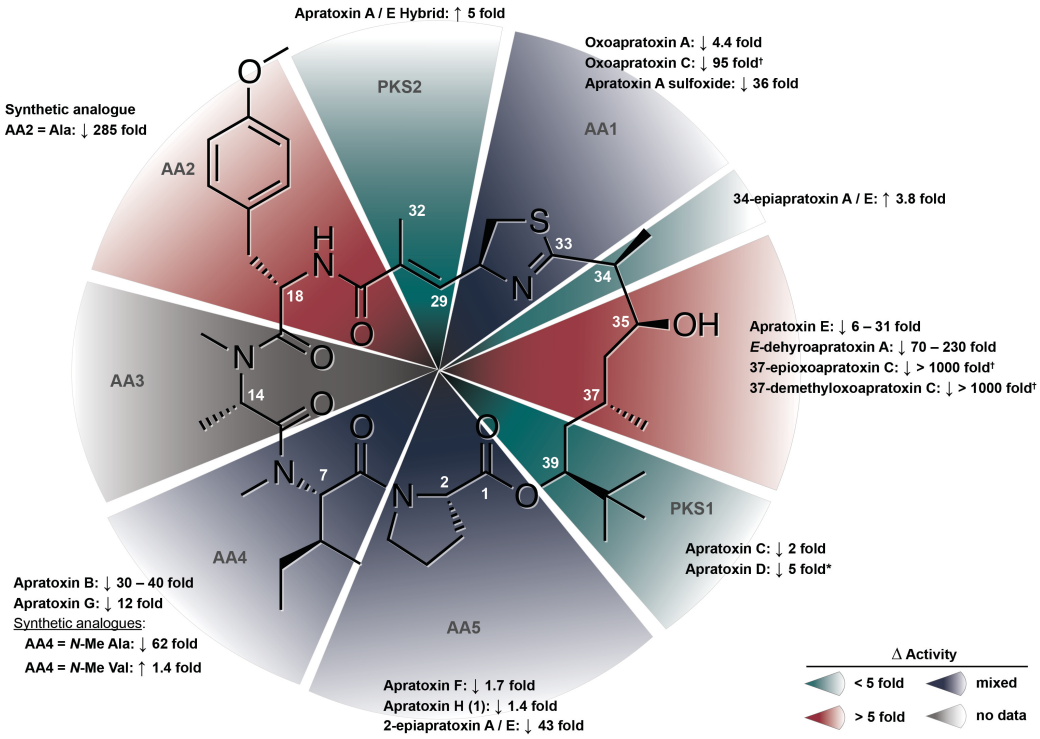

Figure 3.9. Structure-activity relationships (SAR) profile of the apratoxins modified from Tidgewell et al. (2010) to include cytotoxicity data for **1** and **2** relative to apratoxin A, and the reported analogues. Individual units within the core structure of apratoxin A are highlighted to show whether modifications significantly reduce activity (red), or show potency comparable with, or superior to, that of apratoxin A (green). * = indicates an indirect comparison across different cell lines. † = cytotoxicity relative to oxoapratoxin A.

compound **1** should afford greater conformational flexibility within the AA5 / *tert*-butyl region of the apratoxin scaffold, which does not seemingly affect their activity (Figure 3.9). However, in the apratoxin A/E hybrid, a change in the C-2 configuration of proline resulted in a 226–fold loss of cytotoxicity, suggesting that the overall stereostructure within this region of the molecule is critical for potent cytotoxicity (Chen et al., 2011). Thus, medicinal chemistry efforts focused on further modifications of the thiazoline and proline ring systems flanking the polyketide portion of the apratoxin scaffold may fine tune apratoxin selectivity and potency and greatly enhance

the SAR with respect to the overall geometry required for this highly cytotoxic molecule.

Apratoxins F, G and H (**1**) are the only naturally occurring apratoxin analogues containing amino acid substitutions, which may stem from relaxed substrate specificity within the adenylation domains of their respective biosynthetic enzymes. Coincidentally, the enzyme responsible for conversion of L-lysine to L-pipecolate in the biosynthesis of the immunosuppressants rapamycin and FK506 bears a close resemblance to ornithine cyclodeaminases, which convert L-ornithine to L-proline (Gatto et al., 2006). The ability of the final module of the apratoxin biosynthetic pathway to activate and incorporate L-lysine and L-pipecolate is therefore plausible. However, the incorporation of *N*-Me-Ala at this terminal position in apratoxin F and G likely results from changes to several of the critical binding pocket residues that mediate substrate specificity or the presence of multiple, cryptic adenylation (A) domains (Challis et al., 2000). Consistent with these observations, the recently annotated apratoxin biosynthetic gene cluster from an apratoxin-producing *Moorea bouillonii* cyanobacterium revealed that the final module contained two A-domains and a methyl transferase (MT; Grindberg et al., 2011). The presence of a MT in this module explains the incorporation of an *N*-methyl group in apratoxin F and G, but not the final alanine residue. Furthermore, this MT is likely not functional in the apratoxin A pathway due to the specificity for proline of the neighboring A-domain. Although the functionality of the second domain could not be predicted accurately due to the absence of the highly conserved active site residue lysine (Grindberg et al., 2011), it is likely that such a deletion accounts for the relaxed substrate specificity observed within this domain.

In an effort to characterize the evolutionary relationship of the apratoxin-producing strains of *Moorea* sp., which have been misidentified historically as *Lyngbya bouillonii*, *Lyngbya majuscula* and *Lyngbya sordida* (Engene et al., 2012), a phylogenetic analysis was performed utilizing the 16S rRNA gene (Figure 3.10).

Noteworthy is that Apratoxins A–C were isolated from collections of *Moorea* sp. made from Guam and Palau (Luesch et al., 2002; Luesch et al., 2001), while collections of *Moorea* sp. inhabiting Papua New Guinea (Gutiérrez et al., 2008) and Palmyra Atoll (Tidgewell et al., 2010) have afforded apratoxins A–D and apratoxins F and G, respectively (Figure 3.10). Collectively, these strains, coupled with our apratoxin-producing Red Sea *Moorea* sp., share 98.9% sequence homology within their SSU 16S rRNA gene, suggesting that these organisms are closely related species. Furthermore, this distinct cluster of *Moorea* spp. seemingly share a nearly identical biosynthetic pathway for the production of apratoxins, which is likely due to the presence of putative transposases flanking the boundaries of this biosynthetic cluster (Grindberg et al., 2011), leading to its mobility and horizontal gene transfer. Remarkably, however, the apratoxins have only been reported from *M. bouillonii*, and *M. producens*, suggesting that the successful horizontal gene transfer of this relatively large (57.4 kb) biosynthetic gene cluster has either not occurred outside of this clade, or has thus far evaded detection. Additionally, transposase genes were not detected between any of the genes within the biosynthetic cluster (Grindberg et al., 2011). Thus, many of the apratoxin analogues have likely resulted from the activation of several cryptic genes within the apratoxin biosynthetic pathway, which are likely regulated by environmental and epigenetic cues present within each organism's unique niche. Furthermore, temporal changes in the production of secondary metabolites are often observed for many marine microorganisms and invertebrates as a response to biotic interactions, or to preserve primary biological functions, both of which vary seasonally (Esquenazi et al., 2011; Humair et al., 2009; López-Legentil et al., 2006). Luesch and co-workers (2008) reported the differential production of apratoxin A and a new analogue, apratoxin E, based on the depth from which a Guamanian *Moorea bouillonii* cyanobacterium was collected, and the presence or absence of the closely associated red alpheid shrimp, *Alpheus frontalis*. In agreement with these observations, the Red Sea *Moorea producens* strain was grown in BG-11 medium that

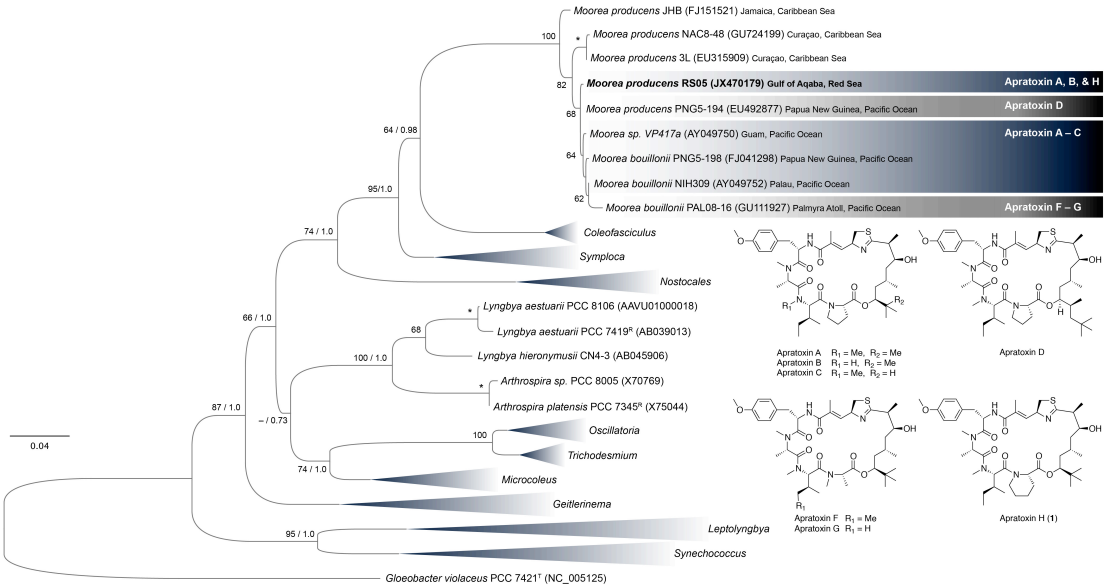

Figure 3.10. Phylogenetic relationship of the apratoxin-producing cyanobacteria with other marine filamentous cyanobacteria based on SSU (16S) rRNA gene sequences. Labels on the terminal nodes indicate the taxa, strain, GenBank accession numbers in parenthesis, and collection sites for relevant strains. Reference (^{R}) or type strains (^{T}) are included within each cyanobacterial group. The support values at important nodes are indicated as bootstrap and posterior probability for the maximum-likelihood (PhyML) and Bayesian inference (MrBayes) methods (* = bootstrap of > 98% and a posterior probability of 1.0). Support values < 60 are not indicated. The scale bar indicates 0.04 expected nucleotide substitutions per site.

had been modified to closely resemble the relatively extreme environmental conditions of the cyanobacterium's natural environment (pH 8.4 and salinity 41‰), which may have contributed to the production of the previously unreported apratoxin analogue, apratoxin H (**1**). Given the recent insights into the biosynthetic pathway of the apratoxins (Grindberg et al., 2011), it is remarkable that relatively few apratoxin analogues have been reported from research groups that have focused intently on apratoxin-producing strains of cyanobacteria. This may be due to different isolation schemes employed where these relatively minor analogues may be missed due to low abundance and/or complexity of the metabolite profile. Notably, additional apratoxin analogues were detected in our extracts of the cultured *Moorea producens* RS05

cyanobacterium. However, these minor components were not able to be purified in sufficient quantity. Thus, a more meticulous examination of extract components from this and other apratoxin-producing cyanobacteria collected with temporal and/or environmental variations in mind may reveal additional, more diverse apratoxin analogues.

Experimental

General Experimental Procedures. Optical rotations were measured on a JASCO P-1010 polarimeter. UV spectra and CD measurements were recorded using a JASCO J-815 spectropolarimeter. IR spectra were recorded on a Thermo Scientific Nicolet IR100 FT-IR Spectrometer. NMR data were acquired in $CDCl_3$ referenced to residual $CHCl_3$ chemical shifts (δ_C 77.2, δ_H 7.26) on a Bruker Avance III 700 MHz spectrometer equipped with a 5mm ^{13}C cryogenic probe for compound **2**. NMR data for **1** were acquired in $CDCl_3$ on a Bruker Avance III 500 MHz spectrometer equipped with a 5 mm TXI probe. High-resolution mass spectrometry was performed in positive ion mode on an AB SCIEX Triple TOF 5600 mass spectrometer. LC-ESIMS^3 data were obtained on an AB SCIEX 3200 Q TRAP mass spectrometer. HPLC was performed using a Shimadzu dual LC-20AD solvent delivery system with a Shimadzu SPD-M20A UV/VIS photodiode array detector.

Collection, Isolation and Culture of the Red Sea *Moorea producens* strain RS05. A dark brown filamentous assemblage of cyanobacteria was collected by hand using snorkel from the Nabq Mangroves (1 – 5 ft) in the Gulf of Aqaba near Sharm el-Sheikh, Egypt (N 27° 21.146' E 33° 54.472') on May 31, 2007 (collection code Nabq-4). Cyanobacterial isolation, morphological characterization and culturing was performed as described previously (Thornburg et al., 2011).

DNA Extraction, Amplification of Cyanobacterial 16S rRNA. Genomic DNA was extracted and amplified by polymerase chain reactions (PCR) as previously described (Thornburg et al., 2011). The 16S rRNA partial gene sequences were inspected visually and assembled using CAP3 (Huang & Madan, 1999). The resulting contig was analyzed for chimeric sequences using Pintail (Ashelford et al., 2005) and compared to sequences in the Ribosomal Database Project database (http://rdp.cme.msu.edu) and GenBank (http://www.ncbi.nlm.nih.gov). The consensus sequence was deposited in GenBank under accession number JX470179.

Phylogenetic Analysis. The evolutionary relationship of the Red Sea *Moorea producens* strain with other groups of cyanobacteria was determined as described in Chapter Two of this thesis.

Extraction and Isolation of Compounds 1, 2, Apratoxin A and Lyngbyabellin B. Culture collections of *Moorea producens* RS05 (30 × 1.5 L cultures) grown over a span of two years yielded 1.32 g organic extract (CH_2Cl_2-MeOH, 2:1). The organic extract was subjected to bioassay-guided fractionation via NP VLC using a stepped solvent gradient of hexanes to EtOAc to MeOH to produce nine fractions (A – I). The fractions eluting with 20% EtOAc – hexanes (fraction F) and 100% EtOAc (fraction G) showed potent toxicity to brine shrimp and were further separated C_{18} reversed-phase (RP_{18}) solid phase extraction (SPE) using a stepped solvent gradient from 60% MeOH-H_2O to 100% MeOH, followed by 100% CH_2Cl_2. Isocratic RP-HPLC (column: Synergi Fusion-RP, 10 x 250 mm, 90% MeOH-H_2O, 3.5 mL/min) of the SPE fractions eluting in 80% MeOH-H_2O for fraction F and G yielded lyngbyabellin B (4.6 mg, t_R = 5.9 min.) and three impure compounds from each fraction with matching UV profiles and retention times. Corresponding peaks were combined from each fraction and targeted for further purification by RP HPLC (Synergi Max, 4.6 x 250 mm) with 80% MeOH-H_2O (0.8 mL/min), yielding **2** (0.9 mg, t_R = 14.1 min.), or 90% MeOH-H_2O (0.7 mL/min), yielding apratoxin A (41.0 mg, t_R = 9.3 min.) and **1** (3.5 mg, t_R = 10.8 min). LC-MS profiling (Synergi Fusion-RP, 2 x 100 mm, 0.2 mL/min, linear gradient of 65 to 100% MeCN in 0.1% (v/v) aqueous TFA) of fraction F also showed an $[M + H]^+$ *m/z* 665/667/669 (100:75:20) ion cluster and $[M + H]^+$ *m/z* 826.2, suggesting a trace amount of hectochlorin and apratoxin B/C, respectively.

Apratoxin H (1): white, amorphous solid; $[\alpha]^{30}_D$ –207 (*c* 0.10, MeOH); UV (MeOH) λ_{max} (log ε) 195 (4.85), 226 (4.45), 284 (3.23); FTIR (neat) ν_{max} 3428 (br), 2962, 2934, 2874, 1738, 1626, 1512, 1456, 1385, 1280, 1247, 1180, 1074 cm^{-1}; ^1H and ^{13}C NMR data, see Table 3.1; HRTOFMS *m/z* 876.5041 $[M + Na]^+$ (calcd for

$C_{46}H_{71}N_5O_8SNa$, 876.4921), *m/z* 854.5074 $[M + H]^+$ (calcd for $C_{46}H_{72}N_5O_8S$, 854.5102).

Apratoxin A sulfoxide (2): white, amorphous solid; $[\alpha]^{30}_D$ –94 (*c* 0.10, MeOH); UV (MeOH) λ_{max} (log ε) 193 (4.67), 226 (4.26), 284 (3.14); FTIR (neat) ν_{max} 3402 (br), 2964, 2932, 2872, 1740, 1626, 1512, 1453, 1384, 1277, 1247, 1178, 1072, 1031 cm^{-1}; ^1H and ^{13}C NMR data, see Supporting Information (Table S-3.1); HRTOFMS *m/z* 856.4897 $[M + H]^+$ (calcd for $C_{45}H_{70}N_5O_9S$, 856.4894).

Apratoxin A: white, amorphous solid; $[\alpha]^{30}_D$ –198 (*c* 0.10, MeOH); UV (MeOH) λ_{max} (log ε) 193 (4.97), 226 (4.41), 269 (3.92); FTIR (neat) ν_{max} 3422 (br), 2965, 2933, 2876, 1742, 1625, 1512, 1456, 1385, 1277, 1248, 1180, 1074 cm^{-1}; ^1H and ^{13}C NMR data, see Supporting Information (Figures S-3.14 and S-3.15); HRTOFMS *m/z* 862.4666 $[M + Na]^+$ (calcd for $C_{45}H_{69}N_5O_8SNa$, 862.4764), *m/z* 840.4927 $[M + H]^+$ (calcd for $C_{45}H_{70}N_5O_8S$, 840.4945).

Lyngbyabellin B: white, amorphous solid; $[\alpha]^{30}_D$ –135 (*c* 0.10, MeOH); UV (MeOH) λ_{max} (log ε) 196 (4.48), 240 (3.98); HRTOFMS *m/z* 679.1775 $[M + H]^+$ (calcd for $C_{28}H_{41}Cl_2N_4O_7S_2$, 679.1794).

Absolute Configuration of Apratoxin H (1) and Apratoxin A sulfoxide (2). The amino acid standards relevant to compounds **1** and **2** were obtained commercially and prepared as 50 mM solutions in H_2O. Each standard was then derivatized for Marfey's analysis by adding 1 M $NaHCO_3$ (10 μL) and *N*-α-(5-fluoro-2,4-dinitrophenyl-)-L-leucinamide (L-FDLA or D-FDLA, 1% w/v in acetone, 50 μL) to 25 μL of each standard solution. The mixture was heated at 40 °C for 1 h with continuous stirring, cooled to room temperature, acidified with 2N HCl (5 μL), evaporated to dryness and resuspended in 1:1 MeCN-H_2O (250 μL).

Approximately 0.4 mg of **1** and 0.2 mg of **2** were dissolved separately in 3 mL CH_2Cl_2 (-78 °C). Ozone was then bubbled through each solution for 15 min. The solution was dried under a stream of N_2 gas, followed by an oxidative workup of the residue (0.6 mL of H_2O_2-HCOOH 1:2 at 70 °C for 20 min). The oxidation product was

concentrated under vacuum and hydrolyzed with 6N HCl (1 mL) in an Ace high-pressure tube, 1200W microwave for 50 s and immediately cooled to 0 °C and evaporated to dryness. The hydrolyzed products were resuspended in 50 μL MeCN:H_2O (1:10) and derivatized for Marfey's analysis in a similar manner to the derivatized chromatographic standards. The Marfey's products of **1** and **2** were resuspended in 1:1 MeCN-H_2O (100 μL) and analyzed by LC-MS (Kinetex XB-C_{18} 110A, 4.6 x 100 mm, 2.6 μm, 1.5 mL/min, UV and ESIMS detection, 340 nm and negative ion mode, respectively) using a linear gradient of 30 to 70% MeCN (containing 0.1% [v/v] formic acid) and 0.1% (v/v) formic acid in H_2O over 15 min. The retention time (t_R min, base peak *m/z*) of the residues in the hydrolysate of **1** matched standards for *N*-Me-L-Ala (5.29, 396.2), D-Cya (2.12, 462.1), *N*-Me-L-Ile (7.88, 438.2), L-Pip (7.10, 422.3) and *O*-Me-L-Tyr (7.20, 488.3). The retention times for the residues in the hydrolysate of **2** were consistent with the results for **1**, with the exception of an L-Pro (4.54, 408.2) standard rather than L-Pip matching the corresponding residue in the hydrolysate of **2**. The retention times (t_R min, base peak *m/z*) of the other amino acid standards analyzed were: *N*-Me-D-Ala (5.49, 396.2), L-Cya (2.22, 462.1), *N*-Me-D-Ile (9.48, 438.2), *N*-Me-L-*allo*-Ile (8.03, 438.2), *N*-Me-D-*allo*-Ile (9.58, 438.2), D-Pip (6.56, 422.3), D-Pro (5.92, 408.2) and *O*-Me-D-Tyr (8.78, 488.3).

Biological Assays. Cytotoxicity of the organic extract and crude fractions was evaluated against brine shrimp (*Artemia salina*) as previously described (Carballo et al., 2002; McLaughlin et al., 1998) with some modifications. Samples were added to 24-well plates containing newly hatched (24 h) brine shrimp (10 to 15 per well) in artificial seawater at final concentrations ranging from 1 to 100 ppm. Brine shrimp toxicity was determined after a 24 h incubation period (28 °C) by counting the number of dead shrimp verses total number in each well.

Cytotoxicity of the purified compounds was evaluated in human NCI-H460 lung cancer cells (ATCC, Manassas, VA) as previously described (Thornburg et al., 2011),

with minor modifications. Cells were seeded into 96-well plates (6,000 cells per well) in 50 μL of medium 12 h before treatment. Approximately 2 h before treatment, test samples were generated from a stock solution (6 mg/mL, 100% DMSO) that was serially diluted in serum-free medium. Following aspiration of seed growth medium, test samples (50 μL) were added to seeded cells at final concentrations ranging from 0.00595 nM to 17.85 μM. Each 96-well plate also contained untreated and vehicle-treated control cells. Cell viability was determined after 48 h treatment using a standard 3-(4,5-dimethylthiazol-2-yl)-2,5,diphenyly tetrazolium bromide (MTT) assay as previously described (Thornburg et al., 2011). The cytotoxicity of each purified compound was assessed in at least three independent cultures with the viability of vehicle-treated control cells defined as 100% in all experiments. Dose response curves were plotted using GraphPad Prism® (v5.0) and IC_{50} values were derived from nonlinear regression analysis.

Acknowledgement

We thank the Red Sea Protectorate for permission to make collections of Red Sea cyanobacteria, and Brian Arbogast and Jeff Morré of the Environmental Health Sciences Center at OSU for mass spectrometric data acquisition (NIEHS P30 ES00210). The National Science Foundation (CHE-0722319) and the Murdock Charitable Trust (2005265) are acknowledged for their support of the OSU Natural Products and Small Molecule Nuclear Magnetic Resonance. Funding was provided by the OSU College of Pharmacy.

Supporting Information

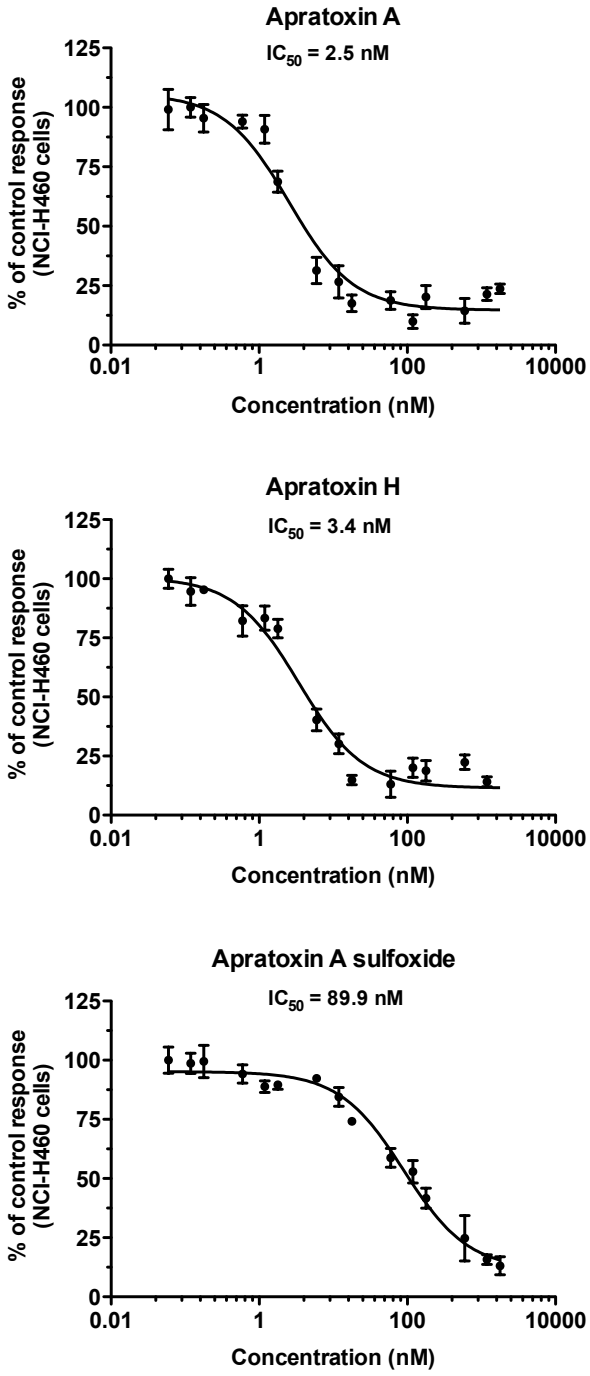

Figure S-3.1. Dose-response curves of apratoxin A, apratoxin H (**1**) and the oxidized apratoxin A analogue (**2**) in the human NCI-H460 lung cancer cell line (n = 3). Cell viability was assessed after 48 hours using a colorimetric MTT cell viability assay and is reported as the percentage of viable cells relative to the vehicle control.

Table S-3.1. NMR Spectroscopic Data for Apratoxin A sulfoxide (**2**) in $CDCl_3$ (700 MHz).

unit	position	δ_C, mult.	δ_H, mult. (*J* in Hz)[a]	COSY	HMBC	ROESY
Pro	1	172.6, C				
	2	59.8, CH	4.22, br t (7.4)	H-3a, H-3b	1, 3	H-3a, H-3b, H-4b
	3a	29.5, CH_2	1.90, m	H-2, H-3b	1, 4	H-2
	3b		2.26, m	H-2, H-3a	1, 4, 5	H-2
	4a	25.7, CH_2	1.92, m	H-5a, H-5b		H-5b
	4b		2.06, m	H-5a, H-5b	2, 3	H-2, H-5b
	5a	48.0, CH_2	3.69, m	H-4a, H-4b, H-5b	3, 4	H-5b, H-7
	5b		4.18, m	H-4a, H-4b, H-5a	3, 4	H-4a, H-4b, H-5a, H-7
N-Me-Ile	6	170.5, C				
	7	57.3, CH	5.23, d (11.5)	H-8	6, 8	H-5a, H-5b, H-8, H_3-12
	8	32.2, CH	2.18, m	H-7 H_3-11	11	H-7, H_3-11, H_3-12
	9a	25.0, CH_2	0.99, m	H-9b	10, 11	H-9b
	9b		1.36, m	H-9a, H_3-10		H-9a, H_3-10
	10	9.6, CH_3	0.95, d (7.5)	H-9b	8, 9	H-9b
	11	14.5, CH_3	0.97, d (7.3)	H-8	7, 8, 9	H-8
	12	30.5, CH_3	2.66, s		7, 13	H-7, H-8, H-14, H-29, OH
N-Me-Ala	13	170.2, C				
	14	60.8, CH	3.31, m	H_3-15	13, 15	H_3-12, H_3-15, H_3-16
	15	14.1, CH_3	1.23, d (6.6)	H-14	13, 14	H-14, H_3-16
	16	36.9, CH_3	2.82, s		14, 17	H-14, H-18, H_3-15, OH
O-Me-Tyr	17	170.5, C				
	18	50.8, CH	5.05, m	H-19a, H-19b, NH	17, 19	H_3-16, H-19a, H-19b, H-21/25, NH
	19a	37.2, CH_2	2.88, dd (-12.5, 4.5)	H-18, H-19b	17, 18, 20, 21/25	H-18, H-19b
	19b		3.14, m	H-18, H-19a	17, 18, 20, 21/25	H-18, H-19a, NH
	20	128.4, C				
	21/25	130.8, CH	7.17, d (8.5)	H-22/24	19, 21/25, 22/24, 23	H-18, H_3-26
	22/24	114.1, CH	6.80, d (8.5)	H-21/25	20, 22/24, 23	H_3-26
	23	158.9, C				
	26	55.5, CH_3	3.79, s		23	H-21/25, H-22/24
	NH		6.05, d (9.5)	H-18	27	H-18, H-19b, H_3-32

Table S-3.1 (continued). NMR Spectroscopic Data for Apratoxin A sulfoxide(**2**) in $CDCl_3$ (700 MHz).

unit	position	δ_C, mult.	δ_H, mult. (*J* in Hz)[a]	COSY	HMBC	ROESY
moCys	27	169.5, C				
	28	133.8, C				
	29	135.0	5.90, d (9.9)	H-30, H_3-32	27, 30, 31, 32	H_3-12, H-30, H-31a, H-32
	30	71.8, CH	5.70, m	H-29, H-31a, H-31b	28, 29, 31, 33	H-29, H-31a, H-31b
	31a	57.0, CH_2	2.78, dd (-13.9, 5.7)	H-30, H-31b	29, 30, 33	H-29, H-30, H-31b
	31b		3.32, dd (-14.0, 5.9)	H-31a	29, 33	H-30, H-31a
	32	13.6, CH_3	2.0, s	H-29	27, 28, 29	H-29, H-30, NH
polyketide	33	177.2, C				
	34	48.7, CH	2.84, dq (10.5, 7.0)	H-35, H_3-44	33, 35, 44	H-35, H-36b, H_3-44, OH
	35	70.8, CH	3.89, dddd (11.1, 10.8, 10.5, 3.5)	H-34, H-36a, H-36b, OH		H-34, H-36a H_3-44, H_3-45, OH
	36a	37.9, CH_2	1.24, m	H-35, H-36b, H-37	38	H-35, H-36b
	36b		1.61, m	H-35, H-36a, H-37	34, 36, 45	H-34, H-36a, H-39, OH
	37	24.7, CH	2.12, m	H-36a, H-36b, H-38b, H_3-45		H-39, H_3-45
	38a	37.6, CH_2	1.31, ob	H-38b, H-39	37	H-38b, H-39
	38b		1.82, m	H-37, H-38a	36	H-38a, H-39
	39	77.7, CH	4.98, dd (12.6, 2.2)	H-38a	1, 40, 41/42/43	H-36b, H-37, H-38a, H-38b, H_3-41/42/43
	40	35.1, C				
	41/42/43	3 × 26.3, CH_3	3 × 0.89, s		39, 40, 41/42/43	H-39
	44	15.7, CH_3	1.35, d (7.0)	H-34	33, 34, 35	H-34, H-35
	45	20.0, CH_3	1.01, d (6.5)	H-37	37, 38	H-35, H-37
	OH		4.65, d (11.5)	H-35	35	H_3-12, H_3-16, H-34, H-35, H-36b, H-37

ob = obscured.

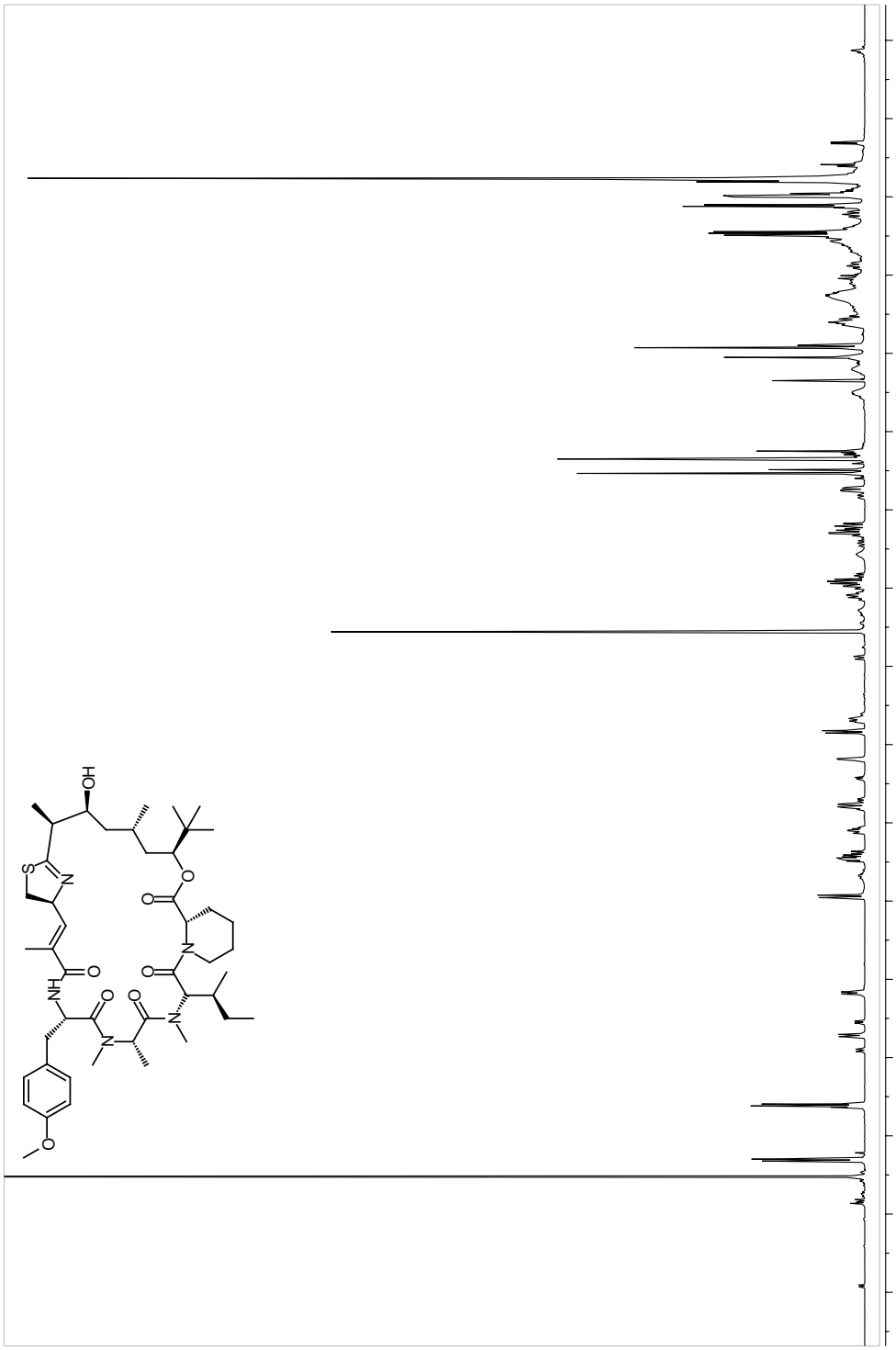

Figure S-3.2. ^{1}H NMR spectrum for apratoxin H (**1**) in $CDCl_3$ (700 MHz).

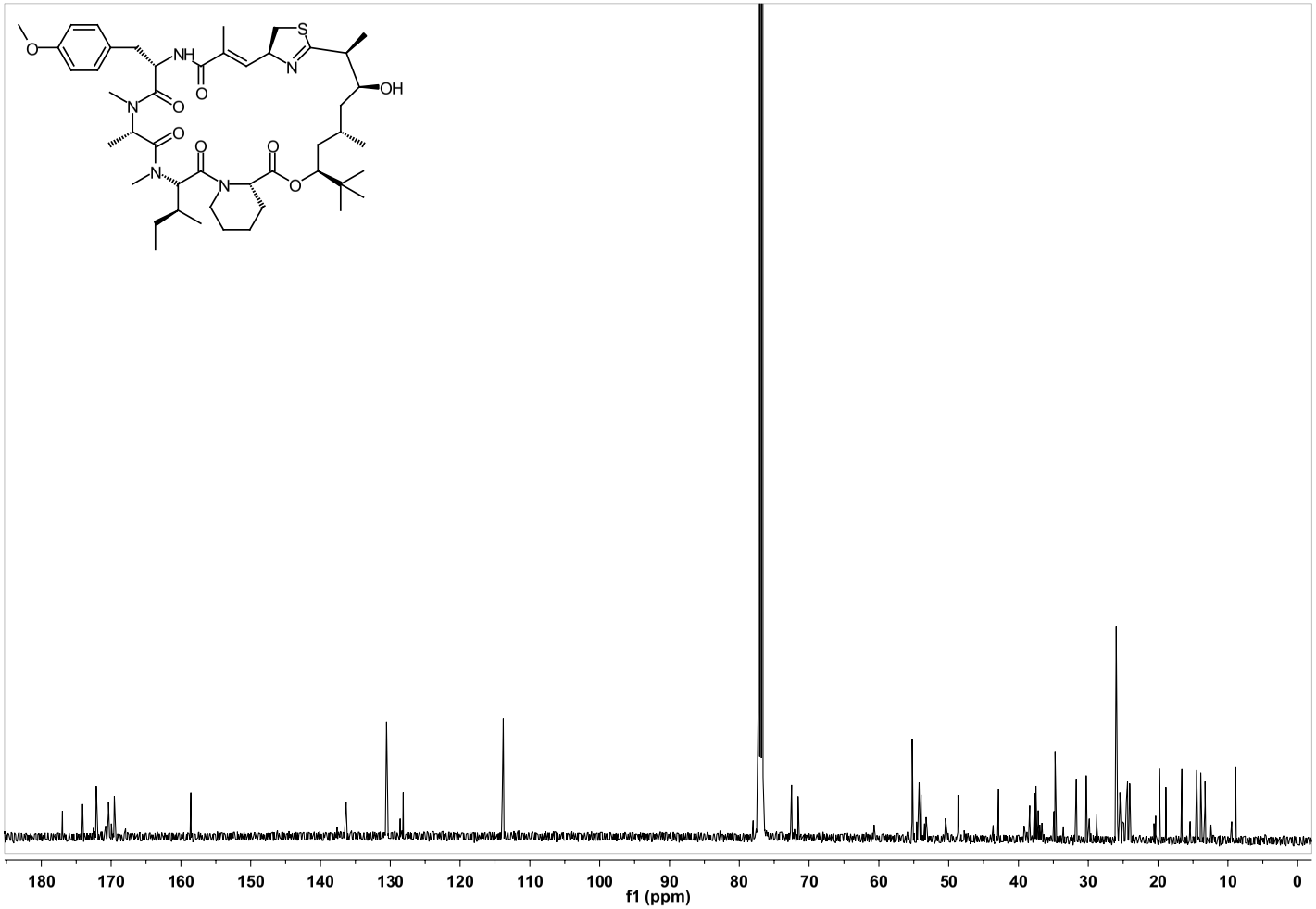

Figure S-3.3. ^{13}C NMR spectrum for apratoxin H (**1**) in $CDCl_3$ (125 MHz).

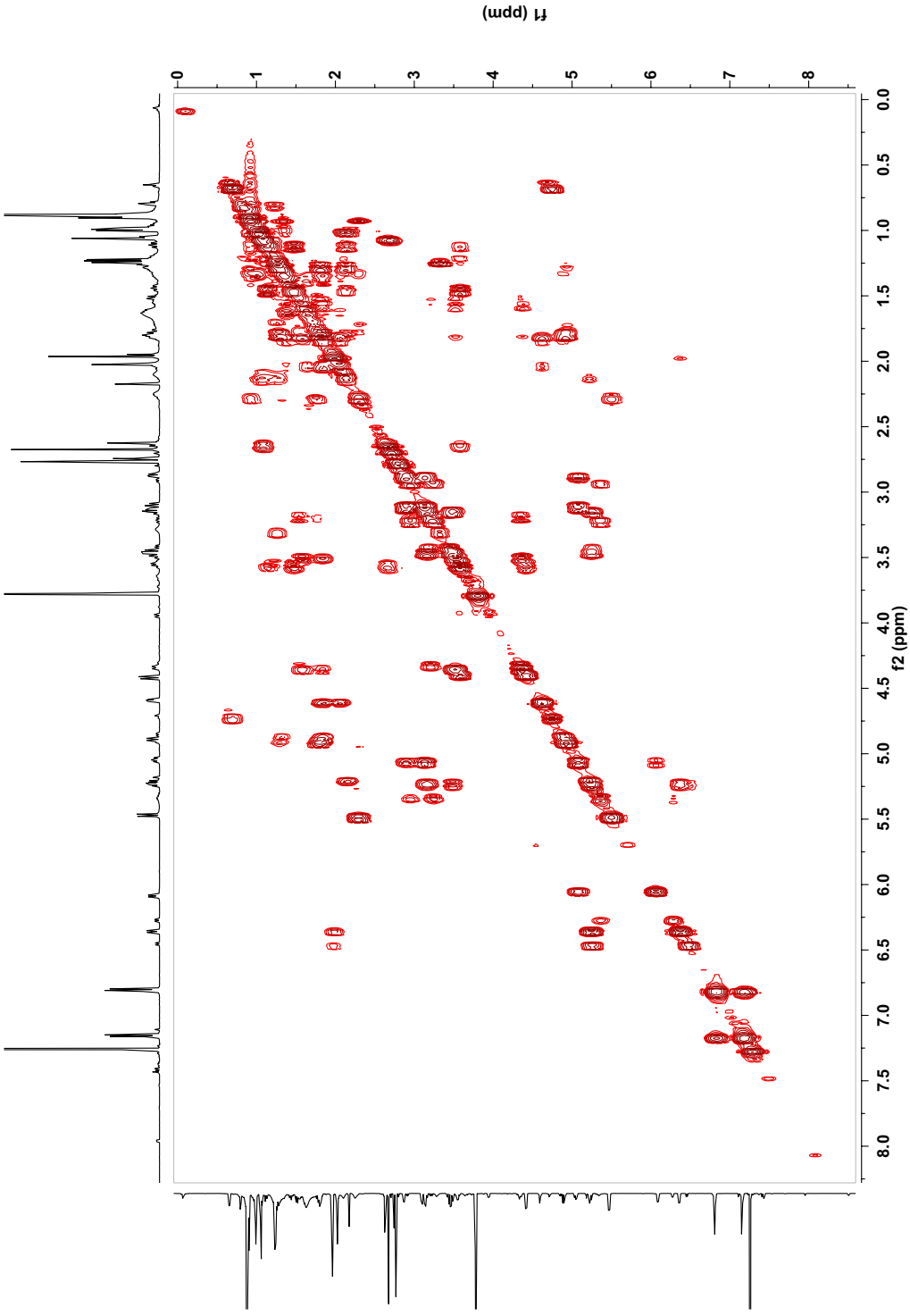

Figure S-3.4. DQF COSY spectrum for apratoxin H (**1**) in $CDCl_3$ (500 MHz).

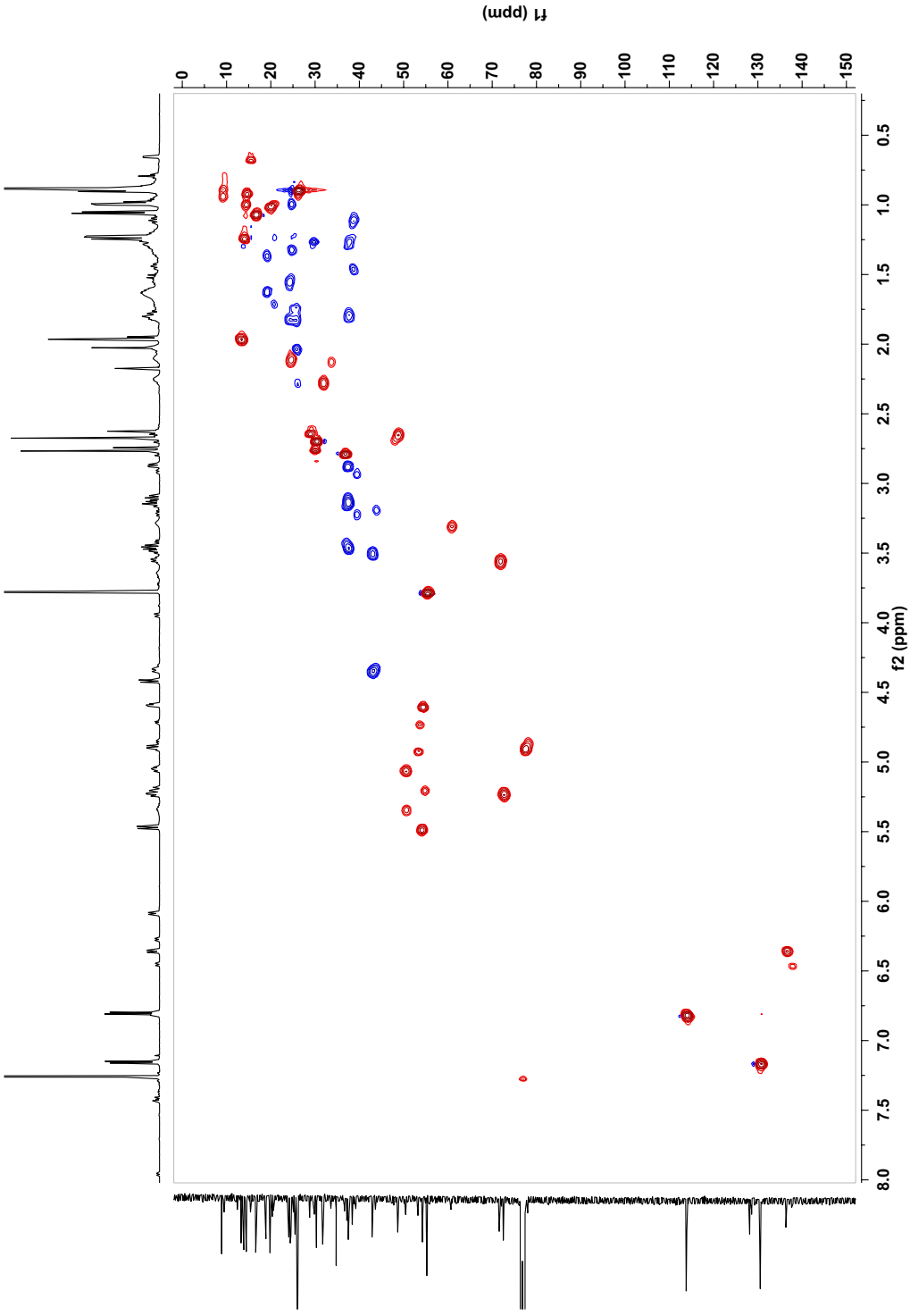

Figure S-3.5. Multiplicity-edited HSQC spectrum for apratoxin H (**1**) in $CDCl_3$ (500 MHz).

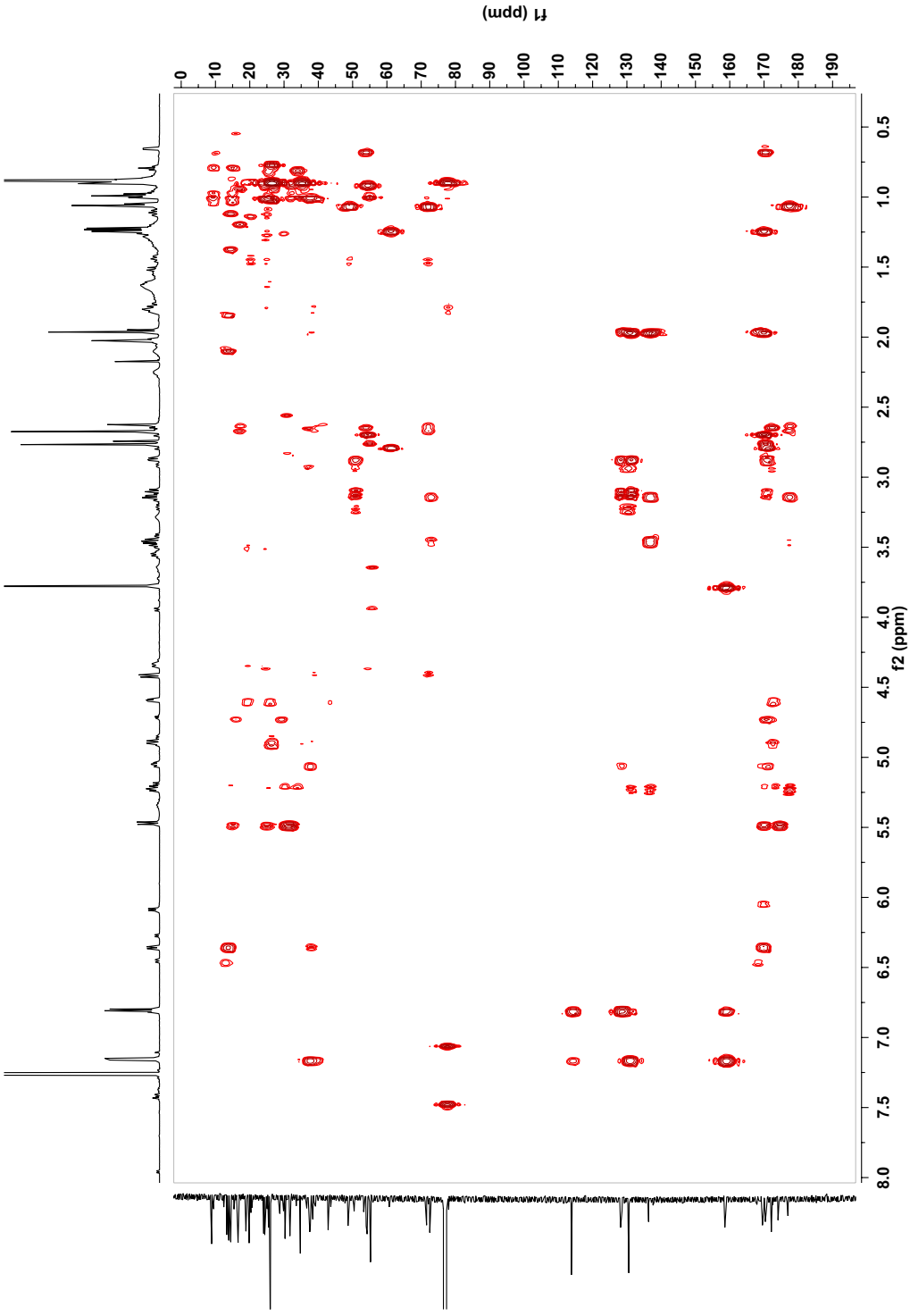

Figure S-3.6. HMBC spectrum for apratoxin H (**1**) in $CDCl_3$ (500 MHz).

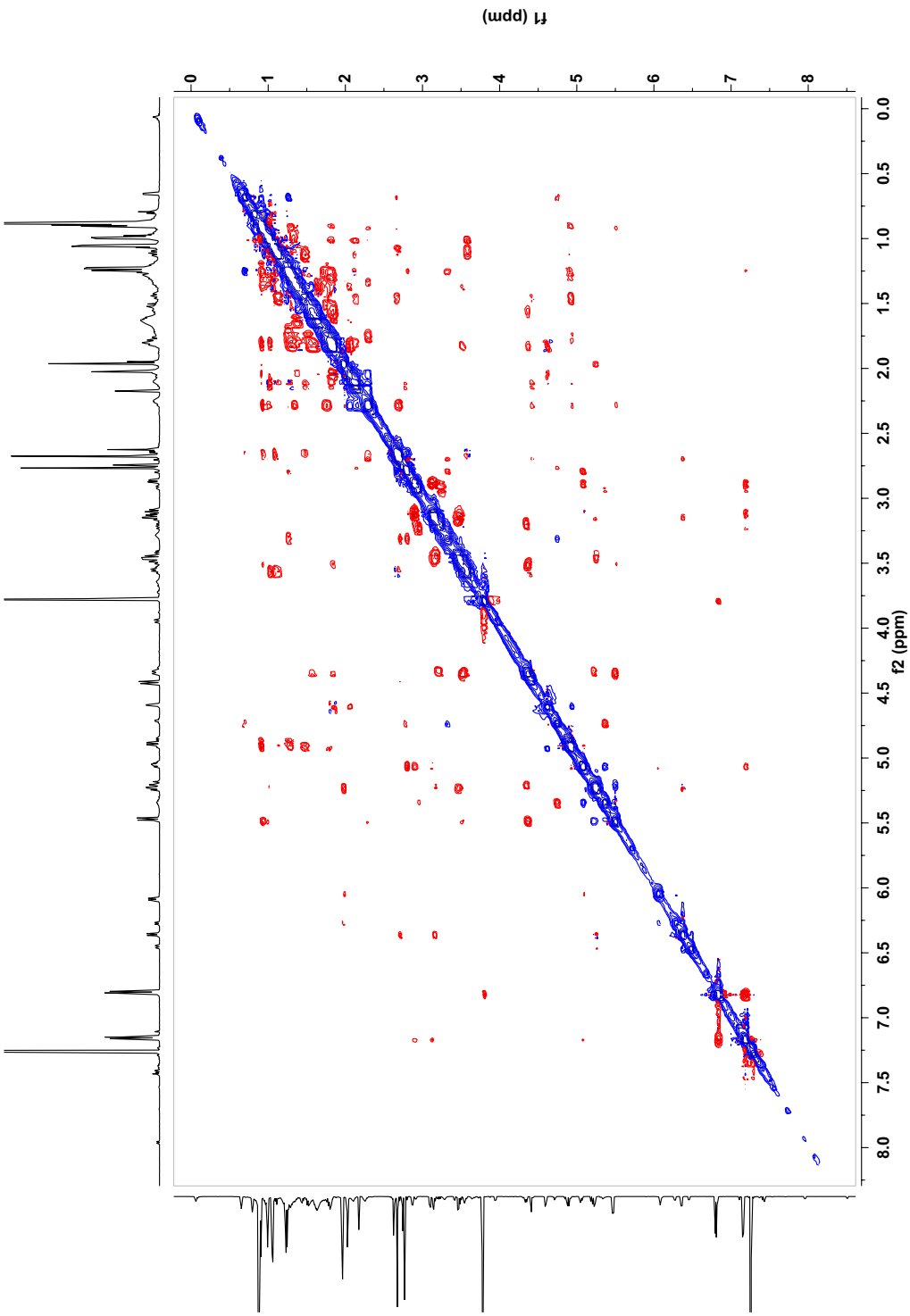

Figure S-3.7. ROESY spectrum for apratoxin H (**1**) in $CDCl_3$ (500 MHz).

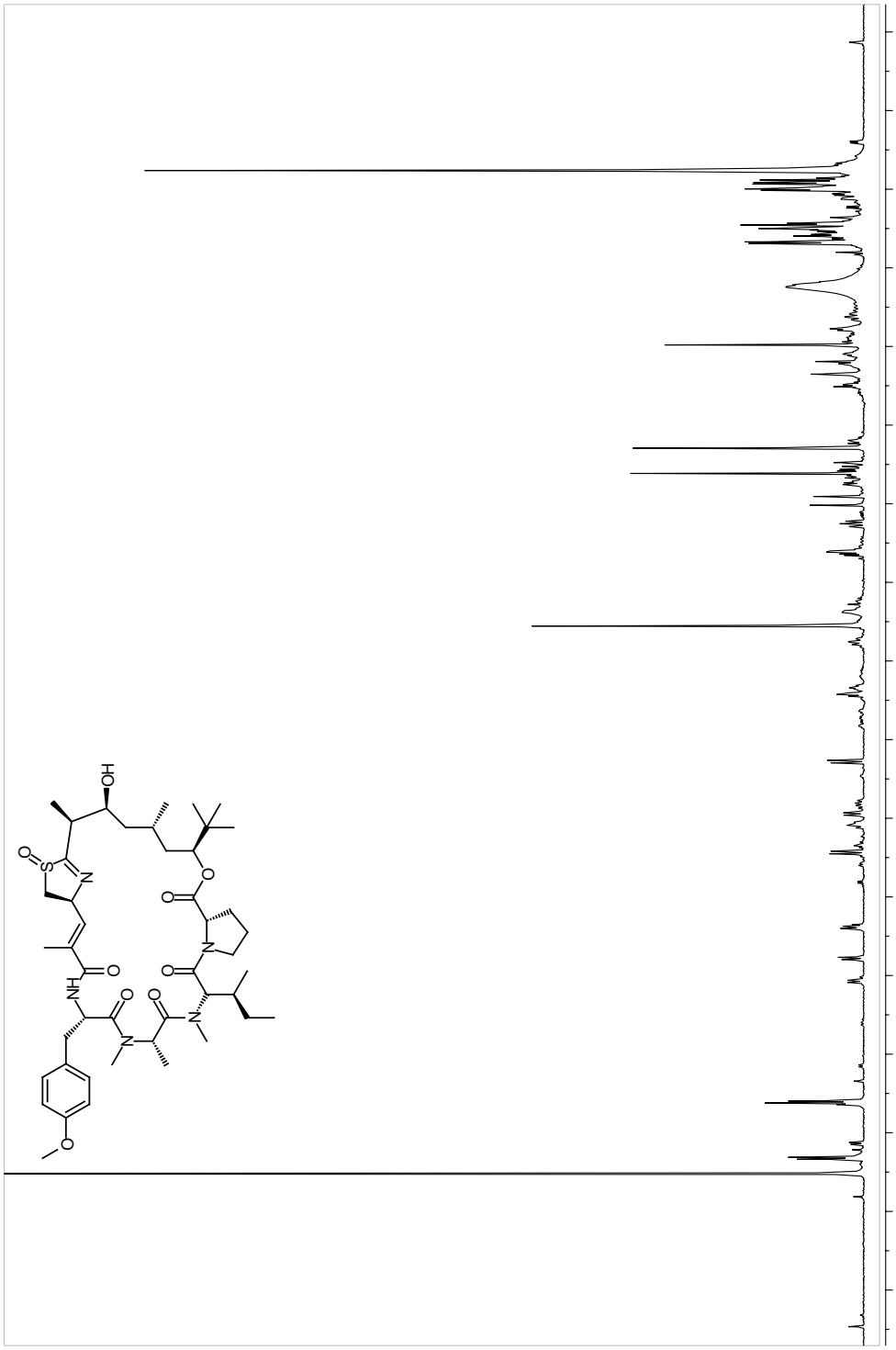

Figure S-3.8. ^{1}H NMR spectrum for apratoxin A sulfoxide (**2**) in $CDCl_3$ (700 MHz).

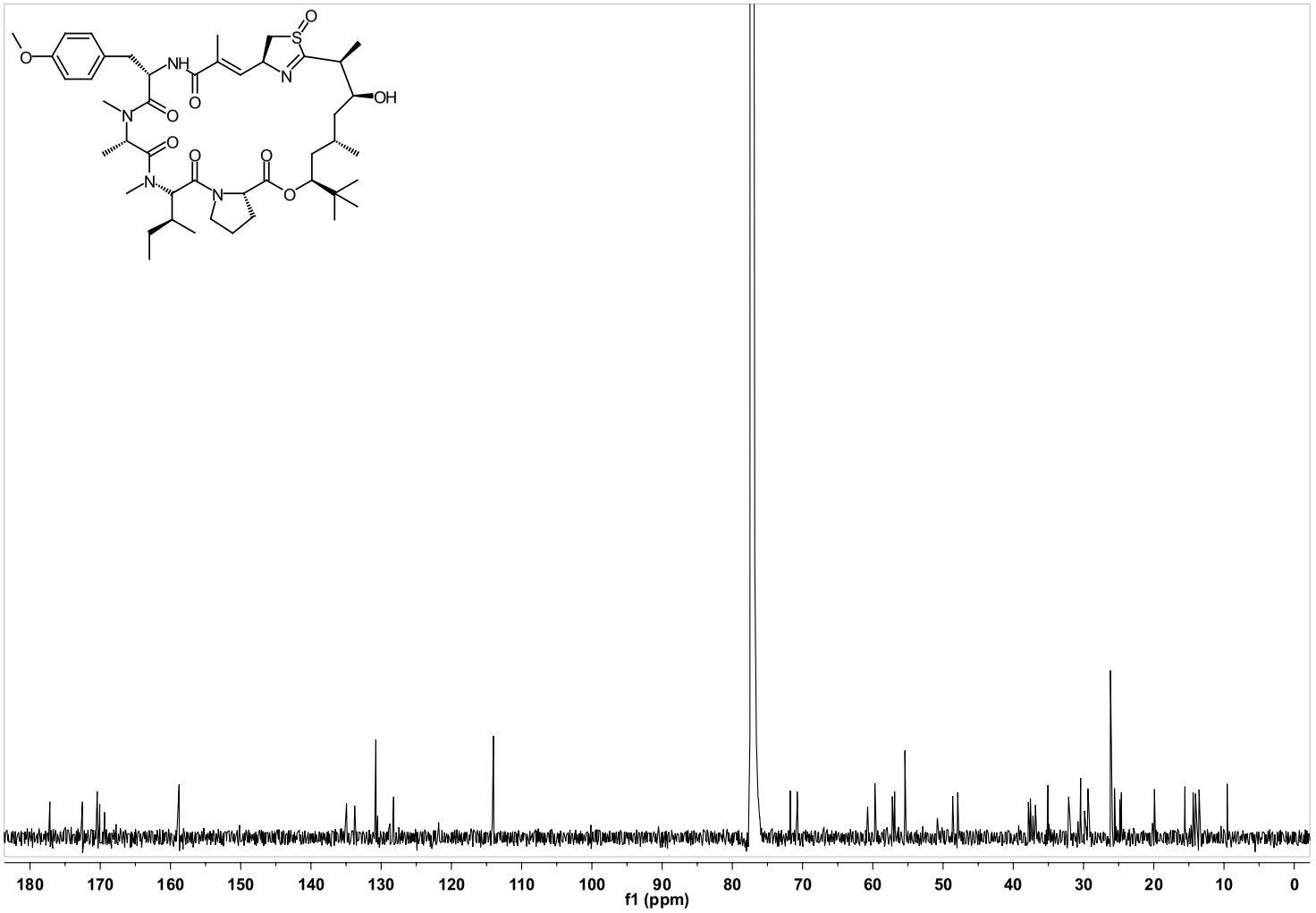

Figure S-3.9. ^{13}C NMR spectrum for apratoxin A sulfoxide (**2**) in $CDCl_3$ (175 MHz).

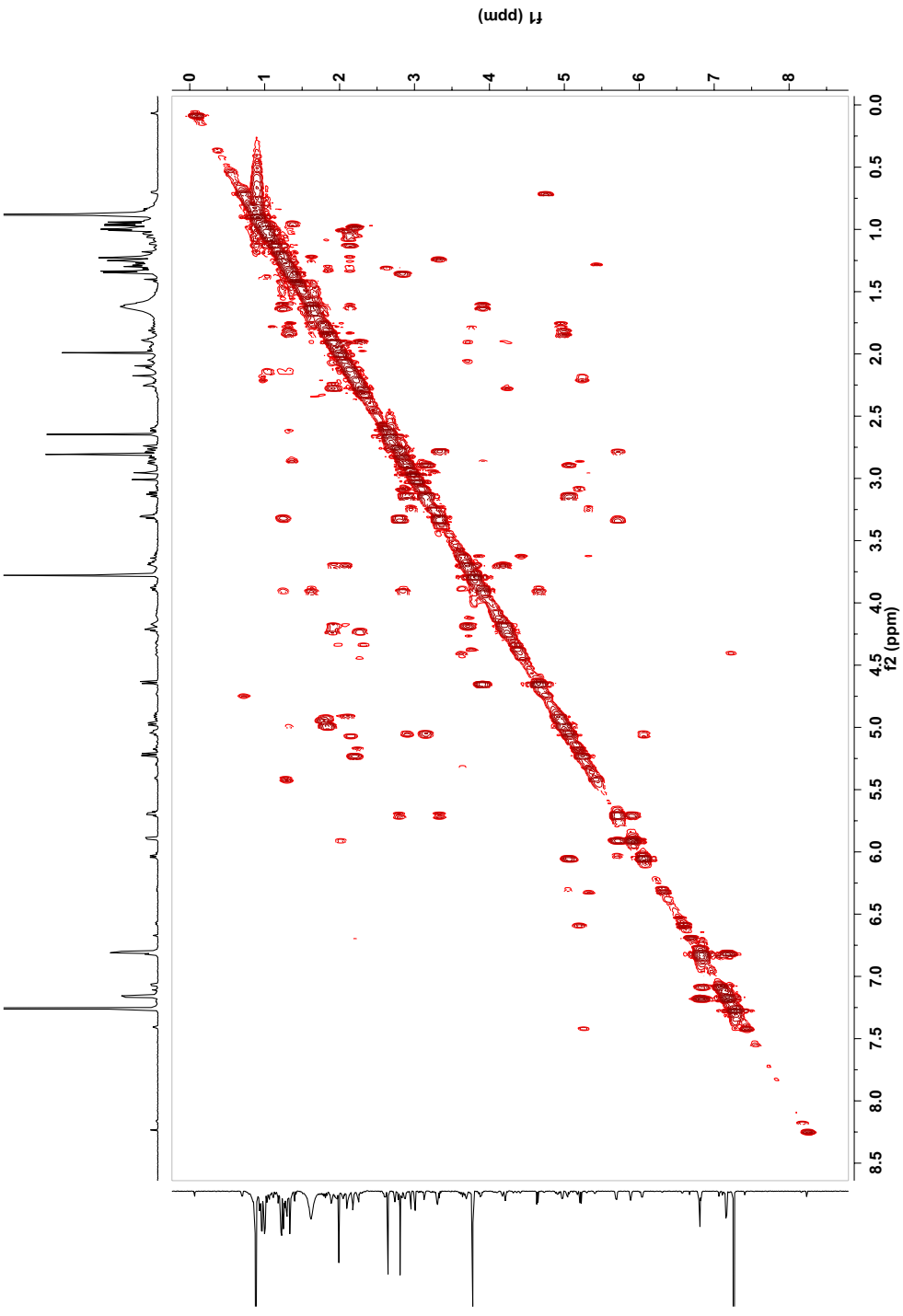

Figure S-3.10. COSY spectrum for apratoxin A sulfoxide (**2**) in $CDCl_3$ (700 MHz).

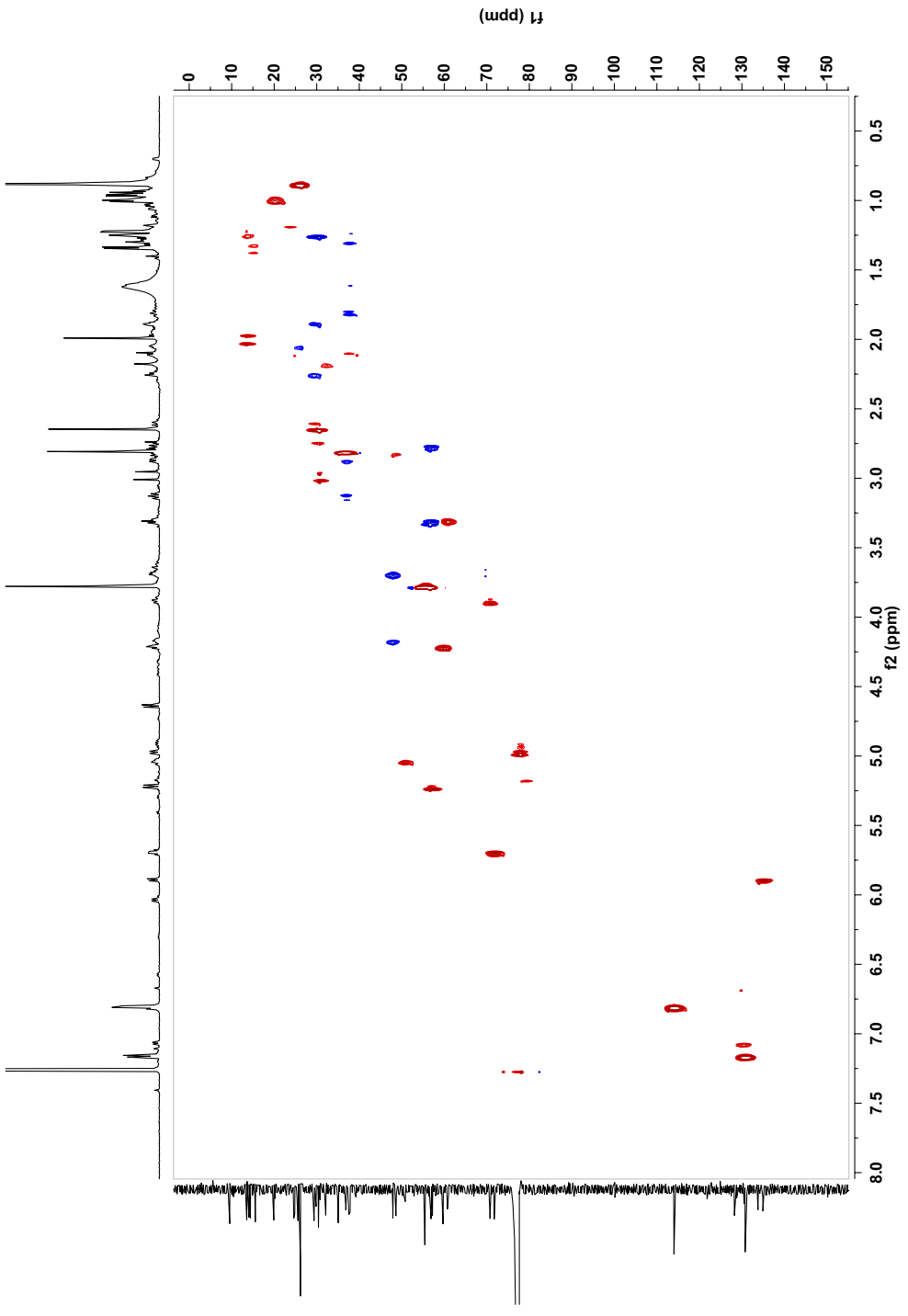

Figure S-3.11. Multiplicity-edited HSQC spectrum for apratoxin A sulfoxide (**2**) in $CDCl_3$ (700 MHz).

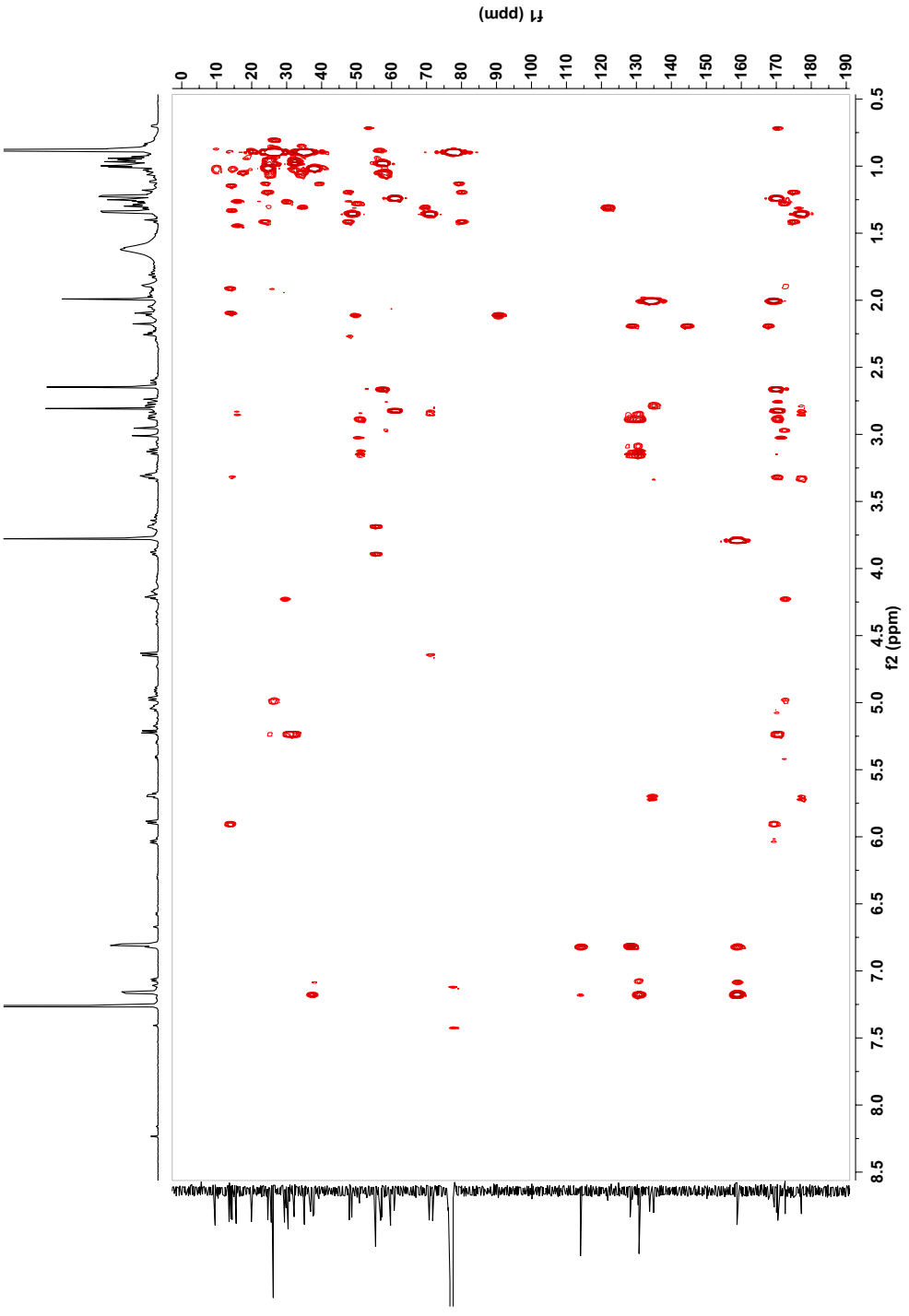

Figure S-3.12. HMBC spectrum for apratoxin A sulfoxide (**2**) in $CDCl_3$ (700 MHz).

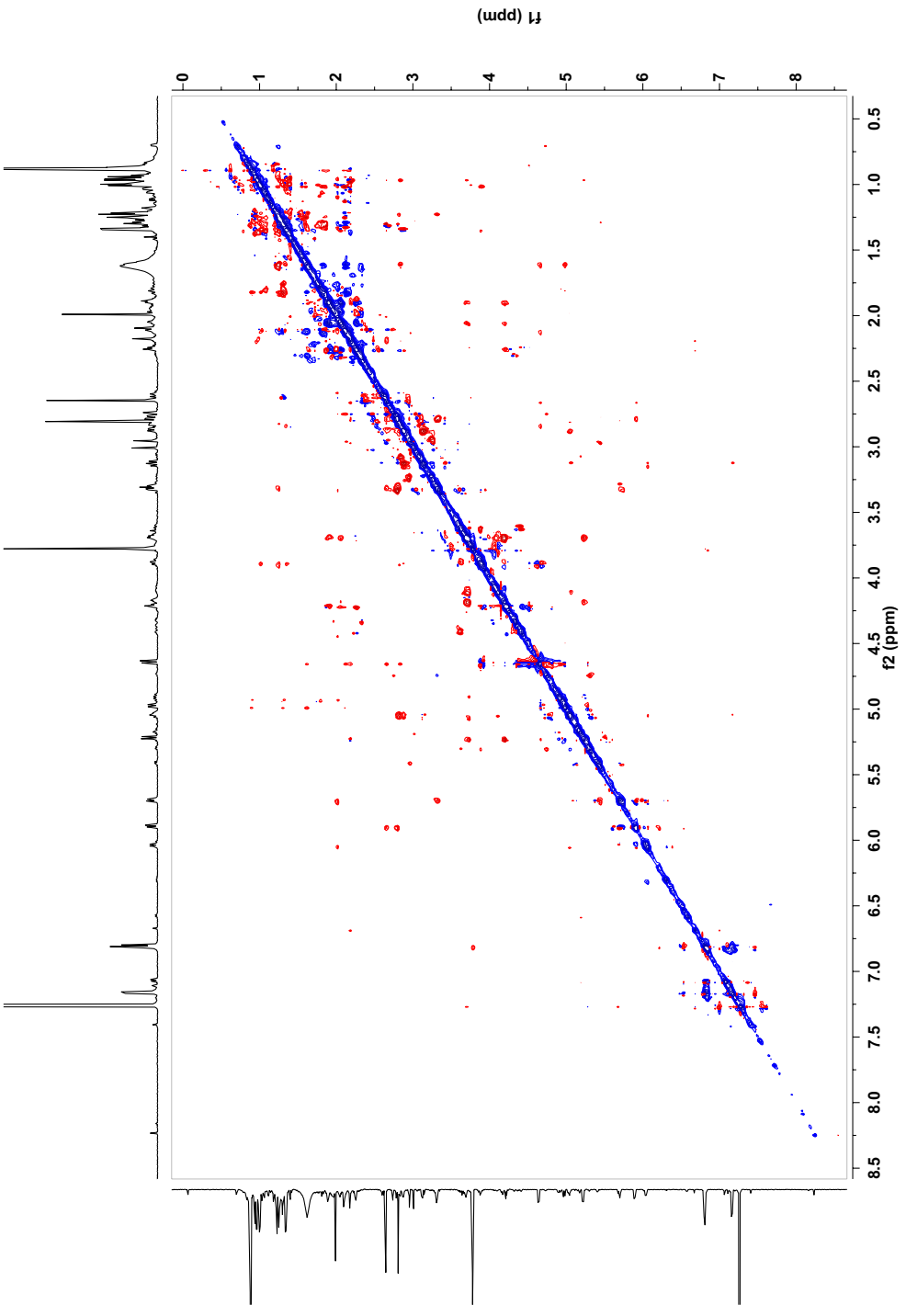

Figure S-3.13. ROESY spectrum for apratoxin A sulfoxide (**2**) in $CDCl_3$ (700 MHz).

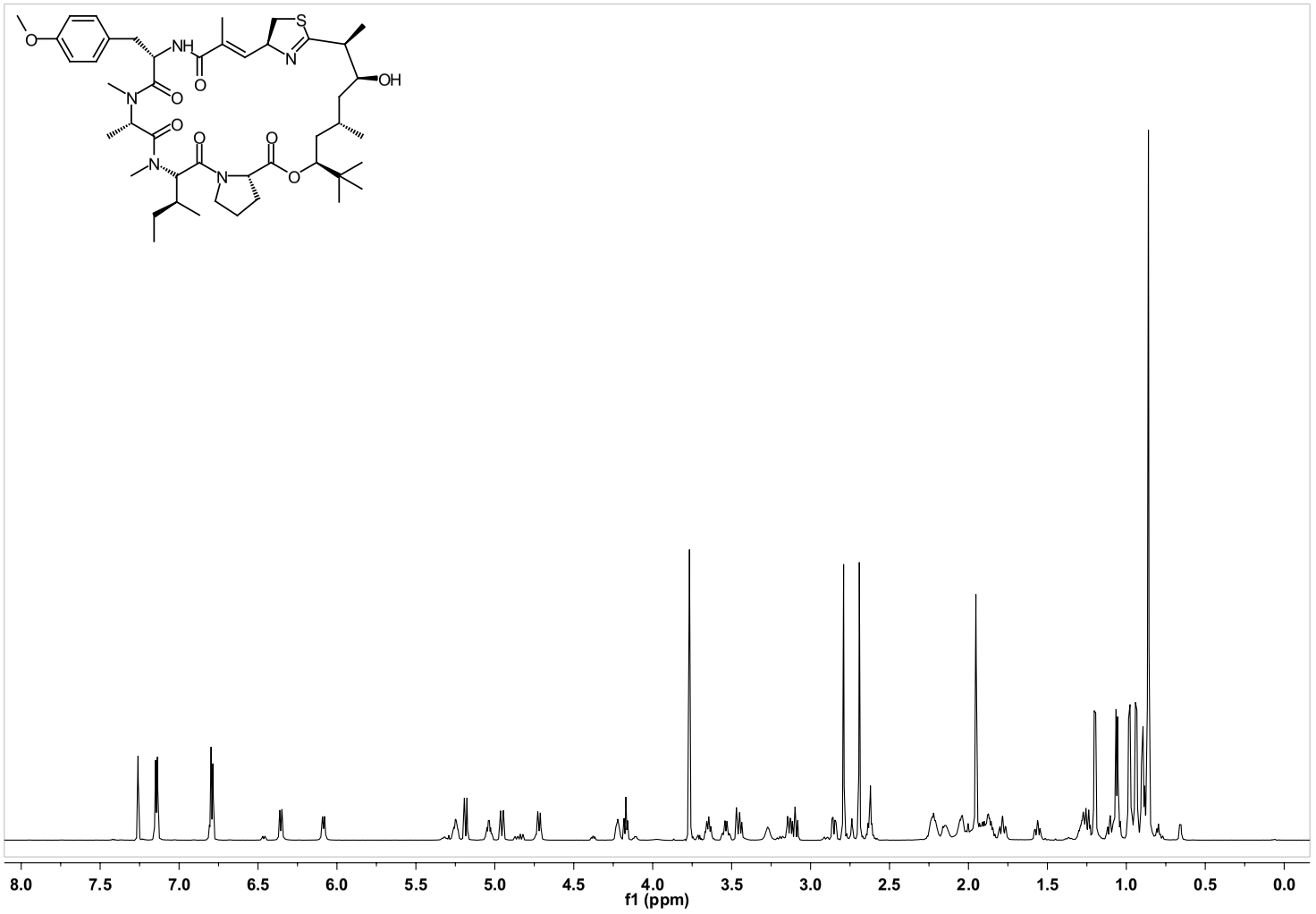

Figure S-3.14. ^{1}H NMR spectrum for apratoxin A in $CDCl_3$ (700 MHz).

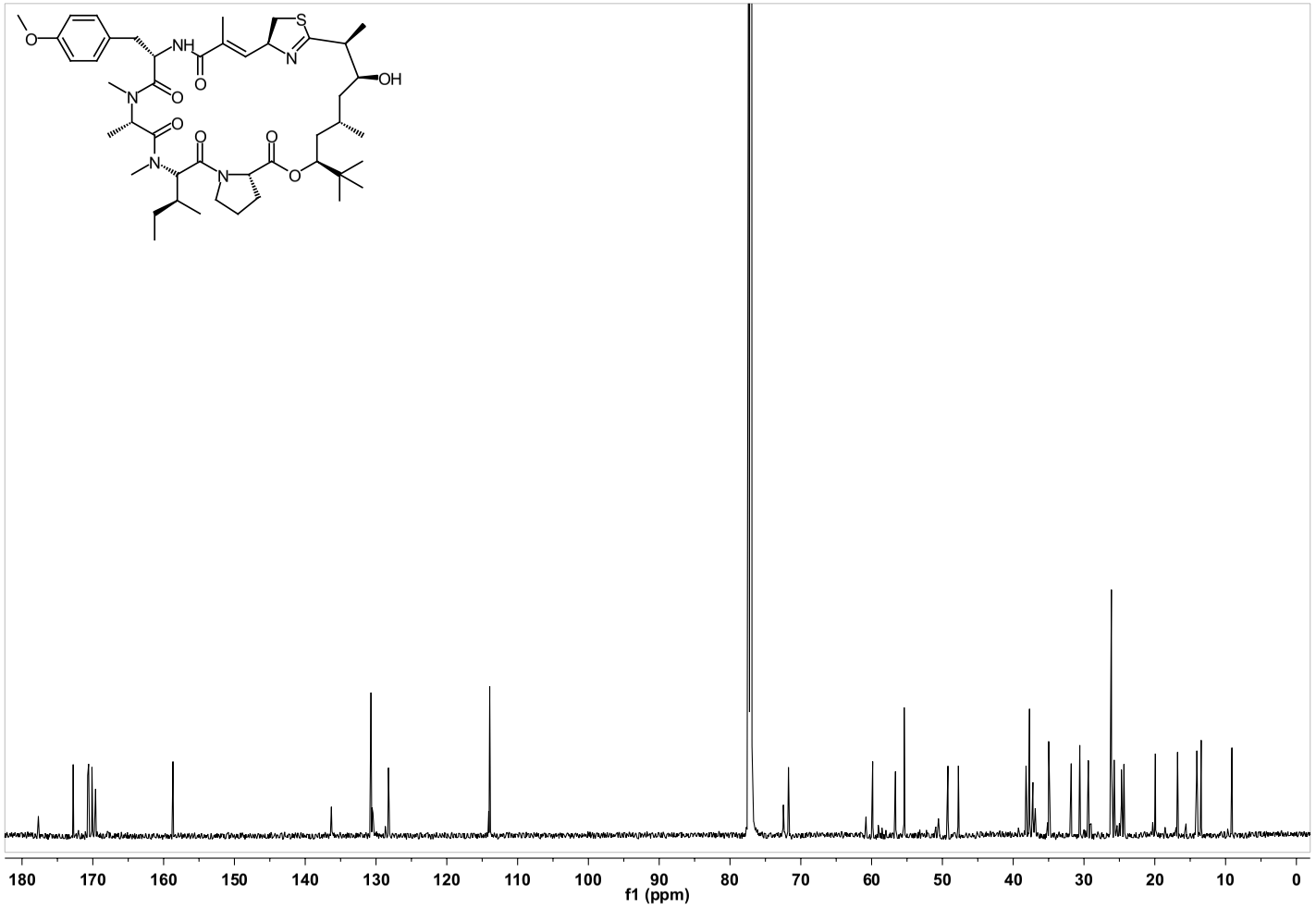

Figure S-3.15. ^{13}C NMR spectrum for apratoxin A in $CDCl_3$ (175 MHz).

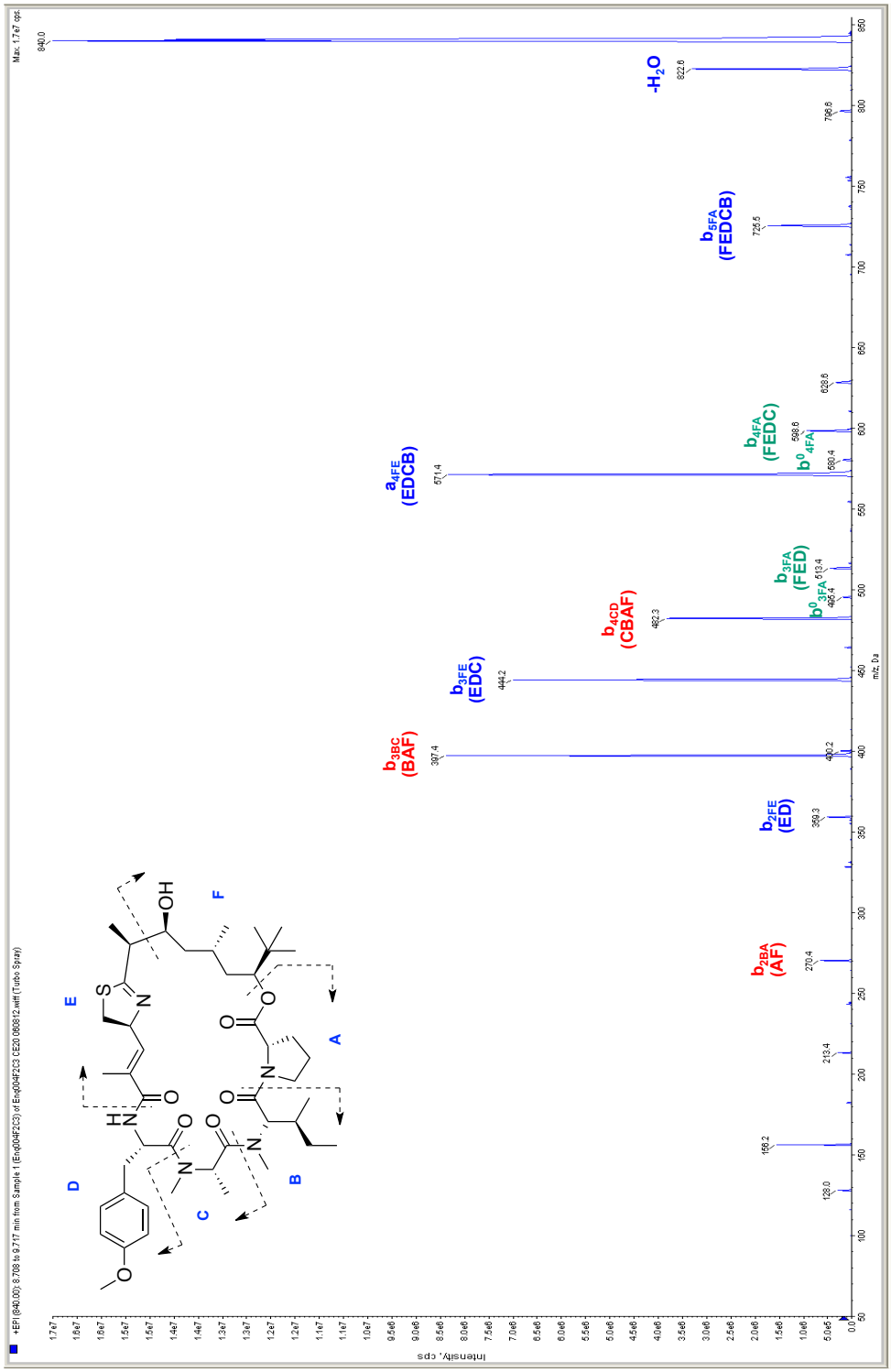

Figure S-3.16. Annotated MS/MS spectrum of apratoxin A [collision energy (CE), 25; declustering potential (DP), 33; entrance potential (EP), 10; T = 400 °C].

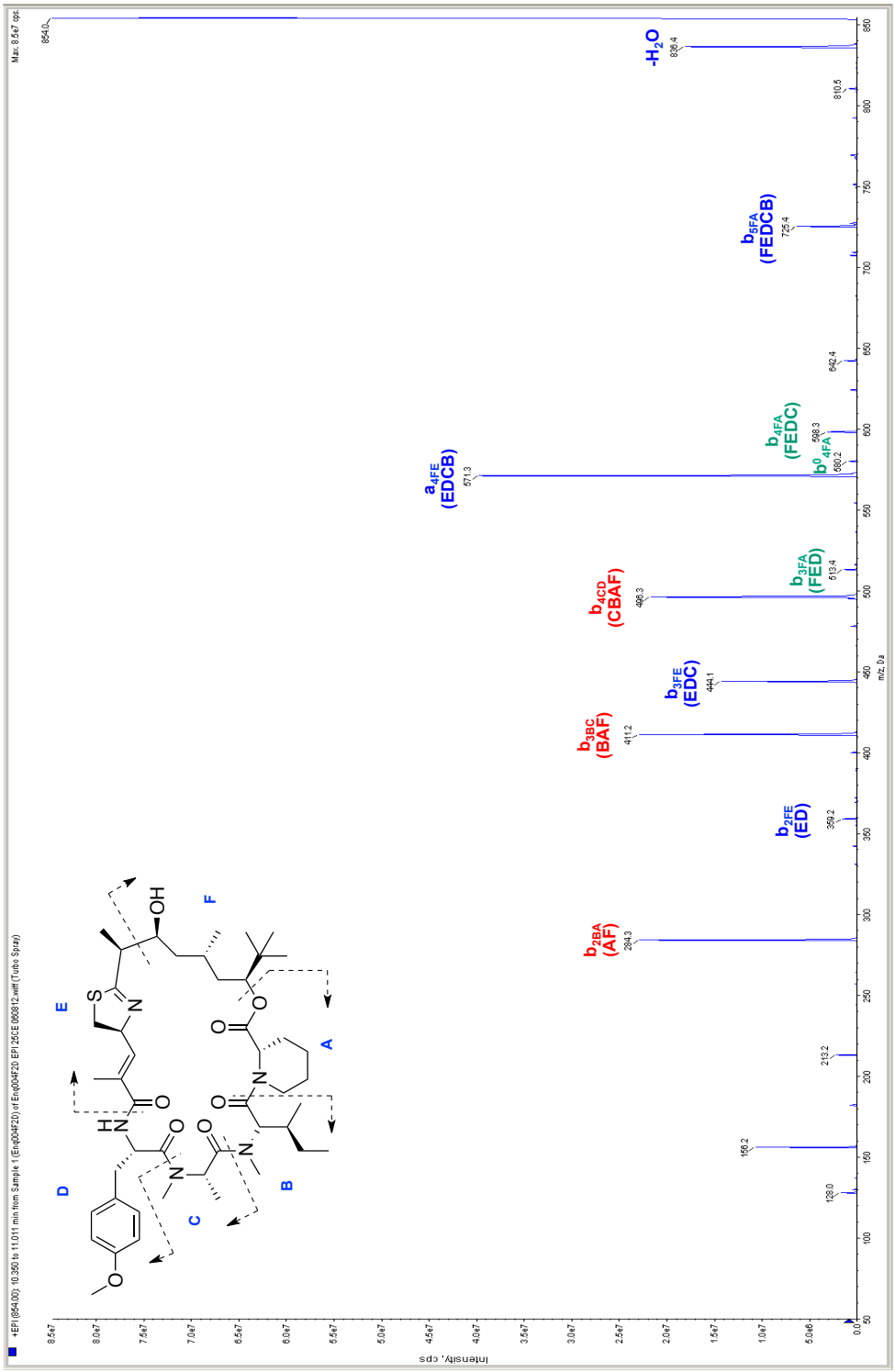

Figure S-3.17. Annotated MS/MS spectrum of apratoxin H (**1**) [collision energy (CE), 25; declustering potential (DP), 33; entrance potential (EP), 10; T = 400 °C].

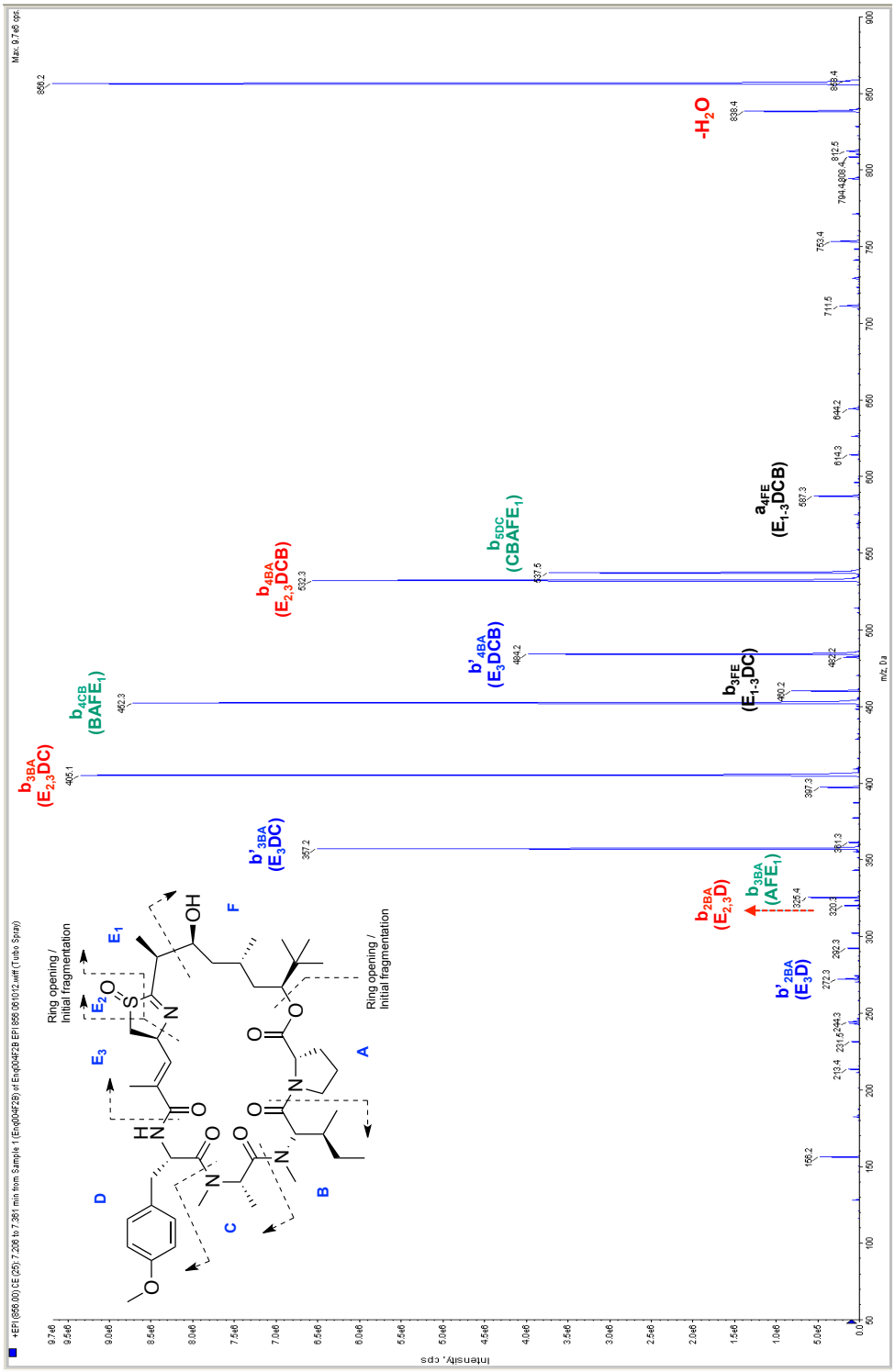

Figure S-3.18. Annotated MS/MS spectrum of apratoxin A sulfoxide (**2**) [collision energy (CE), 25; declustering potential (DP), 33; entrance potential (EP), 10; T = 400 °C].

References

Ashelford, K. E., Chuzhanova, N. A., Fry, J. C., Jones, A. J., & Weightman, A. J. (2005). At Least 1 in 20 16S rRNA Sequence Records Currently Held in Public Repositories Is Estimated To Contain Substantial Anomalies. *Appl. Environ. Microbiol., 71*(12), 7724-7736.

Banker, R., & Carmeli, S. (1998). Tenuecyclamides A−D, Cyclic Hexapeptides from the Cyanobacterium *Nostoc spongiaeforme* var. *tenue*. *J. Nat. Prod., 61*(10), 1248-1251.

Baumann, H. I., Keller, S., Wolter, F. E., Nicholson, G. J., Jung, G., Süssmuth, R. D., & Jüttner, F. (2007). Planktocyclin, a Cyclooctapeptide Protease Inhibitor Produced by the Freshwater Cyanobacterium Planktothrix rubescens. *J. Nat. Prod., 70*(10), 1611-1615.

Carballo, J., Hernandez-Inda, Z., Perez, P., & Garcia-Gravalos, M. (2002). A comparison between two brine shrimp assays to detect in vitro cytotoxicity in marine natural products. *BMC Biotechnol., 2*(1), 17.

Challis, G. L., Ravel, J., & Townsend, C. A. (2000). Predictive, structure-based model of amino acid recognition by nonribosomal peptide synthetase adenylation domains. *Chem. Biol., 7*(3), 211-224.

Chen, Q. Y., Liu, Y., & Luesch, H. (2011). Systematic Chemical Mutagenesis Identifies a Potent Novel Apratoxin A/E Hybrid with Improved in Vivo Antitumor Activity. *ACS Med. Chem. Lett., 2*(11), 861-865.

Engene, N., Rottacker, E. C., Kaštovský, J., Byrum, T., Choi, H., Ellisman, M. H., Komárek, J., & Gerwick, W. H. (2012). Moorea producens gen. nov., sp. nov. and Moorea bouillonii comb. nov., tropical marine cyanobacteria rich in bioactive secondary metabolites. *Int. J. Syst. Evol. Microbiol., 62*(Pt 5), 1171-1178.

Esquenazi, E., Jones, A. C., Byrum, T., Dorrestein, P. C., & Gerwick, W. H. (2011). Temporal dynamics of natural product biosynthesis in marine cyanobacteria. *Proc. Natl. Acad. Sci., 108*(13), 5226-5231.

Francisco, J. A., Cerveny, C. G., Meyer, D. L., Mixan, B. J., Klussman, K., Chace, D. F., Rejniak, S. X., Gordon, K. A., DeBlanc, R., Toki, B. E., Law, C. L., Doronina, S. O., Siegall, C. B., Senter, P. D., & Wahl, A. F. (2003). cAC10-vcMMAE, an anti-CD30-monomethyl auristatin E conjugate with potent and selective antitumor activity. *Blood, 102*(4), 1458-1465.

Gatto, G. J., Boyne, M. T., Kelleher, N. L., & Walsh, C. T. (2006). Biosynthesis of Pipecolic Acid by RapL, a Lysine Cyclodeaminase Encoded in the Rapamycin Gene Cluster. *J. Am. Chem. Soc., 128*(11), 3838-3847.

Grindberg, R. V., Ishoey, T., Brinza, D., Esquenazi, E., Coates, R. C., Liu, W.-t., Gerwick, L., Dorrestein, P. C., Pevzner, P., Lasken, R., & Gerwick, W. H. (2011). Single Cell Genome Amplification Accelerates Identification of the Apratoxin Biosynthetic Pathway from a Complex Microbial Assemblage. *PLoS ONE, 6*(4), e18565.

Gunasekera, S. P., Ritson-Williams, R., & Paul, V. J. (2008). Carriebowmide, a New Cyclodepsipeptide from the Marine Cyanobacterium *Lyngbya polychroa*. *J. Nat. Prod., 71*(12), 2060-2063.

Gutiérrez, M., Suyama, T. L., Engene, N., Wingerd, J. S., Matainaho, T., & Gerwick, W. H. (2008). Apratoxin D, a Potent Cytotoxic Cyclodepsipeptide from Papua New Guinea Collections of the Marine Cyanobacteria *Lyngbya majuscula* and *Lyngbya sordida*. *J. Nat. Prod., 71*(6), 1099-1103.

Hara, M., Asano, K., Kawamoto, I., Takiguchi, T., Katsumata, S., Takahashi, K., & Nakano, H. (1989). Leinamycin, a new antitumor antibiotic from *Streptomyces*; producing organism, fermentation and isolation. J. Antibiot., 42(12), 1768-1774.

Huang, X., & Madan, A. (1999). CAP3: A DNA Sequence Assembly Program. *Genome Res., 9*(9), 868-877.

Humair, B., Gonzalez, N., Mossialos, D., Reimmann, C., & Haas, D. (2009). Temperature-responsive sensing regulates biocontrol factor expression in *Pseudomonas fluorescens* CHA0. *ISME J, 3*(8), 955-965.

Ireland, C. M., Durso, A. R., Newman, R. A., & Hacker, M. P. (1982). Antineoplastic cyclic peptides from the marine tunicate *Lissoclinum patella*. *J. Org. Chem., 47*(10), 1807-1811.

Liu, W. T., Ng, J., Meluzzi, D., Bandeira, N., Gutierrez, M., Simmons, T. L., Schultz, A. W., Linington, R. G., Moore, B. S., Gerwick, W. H., Pevzner, P. A., & Dorrestein, P. C. (2009). Interpretation of Tandem Mass Spectra Obtained from Cyclic Nonribosomal Peptides. *Anal. Chem., 81*(11), 4200-4209.

Liu, Y., Law, B. K., & Luesch, H. (2009). Apratoxin A Reversibly Inhibits the Secretory Pathway by Preventing Cotranslational Translocation. *Mol. Pharmacol., 76*(1), 91-104.

López-Legentil, S., Bontemps-Subielos, N., Turon, X., & Banaigs, B. (2006). Temporal Variation in the Production of Four Secondary Metabolites in a Colonial Ascidian. *J. Chem. Ecol., 32*(9), 2079-2084.

Luesch, H., Yoshida, W. Y., Moore, R. E., & Paul, V. J. (2002). New apratoxins of marine cyanobacterial origin from guam and palau. *Bioorg. Med. Chem., 10*(6), 1973-1978.

Luesch, H., Yoshida, W. Y., Moore, R. E., Paul, V. J., & Corbett, T. H. (2001). Total Structure Determination of Apratoxin A, a Potent Novel Cytotoxin from the

Marine Cyanobacterium *Lyngbya majuscula*. *J. Am. Chem. Soc., 123*(23), 5418-5423.

Ma, D., Zou, B., Cai, G., Hu, X., & Liu, J. O. (2006). Total Synthesis of the Cyclodepsipeptide Apratoxin A and Its Analogues and Assessment of Their Biological Activities. *Chem. Euro. J., 12*(29), 7615-7626.

Matthew, S., Schupp, P. J., & Luesch, H. (2008). Apratoxin E, a Cytotoxic Peptolide from a Guamanian Collection of the Marine Cyanobacterium *Lyngbya bouillonii*. *J. Nat. Prod., 71*(6), 1113-1116.

Mau, C. M. S., Nakao, Y., Yoshida, W. Y., Scheuer, P. J., & Kelly-Borges, M. (1996). Waiakeamide, a Cyclic Hexapeptide from the Sponge *Ircinia dendroides*. *The J. Org. Chem., 61*(18), 6302-6304.

McLaughlin, J. L., Rogers, L. L., & Anderson, J. E. (1998). The Use of Biological Assays to Evaluate Botanicals. *Drug Inf. J., 32*(2), 513-524.

Ngoka, L., & Gross, M. (1999). A nomenclature system for labeling cyclic peptide fragments. *J. Am. Soc. Mass. Spectrom., 10*(4), 360-363.

Ogino, J., Moore, R. E., Patterson, G. M. L., & Smith, C. D. (1996). Dendroamides, New Cyclic Hexapeptides from a Blue-Green Alga. Multidrug-Resistance Reversing Activity of Dendroamide A. *J. Nat. Prod., 59*(6), 581-586.

Pearce, A. N., Chia, E. W., Berridge, M. V., Clark, G. R., Harper, J. L., Larsen, L., Maas, E. W., Page, M. J., Perry, N. B., Webb, V. L., & Copp, B. R. (2007). Anti-inflammatory Thiazine Alkaloids Isolated from the New Zealand Ascidian Aplidium sp.: Inhibitors of the Neutrophil Respiratory Burst in a Model of Gouty Arthritis. *J. Nat. Prod., 70*(6), 936-940.

Portmann, C., Blom, J. F., Kaiser, M., Brun, R., Jüttner, F., & Gademann, K. (2008). Isolation of Aerucyclamides C and D and Structure Revision of Microcyclamide 7806A: Heterocyclic Ribosomal Peptides from Microcystis aeruginosa PCC 7806 and Their Antiparasite Evaluation. *J. Nat. Prod., 71*(11), 1891-1896.

Rashid, M. A., Gustafson, K. R., Boswell, J. L., & Boyd, M. R. (2000). Haligramides A and B, Two New Cytotoxic Hexapeptides from the Marine Sponge *Haliclona nigra*. *J. Nat. Prod., 63*(7), 956-959.

Seattle Genetics. (2013). *CD30-Directed Adcetris® (brentuximab vedotin).* Retrieved January 21, 2013, from www.seattlegenetics.com/adcetris

Sera, Y., Adachi, K., Fujii, K., & Shizuri, Y. (2003). A New Antifouling Hexapeptide from a Palauan Sponge, Haliclona sp. *J. Nat. Prod., 66*(5), 719-721.

Simmons, T. L., Andrianasolo, E., McPhail, K., Flatt, P., & Gerwick, W. H. (2005). Marine natural products as anticancer drugs. *Mol. Cancer Ther., 4*(2), 333-342.

Thornburg, C. C., Thimmaiah, M., Shaala, L. A., Hau, A. M., Malmo, J. M., Ishmael, J. E., Youssef, D. T. A., & McPhail, K. L. (2011). Cyclic Depsipeptides,

Grassypeptolides D and E and Ibu-epidemethoxylyngbyastatin 3, from a Red Sea *Leptolyngbya* Cyanobacterium. *J. Nat. Prod., 74*(8), 1677-1685.

Tidgewell, K., Engene, N., Byrum, T., Media, J., Doi, T., Valeriote, F. A., & Gerwick, W. H. (2010). Evolved Diversification of a Modular Natural Product Pathway: Apratoxins F and G, Two Cytotoxic Cyclic Depsipeptides from a Palmyra Collection of *Lyngbya bouillonii*. *ChemBioChem, 11*(10), 1458-1466.

Chapter Four

Leptochelin, a Cytotoxic Metal Ion Chelator from a *Leptolyngbya* Cyanobacterium

Christopher C. Thornburg, Florina A. Vulpanovici, Jeffrey D. Serrill, Edward A. Mitchell, Jane E. Ishmael, Diaa T.A. Youssef, William H. Gerwick, and Kerry L. McPhail

Abstract

The cyclic depsipeptide leptochelin, isolated from a cyanobacterium of the genus *Leptolyngbya*, is a marine natural product with a uniquely modified chemical scaffold. The planar structure was established by a combination of NMR spectroscopy and mass spectrometry, including ^{1}H-^{15}N and ^{13}C INADEQUATE 2D NMR data obtained from natural abundance and ^{13}C-enriched samples, respectively. The absolute configuration has yet to be established due to a combination of unusual and diverse structural units including 2,4-diamino-3-hydroxy-2-methylpentanoic acid (DHMPA), 3-(2-chloro-1-hydroxyethyl)-2-methyloxirane-2-carboxylic acid, glyceric acid, 3-chlorosalicylic acid, 2-methylcysteine and bromo-phenylalanine. Importantly, a Zn-leptochelin complex, which displays a significant increase in potency, provides evidence for the metal-binding capability and coordination of several key functional groups within leptochelin. Leptochelin showed selective cytotoxicity to human NCI-H460 lung cancer cells (IC_{50} = 153 nM) compared to HeLa cervical carcinoma cells (IC_{50} = > 1 μM), and the metal-bound form was also significantly more potent against both cell lines, suggesting a unique metal-dependent mechanism.

Introduction

The enormous chemical diversity and biochemical specificity of natural product structures have long been recognized as superior to synthetic and combinatorial compounds (Koehn & Carter, 2005). Accordingly, the capacity of marine cyanobacteria to produce structurally diverse, highly bioactive secondary metabolites with a broad spectrum of biological activities makes them a logical source for obtaining chemically diverse natural products (Nunnery et al., 2010; Tidgewell et al., 2010). More specifically, marine cyanobacterial natural products contain a high degree of N- and C-methylation, α/β-hydroxy acids, ketide extended and β-amino acids, heterocycles, and halogen atoms, which stem from the convergence of multiple biosynthetic pathways (Sattely et al., 2008). The production of such a diverse, multifunctional array of secondary metabolites, although energetically costly, provides a selective advantage to microorganisms living in dense communities and/or nutrient limited environments (Cronin, 2001). However, the primary function of many cyanobacterial metabolites remains largely unknown (Leao et al., 2012).

A number of distinct functional groups within a given metabolite may offer insight into its primary function. For example, *N*-acyl homoserine lactones, and variations thereof, are typically used as chemical signals within bacterial communities, while metabolites containing catecholate, carboxylate or hydroxamate functional groups dominate marine siderophores (Wright et al., 2012). Siderophores are low molecular weight metabolites that facilitate iron uptake due to their high affinity for ferric iron (Fe^{3+}), an essential growth factor for phytoplankton, cyanobacteria and heterotrophic bacteria (Vraspir & Butler, 2009). In mammalian cells, the rate-limiting enzyme in DNA synthesis, iron-dependent ribonucleotide reductase (RNR), is activated by the generation and transfer of tyrosyl radicals between its two subunits (RNR1 and RNR2), which occurs through reactions of molecular oxygen with the diferric iron center of the RNR2 subunit (Richardson et al., 2009). An increase in RNR

activity in neoplastic cells suggests that iron chelators may be used for selective inhibition of tumor cell growth (Shao et al., 2006). Indeed, several iron chelators, originally developed for the treatment of iron overload due to transfusion-dependent anemias (Payne et al., 2008), have been explored as potential antitumor agents. Desferrioxamine B (**1**, DFO, Desferal®) is a siderophore from the bacterium *Streptomyces pilosus* (Bickel et al., 1960) that has shown anti-proliferative activity in various cancer cells (Richardson et al., 2009). However, DFO exhibits poor bioavailability and failed to show anticancer activity in several clinical trials (Yu et al., 2006). Alternatively, several thiosemicarbazone-based iron chelators, including Triapine® (**2**), Dp44mT (**3**) and derivatives thereof, have shown promise as anticancer agents given their ability to bind intracellular iron and generate reactive oxygen species (ROS), leading to either inactivation of RNR or apoptosis (Li et al., 2001; Liu et al., 1992; Lukmantara et al., 2013; Yuan et al., 2004).

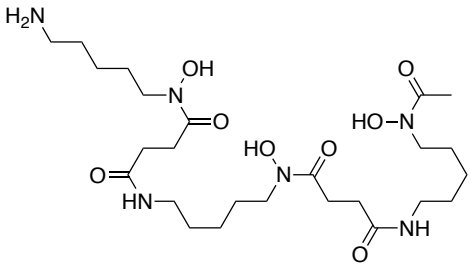

desferrioxamine B (**1**)

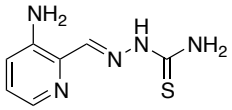

Triapine® (**2**)

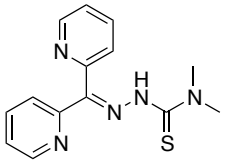

Dp44mT (**3**)

Like iron, other trace metals such as cobalt (Co), nickel (Ni), copper (Cu) and zinc (Zn) are essential cofactors for enzymes and proteins in marine microorganisms (Wright et al., 2012). However, depending on their chemical speciation, trace metals that are vital for growth can also have toxic effects on various metabolic processes. Thus, to balance their positive and negative effects, the specificity and degree of complexation of a trace metal with a given chelator is critical (Vraspir & Butler,

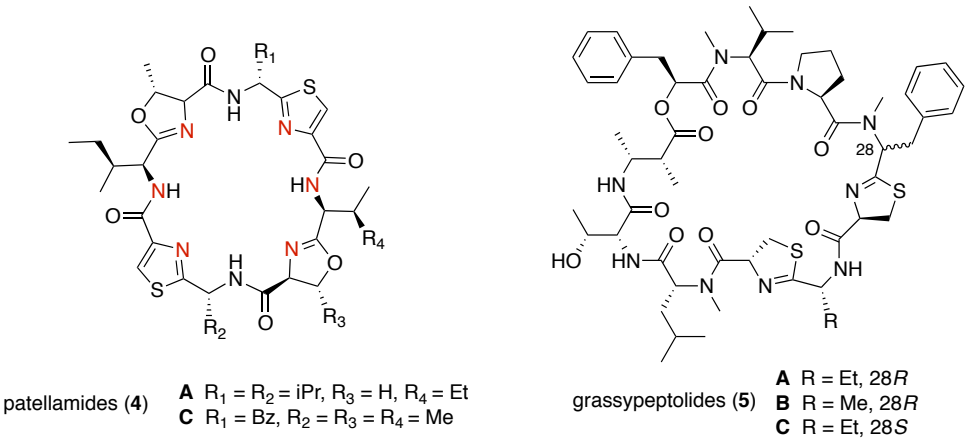

Figure 4.1. Structures of patellamides A and C with the thiazole (T), amine (A) and oxazole (O) nitrogens or TAO metal binding domains shown in red. The structurally similar grassypeptolides (**5**) are also capable of binding Cu^{2+} and Zn^{2+} ions.

2009). For example, a number of azole-containing cyclic peptides from marine cyanobacteria, such as the patellamides (**4**, Morris, Jaspars et al., 2001) and grassypeptolides (**5**, Kwan et al., 2010; Figure 4.1), adopt unique conformations that allow them to preferentially bind Cu^{2+} and Zn^{2+} ions within their central cavities. The binding of such redox-active metals may protect copper-sensitive organisms, as the complexed form of copper is less toxic (Vraspir & Butler, 2009), or it may serve as an activating mechanism to confer biological activity on the complexing metabolite (Kwan & Luesch, 2010). A prime example is that of the chemotherapeutic agent bleomycin (**6**, Bleonoxane® = ~60% bleomycin A_2 and ~30% bleomycin B_2; Figure 4.2), from the terrestrial actinomycete *Streptomyces verticillus* (Umezawa et al., 1966). The pyrimidine moiety of bleomycin (Figure 4.2), together with the bithiazole tail, binds DNA, while the metal-binding domain binds Fe(II) or Cu(I) and molecular oxygen to enable sequence selective DNA binding and cleavage (Chen & Stubbe, 2005).

A potential target of Zn^{2+} chelators are metal-dependent histone deacetylases (HDACs), which play a role in the global repression of gene transcription, including a

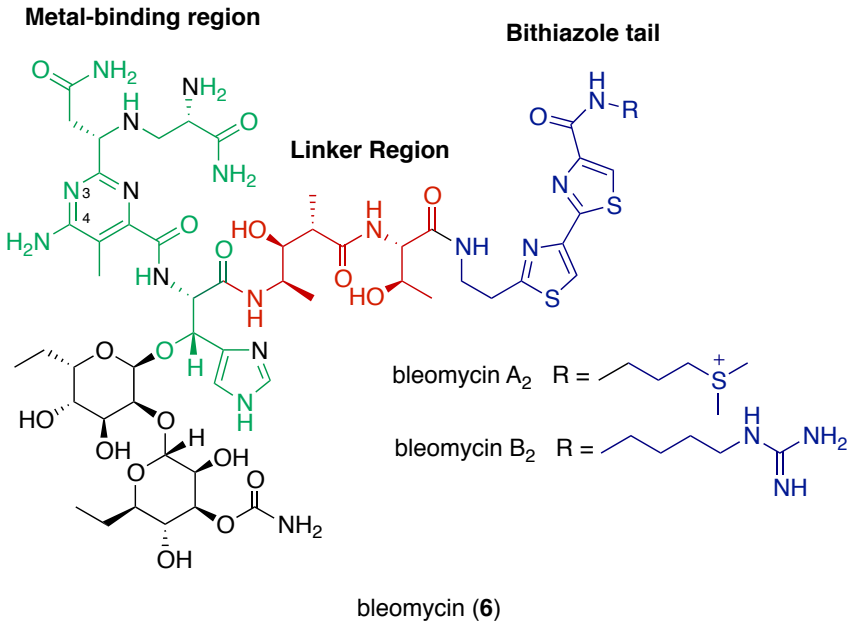

Figure 4.2. Structure of bleomycins (**6**) and derivates that comprise Bleonoxane®. The metal-binding region is in green with the coordinating nitrogen atoms shown in black. (Chen & Stubbe, 2005).

number of key oncogenes and tumor suppressor genes (de Ruijter et al., 2003; Haberland et al., 2009). Thus, inhibition of HDAC activity has broad implications for the reversal of aberrant acetylation levels associated with a variety of disease states, and several HDAC inhibitors have been evaluated clinically (Guan & Fang, 2010). A key feature of the more potent HDAC inhibitors is the presence of a functional group capable of binding the catalytic Zn(II) ion of HDAC. Perhaps the most potent inhibitor of HDAC enzymes known is largazole (**7**), which was isolated from a marine cyanobacterium *Symploca* sp. (Taori et al., 2008). Largazole shares a similar structure and mechanism of action to the HDAC inhibitor romidepsin (**8**, Istodax®), which was recently approved for the treatment of cutaneous T-cell lymphoma (Guan & Fang, 2010). Notably, both structures are modified *in vivo* to yield a free thiol group capable of binding the active site Zn(II) ion of HDACs (Figure 4.3; Cole et al., 2011). However, the rigid thiazoline-thiazole ring system within the macrocycle of largazole

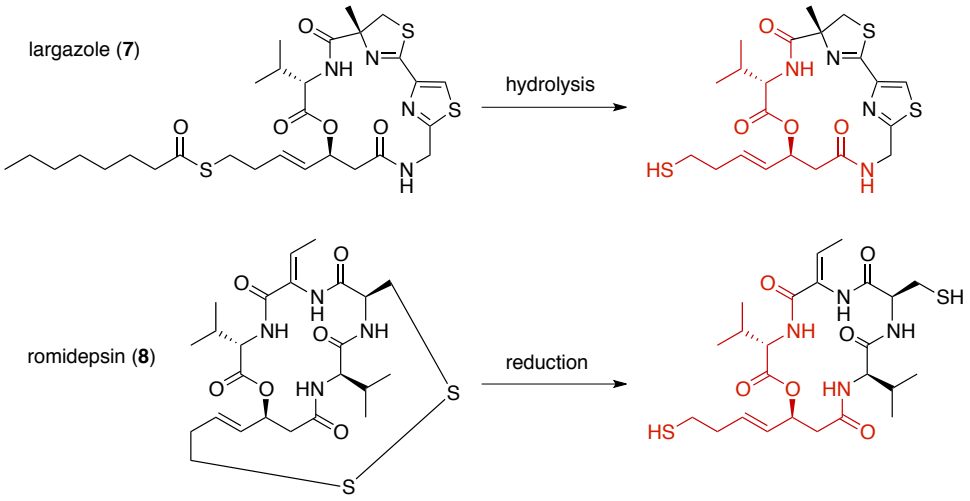

Figure 4.3. Structures of the potent HDAC inhibitors largazole (**7**) and romidepsin (**8**, Istodax®). The thioester linkage of largazole is hydrolyzed, while the disulfide bond of romidepsin is reduced *in vivo* to allow thiol-binding of the active site Zn^{2+} of HDACs. Identical portions of each structure are highlighted in red.

provides an ideal conformation for binding the opening of the HDAC active site, which may account for the observed specificity for class I isoforms (Hong & Luesch, 2012).

Based on the diversity of functional groups capable of binding trace metals, a large number of marine metabolites are proposed to function as metal ligands. However, relatively few siderophore structures and metal chelators have been isolated from marine bacteria (Vraspir & Butler, 2009; Wright et al., 2012). In the course of investigating the biosynthetic capacity of laboratory-cultured cyanobacteria from the Red Sea, we have directly isolated a highly modified, halogenated depsipeptide (**9**) complexed with Zn^{2+} from a *Leptolyngbya* cyanobacterium, as well as the known brominated macrolide phormidolide (**10**, Williamson et al., 2002). Notably, the metal-free compound was isolated previously by the Gerwick group (ca. 2001; Vulpanovici 2003) from a phormidolide-producing Indonesian *Leptolyngbya* strain that shares 99.9% sequence homology with our Red Sea isolate. Although extensive NMR

spectroscopic data were obtained for this compound, including a ^{13}C INADEQUATE NMR spectrum for a ^{13}C-labeled sample, the planar structure was not fully assigned, and an acknowledged incorrect structure was presented (Vulpanovici, 2003). Here we report the resolved planar structure and biological activity of leptochelin (**9**) and the Zn^{2+} complexed form, the latter of which shows a 2 to 4.5–fold increase in cytotoxicity against human NCI-H460 lung cancer cells (IC_{50} = 73 nM) and HeLa cervical carcinoma cells (IC_{50} = 239 nM), respectively.

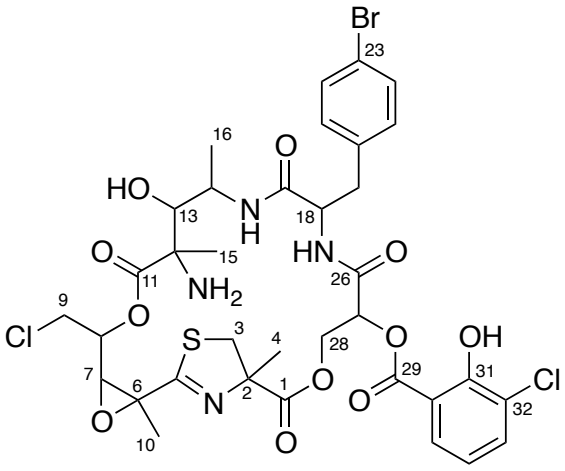

leptochelin A (**9**)

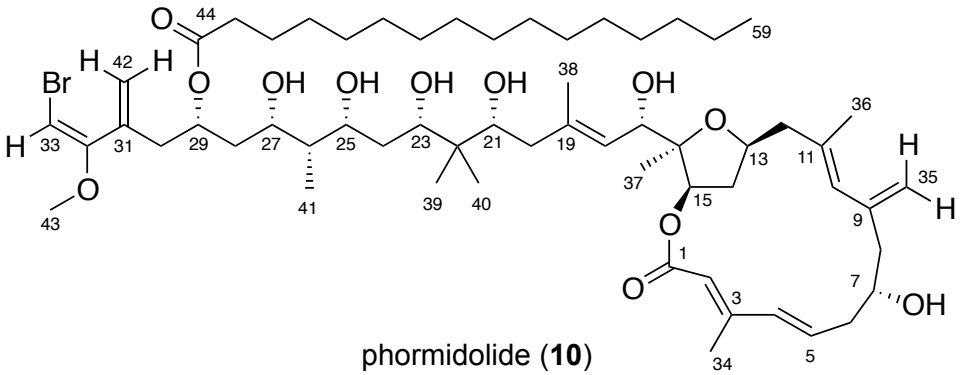

phormidolide (**10**)

Results and Discussion

A mat-forming marine cyanobacterium was obtained by hand using scuba from a hard coral substrate in the Red Sea. A glycerol-preserved portion of this collection was prepared for transport and later reanimated in our laboratory with enrichment medium as previously described (Thornburg et al., 2011) to yield several live cyanobacterial isolates. One of these monoclonal isolates, *Leptolyngbya* sp. RS02, was cultured over the span of four years, and an organic extract of the culture material was subjected to bioassay-guided fractionation via normal phase vacuum liquid chromatography (NP VLC) using a stepped solvent gradient of hexanes to EtOAc to MeOH. The fractions eluting with 100% EtOAc (G) and 25% MeOH–EtOAc (H) were moderately toxic to brine shrimp (10 mg/mL reduced cell viability by 70 and 43%, respectively). Therefore, the G fraction was separated by C_{18} reversed-phase (RP) solid-phase extraction (SPE) and RP-HPLC to yield the known inactive metabolite phormidolide (**10**, 16.0 mg) as the major component and a putative phormidolide analogue (0.1 mg) that was highly cytotoxic to mouse Neuro-2a neuroblastoma cells (30 μg/mL reduced cell viability by 80%). In our attempt to isolate more of this active phormidolide analogue from the less cytotoxic H fraction, an additional unrelated metabolite (**9**, 1.1 mg) that was highly cytotoxic to human NCI-H460 lung cancer cells (IC_{50} = 73 nM) was discovered. ^{1}H and ^{13}C NMR data for the latter compound matched an extensively characterized (NMR and MS), yet unresolved, structure from a phormidolide-producing Indonesian *Leptolyngbya* sp. (Vulpanovici, 2003). However, a difference in mass, coupled with a distinct isotope pattern (Figure 4.4), suggested that our Red Sea *Leptolyngbya* compound was a zinc complexed form of the unresolved compound, which we have now named leptochelin (**9**) for its chelating properties. Notably, since the original isolation of **9** (ca. 2001), several attempts to re-isolate this structurally intriguing compound have been futile. This is likely due to the compound's ability to form metal complexes, which alter the compound's behavior with respect to the

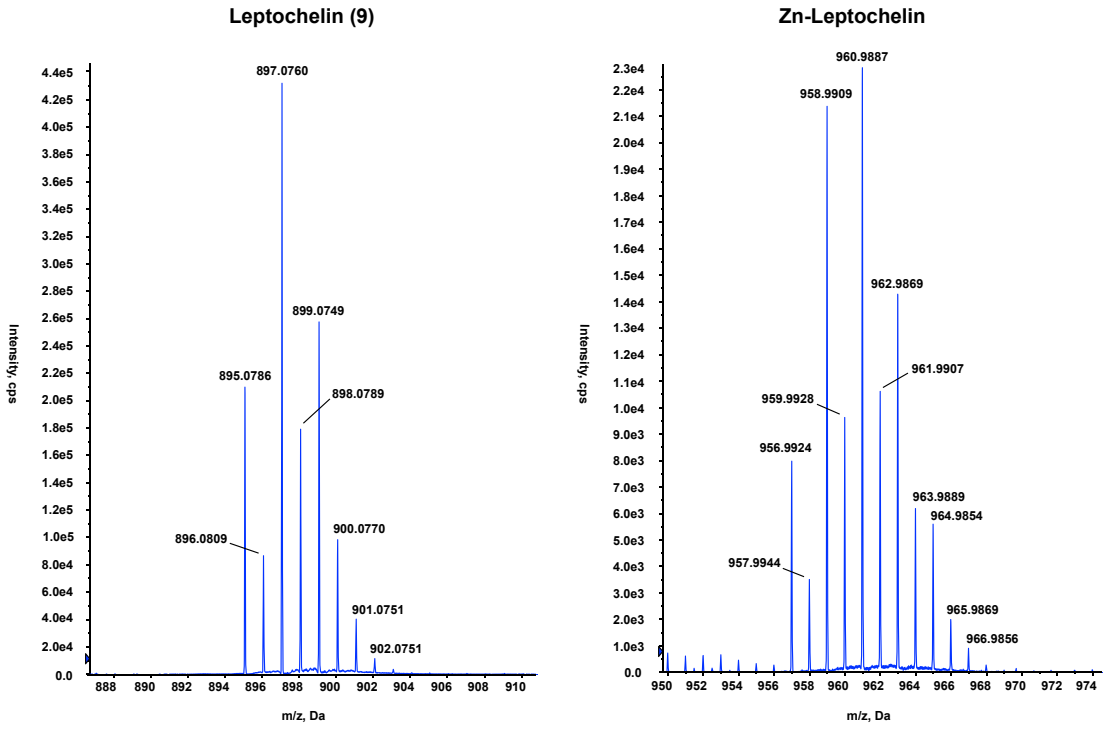

Figure 4.4. HRTOFMS spectra showing the distinct isotope patterns observed for unbound/free leptochelin (**9**) and the Zn(II) adduct.

original isolation scheme. Thus, to directly compare the two compounds by MS and NMR more effectively, approximately 6.0 mg of uncomplexed compound **9** (stored at OSU) was supplied by Dr. W. H. Gerwick, Scripps institution of Oceanography, University of California, San Diego, and is gratefully acknowledged.

Newly acquired HRTOFMS data for **9** showed a pseudomolecular ion $[M + Na]^+$ at *m/z* 895.0786 (Δ 0.3 mDa) and a complex isotope pattern consistent with the presence of several heteroatoms (Figure 4.4). Analysis of this isotope pattern, coupled with ^{1}H and ^{13}C NMR data, established a molecular formula of $C_{35}H_{39}N_4O_{11}SCl_2Br$, and implied 17 degrees of unsaturation. The atomic composition of the Zn-leptochelin molecular ion was established as $C_{35}H_{37}N_4O_{11}SCl_2BrZnNa$ from HRTOFMS data ($[M – 2H + Zn + Na]^+$ *m/z* 956.9924, Δ 0.0 mDa). Although the original NMR dataset (acquired ~2002) for **9** was quite extensive, and obtained on nearly 10–fold more

Table 4.1. NMR Spectroscopic Data for Leptochelin (**9**) and Zn-Leptochelin in $CDCl_3$.

	Leptochelin		Zn-Leptochelin	
No.	δ_H, mult. (*J* in Hz)[a]	δ_C or δ_N, mult.[a]	δ_H, mult. (*J* in Hz)	δ_C, mult.
1		178.9, C		179.0, C
2		85.4, C		84.3, C
3a	3.42, d (-11.7)	41.8, CH_2	3.44, d (-11.7)	42.1, CH_2
3b	3.59, d (-11.7)		3.59, d (-11.7)	
4	1.45, s	22.9, CH_3	1.47, s	22.6, CH_3
N(1)		285.1[b], N		
5		176.8, C		176.3, C
6		61.5, C		61.6, C
7	3.67, d (8.1)	64.4, CH	3.72, d (8.2)	64.3, CH
8	3.92, m	75.4, CH	4.00, br m	75.0, CH
9a	3.72, m	37.8, CH_2	3.79, dd (2.7, 8.6)	38.2, CH_2
9b	3.88, m		3.93, dd (1.0, 10.2)	
10	1.56, s	21.1, CH_3	1.543, s	20.9, CH_3
11		186.5, C		185.0, C
12		62.7, C		61.7, C
13	3.84, br	77.9, CH	3.86, d (2.7)	78.0, CH
14	4.51, m	50.2, CH	4.53, pd (7.6, 3.0)	50.3, CH
15	1.53, s	31.1, CH_3	1.541, s	30.8, CH_3
16	1.18, d (7.1)	15.4, CH_3	1.16, d (7.6)	15.5, CH_3
NH(2a)	1.52, obs	39.7[c], NH_2	1.63, obs	
NH(2b)	3.29, obs		3.56, br d (-11.6)	
OH-13	4.59, d (1.5)		4.64, br s	
NH(3)	10.09, d (7.7)	121.0[c], NH	10.16, d (7.7)	
17		175.2, C		175.3, C
18	4.42, m	57.8, CH	4.41, ddd (3.6, 7.0, 11.0)	58.1, CH
19a	2.92, dd (2.4, 11.7)	37.1, CH_2	2.93, dd (2.4, 11.7)	37.1, CH_2
19b	3.26, dd (3.4, 14.4)		3.25, dd (3.5, 14.2)	
20		135.7, C		135.7, C
21/25	7.22, d (8.2)	130.9, CH	7.24, d (8.3)	130.9, CH
22/24	7.46, d (8.2)	131.9, CH	7.47, d (8.3)	131.9, CH
23		121.0, C		121.0, C
NH(4)	8.07, d (7.0)	125.0[c], NH	8.27, d (7.0)	
26		173.0, C		172.9, C
27	4.509, m	67.4, CH	4.57, br dd (8.5, 9.5)	67.2, CH
28a	4.34, m	69.4, CH_2	4.34, br dd (8.4, 8.4)	69.1, CH_2
28b	4.44, m		4.46, br dd (8.8, 9.6)	
29		171.0, C		170.5, C
30		117.9, C		118.5, C
31		165.0, C		165.6, C
32		111.2, C		109.8, C
33	7.58, dd (1.9, 7.8)	137.5, CH	7.59, dd (1.7, 7.4)	137.7, CH
34	6.30, t (7.8)	112.8, CH	6.30, t (7.8)	112.8, CH
35	7.62, dd (1.9, 7.8)	130.2, CH	7.62, dd (1.7, 8.1)	130.5, CH
OH-31				

NMR data recorded at 600 MHz for leptochelin (9) and 700 MHz for Zn-leptochelin.

[a] Data for ^1H and ^{13}C obtained from Vulpanovici (2003).

[b]Assigned from ^{15}N-GHMBC (500 MHz). [c]Assigned from ^{15}N-HSQC (600 MHz). obs = obscured.

compound, the ^{1}H and ^{13}C NMR spectra for Zn-leptochelin exhibited fewer overlapped signals compared to those for unbound **9** (see Supporting Information), which is possibly due to a more rigid conformation provided by the bound zinc species. Thus, the planar structure of leptochelin (**9**) was established through the combined analysis of the two NMR datasets for unbound leptochelin and Zn-leptochelin. Several distinct features were deduced from the ^{1}H, ^{13}C and multiplicity-edited HSQC NMR spectra for Zn-leptochelin that suggested it was derived from a mixed nonribosomal peptide synthetase (NRPS) and polyketide synthase (PKS) biosynthetic pathway (Table 4.1). These included the presence of two substituted aromatic spin systems (δ_H 6.3–7.62), two NH doublets (δ_H 8.27 and δ_H 10.16), two putative α-H multiplets (δ_H 4.41 and 4.53), four methylenes (δ_H 2.93–4.46), six putative ester/amide carbonyl ^{13}C signals (δ_C 170.5–185.0), four oxymethines (δ_C 64.3–78.0) and four methyl groups (δ_C 30.8, 22.6, 20.9, 15.5). Interpretation of COSY and HMBC correlations (Supporting Information, Tables S-4.1 and S-4.2) further defined the two aromatic spin systems as a *para*-substituted bromo-phenylalanine (4-Br-Phe), indicated by two mutually coupled 2H doublets (δ_H 7.47 and 7.24), and a 3-chloro-2-hydroxybenzoic acid (3-chlorosalicylic acid, 3-CSA) moiety. An HMBC correlation to the benzoic acid carbonyl resonance ($\delta_{C\text{-}29}$ 170.5) from a midfield methine multiplet (δ_H 4.57), in turn coupled to a midfield methylene ^{13}C resonance ($\delta_{C\text{-}28}$ 69.1) and a second deshielded quaternary ^{13}C signal ($\delta_{C\text{-}26}$ 172.9), was consistent with a 2,3-dihydroxypropanoic acid (Dhpa) residue connected to the chlorosalicylic acid moiety (Table A-4.2). The Dhpa carboxylate (C-26) was connected to the amino terminus of the 4-Br-Phe residue in an amide linkage on the basis of an HMBC correlation from NH-4 (δ_H 8.27) to carbonyl C-26, thereby establishing a portion of leptochelin (**9**) as –CSA–Dhpa–BrPhe–.

Perhaps one of the most challenging features in the structural elucidation of the leptochelin depsipeptide (**9)** was the presence of an exceptionally high number of quaternary carbons, thereby limiting the amount of information obtained from typical

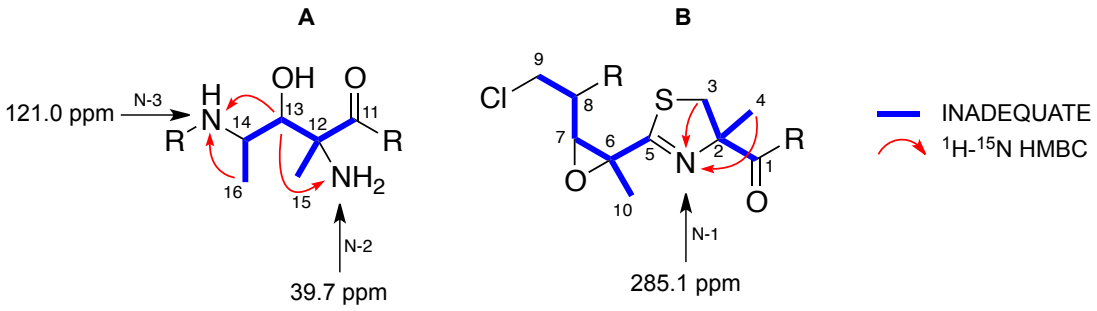

Figure 4.5. Selected ^{13}C-^{13}C (INADEQUATE) and ^{1}H-^{15}N HMBC correlations establishing key fragments containing the 2,4-diamino-3-hydroxy-2-methylpentanoic acid unit (A) and the 4-methyl thiazoline/2-methyloxirane-containing fragment (B) in leptochelin (**9**).

2D NMR experiments (e.g. COSY, HMBC, ROESY, etc.) that could establish key ^{1}H-^{1}H or ^{1}H-^{13}C connections for **9**. Thus, a ^{13}C-enriched sample of leptochelin (**9**), obtained by culturing the Indonesian *Leptolyngbya* sp. in medium supplemented with [U-^{13}C] glucose (Vulpanovici, 2003) during the course of biosynthetic investigations of phormidolide, was subsequently used to acquire an INADEQUATE experiment (Bax et al., 1981). Analysis of the ^{13}C-^{13}C connectivities in this experiment allowed the stepwise tracing of adjacent carbon atoms in leptochelin (**9**). More specifically, connectivities of C-1 to C-4, C-5 to C-10 and C-11 to C-16 visible in the INADEQUATE spectrum for free leptochelin supported several key HMBC and COSY correlations for both free and Zn-bound leptochelin, and clarified several ambiguous connections within the finally assigned unusual fragments (Figure 4.5). From the data acquired for Zn-leptochelin, an AB spin system of an isolated methylene ($\delta_{H\text{-}3}$ 3.44/3.59) showed HMBC correlations to signals for the C-1 carbonyl (δ_C 179.0) and C-5 sp^2-hybridized quaternary carbon (δ_C 176.3), establishing a continuous connection from C-1 to C-10. Within this fragment, HMBC correlations from a methyl singlet ($\delta_{H\text{-}4}$ 1.47) to a midfield resonance for a quaternary carbon ($\delta_{C\text{-}2}$ 84.3), the C-3 methylene and C-1 carbonyl ^{13}C resonances, was consistent with the

presence of an α-methyl thiazoline. Further indication of heterocyclization at this position was evidenced by the downfield shift of the ^{15}N resonance for N-1 (δ_N 285.1) relative to the two amide nitrogens ($\delta_{N\text{-}3}$ 121 and $\delta_{N\text{-}4}$ 125; Martin & Hadden, 2000) in the ^{15}N experiments acquired on free leptochelin. Finally, the adjacent 2-methyloxirane within the C-5 to C-10 portion of this fragment was proposed based on the requirement for an additional unsaturation from the molecular formula and ^{13}C chemical shift data consistent with the attachment of an epoxide oxygen to C-6 (δ_C 61.6) and C-7 (δ_C 64.3). For the C-11 to C-16 fragment (Figure 4.5), careful inspection of the HMBC and HSQC data, revealed two obscured ^1H signals (δ_H 3.56 and 1.63) that shared a mutual COSY correlation. The presence of a primary amine was confirmed by an ^{15}N-HSQC experiment acquired on unbound leptochelin (δ_H 3.29 and 1.53 / δ_N 39.7; Supporting Information, Table S-4.1). Furthermore, HMBC correlations from the free amine ^1H signal at δ_H 3.56 to deshielded quaternary carbon ($\delta_{C\text{-}11}$ 185.0),

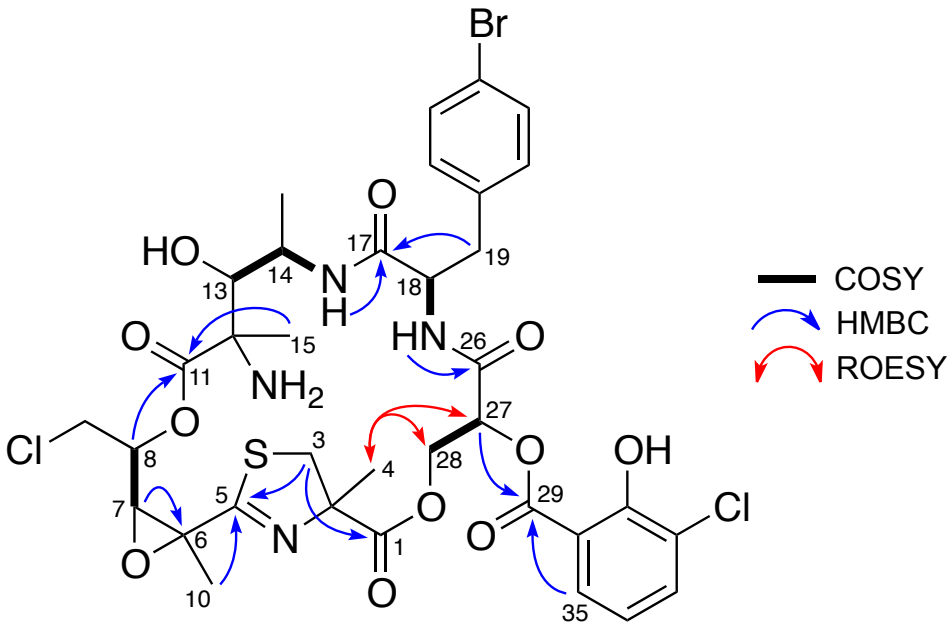

Figure 4.6. Selected 2D NMR correlations connecting the macrocyclic backbone of leptochelin (**9**).

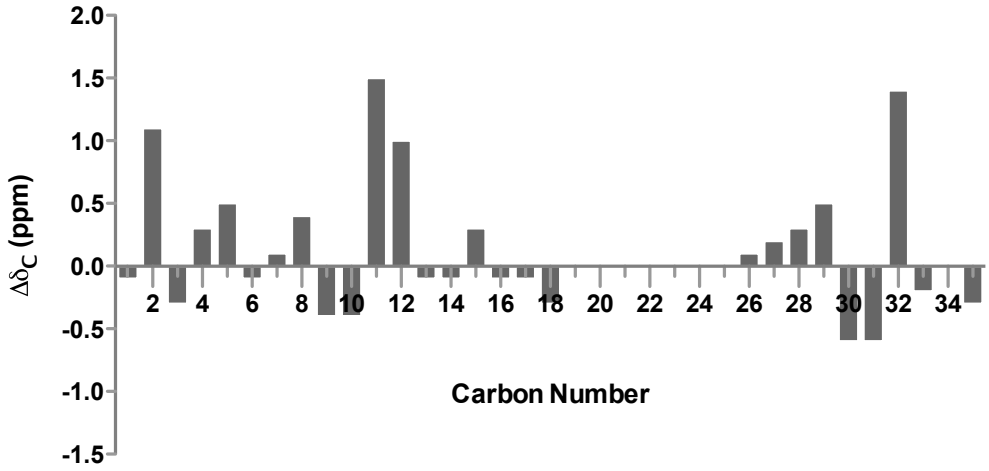

Figure 4.7. Differential ^{13}C NMR chemical shifts for leptochelin (**9**) and Zn-leptochelin ($\Delta = \delta_C$ 9 – δ_C Zn-9).

midfield quaternary carbon ($\delta_{C\text{-}12}$ 61.7) and oxymethine ($\delta_{C\text{-}13}$ 78.0) resonances were consistent with a ^{1}H-^{15}N-gHMBC spectrum for free leptochelin. The latter showed a correlation from oxymethine H-13 (δ 3.84) to the shielded free amine resonance, placing the free amine moiety on C-12 geminal to CH_3-15. Several key HMBC and ROESY (supported by COSY and INADEQUATE) correlations established the macrocyclic backbone and led to the proposed planar structure for leptochelin (**9**, Figure 4.6). Notably, an HMBC correlation from H-8 (δ 4.00) to a deshielded quaternary ^{13}C resonance ($\delta_{C\text{-}11}$ 185.0), and ROE cross peaks observed in Zn-leptochelin between the H_3-4 (δ_H 1.47), H-27 (δ_H 4.57) and H_2-28 (δ_H 4.34/4.46) established the two ester linkages in the molecule. Given the number of highly modified groups within this molecule, X-ray crystallographic analysis is likely the best method to determine the absolute configuration of the nine chiral centers, as well as the coordinating geometry for the bound zinc ion. However, attempts to obtain crystals of **9** large enough for X-ray crystallographic analysis have thus far failed. Despite this setback, there are several key differences in the ^{13}C NMR chemical shifts between unbound **9** and the zinc bound species that indicate possible metal binding sites

(Figure 4.7). Notable are the ^{13}C shift variations observed at the C-2 thiazoline stereocenter, the free amine-substituted C-12 and neighboring carbonyl carbon C-11. In addition, the NH_2 ^{1}H signals (δ_H 1.63/3.56) for Zn-leptochelin were shifted slightly downfield compared to those for unbound **9** (δ_H 1.52/3.29). Overall, these chemical shift differences suggest that each of these functional groups may coordinate the binding of Zn^{2+} in leptochelin (**9**). Most intriguing is the ^{13}C shift variation observed at C-32 (Δ 1.4 ppm), the chlorine-bearing aromatic carbon vicinal to the phenolic carbon (C-31) of the benzoic acid moiety. Although the C-31 shift chemical difference is relatively minimal (< 0.5 ppm), it is conceivable that the C-31 –OH and the C-32 chlorine substituent may also coordinate Zn^{2+} in a manner similar to that of catechol-containing siderophores. However, it is also possible that only the hydroxyl oxygen participates in the binding of Zn^{2+}; in doing so, the change in electron delocalization around the aromatic ring causes shielding of C-32. Importantly, all of the ^{1}H NMR signals observed in the spectrum for unbound **9** were also present in the spectrum for Zn-leptochelin (Table 4.1), suggesting that deprotonation is not required for the binding of the zinc. Thus, the loss of two protons observed in the HRESIMS spectrum of Zn-leptochelin likely occurs during the ionization process. However, it should be noted that the C-31 –OH ^{1}H signal was not observed in either of the ^{1}H NMR spectra. Nonetheless, the binding of zinc by leptochelin is quite remarkable, considering that the zinc ion remains bound throughout the chromatographic methods employed in our isolation scheme. This is further supported by the observation of two clearly distinguishable chromatographic peaks representing both leptochelin and Zn-leptochelin A, as well as differences observed in their respective optical rotations, UV absorbances and CD spectra (Supporting Information, Figure S-4.2), which is consistent with reported literature values for the metal-bound patellamides and lissoclinamides (Morris, Jaspars, et al., 2001; Morris, Milne, et al., 2001).

Leptochelin (**9**) possesses a diverse array of modified structural features that likely stem from the interplay of a mixed NRPS/PKS biosynthetic pathway containing

multiple optional domains and/or tailoring enzymes. Furthermore, 3-chlorosalicylic acid is probably derived from benzoic acid via the shikimate pathway (Dewick, 2009), which undergoes halogenation at some point during or post assembly. Another intriguing structural element is the 4-methylthiazoline fused to the 2-methyloxirane-containing unit. Notably, a methylated thiazoline was not proposed in the original structure (Vulpanovici, 2003). In fact, α-methyl thiazolines have only recently been reported from marine cyanobacteria, such as in largazole (Taori et al., 2008), the hoiamides (Choi et al., 2010), and grassypeptolides D and E from our group (Thornburg et al., 2011). Remarkably, this is the second Red Sea *Leptolyngbya* sp. identified to produce methylated thiazolines. Thus, to gain some insight into the taxonomic relationship of our different α-methyl thiazoline-producing strains, a phylogenetic analysis based on the SSU (16S) rRNA gene sequences from the grassypeptolide-producing Red Sea *Leptolyngbya* sp. RS03 (GenBank acc. no. JF518829), the leptochelin-producing Red Sea *Leptolyngbya* sp. RS02 (GenBank acc. no. JX481735) and the leptochelin-producing Indonesian *Leptolyngbya* sp. was performed. The analysis revealed a distinct cluster of *Leptolyngbya* spp. with a shared evolutionary history (Figure 4.8). Morphologically, the two leptochelin-producing strains were identical to one another, which is supported by their identical 16S rRNA gene sequences. Noteworthy is that these two strains group closely with the marine *Leptolyngbya* reference strain *Leptolyngbya ectocarpi* ATCC 29409, which exhibits a thin bright-red mat compared to the thick deep-purple mats of the leptochelin-producing *Leptolyngbya* spp (see Appendix). Interestingly, a systematic classification of the grassypeptolide-producing strain, which exhibits small purple tufts that adhere to the bottom of the culture flask, indicated that this organism is *Leptolyngbya ectocarpi* (Gomont) Anagnostidis et Komárek (Komárek & Anagnostidis, 2005; Thornburg et al., 2011). However, this latter strain is evolutionarily distant from the reference strain compared to the leptochelin-producers. These morphological

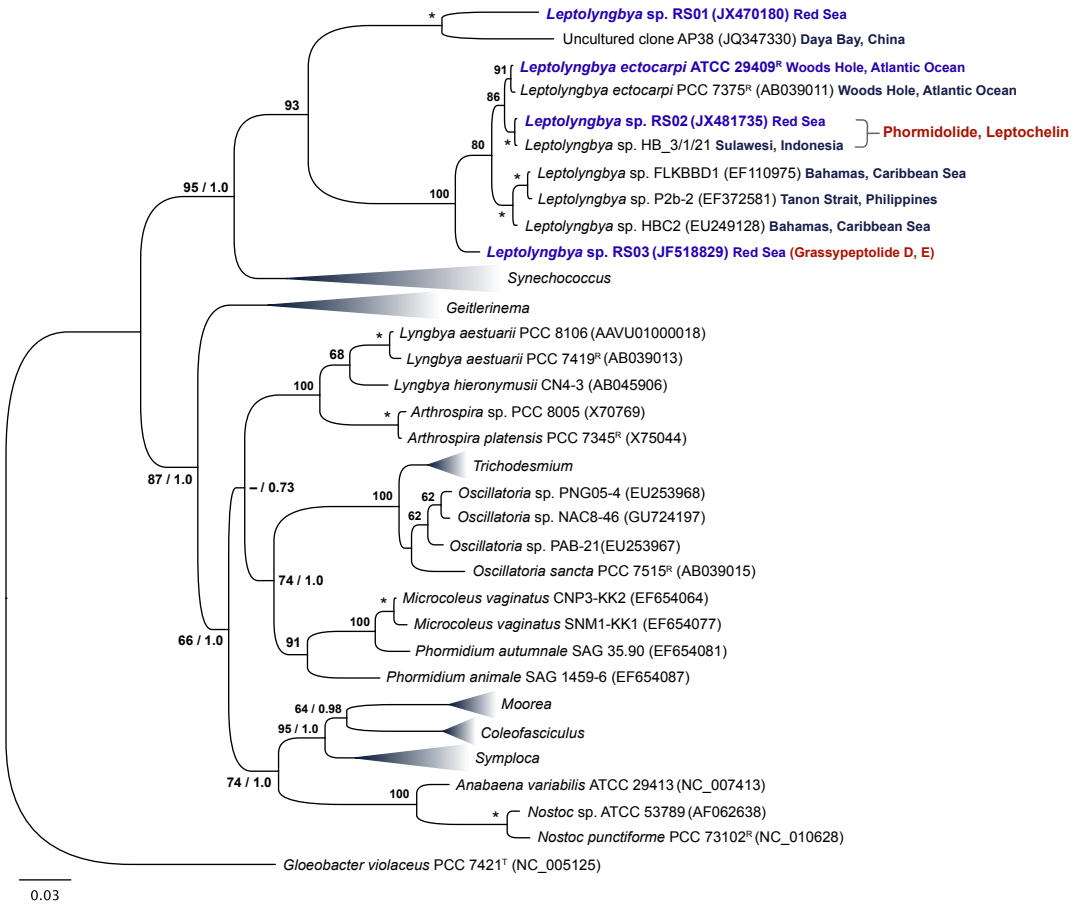

Figure 4.8. Phylogenetic relationship of the leptochelin-producing cyanobacteria with other marine filamentous cyanobacteria based on SSU (16S) rRNA gene sequences. Labels on the terminal nodes indicate the taxa, strain, GenBank accession numbers in parenthesis, and collection sites for relevant strains. Reference (^{R}) or type strains (^{T}) are included within each cyanobacterial group. The support values at important nodes are indicated as bootstrap and posterior probability for the maximum-likelihood (PhyML) and Bayesian inference (MrBayes) methods (* = bootstrap of > 98% and a posterior probability of 1.0). Support values < 60 are not indicated. The scale bar indicates 0.03 expected nucleotide substitutions per site.

differences, coupled with the 16S rRNA data, further support the need for the inclusion of phylogenetics into the taxonomic classification of cyanobacteria.

The less conserved internal transcribed spacer (ITS) region linking the 16S and 23S ribosomal genes has been used to probe the subgeneric relationship of

cyanobacteria (Boyer et al., 2001; Otsuka et al., 1999). Given that the seemingly identical leptochelin-producing strains of *Leptolyngbya* sp. were isolated from geographically distant collection sites, yet maintained in the same culture laboratory, additional housekeeping genes were investigated to gain further insight into their relatedness. These included the less conserved 16S–23S ITS region, as well as the RNA polymerase gamma subunit (*rpoC1*) gene. Although the sequence data for the 16S–23S ITS region did show several base pair substitutions (99.9% sequence identity) between the two leptochelin-producing *Leptolyngbya* spp., we cannot rule out the possibility of the existence of multiple rRNA operons within these strains. However, it should be noted that only one band of identical length was obtained for the 16S plus ITS region for each isolate using several different primer sets. This is consistent with the presence of only a single rRNA operon or multiple identical operons (Boyer et al., 2001). Furthermore, the *rpoC1* gene sequence was identical between the two strains. Thus, it is likely that these two *Leptolyngbya* spp. are the same strain isolated from geographically distant locations, which is plausible considering that the ocean currents connecting the Indian Ocean to the Red Sea may serve as a biological corridor. This "transport" phenomenon may also be reflected in the similarities observed between our apratoxin H-producing Red Sea *Moorea producens* strain RS05 (GenBank acc. no. JX470179) and the apratoxins F and G-producing Palmyra Atoll *Moorea bouillonii* strain PAL08-16 (GenBank acc. no. GU111927), which share 99.5% sequence identity between their respective (SSU) 16S rRNA genes. Notably, the two apratoxin-producing strains were maintained in different culture collections.

Leptochelin (**9**) displayed potent cytotoxicity to human NCI-H460 lung cancer cells (IC_{50} = 153 nM). In contrast, it was nearly 7–fold less cytotoxic to HeLa cervical carcinoma cells (IC_{50} = > 1.0 μM), suggesting some level of cancer cell selectivity (Supporting Information, Figure S-4.1). Remarkably, the zinc bound form of leptochelin resulted in a 2 to 4.5–fold reduction, respectively in IC_{50} values across for

the two cell lines. Thus, it is tempting to speculate that leptochelin may demonstrate a cell-specific, metal-dependent mechanism (e.g. inhibition of a specific metalloenzyme via selective chelation of its metal cofactor), and a non-specific metal-dependent mechanism of action, whereby an exogenously bound zinc ion confers activity on leptochelin (e.g. through the generation of intracellular ROS via a redox mechanism). Importantly, ROS can activate several signaling cascades in mammalian cells, and thus either contribute to cellular proliferation or induce antiproliferative effects depending upon the cell type and concentration of individual reactive species (Storz, 2005). As such, altering the redox status of cancer cells has become an attractive target for anticancer therapeutics. For example, ATN-224 (choline tetrathiomolybdate) selectively chelates the copper ion in superoxide dismutase 1 (SOD1), a Cu/Zn-dependent enzyme that regulates ROS in cells by converting superoxide anions (O_2^-) into H_2O_2 and O_2 (P. Huang et al., 2000). This leads to an inhibition of cell proliferation and angiogenesis in endothelial cells (Juarez et al., 2006). Noteworthy is that SOD1 is overexpressed in a number of human lung adenocarcinomas, including human lung cancer epithelial H460 cells (Somwar et al., 2011). Thus, possible SOD1 inhibition by leptochelin would be predicted to lead to an increase in the steady-state levels of superoxide anion in the cell, which has been shown to decrease cell migration and invasion in H460 cells (Luanpitpong et al., 2010). Furthermore, the generation of mitochondrial-derived ROS is an early and necessary event for the initiation of bortezomib-induced apoptotic signaling in H460 cells (Ling et al., 2003). Lastly, it should be noted that the presence of both iron and copper bound species of leptochelin were identified during preliminary LC-MS profiling, but have not yet been obtained in pure form. Thus, further characterization of the metal binding capabilities of leptochelin with respect to selectivity and affinity may provide valuable information for its potential cellular target. In addition, the differential activity observed for leptochelin, coupled with the numerous potential targets of metal chelators,

necessitates further investigation as to the mechanism of action and cancer chemotherapeutic potential of leptochelin (**9**).

Experimental

General Experimental Procedures. Optical rotations were measured on a JASCO P-1010 polarimeter. UV spectra and CD measurements were recorded using a JASCO J-815 spectropolarimeter. IR spectra were recorded on a Thermo Scientific Nicolet IR100 FT-IR Spectrometer. NMR data for leptochelin were acquired in $CDCl_3$ referenced to residual $CHCl_3$ chemical shifts (δ_C 77.2, δ_H 7.26) on a Bruker DRX 600 MHz spectrometer (5mm TXI probe) and a Bruker DPX 400 MHz spectrometer (Vulpanovici, 2003). ^{15}N spectra were referenced to a 100 mM solution of formamide in $CDCl_3$ ($HCONH_2 = 0$ ppm). NMR data for Zn-leptochelin A were acquired in $CDCl_3$ on a Bruker Avance III 700 MHz spectrometer equipped with a 5mm ^{13}C cryogenic probe and a Bruker Avance III 500 MHz spectrometer equipped with a 5 mm TXI probe. HRESIMS for each compound was performed in positive ion mode on an AB SCIEX Triple TOF 5600 mass spectrometer. Individual isotope patterns were analyzed using the Formula Finder tool in PeakView®, a stand-alone software package developed specifically for the AB SCIEX TripleTOF 5600 system. LC-ESIMS data were obtained on an AB SCIEX 3200 Q TRAP mass spectrometer. HPLC was performed using a Shimadzu dual LC-20AD solvent delivery system with a Shimadzu SPD-M20A UV/VIS photodiode array detector.

Collection, Isolation and Culture of the Red Sea *Leptolyngbya* sp. strain RS02. A cyanobacterial mat of apparent mixed assemblage was collected by hand using scuba from a hard coral surface (24–30 ft) in the Red Sea on May 26, 2007 (collection code EHu-05-26-07-4). Cyanobacterial isolation, morphological characterization and culturing was performed as described previously (Thornburg et al., 2011). For collection, isolation and culture of the Indonesian *Leptolyngbya* sp. see Vulpanovici (2003).

DNA Extraction and Amplification of Cyanobacterial genes. Genomic DNA was extracted and 16S rRNA genes amplified by polymerase chain reactions (PCR) as

previously described (Thornburg et al., 2011). The 16S–23S ITS region was PCR amplified using the primers described in Boyer et al. (2001), and the RNA polymerase gamma-subunit (*rpoC1*) genes with the degenerate primers described in Engene et al. (2010): LrpoC1-F (5′-CYTGYTTNCCYTCDATDATRTC-3′) and LrpoC1-R (5′-YTNAARCCNGARATGGAYGG-3′). The 16S rRNA partial gene sequences and their respective ITS regions were inspected visually and assembled using CAP3 (X. Huang & Madan, 1999). The resulting contig was analyzed for chimeric sequences using Pintail (Ashelford et al., 2005) and compared to sequences in the Ribosomal Database Project database (http://rdp.cme.msu.edu) and GenBank (http://www.ncbi.nlm.nih.gov). The 16S rRNA consensus sequence was deposited in GenBank under accession number JX481735.

Phylogenetic Analysis. The evolutionary relationship of the Red Sea *Leptolyngbya* strain with other groups of cyanobacteria was determined as described in Chapter Two of this thesis.

Extraction and Isolation of Zn-leptochelin. Cultures of *Leptolyngbya* sp. RS02 (10 × 1.5 L cultures grown for 6 months) were harvested by filtration on glass-fiber filters and extracted in organic solvent (CH_2Cl_2-MeOH, 2:1) to afford 2.05 g of extract. The organic extract was subjected to bioassay-guided fractionation via NP VLC using a stepped solvent gradient of hexanes to EtOAc to MeOH to produce six fractions (A, C, E, G, H and I). The fraction eluting with 25% MeOH–EtOAC (H) was moderately toxic to brine shrimp and further separated by RP_{18} SPE using a stepped solvent gradient of MeOH–H_2O from 50% MeOH–H_2O to 100% MeOH, followed by 100% CH_2Cl_2. The RP_{18} SPE fraction eluting in 85% MeOH was subjected to RP-HPLC using a combined isocratic and gradient profile (column: Synergi Polar-RP, 10 x 250 mm, 75% MeOH-H_2O for 30 min., increasing to 100% MeOH for 30 min., 3.0 mL/min) to yield Zn-leptochelin A (1.1 mg, t_R = 46.8 min.). LC-MS profiling (Synergi Fusion-RP, 2 x 100 mm, 0.2 mL/min, 70% MeOH in 0.1% (v/v) aqueous FA) of fraction H also showed an ion cluster for $[M - 4H + Fe + Na]^+$ at *m/z* 947/949/951/953

suggesting the presence of Fe-leptochelin. Furthermore, a cluster spanning *m/z* 955 to 965 $[M - 2H + X + Na]^+$ suggested the presence of two overlapping ion clusters for Zn^{2+} and Cu^{2+} bound species. However, only the Zn-bound form was isolated in our HPLC protocol. For the isolation of leptochelin (**9**) see Vulpanovici (2003).

Leptochelin (9): white, amorphous solid; $[\alpha]^{30}_D$ –84.4 (*c* 0.10, $CHCl_3$); UV (MeOH) λ_{max} (log ε) 197 (4.77), 213 (4.57), 255 (4.14), 318 (3.55), 352 (3.37); FTIR (neat) ν_{max} 3333 (br), 3241, 3004, 2921, 2849, 1678, 1611, 1529, 1466, 1379, 1243, 1151, 1074, 1011 cm^{-1}; ^1H and ^{13}C NMR data, see Table 4.1; HRTOFMS $[M + Na]^+$ *m/z* 895.0786 (calcd for $C_{35}H_{39}N_4O_{11}SCl_2BrNa$, 895.0789).

Zn-Leptochelin: clear, yellow glass; $[\alpha]^{30}_D$ –210.5 (*c* 0.10, $CHCl_3$); UV (MeOH) λ_{max} (log ε) 196 (4.81), 225 (4.56), 258 (4.16), 356 (3.77); FTIR (neat) ν_{max} 3338 (br), 2925, 1682, 1606, 1543, 1521, 1512, 1453, 1383, 1244, 1247, 1152, 1072, 1026 cm^{-1}; ^1H and ^{13}C NMR data, see Table 4.1; HRTOFMS $[M - 2H + Zn + Na]^+$ *m/z* 956.9924 (calcd for $C_{35}H_{37}N_4O_{11}SCl_2BrZnNa$, 956.9924).

Biological Assays. Cytotoxicity of the organic extract and crude fractions was evaluated against brine shrimp (*Artemia salina*) as previously described (Carballo et al., 2002; McLaughlin et al., 1998) with some modifications. Samples were added to 24-well plates containing newly hatched (24 h) brine shrimp (10 to 15 per well) in artificial seawater at final concentrations ranging from 1 to 100 ppm. Brine shrimp toxicity was determined after a 24 h incubation period (28 °C) by counting the number of dead shrimp verses total number in each well.

Cytotoxicity of the purified compounds was evaluated in human NCI-H460 lung cancer and HeLa cervical carcinoma cells (ATCC, Manassas, VA) as previously described (Thornburg et al., 2011), with minor modifications. Cells were seeded into 96-well plates (5,000 cells per well) in 50 μL of medium 16 h before treatment. Approximately 2 h before treatment, test samples were generated from a stock solution (6 mg/mL, 100% DMSO) that was serially diluted in serum-free medium. Following aspiration of seed growth medium, test samples (50 μL) were added to seeded cells at

final concentrations ranging from 0.01 nM to 10.0 μM. Each 96-well plate also contained untreated and vehicle-treated control cells. Cell viability was determined after 48 h treatment using a standard 3-(4,5-dimethylthiazol-2-yl)-2,5,diphenyly tetrazolium bromide (MTT) assay as previously described (Thornburg et al., 2011). The cytotoxicity of each purified compound was assessed in at least three independent cultures with the viability of vehicle-treated control cells defined as 100% in all experiments. Dose response curves were plotted using GraphPad Prism® (v5.0) and IC_{50} values were derived from nonlinear regression analysis.

Acknowledgement

We thank the Red Sea Protectorate for permission to make collections of Red Sea cyanobacteria, and Jeff Morré of the Environmental Health Sciences Center at OSU for mass spectrometric data acquisition (NIEHS P30 ES00210). The National Science Foundation (CHE-0722319) and the Murdock Charitable Trust (2005265) are acknowledged for their support of the OSU Natural Products and Small Molecule Nuclear Magnetic Resonance. Funding was provided by the OSU College of Pharmacy.

Supporting Information

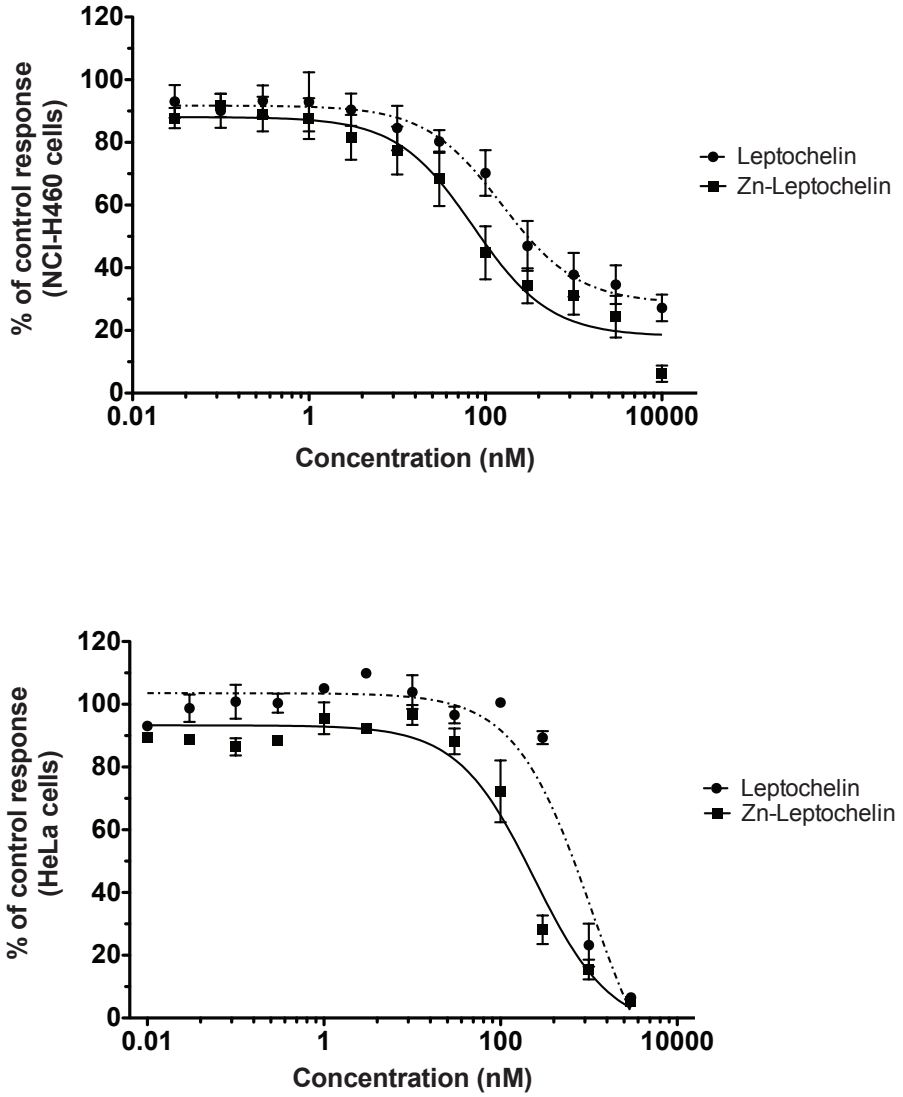

Figure S-4.1. The dose response curves for leptochelin (**9**) and Zn-leptochelin in human NCI-H460 (n = 3) and HeLa cervical carcinoma cell lines (n = 3). Cell viability was assessed after 48 hours using a colorimetric MTT cell viability assay and is reported as the percentage of viable cells relative to the vehicle control.

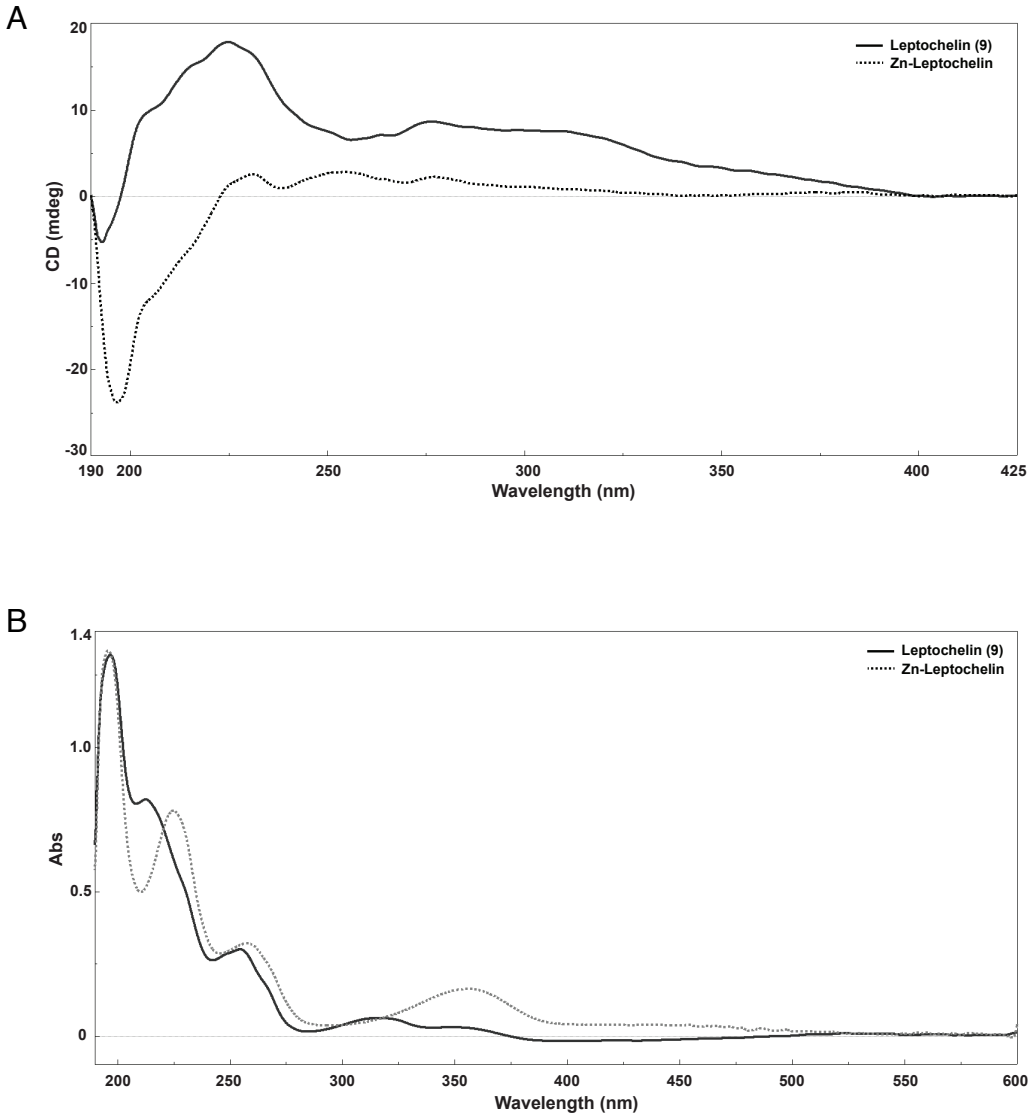

Figure S-4.2. CD (A) and UV (B) spectra for leptochelin (**9**, blue) and Zn-leptochelin (red).

Table S-4.1. NMR Spectroscopic Data for Leptochelin (**9**) in $CDCl_3$.

No.	δ_C[a] or δ_N, mult.	δ_H, mult. (*J* in Hz)[a]	HSQC-TOCSY[a]	HMBC[a]	^{15}N-HMBC	INADEQUATE[a]
1	178.9, C					2
2	85.4, C					1, 3, 4
3a	41.8, CH_2	3.42, d (-11.7)		2, 4, 5	N(1)	2
3b		3.59, d (-11.7)		1, 2, 4		
4	22.9, CH_3	1.45, s		1, 2, 3	N(1)	2
N(1)	285.1[b], N					
5	176.8, C					6
6	61.5, C					5, 7, 10
7	64.4, CH	3.67, d (8.1)	8, 9	6, 8, 9, 10		6, 8
8	75.4, CH	3.92, m	7, 9	7, 9, 11		7, 9
9a	37.8, CH_2	3.72, m	7, 8, 9	7, 8		8
9b		3.88, m		7, 8, 11		
10	21.1, CH_3	1.56, s		5, 6, 7		6
11	186.5, C					12
12	62.7, C					11, 13, 15
13	77.9, CH	3.84, br	14, 16, NH(3)	15	NH(2), NH(3)	12, 14
14	50.2, CH	4.51, m	13, 16, NH(3)	12, 13, 16		13, 16
15	31.1, CH_3	1.53, s		11, 12, 13		12
16	15.4, CH_3	1.18, d (7.1)	13, 14, NH(3)	13, 14	NH(4)	14
NH(2a)	39.7[c], NH_2	1.52, obs				
NH(2b)		3.29, obs		11, 12, 13, 14		
OH-13		4.59, d (1.5)				
NH(3)	121.0[c], NH	10.09, d (7.7)		14, 16, 17		
17	175.2, C					18
18	57.8, CH	4.42, m	19, NH(4)	17, 19, 26		17, 19
19a	37.1, CH_2	2.92, dd (2.4, 11.7)	18	17, 18, 20, 21/25	NH(4)	18, 20
19b		3.26, dd (3.4, 14.4)		18, 20, 21/25	NH(4)	
20	135.7, C					19, 21/25
21/25	130.9, CH	7.22, d (8.2)		19, 22/24, 23		20
22/24	131.9, CH	7.46, d (8.2)		20, 21/25, 23		23
23	121.0, C					22/24
NH(4)	125.0[c], NH	8.07, d (7.0)		18, 19, 26		
26	173.0, C					27
27	67.4, CH	4.509, m		26, 28, 29		26, 28
28a	69.4, CH_2	4.34, m		26, 27, 29		27
28b		4.44, m		26, 27, 29		
29	171.0, C					
30	117.9, C					35
31	165.0, C					32
32	111.2, C					31
33	137.5, CH	7.58, dd (1.9, 7.8)	34	30, 31, 35		34
34	112.8, CH	6.30, t (7.8)	33, 35	30, 32		33, 35
35	130.2, CH	7.62, dd (1.9, 7.8)	34, 35	29, 31, 33		30, 34
OH-31						

[a]All data, with the exception of ^{15}N data, from Vulpanovici (2003) with the numbering scheme modified to match that of Zn-leptochelin. ^{1}H and ^{13}C NMR data recorded at 600 MHz and 150 MHz, respectively. [b]Assigned from ^{15}N-gHMBC (500 MHz). [c]Assigned from ^{15}N-HSQC (600 MHz) acquired by K. McPhail, 2002.

Table S-4.2. NMR Spectroscopic Data for Zn-Leptochelin Complex in $CDCl_3$.

No.	δ_C, mult.	δ_H, mult. (*J* in Hz)	COSY	HMBC	ROESY
1	179.0, C				
2	84.3, C				
3a	42.1, CH_2	3.44, d (-11.7)	H-3b	2, 4, 5	H_3-4
3b		3.59, d (-11.7)	H-3a	1, 2, 4	
4	22.6, CH_3	1.47, s		1, 2, 3	H-3a, H-27, H-28b
N(1)					
5	176.3				
6	61.6, C				
7	64.3, CH	3.72, d (8.2)	H-8	6, 8, 9, 10	H_3-10
8	75.0, CH	4.0, br m	H-8, H-9a, H-9b	7, 9, 11	H_3-10, H_3-16
9a	38.2, CH_2	3.79, dd (2.7, 8.6)	H-8, H-9b	7, 8	
9b		3.93, dd (1.0, 10.2)	H-8, H-9a	7, 8, 11	
10	20.9, CH_3	1.543, s		5, 6, 7	H-7
11	185.0, C				
12	61.7, C				
13	78.0, CH	3.86, d (2.7)	H-14	15	H-14, H_3-15, H_3-16
14	50.3, CH	4.53, pd (7.6, 3.0)	H-13, H_3-16, NH(3)	12, 13, 16	H-13, H_3-16, NH(3)
15	30.8, CH_3	1.541, s		11, 12, 13	H-13
16	15.5, CH_3	1.16, d (7.6)	H-14	13, 14	H-8, H-13, H-14, NH(3)
NH(2a)		1.63, ob	NH(2b)		[a]NH(2b)
NH(2b)		3.56, br d (-11.6)	NH(2a)	11, 13	[a]NH(2a), NH(3)
OH-13		4.64, br s			
NH(3)		10.16, d (7.7)	H-14	14, 16, 17	H-14, H_3-16, H-19a, NH(2a), NH (2b), NH(4)
17	175.3, C				
18	58.1, CH	4.41, ddd (3.6, 7.0, 11.0)	H-19a, H-19b, NH(4)	19	H-19a, H-19b, H-21/25
19a	37.1, CH_2	2.93, dd (2.4, 11.7)	H-18, H-19b	17, 18, 20, 21/25	H-18, H-19b, H-21/25, NH(3), NH(4)
19b		3.25, dd (3.5, 14.2)	H-18, H-19a	18, 20, 21/25	H-18, H-19a, H-21/25
20	135.7, C				
21/25	130.9, CH	7.24, d (8.3)	H-22, H-24	19, 22/24, 23	H-18, H-19a, H-19b, NH(4)
22/24	131.9, CH	7.47, d (8.3)	H-21, H-25	20, 21/25, 23	
23	121.0, C				
NH(4)		8.27, d (7.0)	H-18	18, 19, 26	H-19a, H-21/25, H-27, H-28a, H-28b, NH(3)
26	172.9, C				
27	67.2, CH	4.57, br dd (8.5, 9.5)	H-28a, H-28b	26, 28, 29	H_3-4, NH(4)
28a	69.1, CH_2	4.34, br dd (8.4, 8.4)	H-27, H-28b	26, 27, 29	NH(4)
28b		4.46, br dd (8.8, 9.6)	H-27, H-28a	26, 27, 29	H_3-4, NH(4)
29	170.5, C				
30	118.5, C				
31	165.6, C				
32	109.8, C				
33	137.7, CH	7.59, dd (1.7, 7.4)	H-34	30, 31, 35	H-34
34	112.8, CH	6.30, t (7.8)	H-33, H-35	30, 32	H-33, H-35
35	130.5, CH	7.62, dd (1.7, 8.1)	H-34	29, 31, 33	H-34
OH-31					

^1H and ^{13}C NMR data recorded at 700 MHz and 175 MHz, respectively. [a]COSY artifact observed in ROESY spectrum. ob = obscured.

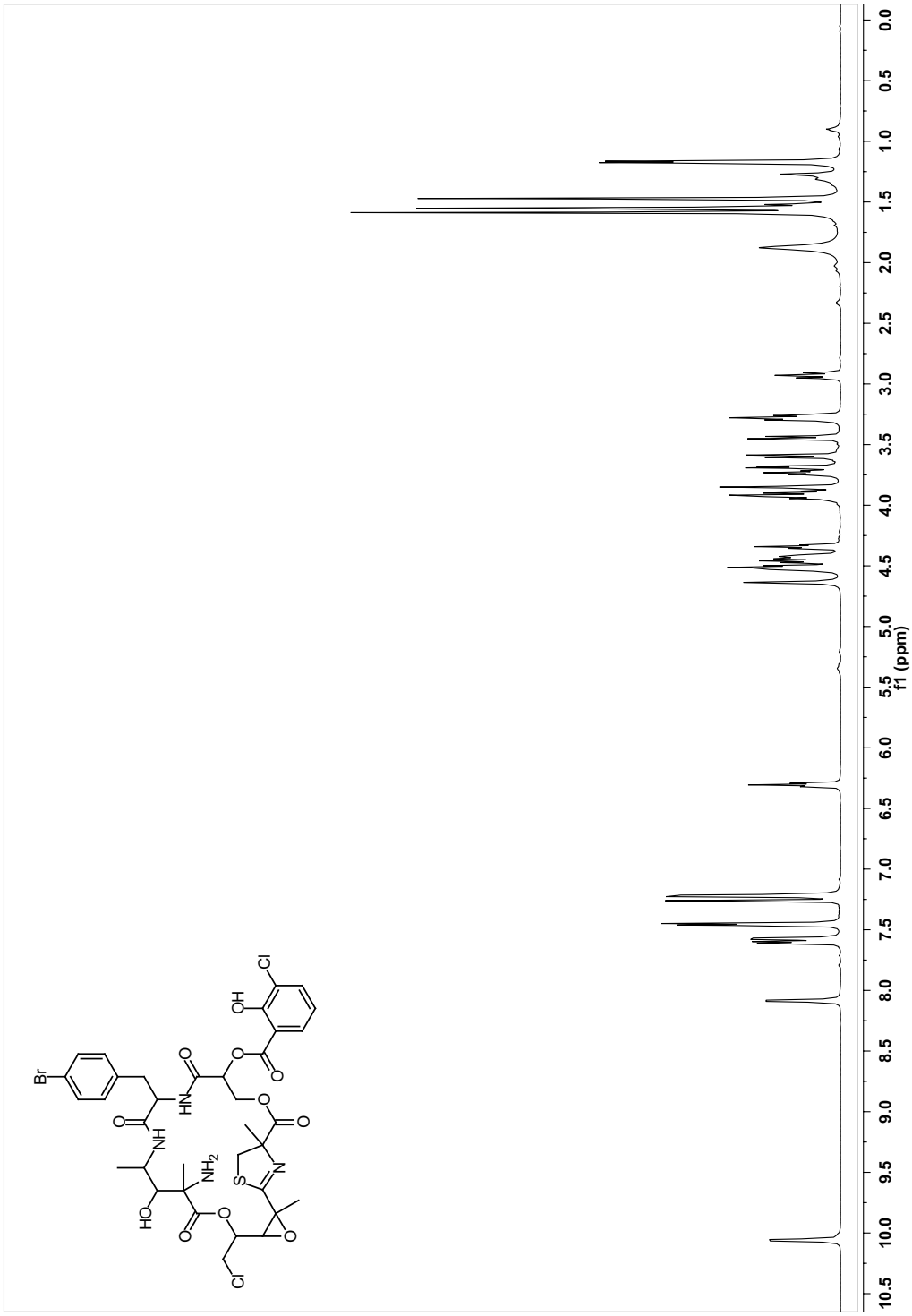

Figure S-4.3. ^{1}H NMR spectrum for leptochelin (**9**) in $CDCl_3$ (600 MHz).

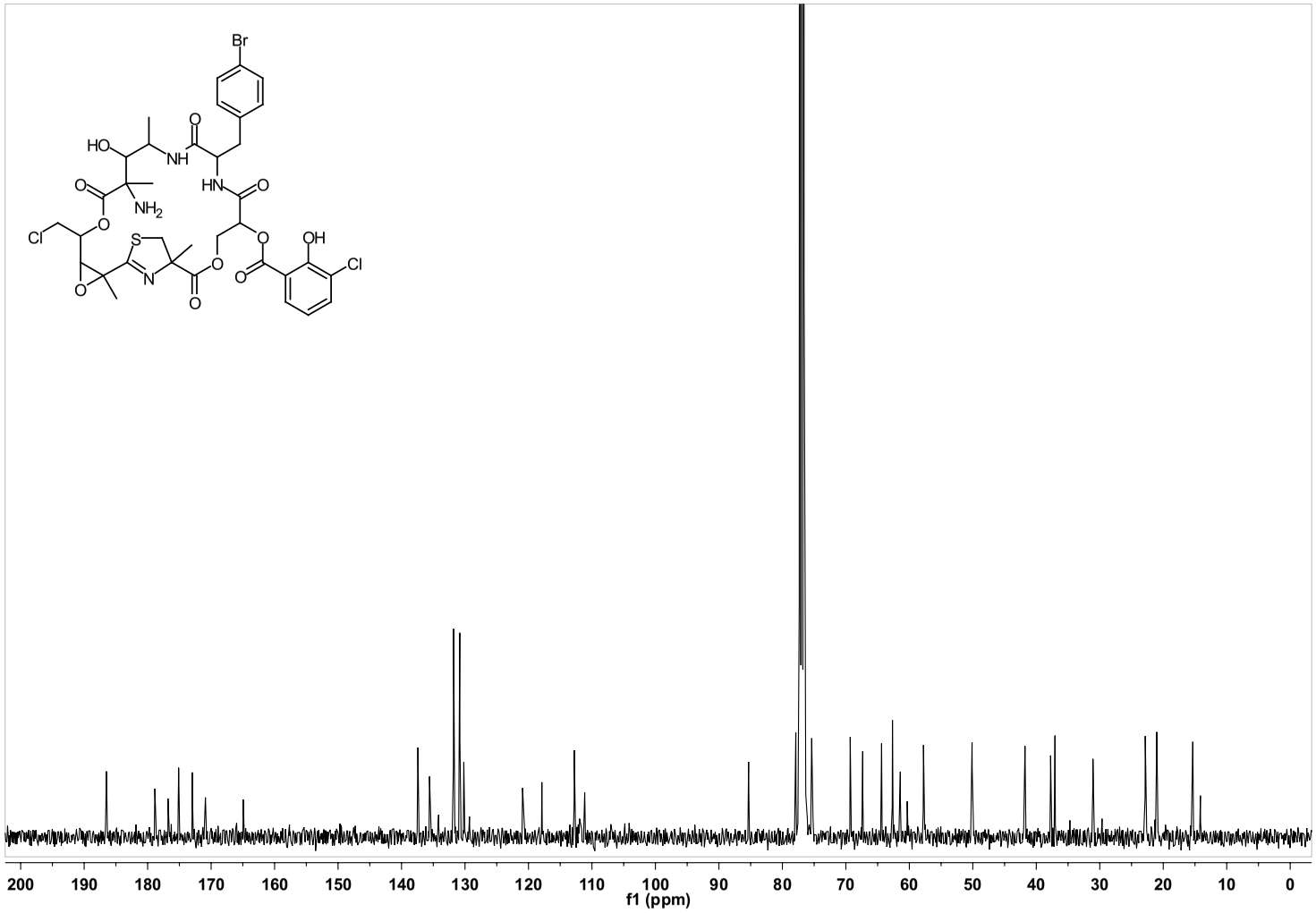

Figure S-4.4. ^{13}C NMR spectrum for leptochelin (**9**) in $CDCl_3$ (150 MHz).

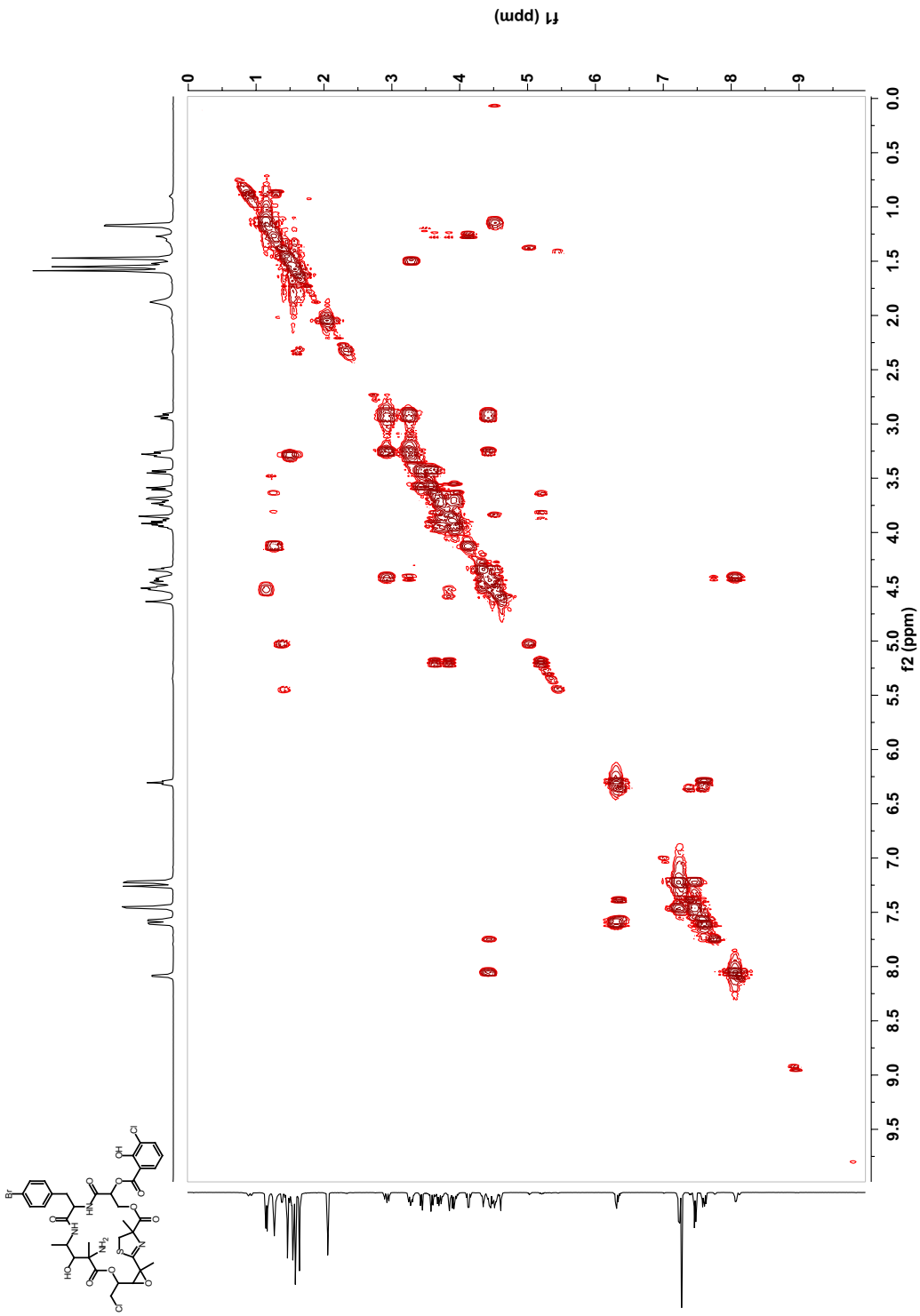

Figure S-4.5. COSY spectrum for leptochelin (**9**) in $CDCl_3$ (600 MHz).

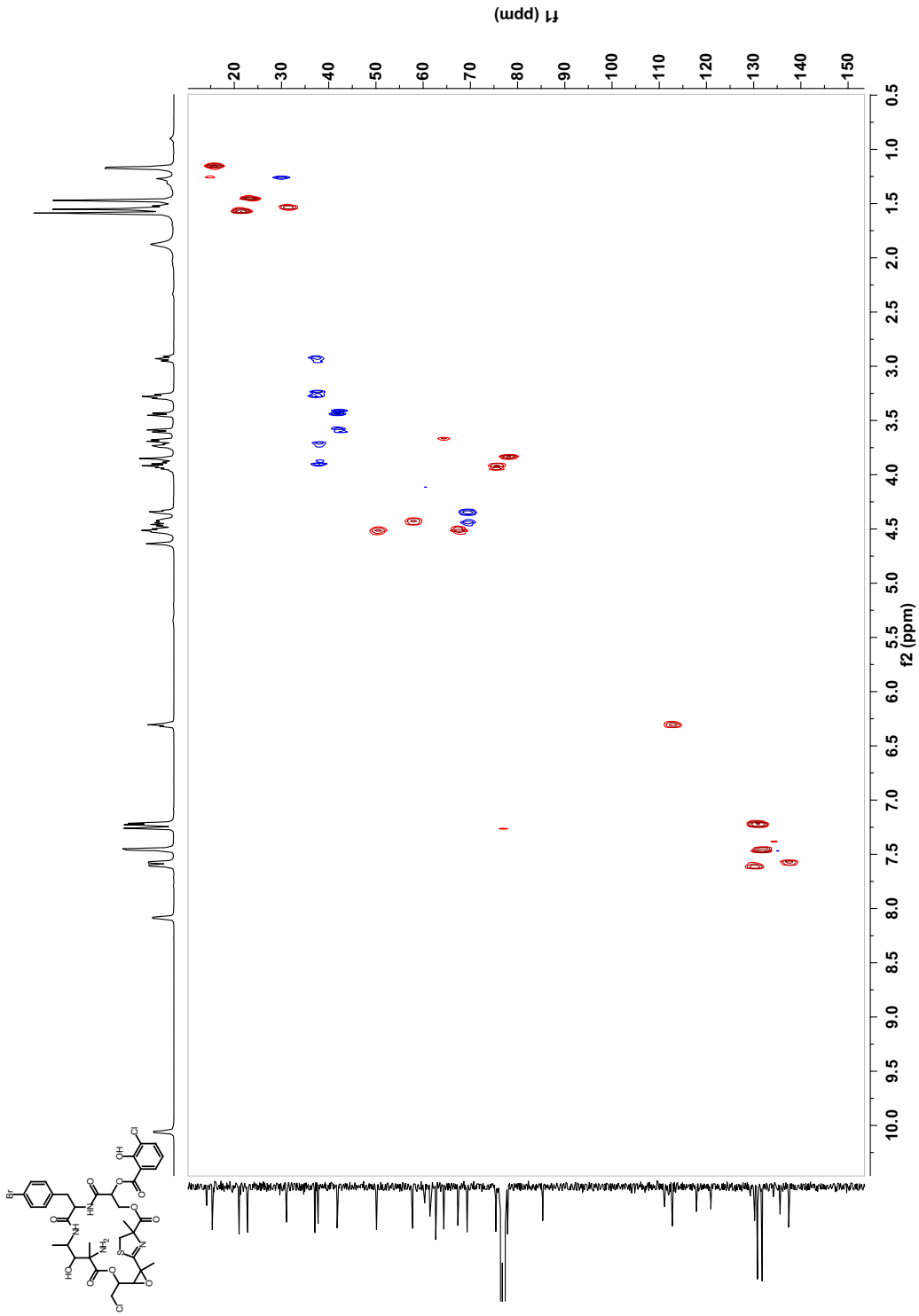

Figure S-4.6. Multiplicity-edited HSQC spectrum for leptochelin (**9**) in $CDCl_3$ (600 MHz).

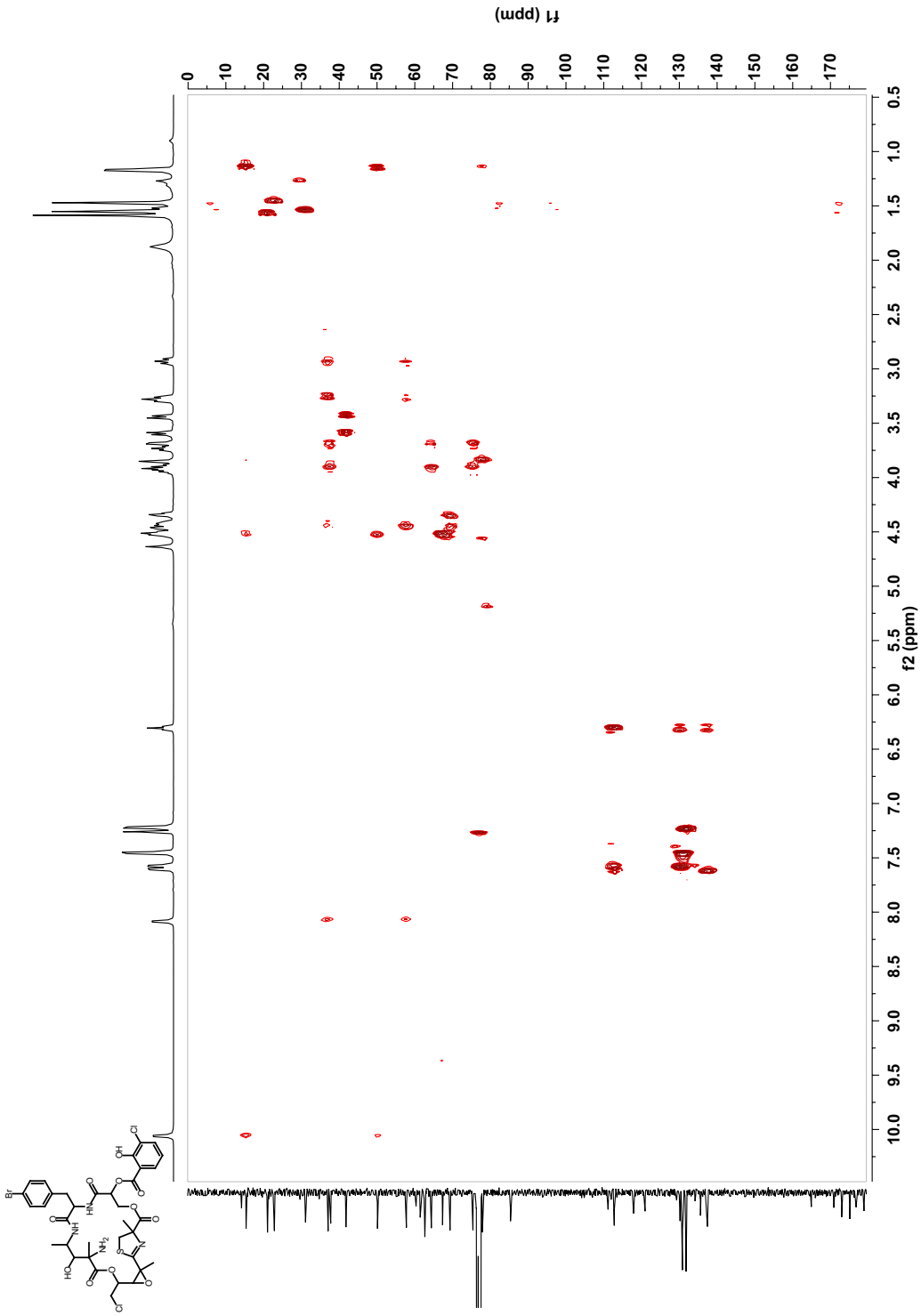

Figure S-4.7. HSQC-TOCSY spectrum for leptochelin (**9**) in $CDCl_3$ (600 MHz).

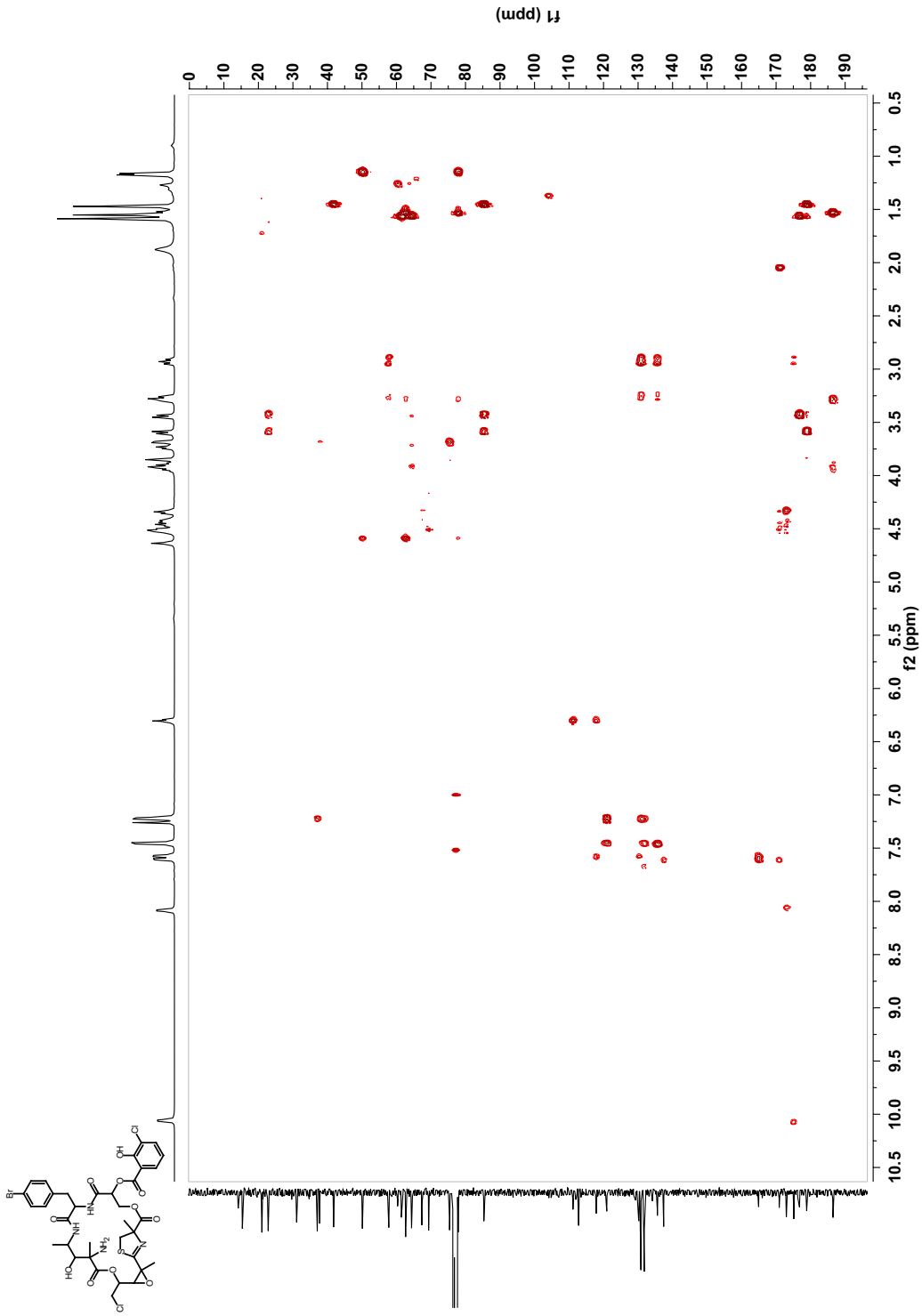

Figure S-4.8. HMBC spectrum for leptochelin (**9**) in $CDCl_3$ (600 MHz).

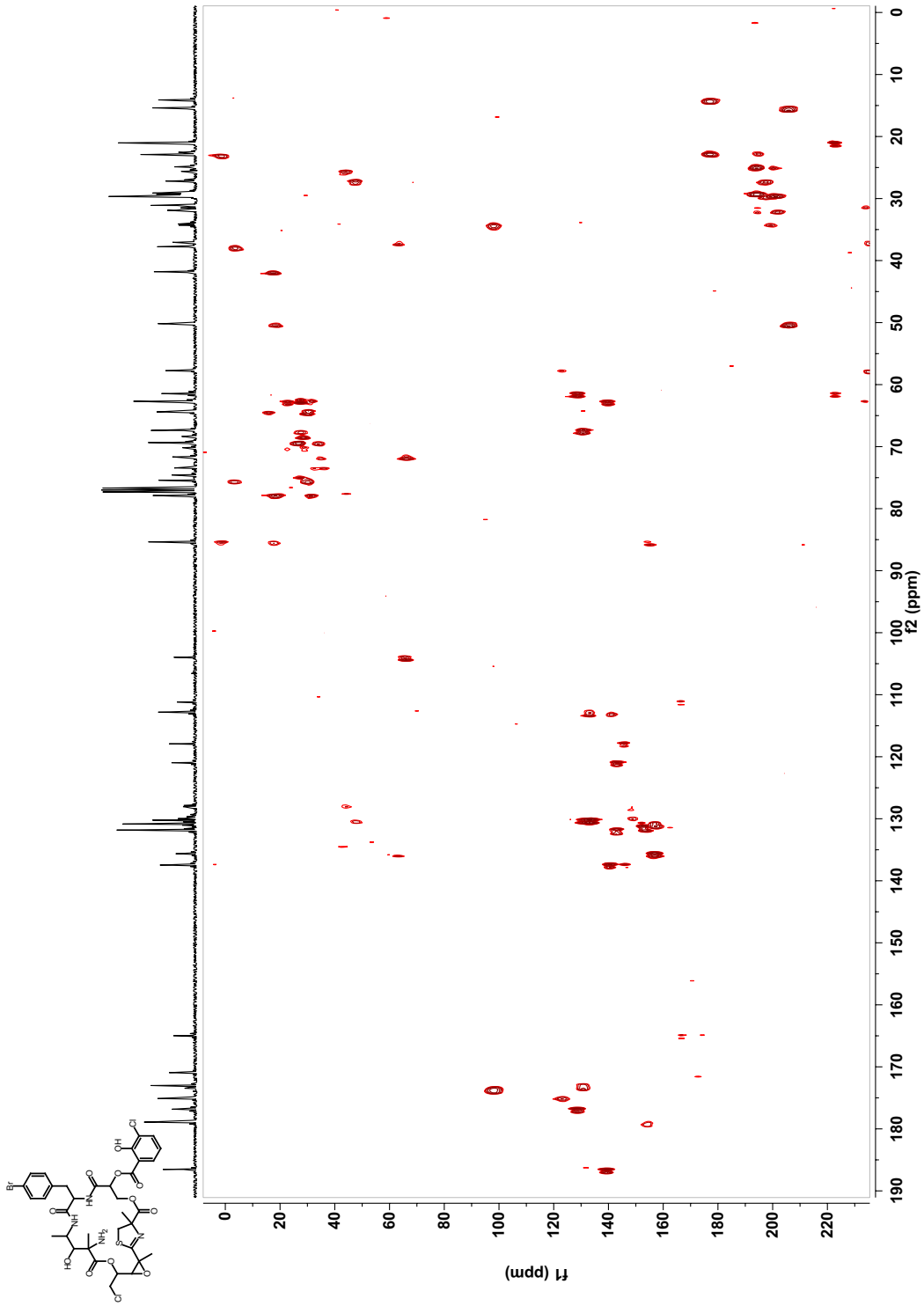

Figure S-4.9. ^{13}C INADEQUATE NMR spectrum for ^{13}C-labeled leptochelin (**9**) in $CDCl_3$ (400 MHz).

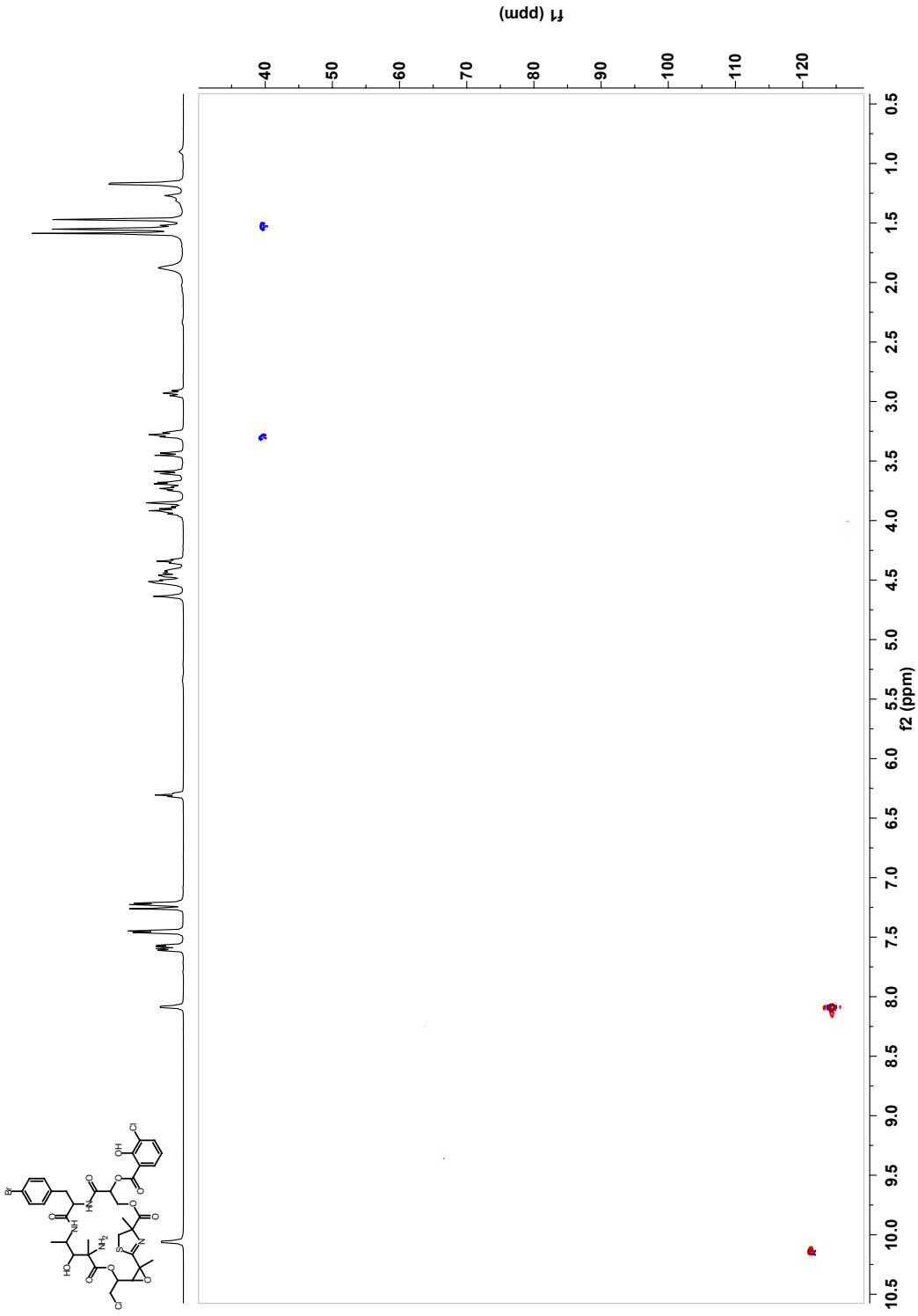

Figure S-4.10. ^{1}H-^{15}N multiplicity-edited HSQC spectrum for leptochelin (**9**) in $CDCl_3$ (600 MHz).

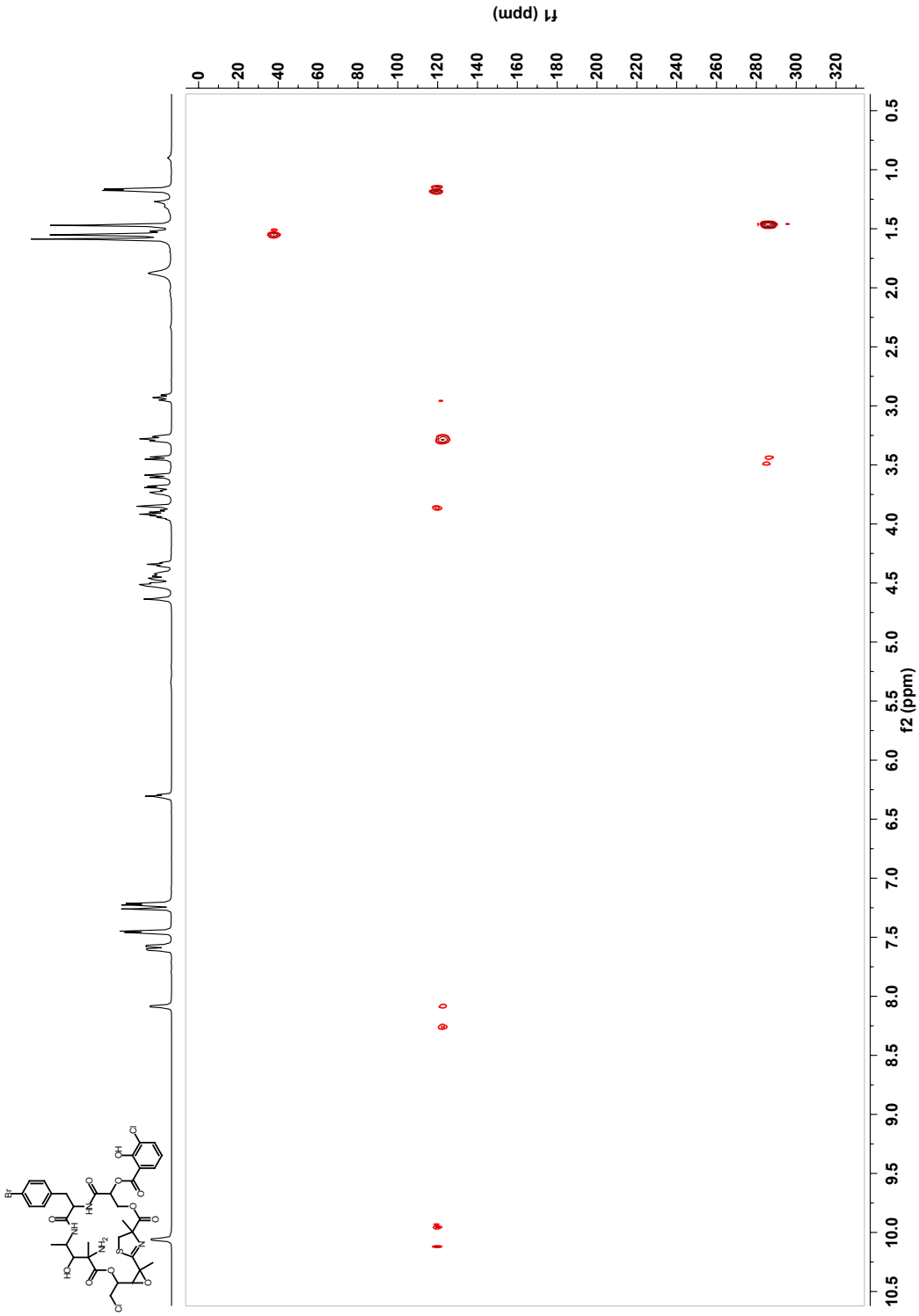

Figure S-4.11. ^{1}H-^{15}N gHMBC spectrum for leptochelin (**9**) in $CDCl_3$ (500 MHz).

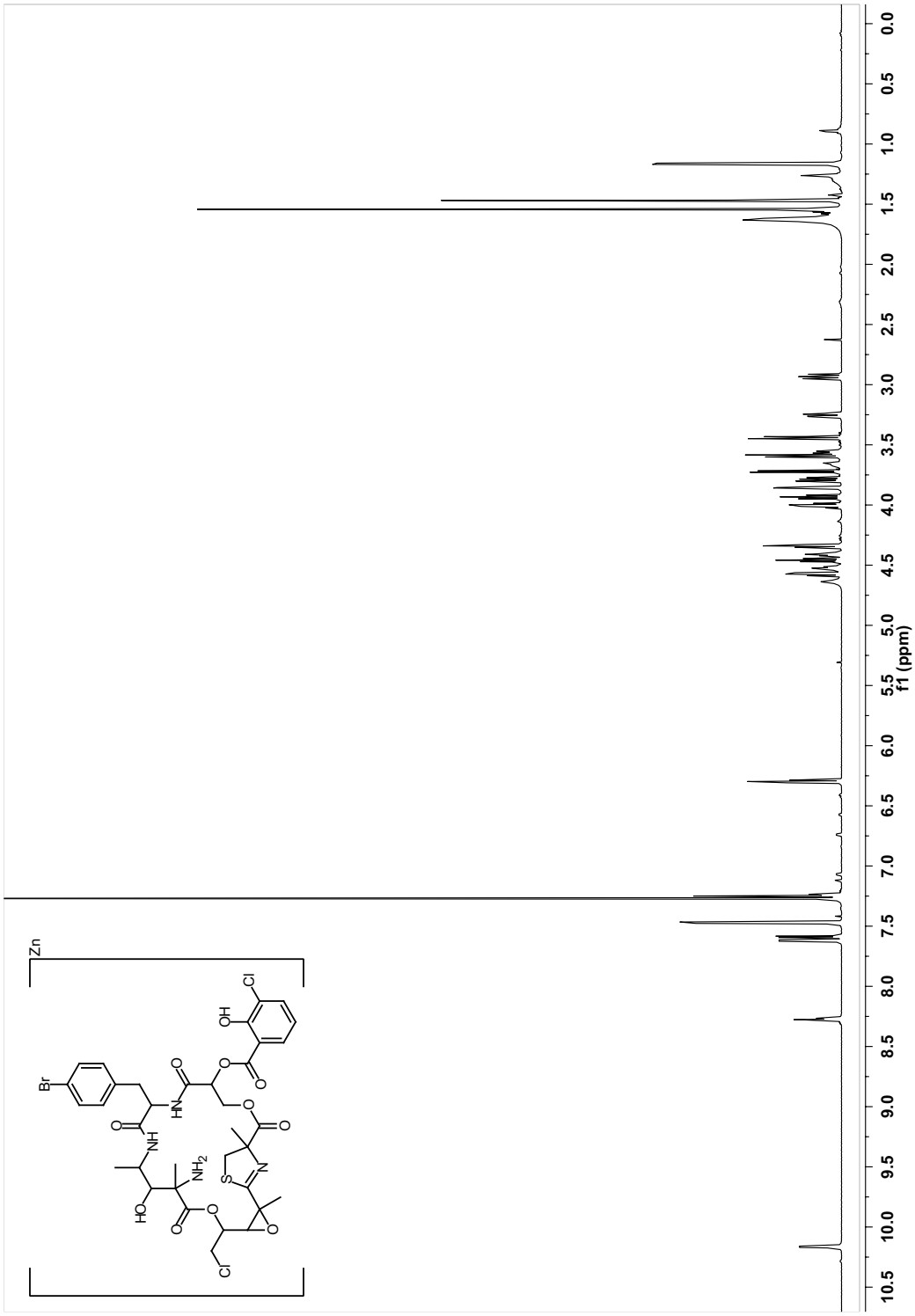

Figure S-4.12. ^{1}H NMR spectrum for Zn-leptochelin in $CDCl_3$ (700 MHz).

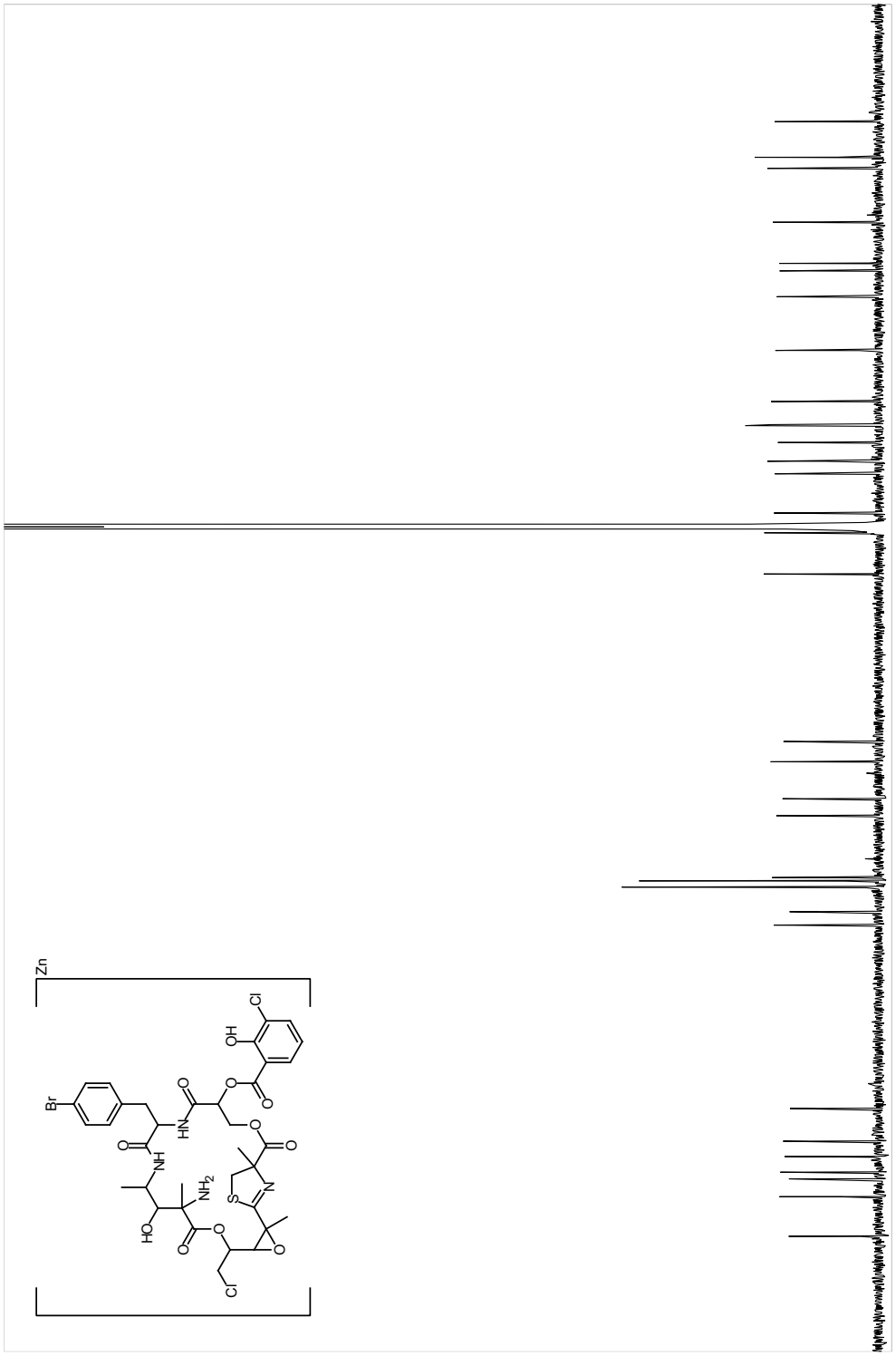

Figure S-4.13. ^{13}C NMR spectrum for Zn-leptochelin in $CDCl_3$ (175 MHz).

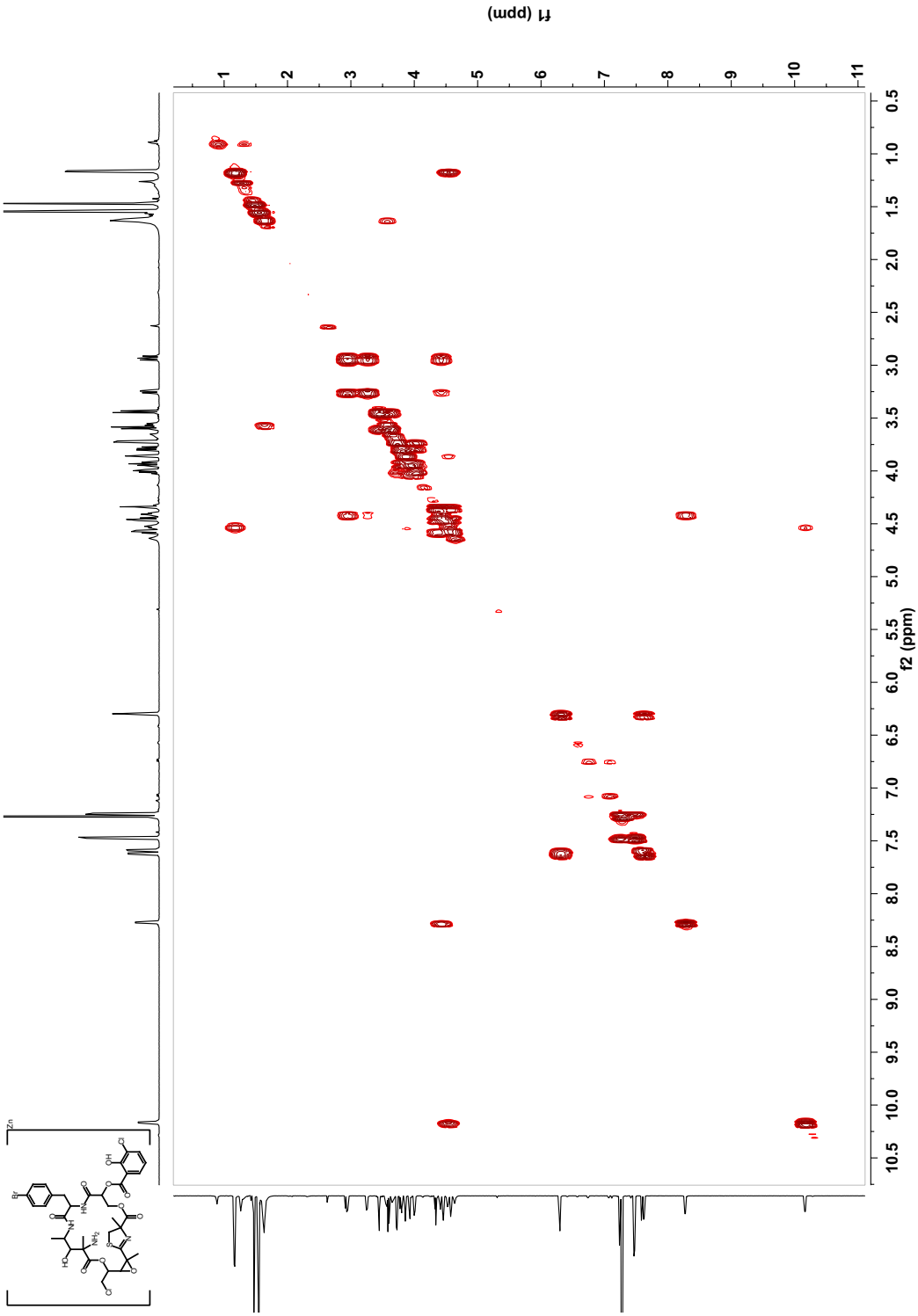

Figure S-4.14. COSY spectrum for Zn-leptochelin in $CDCl_3$ (500 MHz).

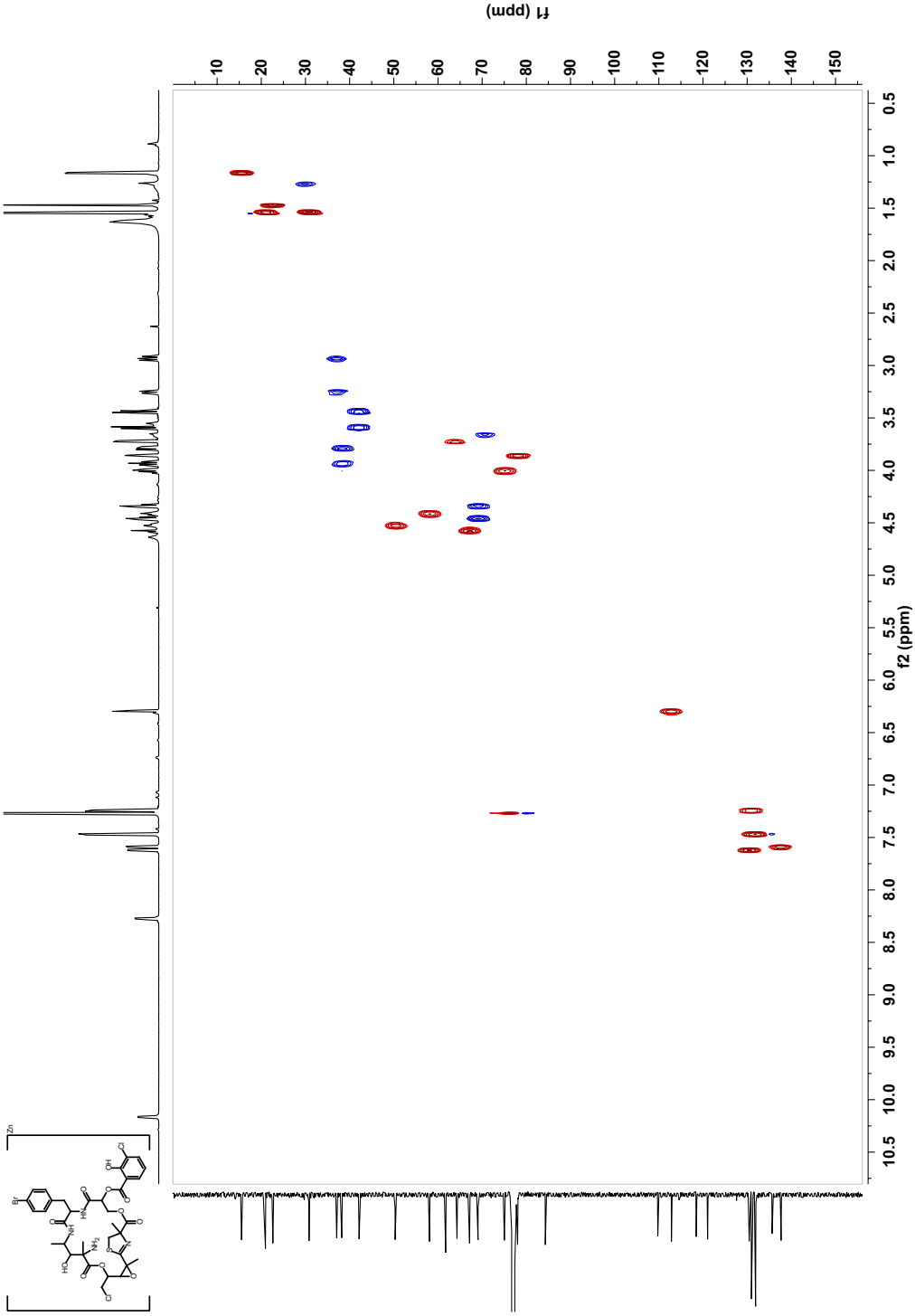

Figure S-4.15. Multiplicity edited HSQC spectrum for Zn-leptochelin in $CDCl_3$ (700 MHz).

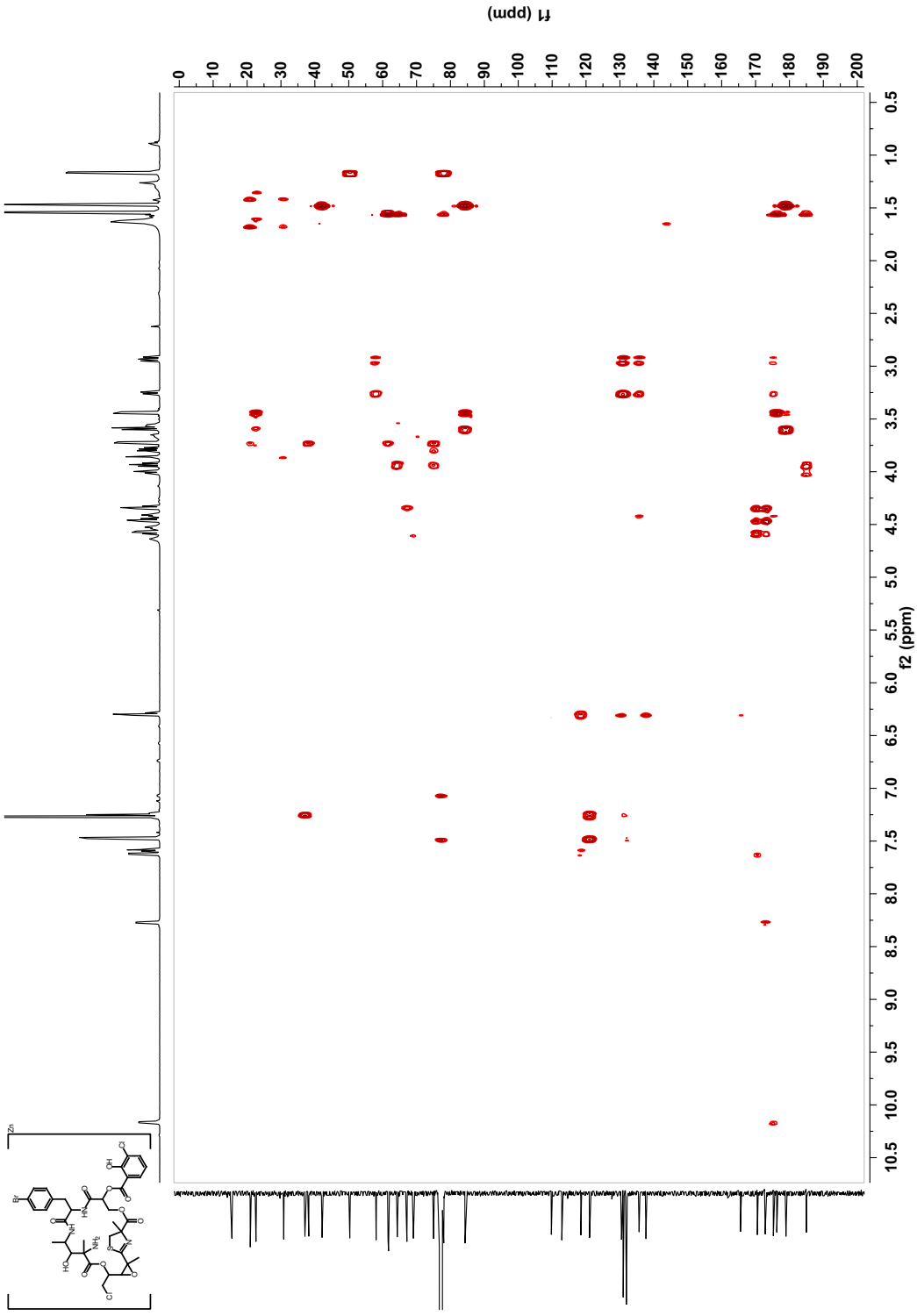

Figure S-4.16. HMBC spectrum for Zn-leptochelin in $CDCl_3$ (500 MHz).

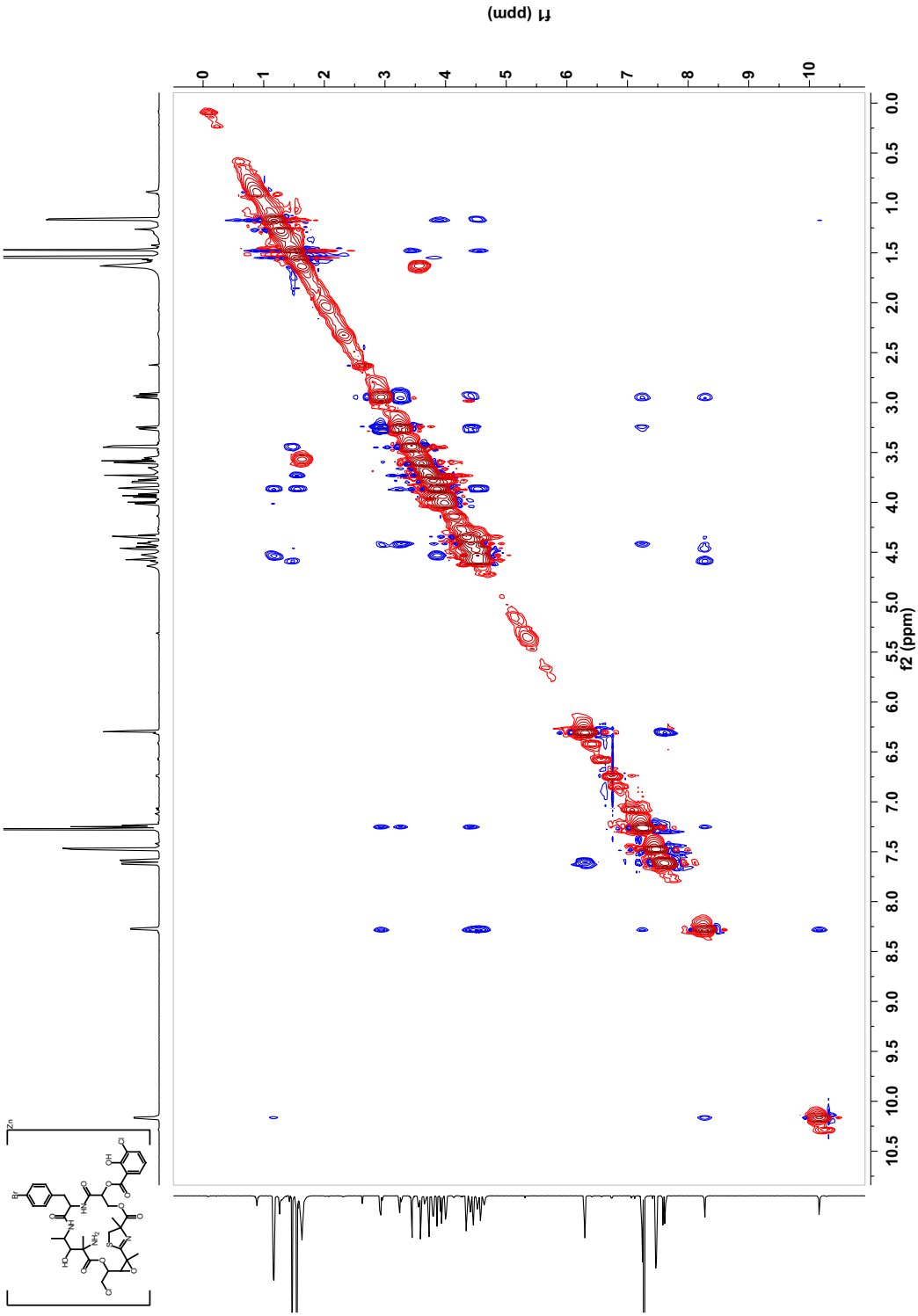

Figure S-4.17. ROESY spectrum for Zn-leptochelin in $CDCl_3$ (500 MHz).

References

Ashelford, K. E., Chuzhanova, N. A., Fry, J. C., Jones, A. J., & Weightman, A. J. (2005). At Least 1 in 20 16S rRNA Sequence Records Currently Held in Public Repositories Is Estimated To Contain Substantial Anomalies. *Appl. Environ. Microbiol., 71*(12), 7724-7736.

Bax, A., Freeman, R., Frenkiel, T. A., & Levitt, M. H. (1981). Assignment of carbon-13 NMR spectra via double-quantum coherence. *J. Magn. Reson. (1969), 43*(3), 478-483.

Bickel, H., Hall, G. E., Keller-Schierlein, W., Prelog, V., Vischer, E., & Wettstein, A. (1960). Stoffwechselprodukte von Actinomyceten. 27. Mitteilung. Über die Konstitution von Ferrioxamin B. *Helv. Chim. Acta, 43*(7), 2129-2138.

Boyer, S. L., Flechtner, V. R., & Johansen, J. R. (2001). Is the 16S–23S rRNA Internal Transcribed Spacer Region a Good Tool for Use in Molecular Systematics and Population Genetics? A Case Study in Cyanobacteria. *Mol. Biol. Evol., 18*(6), 1057-1069.

Carballo, J., Hernandez-Inda, Z., Perez, P., & Garcia-Gravalos, M. (2002). A comparison between two brine shrimp assays to detect in vitro cytotoxicity in marine natural products. *BMC Biotechnol., 2*(1), 17.

Chen, J., & Stubbe, J. (2005). Bleomycins: towards better therapeutics. *Nat. Rev. Cancer, 5*(2), 102-112.

Choi, H., Pereira, A. R., Cao, Z., Shuman, C. F., Engene, N., Byrum, T., Matainaho, T., Murray, T. F., Mangoni, A., & Gerwick, W. H. (2010). The Hoiamides, Structurally Intriguing Neurotoxic Lipopeptides from Papua New Guinea Marine Cyanobacteria. *J. Nat. Prod., 73*(8), 1411-1421.

Cole, K. E., Dowling, D. P., Boone, M. A., Phillips, A. J., & Christianson, D. W. (2011). Structural Basis of the Antiproliferative Activity of Largazole, a Depsipeptide Inhibitor of the Histone Deacetylases. *J. Am. Chem. Soc., 133*(32), 12474-12477.

Cronin, G. (2001). Resource allocation in seaweeds and marine invertebrates: chemical defense patterns in relation to defence theories. In J. B. McClintock & B. J. Baker (Eds.), *Marine Chemical Ecology* (pp. 325-353). Boca Raton, London, New York, Washington: CRC Press.

de Ruijter, A. J. M., van Gennip, A. H., Caron, H. N., Kemp, S., & van Kuilenburg, A. B. P. (2003). Histone deacetylases (HDACs): characterization of the classical HDAC family. *Biochem. J., 370*(3), 737-749.

Dewick, P. M. (2009). The Shikimate Pathway: Aromatic Amino Acids and Phenylpropanoids *Medicinal Natural Products* (pp. 137-186): John Wiley & Sons, Ltd.

Engene, N., Coates, C. R., & Gerwick, W. H. (2010). 16S rRNA gene heterogeneity in the filamentous marine cyanobacterial genus *Lyngbya*. *J. Phycol., 46*(3), 591-601.

Guan, P., & Fang, H. (2010). Clinical development of histone deacetylase inhibitor romidepsin. *Drug Discov. Ther., 4*(6), 388-391.

Haberland, M., Montgomery, R. L., & Olson, E. N. (2009). The many roles of histone deacetylases in development and physiology: implications for disease and therapy. *Nat. Rev. Genet., 10*(1), 32-42.

Hong, J., & Luesch, H. (2012). Largazole: From discovery to broad-spectrum therapy. *Nat. Prod. Rep., 29*(4), 449-456.

Huang, P., Feng, L., Oldham, E. A., J., K. M., & Plunkett, W. (2000). Superoxide dismutase as a target for the selective killing of cancer cells. *Nature, 407*(6802), 390.

Huang, X., & Madan, A. (1999). CAP3: A DNA Sequence Assembly Program. *Genome Res., 9*(9), 868-877.

Juarez, J. C., Betancourt, O., Pirie-Shepherd, S. R., Guan, X., Price, M. L., Shaw, D. E., Mazar, A. P., & Doñate, F. (2006). Copper Binding by Tetrathiomolybdate Attenuates Angiogenesis and Tumor Cell Proliferation through the Inhibition of Superoxide Dismutase 1. *Clin. Cancer. Res., 12*(16), 4974-4982.

Koehn, F. E., & Carter, G. T. (2005). The evolving role of natural products in drug discovery. *Nat. Rev. Drug Discov., 4*(3), 206-220.

Komárek, J., & Anagnostidis, K. (2005). Cyanoprokaryota 2. Teil/ 2nd Part: Oscillatoriales. In B. Büdel, L. Krienitz, G. Gärtner & M. Schagerl (Eds.), *Süßwasserflora von Mitteleuropa 19/2* (pp. 759). Heidelberg: Elsevier/ Spektrum.

Kwan, J. C., & Luesch, H. (2010). Weapons in Disguise—Activating Mechanisms and Protecting Group Chemistry in Nature. *Chem. Eur. J., 16*(44), 13020-13029.

Kwan, J. C., Ratnayake, R., Abboud, K. A., Paul, V. J., & Luesch, H. (2010). Grassypeptolides A-C, Cytotoxic Bis-thiazoline Containing Marine Cyclodepsipeptides. *J. Org. Chem., 75*(23), 8012-8023.

Leao, P. N., Engene, N., Antunes, A., Gerwick, W. H., & Vasconcelos, V. (2012). The chemical ecology of cyanobacteria. *Nat. Prod. Rep., 29*(3), 372-391.

Li, J., Zheng, L. M., King, I., Doyle, T. W., & Chen, S. H. (2001). Syntheses and antitumor activities of potent inhibitors of ribonucleotide reductase: 3-amino-4-methylpyridine-2-carboxaldehyde-thiosemicarba-zone (3-AMP), 3-amino-pyridine-2-carboxaldehyde-thiosemicarbazone (3-AP) and its water-soluble prodrugs. *Curr. Med. Chem., 8*(2), 121-133.

Ling, Y.-H., Liebes, L., Zou, Y., & Perez-Soler, R. (2003). Reactive Oxygen Species Generation and Mitochondrial Dysfunction in the Apoptotic Response to

Bortezomib, a Novel Proteasome Inhibitor, in Human H460 Non-small Cell Lung Cancer Cells. *J. Biol. Chem., 278*(36), 33714-33723.

Liu, M. C., Lin, T. C., & Sartorelli, A. C. (1992). Synthesis and antitumor activity of amino derivatives of pyridine-2-carboxaldehyde thiose micarbazone. *J. Med. Chem., 35*(20), 3672-3677.

Luanpitpong, S., Talbott, S. J., Rojanasakul, Y., Nimmannit, U., Pongrakhananon, V., Wang, L., & Chanvorachote, P. (2010). Regulation of Lung Cancer Cell Migration and Invasion by Reactive Oxygen Species and Caveolin-1. *J. Biol. Chem., 285*(50), 38832-38840.

Lukmantara, A. Y., Kalinowski, D. S., Kumar, N., & Richardson, D. R. (2013). Synthesis and biological evaluation of substituted 2-benzoylpyridine thiosemicarbazones: Novel structure–activity relationships underpinning their anti-proliferative and chelation efficacy. *Bioorg. Med. Chem. Lett., 23*(4), 967-974.

Martin, G. E., & Hadden, C. E. (2000). Long-Range 1H−15N Heteronuclear Shift Correlation at Natural Abundance. *J. Nat. Prod., 63*(4), 543-585.

McLaughlin, J. L., Rogers, L. L., & Anderson, J. E. (1998). The Use of Biological Assays to Evaluate Botanicals. *Drug Inf. J., 32*(2), 513-524.

Morris, L. A., Jaspars, M., Kettenes-van den Bosch, J. J., Versluis, K., Heck, A. J. R., Kelly, S. M., & Price, N. C. (2001). Metal binding of *Lissoclinum patella* metabolites. Part 1: Patellamides A, C and ulithiacyclamide A. *Tetrahedron, 57*(15), 3185-3197.

Morris, L. A., Milne, B. F., Jaspars, M., Jantina Kettenes-van den Bosch, J., Versluis, K., Heck, A. J. R., Kelly, S. M., & Price, N. C. (2001). Metal binding of *Lissoclinum patella* metabolites. Part 2: Lissoclinamides 9 and 10. *Tetrahedron, 57*(15), 3199-3207.

Nunnery, J. K., Mevers, E., & Gerwick, W. H. (2010). Biologically active secondary metabolites from marine cyanobacteria. *Curr. Opin. Biotechnol., 21*(6), 787-793.

Otsuka, S., Suda, S., Li, R., Watanabe, M., Oyaizu, H., Matsumoto, S., & Watanabe, M. M. (1999). Phylogenetic relationships between toxic and non-toxic strains of the genus *Microcystis* based on 16S to 23S internal transcribed spacer sequence. *FEMS Microbiol. Lett., 172*(1), 15-21.

Payne, K., Rofail, D., Baladi, J.-F., Viala, M., Abetz, L., Desrosiers, M.-P., Lordan, N., Ishak, K., & Proskorovsky, I. (2008). Iron chelation therapy: Clinical effectiveness, economic burden and quality of life in patients with iron overload. *Adv Therapy, 25*(8), 725-742.

Richardson, D. R., Kalinowski, D. S., Lau, S., Jansson, P. J., & Lovejoy, D. B. (2009). Cancer cell iron metabolism and the development of potent iron chelators as anti-tumour agents. *Biochim. Biophys. Acta, 1790*(7), 702-717.

Sattely, E. S., Fischbach, M. A., & Walsh, C. T. (2008). Total biosynthesis: in vitro reconstitution of polyketide and nonribosomal peptide pathways. *Nat. Prod. Rep., 25*(4), 757-793.

Shao, J., Zhou, B., Chu, B., & Yen, Y. (2006). Ribonucleotide reductase inhibitors and future drug design. *Curr. Cancer Drug Targets, 6*(5), 409-431.

Somwar, R., Erdjument-Bromage, H., Larsson, E., Shum, D., Lockwood, W. W., Yang, G., Sander, C., Ouerfelli, O., Tempst, P. J., Djaballah, H., & Varmus, H. E. (2011). Superoxide dismutase 1 (SOD1) is a target for a small molecule identified in a screen for inhibitors of the growth of lung adenocarcinoma cell lines. *Proc. Natl. Acad. Sci., 108*(39), 16375-16380.

Storz, P. (2005). Reactive oxygen species in tumor progression. *Front. Biosci., 10*, 1881-1896.

Taori, K., Paul, V. J., & Luesch, H. (2008). Structure and Activity of Largazole, a Potent Antiproliferative Agent from the Floridian Marine Cyanobacterium *Symploca* sp. *J. Am. Chem. Soc., 130*(6), 1806-1807.

Thornburg, C. C., Thimmaiah, M., Shaala, L. A., Hau, A. M., Malmo, J. M., Ishmael, J. E., Youssef, D. T. A., & McPhail, K. L. (2011). Cyclic Depsipeptides, Grassypeptolides D and E and Ibu-epidemethoxylyngbyastatin 3, from a Red Sea *Leptolyngbya* Cyanobacterium. *J. Nat. Prod., 74*(8), 1677-1685.

Tidgewell, K., Clark, B. R., & Gerwick, W. H. (2010). 2.06 - The Natural Products Chemistry of Cyanobacteria. In M. Editors-in-Chief: Lew & L. Hung-Wen (Eds.), *Comprehensive Natural Products II* (pp. 141-188). Oxford: Elsevier.

Umezawa, H., Maeda, K., Takeuchi, T., & Okami, Y. (1966). New antibiotics, bleomycin A and B. *J. Antibiot., 19*(5), 200-209.

Vraspir, J. M., & Butler, A. (2009). Chemistry of Marine Ligands and Siderophores. *Ann. Rev. Mar. Sci., 1*(1), 43-63.

Vulpanovici, F. A. (2003). *Biosynthesis, production and structural studies of secondary metabolites in cultured marine cyanobacteria.* (Doctoral Thesis), Oregon State University.

Williamson, R. T., Boulanger, A., Vulpanovici, A., Roberts, M. A., & Gerwick, W. H. (2002). Structure and Absolute Stereochemistry of Phormidolide, a New Toxic Metabolite from the Marine Cyanobacterium *Phormidium* sp. *J. Org. Chem., 67*(23), 7927-7936.

Wright, S., Raab, A., Feldmann, J., Krupp, E., & Jaspars, M. (2012). Marine Metabolites and Metal Ion Chelation. In E. Fattorusso, W. H. Gerwick & O. Taglialatela-Scafati (Eds.), *Handbook of Marine Natural Products* (pp. 861-892): Springer Netherlands.

Yu, Y., Wong, J., Lovejoy, D. B., Kalinowski, D. S., & Richardson, D. R. (2006). Chelators at the Cancer Coalface: Desferrioxamine to Triapine and Beyond. *Clin. Cancer. Res., 12*(23), 6876-6883.

Yuan, J., Lovejoy, D. B., & Richardson, D. R. (2004). Novel di-2-pyridyl–derived iron chelators with marked and selective antitumor activity: in vitro and in vivo assessment. *Blood, 104*(5), 1450-1458.

Chapter Five

Method Development and Sample Screening for Natural Products from Deep-Sea Hydrothermal Vent Organisms

Christopher C. Thornburg, Edward A. Mitchell, Oliver B. Vining, William W. Chadwick Jr., David A. Butterfield, T. Mark Zabriskie, and Kerry L. McPhail

Text in part from:
Journal of Natural Products
2010, 73(3), pp 489-499
DOI: 10.1021/np900662k

Abstract

Hydrothermal vents are among the most extreme and dynamic environments on Earth. They are characterized by physical extremes of temperature (2–350 ºC) and pressure, steep chemical, pH and temperature gradients, and a complete absence of light. Despite these harsh conditions, the biological, chemical and physical diversity of hydrothermal vents parallels the highly productive terrestrial and shallow water marine environments, which have been rich sources of biologically active compounds. Thus, in collaboration with the NOAA Vents program at Oregon State University and Pacific Marine Environmental Laboratory (PMEL) we have begun investigating the chemical diversity of prokaryotic and eukaryotic organisms that exist in the immediate vicinity of hydrothermal vent flows from Axial Seamount on the Juan de Fuca Ridge. In particular, a diverse collection of deep-vent invertebrates including *Ridgeia piscesae* tubeworms, *Paralvinella palmiformis* palm worms and *Lepetodrilus fucensis* limpets, as well as microbial mats at diffuse vent flows and a blue protozoan mat identified as a folliculinid ciliate (*Folliculinopsis* sp.) have been collected for natural products investigations during the 2009–2012 New Millennium Observatory (NeMO) annual expeditions. Bioassay-guided fractionation following microtiter plate-based antimicrobial assays against both *Staphylococcus aureus* and *Escherichia coli* was used in conjunction with LC-MS/MS and NMR profiling to identify anti-infective natural product leads from extract libraries of these collections, as well as several laboratory-cultured deep-vent actinomycetes.

Introduction

The deep ocean may be defined technically as depths beyond the euphotic zone (upper 200-300 m; Van Dover et al., 2002) where the sea bottom, in darkness, receives less than 1% of organic matter from photosynthetic primary production, oxygen levels and temperatures (down to 2 °C) plummet, and hydrostatic pressures rise to greater than 1,000 atmospheres in the deep trenches (10 m water = 1 atmosphere; Walsh et al., 1981). However, in the realm of natural products chemistry, many logically report depths beyond those readily accessible by SCUBA as "deep". Thus, in a recent, comprehensive deep-sea review, Skropeta considered the range of ocean environments below 50 m (~164 ft), which host a variety of marine invertebrates and microbes adapted to physical extremes in environmental conditions (Skropeta, 2008). The introduction to the latter review provides an informative overview of the deep-sea environment and the effects of the extreme, although very stable, conditions on the gene regulation, macromolecules, and the metabolism of deep-sea organisms.

Once thought to comprise a very low diversity of organisms evolved to occupy a physiologically challenging niche that precluded the intense competition of many shallow water ecosystems, deep-sea benthic communities are now recognized to be highly diverse, although not abundant. In the 1960's, focused efforts to sample the deep ocean floor resulted in unexpected findings of high faunal diversity, even in individual benthic dredge and epi-benthic sled samples from less than 100 to greater than 5,000 m (Sanders & Hessler, 1969). Nevertheless this high diversity, which is on the same order as that found in shallow tropical seas and has been attributed to the seasonal and geological stability of the deep-sea environment, occurs in relatively sparse pockets of slow-growing benthic organisms that are likely limited in density by food scarcity. Therefore, the exceptionally dense and diverse communities within the immediate vicinity of hydrothermal vents were in stark contrast to the surrounding sea bottom when first observed: in 1977, scientists aboard the manned deep submergence

vehicle (DSV) *Alvin* dove in the Galapagos Rift valley (ca. 2,500 m) to investigate recently photographed communities of large suspension-feeding benthic organisms surrounding active hydrothermal vents (Lonsdale, 1977). Hydrothermal vents, considered one of the most extreme environments on Earth, are formed when water heated in the earth's crust by magma is forced explosively to the surface through rock fissures in volcanic regions. At deep-sea vent sites, in addition to physical extremes of temperature (up to 400 ºC) and pressure and a complete absence of light, there are also extremely steep chemical, pH and temperature gradients between vent fluids and the surrounding seawater (Burgess et al., 2007). Remarkably, the growth rates of the deep vent communities proved comparable to organisms from shallow tropical environments (Childress & Fisher, 1992), and ultimately, the presence of extremely high concentrations of chemosynthetic microorganisms led to a new paradigm for primary production in the absence of sunlight (Corliss et al., 1979; Jannasch & Wirsen, 1979). Noteworthy is that the discovery of chemosynthetic symbiosis at deep-sea vent sites lead to the realization that this phenomenon occurs in a wide range of habitats worldwide, typically characterized by high sulfide concentrations and the presence of free-living macroorganisms with reduced digestive systems. This diversity of chemosynthetic habitats, as well as their hosts and symbionts, is engagingly reviewed by Dubilier et al. (2008), and includes sewage outfalls, organic-rich mud flats, some shallow-water coastal sediments, whale and wood falls in the deeper ocean, cold seeps, mud volcanoes and continental margins, in addition to hydrothermal vents.

Deep-sea hydrothermal vents, besides being extreme environments, also represent some of the most dynamic environments on Earth. With unpredictable temperatures, chemical concentrations, flow dynamics and seasonality, a single vent field may often be comprised of completely different fauna from one visit to the next (Childress & Fisher, 1992). As the vent matures and ages, early colonizers are superseded by a succession of other species in parallel with the diminishing thermal flow volume, temperature and amount of hydrogen sulfide (Van Dover, 2000). A

distinction has been made between deep-sea and shallow-water hydrothermal vents on the basis of their biota. Tarasov et al. (2005) have shown a striking change in hydrothermal vent communities at depths of 200 m (660 ft) based on the occurrence of obligate vent fauna. Thus, for the purpose of this study, deep-sea hydrothermal vents are those that occur below 200 m.

In order to discuss deep-sea hydrothermal vents as a potential source for natural products investigations, here we consider the geological setting and geochemical nature of deep-sea vents that impacts the biogeography of vent organisms, chemosynthesis and the known biological and metabolic diversity of eukaryotes and prokaryotes at vent sites, and the handful of small molecule natural products isolated to date directly from deep-sea vent organisms. Of critical importance too are the logistics of collecting deep vent organisms, opportunities for recollection, considering the dynamic nature of vent sites, and the ability to culture natural product-producing deep vent organisms in the laboratory. Importantly, several of these logistics are addressed in this study.

Geology and Distribution of Deep-Sea Hydrothermal Vents

Over 300 deep-sea hydrothermal vent sites are known throughout the world (Desbruyères et al., 2006). These vent sites generally occur along a nearly continuous underwater mountain chain (mid-ocean ridges) totaling more than 75,000 km that remain largely unexplored for hydrothermal activity (Figure 5.1; Van Dover, 2000). Located at the boundaries between the tectonic plates of the Earth's crust, these mid-ocean ridges are the sites of incremental seafloor spreading (spreading centers) at which molten rock (magma) rises towards the Earth's surface as the tectonic plates move in relation to each other. Hydrothermal vent fields may comprise multiple zones of focused hot and diffuse (low-temperature) fluid flows, and range in size from several hundred to several million square meters around ridge axes. Hydrothermal

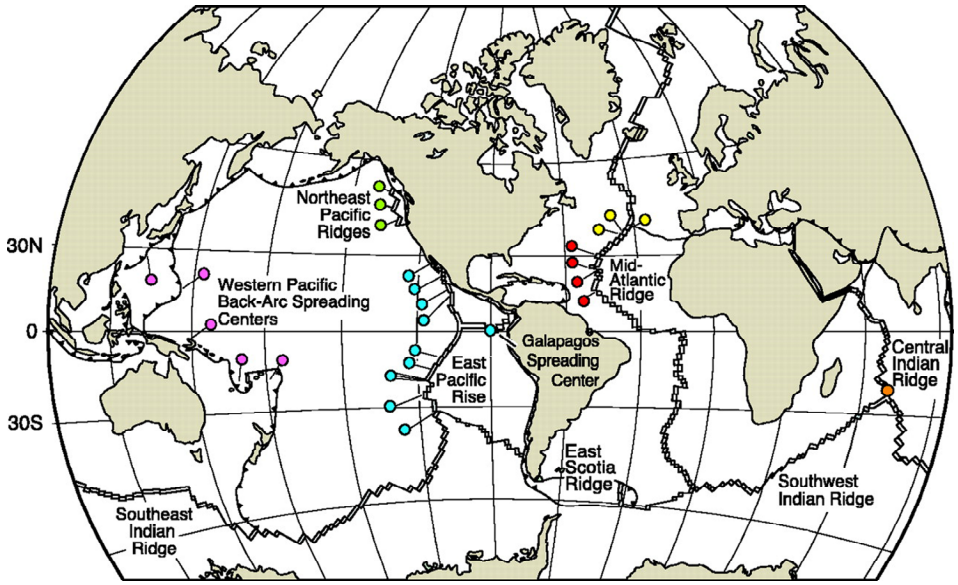

Figure 5.1. Map showing the major mid-ocean ridges and known deep-sea hydrothermal vent biogeographic provinces: Pink, western Pacific; green, northeast Pacific; blue, East Pacific Rise; yellow, Azores; red, Mid-Atlantic Ridge; orange, Indian Ocean. Reproduced with permission from Van Dover et al (2002).

vents are also found behind island arcs along active plate margins in "back-arc spreading centers" and active submarine volcanoes or seamounts located in the center of tectonic plates (Seyfried & Mottl, 1995). As a result of their proximity to the countries primarily involved in deep-sea hydrothermal vent research, the most studied hydrothermal systems are either in the eastern Pacific (East Pacific Rise and the Juan de Fuca, Gorda and Explorer Ridges) or the north-central Atlantic (northern Mid-Atlantic Ridge). The distinct geological settings of different hydrothermal vents impact the extent of venting on both spatial and temporal scales, and thus influence the biogeography of vent organisms. Therefore, variations in mid-ocean ridge crest dynamics between different ocean basins, as well as regional and local differences in ridge morphology (valley depth, etc.), which affect bottom currents, style of venting and vent longevity, make it important to keep in mind the geographical context of the general descriptions of vents and their biota presented here.

Vents are typically characterized by the mineral composition of their emissions and the morphology of structures built up through mineral deposition: variations in fluid composition, temperature, mineralogy, shape and size of deposits exist (Tivey, 1991). As cold seawater penetrates deep into the earth's crust it is heated and chemically modified from interactions with very hot basaltic rock (Edmond et al., 1982). Hot fluids, exiting vents at up to 400 °C, are enriched with transition metals (e.g., aluminum, copper, cobalt, iron, lead, manganese and zinc), silica, sulfides and dissolved gases such as hydrogen and methane (Seyfried & Mottl, 1995; Van Dover, 2000). The rapid mixing of these hydrothermal fluids with the surrounding cold seawater as they exit from the ocean floor causes changes in pH and temperature and the precipitation of metal sulfides and minerals to form particle-rich black plumes and columnar sulfide-rich *black-smoker chimney* structures. At many active vent sites, within a year of a volcanic eruption, mature (> 5 m) black-smoker sulfide chimneys are observed that eventually grow 10-20 m high and may have several high-temperature orifices near the top (Haymon, 1983; Tivey, 1991). *White-smoker chimneys* form around intermediate temperature flows (100-300 °C) that facilitate the precipitation of silica, anhydrite, and barite as white particles. In addition, there are several other structural variations of sulfide-rich mineral deposits, including beehives (with horizontal layering and conduits for diffuse fluid flow), flanges (where pooled hot fluids are trapped beneath the shelf-like structure) and complex sulfide mounds (Van Dover, 2000). The complex mineralization processes ongoing in even mature sulfide structures result in convoluted internal plumbing that may create diffuse warm-water flows at temperatures and mineral fluxes suitable for the growth of organisms. In addition to issuing from porous surfaces of active mineral deposits, low-temperature, diffuse flows may also exit directly from fissures in basalt lavas. One of the largest known hydrothermal deposits, "Godzilla," is an extreme example of a complex sulfide mound (Robigou et al., 1993). This sulfide structure has a diameter of 12-20 m and towers 55 m (180 ft) above the valley floor of the High-Rise vent field,

Juan de Fuca Ridge. Hydrothermal fluids from 30 to 330 °C exit at various tiers of its flanges extending 4 to 5 m (13-16 ft) away from the structure. The extent of this venting may be brought into perspective by the observation that it is common to measure temperature changes from 350 to 10 °C over a distance of just a few centimeters around the majority of high-temperature vent orifices at deep-sea hydrostatic pressures.

In addition to the particular morphology of a deep-sea vent, temperature and chemistry fluxes and the duration of hydrothermal activity has a profound effect on the composition of vent communities. Where rates of seafloor spreading are more rapid, as on the East Pacific Rise, eruptive disturbances are frequent enough that individual chimneys or diffuse-flow areas in a vent field may be present for less than 20 years. Alternately, in areas where volcanism is less frequent, such as the Main Endeavour Field (Juan de Fuca Ridge), some active mounds are thought to be more than 200 years old (Van Dover, 2000).

Biogeography and Diversity of Deep-Sea Vent Eukaryotes

The dense invertebrate communities typically associated with deep-sea hydrothermal vents exist in diffuse, warm-water flows that sustain temperatures of 10-40 and occasionally up to 60 °C (Van Dover, 2000). Despite the high biomass associated with hydrothermal vents, there is much lower macrofaunal species diversity relative to other deep-sea communities. This is likely a result of the dynamic and variable fluid conditions both within and between vent habitats that require specialized physiological and biochemical adaptations (Childress & Fisher, 1992; Van Dover, 2000) and favor the emergence of dominant species that succeed in a range of fluid conditions (Marcus et al., 2009). However, the full extent of the species present within hydrothermal vent communities has yet to be discovered considering the vast

unexplored ocean ridge systems and the report of new species being described every two weeks throughout the 1990's (Childress & Fisher, 1992).

Over 500 eukaryote species, encompassing 12 animal phyla and more than 150 new genera, have been described in the last three decades from deep vent sites. Arthropods (38.8%), mollusks (28.6%) and annelid worms (17.7%) dominate the megafaunal vent communities throughout the world, while cnidarians (4.6%), chordates (3.7%) and sponges (1.9%) are of notable presence (Desbruyères et al., 2006). Although deep ocean currents can disperse larval organisms over vast distances to new hydrothermal fields, many hydrothermal vent fields exhibit a unique range of habitat diversity and a high degree of endemism (Seyfried & Mottl, 1995; Van Dover, 2000). The Galapagos Rift and East Pacific Rise of the Pacific Ocean have similar communities, whereas different vent communities on the Juan de Fuca Ridge (northeast Pacific) share few species (Tunnicliffe & Fowler, 1996). During a visit to a mature hydrothermal vent site in the eastern Pacific, one might expect to observe scattered aggregations or "bushes" of siboglinid polychaetes (e.g., the vestimentiferan tube worms *Riftia pachyptila* or *Ridgeia pisceae*) which, on closer inspection, host a mix of limpets and snails, alvinellid polychaetes (e.g., the palm worm *Paralvinella palmiformis*) and polynoid polychaetes (e.g., the scale worm *Lepidonotopodium piscesae*), all cloaked in a white microbial mat, with occasional hydrothermal vent shrimp and Yeti crabs. On the Mid-Atlantic Ridge, vent sites are characterized instead by an abundance of hydrothermal vent shrimps (*Rimicaris*) swarming over chimneys near high flows that lack the vestimentiferans and alvinellids of the Pacific vent communities (Van Dover, 2000). Nonetheless, at least 40% of the Atlantic genera reported are shared with the Pacific vent fauna. In both oceans, beds of hydrothermal vent clams (*Calyptogena magnifica*) or mussels (*Bathymodiolus thermophilus*) may be observed in lower flow areas. The Kairei and Edmond vent fields of the Indian Ocean contain genera shared with either Atlantic or Pacific vents. However, Indian Ocean

communities are different enough to constitute a separate biogeographic province from either the Atlantic or Pacific (Van Dover et al., 2001).

Unlike communities in other deep-sea reducing habitats (e.g., cold seeps), hydrothermal vent communities change on time-scales of months to years, and frequent volcanic activity along ridge systems with medium to fast seafloor spreading rates may continually reset vent community development allowing repeated primary successions to be documented in conjunction with geo-physical and -chemical parameters (Tsurumi & Tunnicliffe, 2001). Within two years of the eruption of Cleft Segment on the Juan de Fuca Ridge (eastern Pacific), tubeworm-associated assemblages were well-established at diffuse vents. These communities were observed almost annually over the next six years (2-8 years post-eruption), and showed a shift in dominance from the alvinellid polychaete *Paralvinella pandorae* (20-98% of the assemblages at year 2) to the limpet *Lepetodrilus fucensis* by year 7. Most diffuse venting had waned by year 5, and all vents were extinct by year 8. In another more recent report on succession in diffuse flow vent communities after the 1998 eruption at Axial Volcano (central segment, Juan De Fuca Ridge), Marcus et al. (2009) first examined mature pre-eruption communities using data for 21 low temperature vents that were sampled in Axial vent fields in 1986-88 and 1997-99. Species composition proved very similar among mature vents and the collections were dominated by a small subset of taxa, although the relative dominance of the common species depended on vent flow temperature. As observed in earlier studies, alvinellid worms dominate higher temperature vents, while limpets dominate lower temperature vents (< 18 °C). This predictability of mature vent communities bodes well for natural products investigations that require recollections to pursue preliminary results from broad biological activity profiling of initial small-scale, diverse collections.

Post-eruption colonization of new vents depends on the species pool available to colonize a site, as well as the physico-chemical characteristics of a particular vent environment. Marcus et al. (2009) found that *Paralvinella pandorae* colonized and

dominated the new Axial vent communities within the first year post-eruption. *Ridgeia piscesae* tubeworms took up to 30 months to become well established, by which time 23 of the 36 known Axial vent and four new macrofaunal species had arrived. This may coincide with the tapering of high vent flows to a level where temperature and hydrogen sulfide levels were acceptable to juvenile recruits that require both oxygen and sulfide. Interestingly, some rare macrofaunal species showed rapid recruitment and colonization, although they never reached significant abundance. By year 2 after the eruption, biomass of tubeworm-associated species had leveled, but animal densities remained significantly higher than at the mature vents, suggesting that the latter support larger individuals. This knowledge of the rates of colonization, progressive succession and ecology of vent communities at different sites may be critical to the success of natural products investigations that must rely on limited collection opportunities, both spatially and temporally.

Eukaryotic microorganisms from both known and previously undescribed taxa have also been described from deep-sea hydrothermal and cold-seep environments, including those living in association with various invertebrate species. Sequence comparisons of PCR-amplified small subunit (SSU) ribosomal RNA's were used to characterize the diversity of eukaryotic organisms associated with hydrothermal sediments from the Guaymas Basin in the Gulf of California (Edgcomb et al., 2002). Many of these sequences are related to previously uncharacterized eukaryotes or seem to represent early branching within well-characterized eukaryotic clades. These include sequences from certain fungi, green algae, diatoms, water molds, protists, acanthareans and radiolarians. Obviously, sequences of phytoplanktonic taxa, such as green algae and diatoms, could have been deposited through sedimentation from the euphotic zone, and culture-independent molecular surveys do not necessarily reflect viable members within sediment samples. However, Atkins et al. (1998) isolated and cultured 18 strains of flagellated protists representing nine species from four deep-sea hydrothermal vent sites, including the Guaymas Basin. This suggests that many of

these sequences represent truly unique eukaryotic microorganisms capable of adapting to life in extreme and dynamic environments. In addition, the Deep-sea Microorganism Research Group at the Japan Marine Science and Technology Center (JAMSTEC) has identified new species of unicellular fungi, typically designated as yeasts, associated with the tubeworm *Lamellibranchia* sp. and the giant white clam *Calyptogena* sp (Nagahama et al., 2001, 2003). These organisms live in cold-seep environments where high concentrations of methane and hydrogen sulfide flow from the seafloor.

The dominant and ubiquitous vent species highlighted here (arthropods, gastropods and annelids) belong to taxa widely recognized from other environments not to be prolific producers of natural products. However, the vast majority of vent invertebrates host epibiotic or endobiotic extracellular or intracellular symbionts, and in this respect, could be viewed as the equivalent of shallow-water filter feeders such as sponges and tunicates, which are both responsible for tremendous natural products diversity from symbiotic microbes that account for up to 40% of their body mass (Dunlap et al., 2007). Thus, the crucial question becomes the biological and metabolic diversity of the symbiotic, and also free-living, microorganisms associated with the dense vent invertebrate communities (Table 5.1), which in fact support primary production in those vent communities via chemosynthesis. In addition to providing critical food resources to their hosts, epi- and endosymbiotic bacteria have been proposed as sources of natural products for deterring predation within these communities (Kicklighter et al., 2004).

A variety of evidence indicates that nearly all invertebrates associated with hydrothermal vents acquire much if not all of their needs for fixed carbon and nitrogen from microbial symbionts, which are dominated by sulfide-oxidizing bacteria that require a constant supply of sulfide to specialized host tissues (Kelley et al., 2002). For example, adult vestimentiferan tubeworms lack a digestive tract and derive their nutrition solely from culturing sulfur-oxidizing bacteria within a specialized organ

Table 5.1. Representative bacterial counts and phylogenetic diversity reported from different hydrothermal vent niches.

[a]Sample Description	Temp. (°C)	Total Bacteria Cell Count	Phylogenetic Clusters ([b]OTUs)	References
hydrothermal plume	~200	6.3×10^4 – 7.5×10^4 cells mL^{-1}	4 (20)	Sunamura et al., 2004
hydrothermal fluid	2–208	[c]ND	15 (46)	Huber et al., 2003
[d]ISCD (5 days)	2–300	6.8×10^4 – 2.0×10^7 cells g^{-1}	7 (22)	Harmsen et al., 1997; Corre et al., 2001
chimney structure (enrichment cultures)	ND	2.2×10^9 cells mL^{-1}	9 (17)	Postec et al., 2007
tubeworm (*Riftia pachyptila*)	ND	ND	8 (39)	Lopez-Garcia et al., 2002
polychaete worms (*Paralvinella palmiformis*)	ND	ND	8 (93)	Alain et al., 2002
scaly snail (*Crysomallon squamiferum*)	ND	ND	5 (76)	Goffredi et al., 2004
microbial mat	~37	ND	3 (18)	Moyer et al., 1995
hydrothermal sediment	ND	ND	12 (59)	Lopez-Garcia et al., 2003
hydrothermal sediment cores	2–74	ND	9 (36)	Teske et al., 2002

[a]Note that the data referenced are from different geographical location;. [b]Number of operational taxonomic units (OTUs) determined within referenced material; [c]ND, not determined; [d]ISCD, *in situ* colonization device.

known as the trophosome (Cavanaugh et al., 1981; Felbeck, 1981). The trophosome accounts for approximately 16% of the animals' wet weight and consists primarily of symbiont-containing lobes (bacteriocytes), crystals of elemental sulfur and blood vessels (Cavanaugh et al., 1981; Childress & Fisher, 1992). Bacterial densities between 10^9 and 10^{11} cells per gram of wet tissue have been observed within the trophosome of the giant vestimentiferan tubeworm, *Riftia pachyptila*, which is capable of growing up to 2.0 m in length (Desbruyères et al., 2006). Although numerous reports indicate dominance by only a single bacterial phylotype within trophosomes of *R. pachyptila* and other vestimentiferans, new molecular evidence suggests that a more

diverse community may colonize these and other structures within the trunk of these tubeworms (Chao et al., 2007; Harmer et al., 2008). In general, the potential diversity of chemosynthetic symbionts, which may arise from many different bacterial lineages, has only recently been appreciated with the advent of molecular methods that have revealed a remarkable variety of chemosynthetic metabolic pathways (Dubilier et al., 2008) discussed in more detail in the following section. Other examples of vent symbioses include suspension-feeding hydrothermal vent clams and mussels, which gain approximately 45% of their fixed carbon from chemoautolithotrophic (auto-, fixing inorganic carbon; litho-, oxidation of inorganic electron donors) microorganisms associated with their gills (Childress & Fisher, 1992; Fisher et al., 1988). A highly diverse assemblage of episymbionts was identified from the dorsal surface of the extremely thermotolerant polychaete *Alvinella pompejana* (Haddad et al., 1995). Other epibiont communities include microbes "farmed" on dense aggregations of shrimp at Mid-Atlantic Ridge hydrothermal vents. The shrimps compete for space near warm, sulfide-rich water emissions to support their "crop" of microorganisms (Polz et al., 1998). Microorganisms are also associated with iron sulfide-containing sclerites in the foot of a newly described scaly snail, *Crysomallon squamiferum*, from hydrothermal vents in the Indian Ocean (Goffredi et al., 2004). Without these chemosynthetic microorganisms, the rapid growth rates required to prosper and reach reproductive maturity in such an extreme and dynamic environment would not be possible (Childress & Fisher, 1992; Nelson & Fisher, 1995).

Chemosynthesis and the Biogeography and Diversity of Archaea and Bacteria

At deep-sea hydrothermal vents, in the absence of light and in the presence of hydrothermal fluids rich in minerals, reduced compounds (including H_2S, CH_4) and CO_2, chemical energy replaces solar energy as the fuel that supports primary

production by chemosynthetic bacteria and archaea (Kelley et al., 2002; Van Dover, 2000). The Archaea are a distinct domain of microorganisms that have no cell nucleus or membrane-bound organelles (the same as "prokaryotic" Bacteria), but possess unique biochemistry and have several metabolic pathways that are more closely related to those of eukaryotes (especially transcription and translation; Woese, 2004). Bacteria and archaea may be suspended in the ambient water column, hydrothermal plumes, or attached to rocks, sediment or on/in vent animals, which in turn may feed directly on the microbes or engage in symbiotic associations to acquire fixed carbon and nitrogen, as discussed in the previous section (Haymon, 1983; Robigou et al., 1993; Tivey, 1991). Table 5.1 provides a representation of the different vent habitats for microorganisms, with representative bacterial counts and taxonomic diversity reported for each niche.

Gradients of temperature and chemistry (including O_2) in hydrothermal systems support free-living microorganisms with a diverse array of obligate and facultative physiologies and tolerances, and thus microbial diversity correlates closely with major element and volatile chemistry of vent fluids. It has been proposed that individual microorganisms switch freely between autotrophy (inorganic carbon energy sources) and heterotrophy (organic carbon energy sources) depending on environmental conditions, since heterotrophy yields higher energy when available. However, in the absence of a supply of small organic compounds supporting heterotrophic metabolism, chemosynthetic microorganisms produce particulate organic carbon for vent communities, and are important as sinks for reduced hydrothermal compounds in the global cycling of elements (Van Dover, 2000). Since the concentration of H_2S in vent fluids is extremely high (3 to 110 mmol per kg seawater), sulfide oxidation is a dominant microbial chemosynthetic source of energy in vent communities (Kelley et al., 2002). The oxidation of reduced compounds such as HS^-, H_2S, S°, CH_4, H_2, NH_4^+ or Fe(II)- and Mn(II)-containing minerals provides energy for the synthesis of useable organic carbon from inorganic sources such as CO_2 and CH_4 (Jannasch & Wirsen,

1981; Van Dover, 2000). The fixation of CO_2 used by many of these chemoautolithotrophic bacteria is identical to the Calvin-Benson cycle used by plants. While aerobic microbes use O_2 as the electron acceptor during the energy-yielding chemosynthetic reaction, anaerobic hydrothermal microorganisms use CO_2, Fe^{3+}, NO_3^{2-}, or organic compounds (to oxidize H_2; Kelley et al., 2002; Schmidt et al., 2008).

Free-living bacteria and archaea are suspended within buoyant vent plumes at temperatures reaching at least 115 °C, and cell densities several orders of magnitude more abundant than surrounding seawater can be detected hundreds of kilometers away from vent fields (Jannasch & Wirsen, 1979; Juniper et al., 1998). These microorganisms, also form microbial mats of various colors and morphologies on the surface of basalt (Moyer et al., 1994; Santelli et al., 2008), chimney spires (Kormas et al., 2006) and within hydrothermal sediments (Lopez-Garcia et al., 2003), where they serve as food for numerous invertebrate filter-feeding, grazing and deposit-feeding species (Van Dover & Fry, 1994). They likely also play a significant role in early steps of macrofaunal colonization around new vent formations (Alain et al., 2004; Lutz et al., 2001). Many anaerobic microbes are also found deep within the thermal subseafloor (Takai et al., 2004) and chimney walls in close proximity to nutrient-rich, acidic effluent that can vary in temperature from ≤ 25 °C to 350 °C (Winn et al., 1986). A steep temperature gradient exists within only a few centimeters of these walls, where variations in the abundance and diversity of bacteria and archaea occur. Numerous studies have shown that hyperthermophilic archaea increasingly dominate the microbial consortium as effluent temperatures rise from 150 to 300 °C (Harmsen et al., 1997; Schrenk et al., 2003; Takai & Horikoshi, 1999; Takai et al., 2001), although cell densities of both archaea and bacteria decrease in proximity to such extreme temperatures.

Although there has been tremendous scientific interest in the microbial ecology of “hot-spot ecosystems,” such as hydrothermal vents, cold-seeps and gas-hydrate systems, the distribution and diversity of functional and taxonomic groups of bacteria

and archaea within the deep-sea is largely unknown (Jørgensen & Boetius, 2007). The diversity of hydrothermal vent microbial communities cannot truly be assessed by methods that rely solely on artificial cultivation, since 99% of marine microbes are considered unculturable (Amann et al., 1995). These challenges have been overcome in part by the application of a molecular phylogeny-based approach using nucleotide-sequence analysis of the highly conserved gene for the small-subunit (SSU) ribosomal RNA molecule (16S rRNA), (Pace, 1997). This approach has revealed that the global diversity of microorganisms is at least 100 times greater than estimates based on cultivation-dependent surveys; new phylotypes, often representing major new lineages, are consistently shown with each molecular analysis of microbial environments (Pace, 1997; Sogin et al., 2006; Venter et al., 2004). For example, the new archaeal phylum "Nanoarchaeota" (Huber et al., 2002) has been identified by analysis of PCR-amplified SSU rRNA genes from a defined co-culture of hyperthermophilic archaeans, and similar methods have indicated the emergence of a newly defined lineage distributed throughout the global deep-sea vent system referred to as the "Deep-Sea Hydrothermal Vent Euryarchaeoic group" (DHVEG; Takai & Horikoshi, 1999).

At the Josephine Bay Paul Center, Marine Biological Laboratory (Woods Hole, MA) and the Joint Institute for the Study of Atmosphere and Ocean, University of Washington (Seattle, WA), an alternative approach to the more traditional analysis of full-length 16S rRNA amplicons has been developed (Sogin et al., 2006). This approach targets hypervariable regions within 16S rRNAs that can record differences between both divergent and closely-related organisms and thus provide a greater resolution of microbial diversity and relative abundance (Kysela et al., 2005; Sogin et al., 2006). Analysis of 689,720 bacterial and 216,627 archaeal amplicons, targeting the V6 hypervariable region, from two low-temperature (~30 °C) diffuse flow vents in the northeast Pacific Ocean revealed 30,108 unique bacterial sequences forming 18,537 phylotypes and 5,979 unique archaeal tag sequences defining 1,931 phylotypes (Huber

et al., 2007). By comparison, previous assessments from the same sites using traditional PCR-amplified 16S rRNA gene sequence analysis identified only 55 bacterial and 28 archaeal phylotypes [operational taxonomic units (OTUs)] (Huber et al., 2002, 2003). Even more remarkably, this attempt by Huber et al. (2007) to provide an exhaustive characterization of bacterial and archaeal diversity at the study sites was not successful in the case of the bacteria: statistical analyses of the data from even this unparalleled number of bacterial sequences indicated additional, undescribed bacterial diversity at every taxonomic level. Hence, much of the microbial diversity reported from these environments is likely at best a conservative approximation of their true community structure. This strategy of sequencing the 16S rRNA V6 hypervariable region has also been adopted by the International Census of Marine Microbes, one of 14 groups within the Census of Marine Life (CoML) initiative. The goal of the CoML is to provide an on-line database (first consensus released on October 4, 2010), which describes each one of the more than 14 million marine species currently known. Since its inception in 2000, researchers have discovered more than 6,000 potential new species from microbes to whales in near shore habitats to the abyssal plains, including mid-ocean ridges and deep-sea vents (CoML, 2013).

Bacterial diversity at deep-sea hydrothermal vents, as for non-thermal deep-sea environments, spans most of the currently defined lineages including the Actinobacteria (high G+C Gram positives; Teske et al., 2002), Firmicutes (low G+C Gram positives encompassing the Bacilli, Clostridia and Mollicutes; Huber et al., 2003; Lopez-Garcia et al., 2003), and the Bacteroidetes (formerly *Cytophaga-Flexibacter-Bacteroides*) phylum (Alain et al., 2002; Takai et al., 2004). The presence of Actinobacteria, some of which have larger genome sizes (over 9 Mb for some *Streptomyces* and *Rhodococcus* species), is particularly encouraging given that they are the most prolific source of natural product-derived medicines (Bérdy, 2005). A correlation between genome size and secondary metabolic capacity has emerged in recent studies aimed at evaluating how relative usage of the genome varies with

genome size. The functional characterization of 115 completed bacterial genomes in the Genbank database showed that the relative proportion of genes for regulation and secondary metabolism increases with genome size (Konstantinidis & Tiedje, 2004).

Notably, the relative distribution of bacteria among taxonomic groups differs between deep-sea hydrothermal vent and non-vent environments (Figure 5.2). In fact, Actinobacteria form a relatively small portion of the known bacterial diversity at vents (Figure 5.2a) compared to other non-thermal environments (Figure 5.2b). However, the much higher concentrations of bacteria in hydrothermal versus cold sediments, for example (Teske et al., 2002), should lead to greater sampling efficiency at hydrothermal vents and therefore favor these environments as a source of Actinobacteria as well as other likely natural product producers. The Proteobacteria (Gram-negative) form the largest bacterial phylum, comprising approximately one third of all known bacteria, and represent a diverse range of organisms with varying genome sizes and life histories. This phylum includes sulfur-oxidizing bacteria (e.g., *Beggiatoa* species), methanotrophs (e.g., *Methylobacter* species) and nitrifying bacteria (e.g., *Nitrococcus* species) as well as bacteria responsible for animal bioluminescence (e.g., some *Vibrio* species). In addition, *β*-, *γ*- and *δ*-subclasses of Proteobacteria include some gliding forms, predatory species of which have unusually large genome sizes and are thought to secrete antibiotics to weaken or immobilize their prey (Nett & Konig, 2007).

The non-vent deep-sea bacteria comprise highest numbers of *γ*-proteobacteria followed by α-proteobacteria, Firmicutes, Actinobacteria and *δ*-proteobacteria (Figure 5.2b). In contrast, *ε*-proteobacteria dominate deep-sea vent microbial communities, although other subclasses of Proteobacteria (*γ*-, *α*- and *δ*-) and the Aquificae (a small group of thermophilic/hyperthermophilic chemolithotrophic bacteria) are also found widely in a variety of vent habitats including sulfide structures, hydrothermal fluids, sediments and microbial mats (Takai et al., 2006). The *ε*-proteobacteria subclass is ubiquitous in Nature and incorporates sulfur-metabolizing and microaerophilic

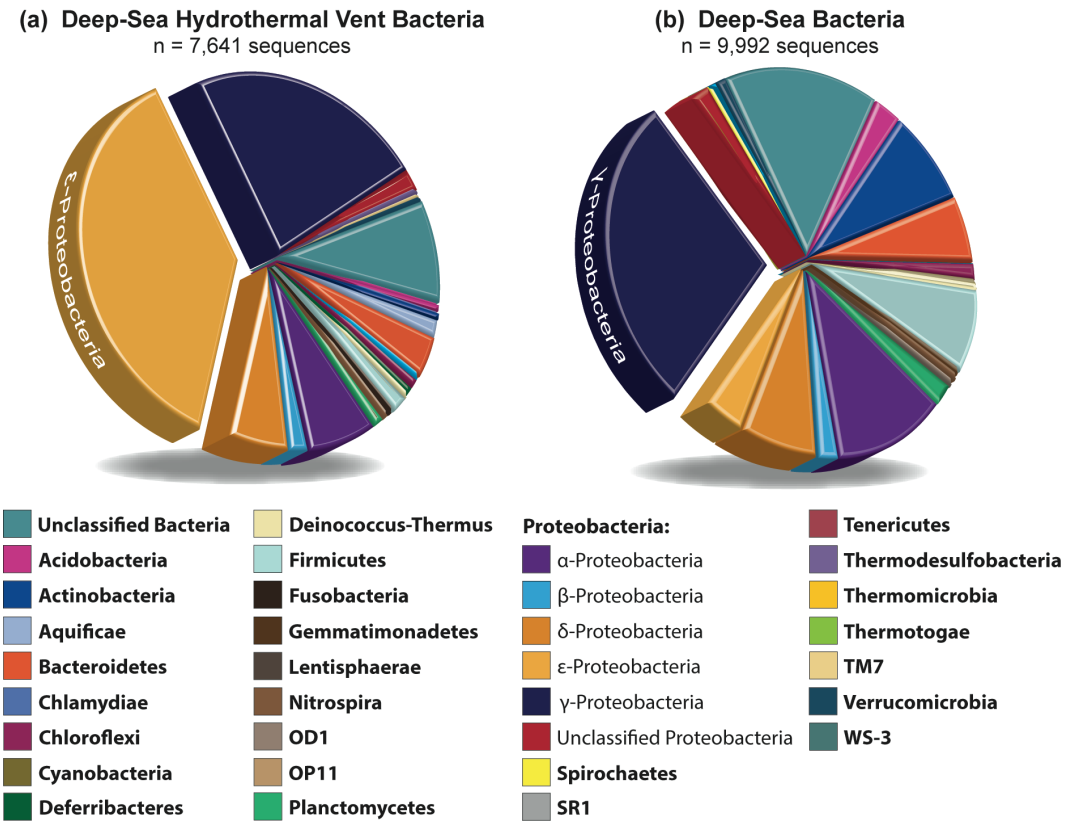

Figure 5.2. Relative abundances of bacterial phyla (including classes of Proteobacteria) found in the deep-sea as determined by 16S rRNA gene sequence analysis and reported in the Ribosomal Database Project (RDP, http:// rdp.cme.msu.edu/): (a) hydrothermal vent samples and (b) non-thermal water column and sediment samples (Cole et al., 2007; Cole et al., 2009). Note that these data do not include 16S rRNA V6 hypervariable region sequences, but those data show comparable diversity and relative abundances of phylogenetic groups (Huber et al., 2007).

bacteria, including many enteric mammalian pathogens (e.g., *Helicobacter* and *Campylobacter* species). The success of ε-proteobacteria, including a high degree of endemism to very specific habitats, is attributed in large part to the genomic plasticity of these bacteria, which lack many DNA-repair genes (Nakagawa et al., 2007). At hydrothermal vents, species of *Arcobacter*, *Sulfurovum*, *Sulforimonas*, *Hydrogenimonas*, *Nitratiruptor* and many other genera play a key role in early steps of

microbial and invertebrate colonization processes through the cycling of sulfur, hydrogen, nitrogen and carbon at vent fields (Alain et al., 2004; Nakagawa et al., 2005; Takai et al., 2006). Although the known genome sizes of members of these genera fall between 1.8 and 2.6 Mb, some ε-proteobacteria have been observed as filamentous aggregations (Cary et al., 1997; Goffredi et al., 2004; Harmsen et al., 1997; Santelli et al., 2008), the formation of which may rely on chemical signaling. Notably, recent metagenomics analyses of water-column bacteria reveal that deep-sea bacterial communities have a larger average genome size than surface-dwelling species and are characterized by a higher metabolic diversity and genomic plasticity (Konstantinidis et al., 2009).

The diversity of archaea within microbial communities associated with active chimney structures can vary from a single species (invertebrate symbionts and populations deep within chimney structures) to more complex communities. To date, phylotypes from every known and newly discovered marine Archaea group have been observed in deep-sea hydrothermal fields throughout the world (Figure 5.3a). While the archaea are generally associated with small genome sizes (< 2-3 Mb), methanogens of the genus *Methanosarcina* have genome sizes of 3 to 5.7 Mb, and are found ubiquitously in diverse habitats. These unusual archaea possess all three known pathways for methanogenesis and can utilize nine different methanogenic substrates. They comprise a significant portion of the largely (formally) unclassified deep-sea archaea (Figure 5.3b), and have also been detected in hydrothermal sediments from the Guaymas Basin (Teske et al., 2002) and high temperature chimneys in the Lost City Hydrothermal Field (Mid-Atlantic Ridge; Brazelton et al., 2006).

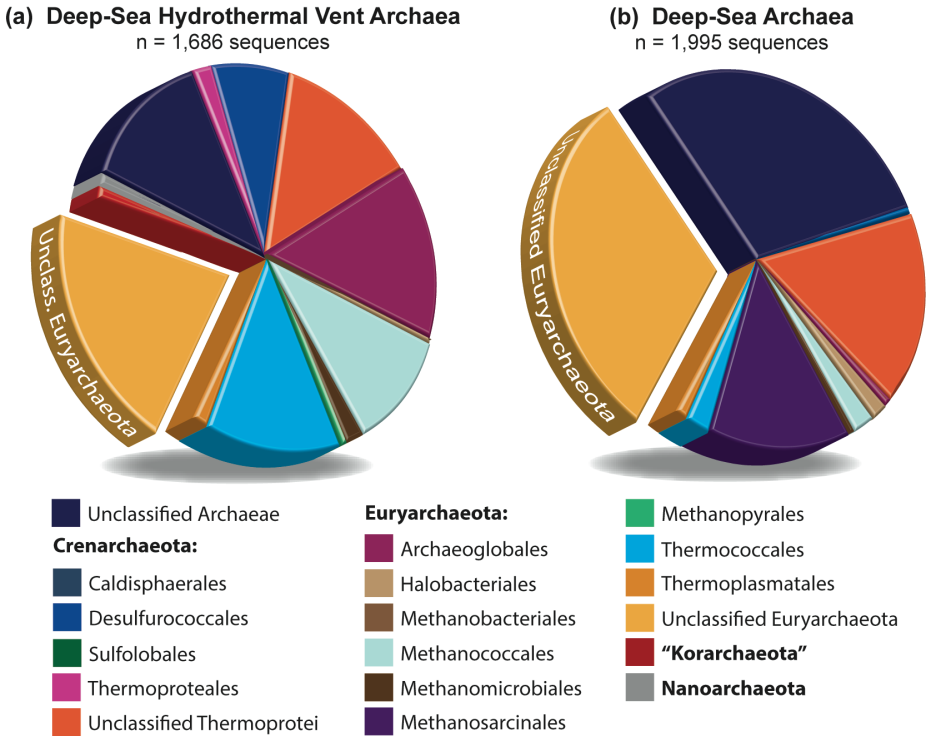

Figure 5.3. Relative abundances of phyla and component classes of archaea found in the deep-sea as determined by 16S rRNA gene sequence analysis and reported in the Ribosomal Database Project (RDP, http://rdp.cme.msu.edu/): (a) hydrothermal vent samples and (b) non-thermal water column and sediment samples (Cole et al., 2007; Cole et al., 2009). Note that these data do not include 16S rRNA V6 hypervariable region sequences, but those data show comparable diversity and relative abundances of phylogenetic groups (Huber et al., 2007).

Natural Products from Deep-Sea Vent Environments

It is widely accepted that the production of natural products represents a critical chemical defense mechanism adopted by organisms that lack physical/structural defenses against predation (Hay, 1996). The occurrence of isolated pockets of dense vent communities in the vast expanse of sea floor otherwise devoid of standing biomass implies the presence of defense mechanisms against predation by generalist

feeders. An obvious conclusion is that the extreme and dynamic nature of deep-sea vent habitats, including high levels of normally toxic abiotic chemical species such as H_2S, is responsible for the persistence of vent communities in the presence of high densities of predatory fishes and crabs. However, Hay and colleagues (2004) have investigated the feeding deterrent effects of H_2S-rich blood from tubeworms and chemical extracts from unpalatable deep-sea vent organism tissues on readily accessible shallow water generalist feeders (two crab and two fish species). Remarkably, none of the predators was deterred from feeding by the presence of H_2S in the offered food. In contrast, food containing chemical extracts from select tissues of certain polychaetes and bivalves was not accepted. Of 12 deep-sea vent species investigated, five possessed tissues that deterred feeding (*Riftia pachyptila*, *Lamellibrachia luymesi*, *Seepiophila jonesi*, *Archinome rosacea*, and *Calyptogena magnifica*). This chemical ecological study provides strong support for the use of natural product chemical defenses by deep-sea vent organisms. Additionally, anaerobic cycling of carbon often requires close associations of interdependent microorganisms, and these microbial interactions may be supported by an efficient communication network of small signaling molecules of potential utility for human health applications.

In addition to the specialized equipment needed to survey and sample the ocean floor, the generally accepted pre-1960's paradigms that the deep ocean lacked invertebrate biological diversity and that most important groups of antibiotic-producing bacteria were not indigenous in the oceans, delayed NPs investigations of the deep sea and also near-shore sediment-derived marine microbes. In the last 35 years, new, more cost-effective technologies in deep-sea research have resulted in literature reports of natural products from deep-sea cnidarians, sponges, echinoderms, bacteria, fungi and archaea collected from bathyal (200-4,000 m) and abyssal (4,000-6,500 m) ocean depths, as reviewed by Skropeta (2008). Nevertheless, the number of natural products from the deep sea (> 200 m) is only 1-2% of the more than

22,000 marine natural products reported in the last fifty years. The Skropeta review provides a graphical profile of the numbers of new compounds isolated through 2007 by depth range (below 50 m), which shows 267 new marine compounds collected from depths below 200 m. Of these, only two new molecules are attributable to deep-sea hydrothermal vent organisms, both archaea. In separate reports, anaerobic cultures of *Thermococcus* S 557 (cultured under N_2, 85 °C) and methanogenic *Methanococcus janaschii* (cultured under H_2, CO_2, 85 °C) produced isoprenyl glycerol ethers **1** (Gonthier et al., 2001) and **2** (Comita et al., 1984), respectively. However, these and other known archaeal glycerol ethers may be classified as primary rather than secondary metabolites: archaea are characterized by the production of thermally and chemically stable ether-containing membrane lipids. The only deep vent *invertebrate* metabolites reported to date are bathymodiolamides A (**3**) and B (**4**; Andrianasolo et al., 2011). These were obtained from the hydrothermal vent mussel *Bathymodiolus thermophilus* collected from around hydrothermal vents at 1,733 m in the Mid-Atlantic Ridge. In an apoptosis induction assay, compounds **3** and **4** inhibited the growth of HeLa cervical carcinoma cells (IC_{50} = 0.4 and 0.5 μM, respectively) and MCF7 breast cancer cells (IC_{50} = 0.1 and 0.2 μM, respectively).

The 2009 reports of the loihichelins and ammonificins A and B may be considered to be the first publications on *new* natural products from deep-sea vent environments. Loihichelins A-F (**5-10**) are amphiphilic peptidic siderophores isolated from cultures of the heterotrophic bacterium *Halomonas* LOB-5 collected from Loihi Seamount (east of Hawaii, -1174 m; Homann et al., 2009), and are related to the amphibactins, aquachelins and marinobactins from ubiquitous marine bacteria (Vraspir & Butler, 2009). With their octapeptide polar head groups and relatively short fatty acid moieties, the loihichelins are the most hydrophilic of the reported amphiphilic siderophores, which all chelate Fe(III) via the bidentate coordination of two ornithine hydroxamate groups and a β-hydroxyaspartate residue. Three 2 L cultures of the bacterium provided 8 mg of loihichelin C for 1D and 2D NMR spectroscopy. These

data confirmed the structural information gained for all six loihichelins by amino acid analysis using Marfey's method, peptide sequencing by tandem mass spectrometry and fatty acid analysis by GC-MS. *Halomonas* strains are broadly distributed in association with deep-sea volcanic weathered basalt and sulfide rocks in low-temperature hydrothermal vent fields, and possess the functional capability of Fe(II) and Mn(II) oxidation (Homann et al., 2009). It is not known whether the loihichelins serve a role only in the acquisition of iron as a trace nutrient or whether they are required for energy generation by *Halomonas* during the metabolism of reduced Fe (II).

Four brominated hydroxyethylamine chroman compounds, ammonificins A–D (**11**–**14**), were reported from the chemolithotrophic bacterium *Thermovibrio ammonificans* (Phylum Aquificae, Order Aquificales), which was isolated from the walls of an active deep-sea hydrothermal vent chimney on the East Pacific Rise (9°50′ N; Andrianasolo et al., 2009; 2012). Optimal growth of this thermophilic anaerobe is seen at 75 °C (pH 5.5, 2% w/v NaCl) in the presence of H_2 and CO_2 with nitrate or sulfur as the electron acceptor, which generates ammonium or hydrogen sulfide, respectively. A 5 L culture produced 40 g wet weight of bacterial mass from which milligram quantities of **11**–**14** were isolated. Interestingly, the original isolation attempt only afforded ammonificins A (**11**) and B (**12**), which did not correlate with the biological activity of the crude extract in an apoptosis induction assay. The authors concluded that this was possibly due to minor inseparable contaminants which could be responsible for the original activity of the parent extract. In re-isolation efforts, these minor components were identified as ammonificins C (**13**) and D (**14**), which induced apoptosis in apoptosis-competent primary baby mouse kidney (BMK) epithelial cells at 2 and 3 μM, respectively. Noteworthy is that staurosporine (an apoptosis inducer) induced apoptosis at 0.1 μM in the same assay. Nevertheless, this is the first report of a natural product that induces apoptosis from a cultured deep-sea hydrothermal vent bacterium.

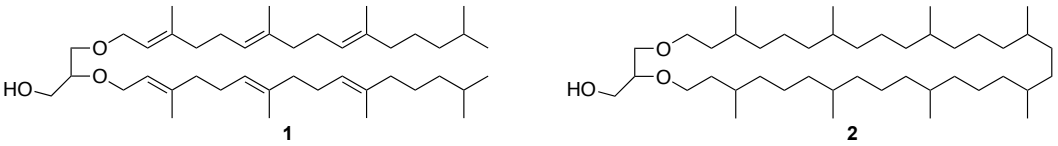

1 **2**

Thermococcus S 557 (archaeon)

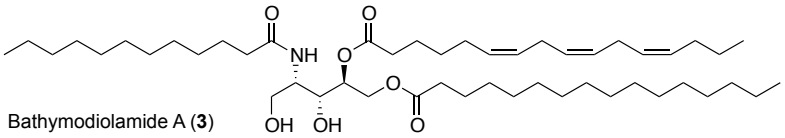

Bathymodiolamide A (**3**)

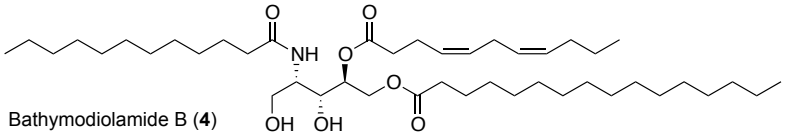

Bathymodiolamide B (**4**)

Bathymodiolus thermophilus (mussel)

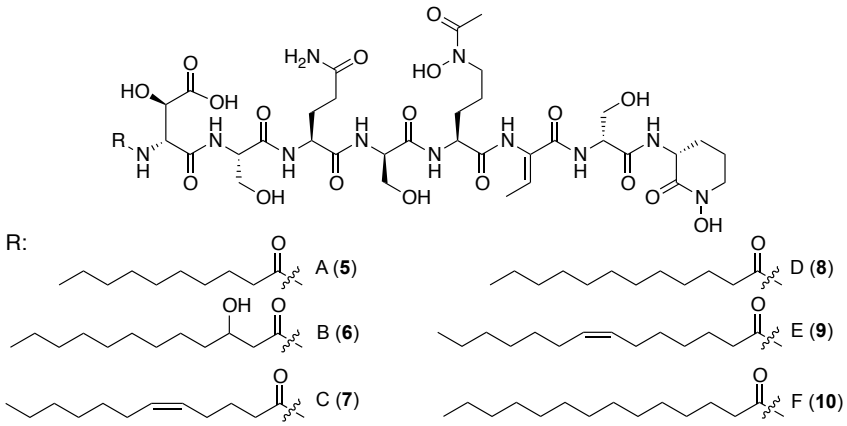

Loihichelins A–F (**5**–**10**)
Halomonas LOB-5 (Proteobacterium)

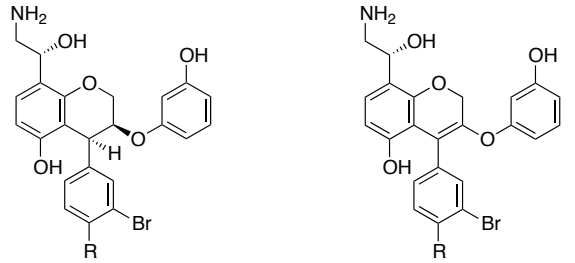

Ammonificin A (**11**) R = OH
Ammonificin B (**12**) R = Br
Ammonificin C (**13**) R = OH
Ammonificin D (**14**) R = Br

Thermovibrio ammonificans
(Aquificae bacterium)

Results and Discussion

Method Development

Collection of Deep-Sea Vent Organisms

Analytical tools for molecular structure elucidation have progressed to permit routine characterization of microgram quantities of pure, unprecedented natural products. However, the characterization of new chemotypes from complex extract mixtures that also comprise a substantial mass of inorganic contaminants still requires significant biomass of source organisms. Ideally, field collections of deep-sea vent invertebrates with their associated symbionts and collectable microbial mats may need to be one half to several liters in volume, with the possibility of recollection, and laboratory cultivation of microorganisms of interest is highly desirable. Therefore, the logistics and potential yields of deep-sea vent collections are critical considerations, together with the observation that to date most hydrothermal vent microorganisms are extremely resistant to routine cultivation.

Deep-water collections can be made in a nonselective sense by dredging, trawling and coring, which in turn damages a significant portion of non-targeted benthic communities and structures. However, advances in deep-sea submersible technology over the last 30 years have made nearly every niche of the deep ocean accessible. Deep-sea submersibles impose minimal environmental impact while allowing important ecological observations and biological collections. However, the costs incurred for only 4-5 hours of collection time precludes their extensive use in routine, non-collaborative collection operations (Cragg et al., 1999; Gage & Tyler, 1991). Thus, sample collections from hydrothermal vents and cold seeps are conducted exclusively by scientific institutions that operate manned submersibles (Human Occupied Vehicles, HOV), remote operated vehicles (ROVs) or autonomous

underwater vehicles (AUVs). As noted above, the most studied hydrothermal systems are in the eastern Pacific and the north-central Atlantic Oceans (Van Dover, 2000). This is mostly due to their proximity to the countries primarily involved in deep-sea hydrothermal vent research. Table 5.2 lists some of the institutions and their associated submersibles with maximum depth. Access to collections of hydrothermal vent samples may occur through research collaboration with these institutions: direct participation in research cruises carrying out submersible operations yields good bulk of field-collected material in our experience.

In collaboration with the NOAA Vents program at Oregon State University and Pacific Marine Environmental Laboratory (PMEL) we have collected several microbial mat and invertebrate samples during the New Millennium Observatory (NeMO) expeditions (2009–2012) to an active deep-sea volcano, Axial Seamount (Figure 5.4). The 2009 and 2010 field collections are the focus of the research presented here. Axial Seamount is located along the Juan de Fuca Ridge in the Pacific Ocean approximately 480 km (300 mi) west of Cannon Beach, Oregon. The caldera of this active submarine volcano (Figure 5.4) contains three distinct hydrothermal fields: a northern vent field (CASM, Canadian American Seamount Expedition), a southwestern vent field (ASHES, Axial Seamount Hydrothermal Emissions Study) and within the 1998 lava flow region along the southeast portion of the caldera (Baker et al., 1999). Since the 1998 eruption, the NeMO Project was initiated to study the geology, chemistry and biology of this active volcano (NeMO, 2013). Notably, an eruption of this volcano was predicted to occur before 2014, which was based on a deflation-inflation cycle observed from bottom pressure recorders that were continuously monitored and maintained during NeMO expeditions from 1998 to 2010. In fact, during the NeMO 2011 cruise extensive new lava flows revealed that a massive eruption had occurred along the upper south rift zone at Axial Seamount (Chadwick et al., 2012; Dziak et al., 2012). Thus, as a part of a decade long study of vent fluid chemistry and microbial diversity, a major focus of many of the NeMO

Table 5.2. Scientific Institutions that Operate Deep-Sea Submersibles.

Institution	Submersible	Maximum Depth (m)
Australia's Commonwealth Scientific Industrial and Research Organization (CSIRO)	AUV ABE	2,500
The Canadian Scientific Submersible Facility	ROV ROPOS	5,000
Florida Atlantic University's Harbor Branch Oceanographic Institution (HBOI)	HOV Johnson-Sea-Link I and II	1,000
The Hawaii Undersea Research Laboratory (HURL)	HOV Pisces IV and V	2,000
Institut français de recherche pour l'exploitation de la mer (Ifremer)	HOV Nautile	6,000
	ROV Victor	6,000
The Japan Marine Science and Technology Center (JAMSTEC)	HOV Shinkai-6500	6,500
	ROV Kaiko	[a]11,000
	ROV Kaiko 7000 (II)	7,000
The Monterey Bay Aquarium Research Institute (MBARI)	ROV Tiburon	4,000
PP Shirshov Institute of Oceanology, Russian Academy of Sciences	HOV Mir I and II	6,000
MARUM-Center for Marine Environmental Sciences, University of Bremen	ROV QUEST 4000	4,000
Woods Hole Oceanographic Institute (WHOI)	HOV Alvin	4,500
Woods Hole Oceanographic Institute (WHOI)	ROV Jason (II)	6,500

[a]lost at sea in 2003. References: (Desbruyeres et al., 2006; Verenium, 2013)

expeditions is to deploy and collect geological monitoring devices and sample hydrothermal vent fluids (Chadwick et al., 2010). As such, many of the ROV's resources for collecting (e.g. single chamber vacuum slurp vs. multiple chamber slurp) and storing large-scale samples (e.g. one small bio-box), as well as the aliquoted time to achieve such tasks, are limited in terms of manageable weight on the submersible and priority. Therefore, in order to maximize sampling potential with minimal impact to the ongoing research efforts of NOAA Vents Program scientists and their collaborators, we developed several lightweight syringes from materials obtained at our local hardware store. Importantly, these syringes could be used by the ROV's manipulator arms to collect small (< 100 mL) or large (> 400 mL) samples of bacterial mats or sediment (Figures 5.5 and 5.6, respectively). During the NeMO 2010 expedition these syringes were used to collect diverse samples of microbial mats and sediment that were the focus of several cultivation experiments.

To collect large biological samples, the ROV Jason II is also capable of collecting microbe-bearing rocks or bulk invertebrate material to stow in its "biological box" (Figures 5.7 and 5.8). In particular, numerous unsuccessful methods were attempted to collect the blue carpet-like mats of the ciliate *Folliculinopsis* sp., which secrete and dwell in chitinous sheaths (loricae) that are strongly attached to the substratum and to each other. Ultimately, a piece of volcanic basalt (9.2 kg) containing a mat of *Folliculinopsis* sp. was collected (Figure 5.7 C; sample J2-525-Mat-22) and processed on board the *R/V Thompson* to remove the organism for natural products investigations. In addition, a bright orange filamentous mat growing on a tubeworm assemblage, which was originally identified as a possible sponge, was collected using the same grab technique employed to collect the blue mat (Figure 5.7 C; sample J2-520-T07). Here we report the biological and chemical profiling of these and other samples collected during the 2009 and 2010 NeMO expeditions (Tables 5.3 and 5.4, respectively).

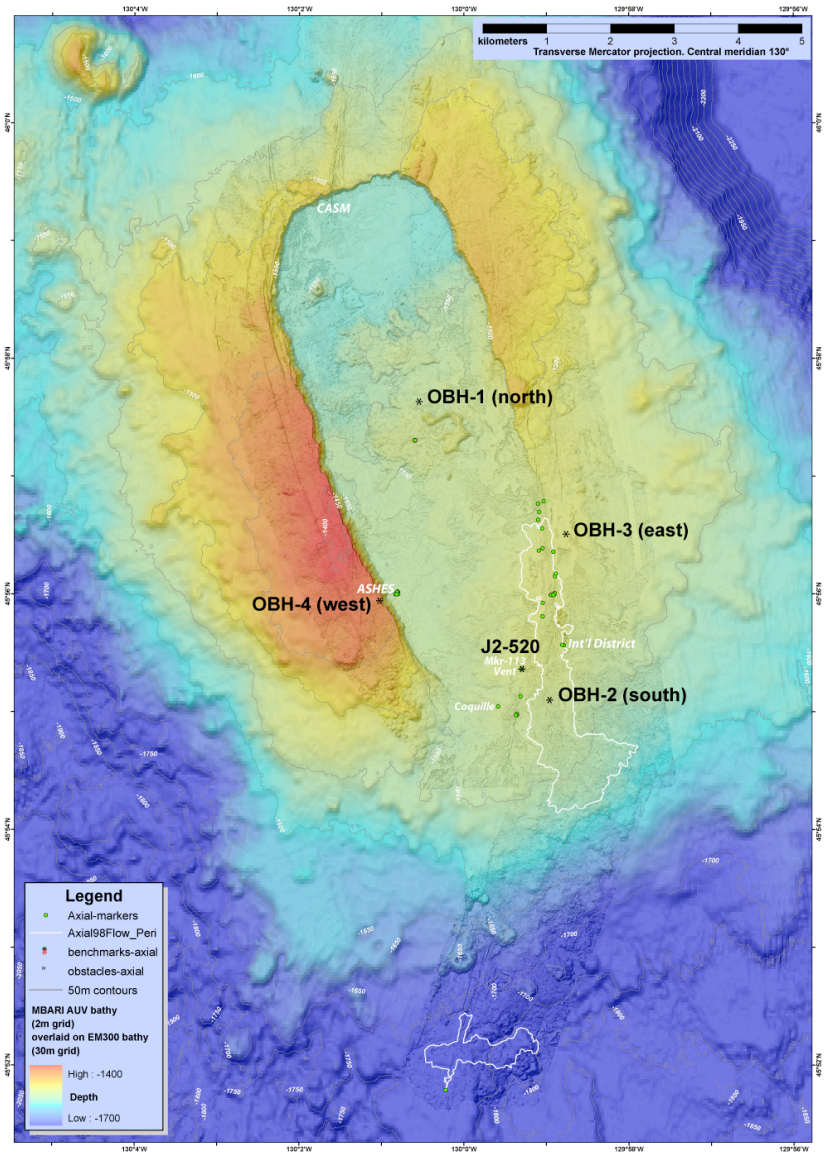

Figure 5.4. Bathymetry map of the Axial Volcano (Seamount) caldera located along the Juan de Fuca Ridge in the Pacific Ocean approximately 480 km (300 mi) west of Cannon Beach, Oregon. J2-520 represents the first logged dive for the ROV Jason II during the 2010 New Millennium Observatory (NeMO) expedition at Marker 113 (-1522 m). Image credit: William W. Chadwick, Jr., Oregon State University.

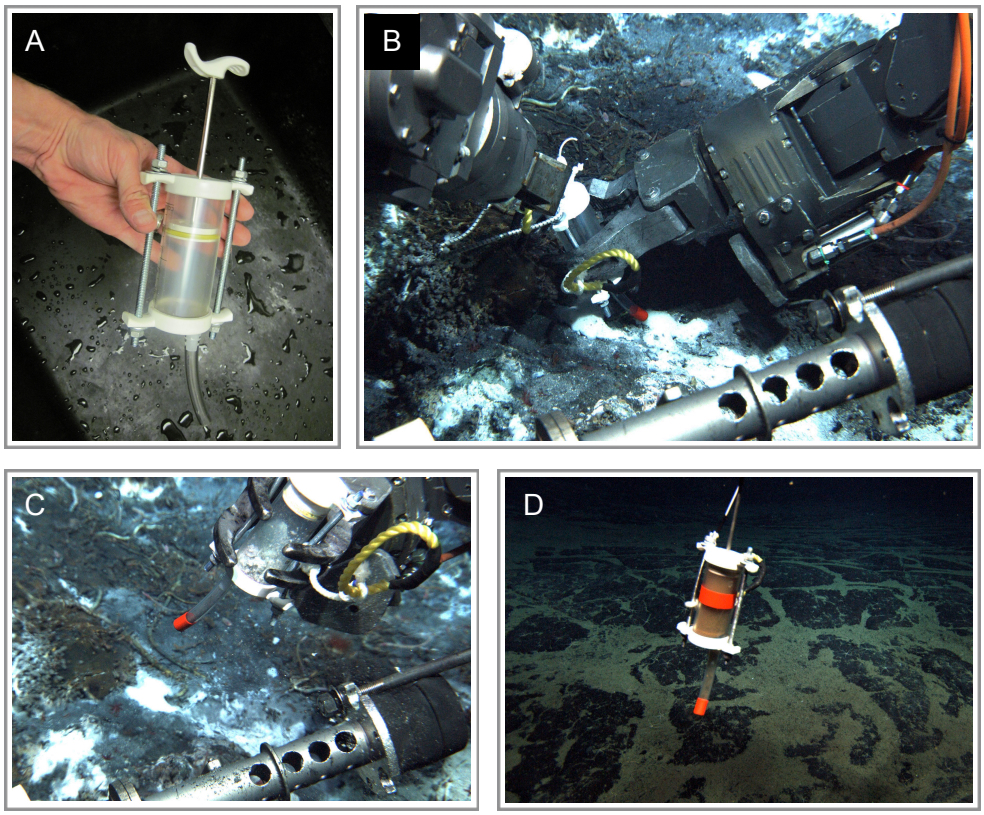

Figure 5.5. (A) Modified Sharpvet nylon syringe (100 mL, *small syringe*) used to collect isolated pockets of microbial mats and/or sediment. (B, C) ROV Jason II using a small syringe to collect a white microbial mat (J2-521-Mat 37) at Mushroom Vent located on the Axial Seamount. (D) Sediment collected with a small syringe near Marker 33 along the east caldera at Axial Seamount (J2-525-SED-01).

Figure 5.6. (A) Picture of a large syringe (400 mL) made from materials purchased from a local hardware store. (B, C) ROV Jason II using a large syringe to collect an orange microbial mat (J2-525-Mat 25) growing on an extinct chimney (El Antiguo; 1522 m) located in the International District of the Axial Seamount. This chimney also appeared to contain veins of ferric iron on which the mat was located. (D) Processing of the J2-525-Mat 25 sample on board the *R/V Thompson*. Individual samples were aliquoted into 50 mL conical tubes for storage at -80 °C or further processed for culture enrichment experiments. (E) Third generation syringe sampler made by a local machine shop, which was designed to be used by the main manipulator arm of the ROV Jason II or HOV Alvin. This syringe (E) was recently used to collect microbial samples during two separate expeditions made in 2012: Axial Seamount (NeMO) and NE Lau Basin (Submarine Ring of Fire).

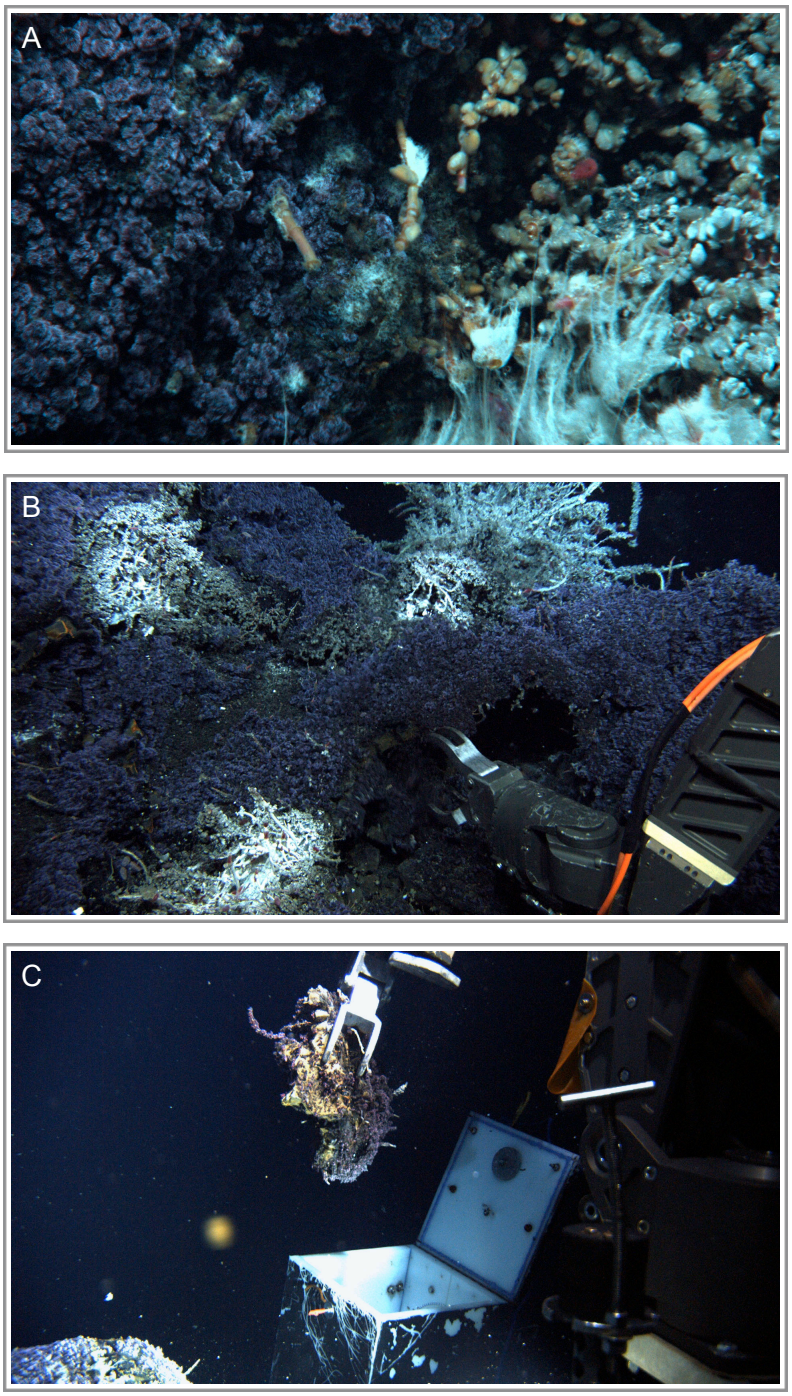

Figure 5.7. (A) Blue carpet-like mats of the marine ciliate *Folliculinopsis* sp. in close proximity to limpets and scale worms covered in white filamentous microbial mats. (B) ROV Jason II manipulator collecting volcanic rock and associated blue mat at Marker N3 (Magic Carpet; 1525 m) on Axial Seamount. (C) Stowing a piece of volcanic basalt (9.2 kg) containing a mat of *Folliculinopsis* sp (J2-525-Mat-22).

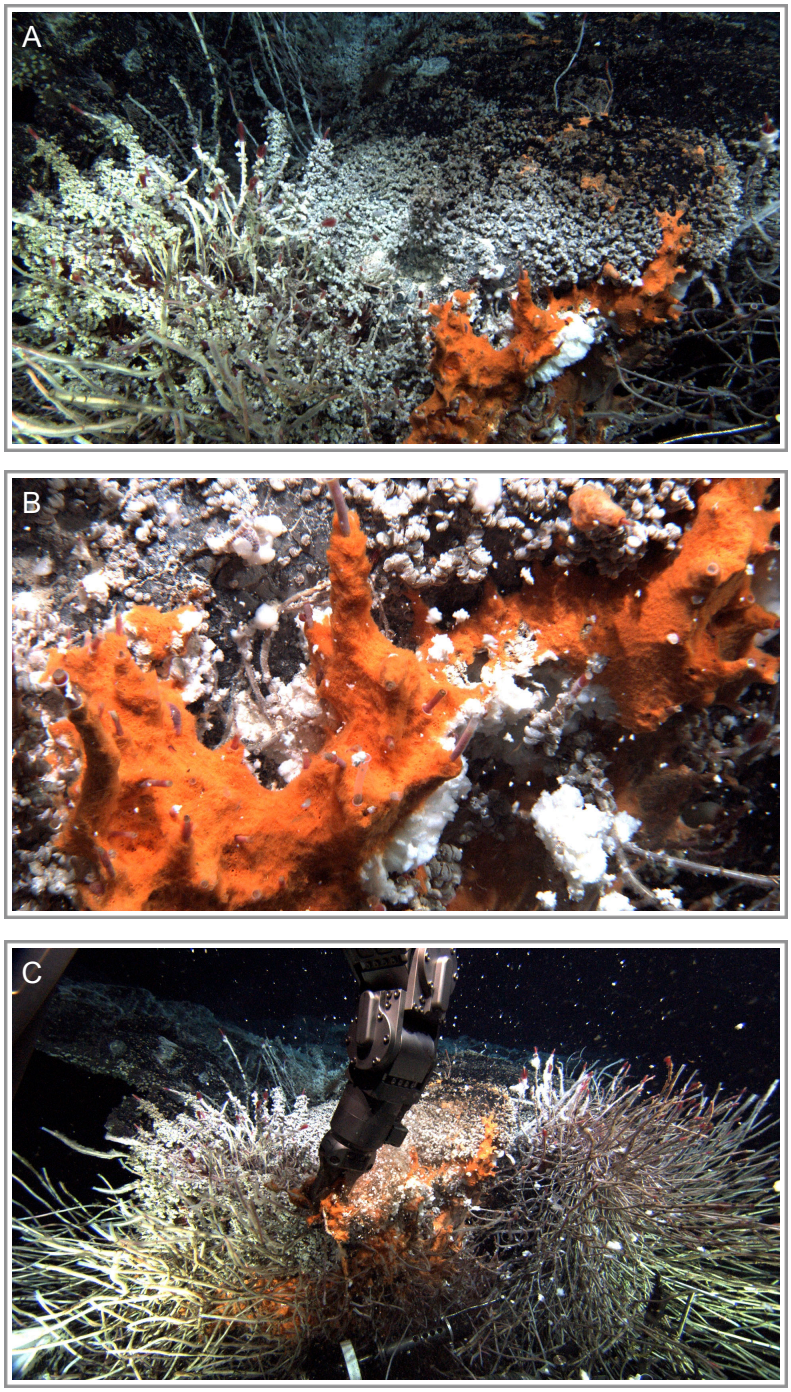

Figure 5.8. (A, B) Orange microbial mat growing on a tubeworm assemblage located near the Marker 113 vent site (1523 m) at Axial Seamount. Tubeworms and the associated orange mat (J2-520-T07) were collected using the ROV Jason II robotic arm (grab technique).

Table 5.3. Summary of June 2009 Axial Seamount collections of deep vent invertebrates for natural product investigations.

Organism description	Number of collections	Range of Collection Volumes
Tubeworms (*Ridgeia piscesae*)	4	1-3 L
Bacterial mats (5 white, 1 peach)	6	50 mL–1.5 L
Blue protozoan mat (*Folliculinopsis* sp.)	1	100 mL
Palm worms (*Paralvinella palmiformis*)	2	100, 600 mL
Pandorae worms (*Paralvinella pandorae*)	1	100 mL
Limpets (*Lepetodrilus fucensis*)	3	300 mL
Scale worms (mixed taxa)	1	100 mL
Mixed (unsorted) collections	3	1 L

Table 5.4. List of August 2010 Axial Seamount collections of deep-vent microbial samples for natural product investigations.

Sample ID	Location	Collection (Method)	Volume	Depth (m)
J2-520-T07	Marker 113	orange filamentous mat/large tubeworms (grab)	500 mL	1522.9
J2-520-Mat-19	Bag City	white microbial mat/limpets (slurp)	10 mL	1531.0
J2-520-Mat-25	Vixen	white microbial mat (large syringe)	50 mL	1533.8
J2-520-Mat-36	Casper	sediment (small syringe)	10 mL	1534.4
J2-521-SED-01	West rim of caldera	sediment (core)	–	1415.0
J2-521-SED-02	West rim of caldera	sediment (core)	–	1415.0
J2-520-SED-03	West rim of caldera	sediment (core)	–	1415.0
J2-521-Mat-08	Styx	orange microbial mat (large syringe)	50 mL	1543.2
J2-521-Mat-17	Gollum	white microbial mat/palm worms (slurp)	50 mL	1541.2
J2-521-Mat-37	Mushroom	white microbial mat (small syringe)	25 mL	1542.0
J2-522-Bio-07	Bag City	white filamentous mat/large tubeworms (grab)	4 L	1531.0
J2-522-Mat-02	Marker 33	white microbial mat/limpets (slurp)	10 mL	1520.0
J2-523-Mat-05	El Gordo (Mkr 151)	white filamentous mat at base of tubeworm assemblage (slurp)	1 L	1521.8
J2-523-Mat-10	9 Meter	blue ciliate mat, *Folliculinopsis* sp. (scraped with temp probe)	1 mL	1518.5
J2-523-Mat-20	Escargot	blue ciliate mat, *Folliculinopsis* sp. (small syringe)	1 mL	1518.0
J2-523-Mat-24	Diva	orange microbial mat (small syringe)	10 mL	1520.0
J2-523-Mat-34	El Antiguo	orange microbial mat (large syringe)	100 mL	1520.0
J2-523-CHY-15	Escargot	chimney spire (grab)	–	1519.6
J2-525-SED-01	East rim of caldera	sediment (small syringe)	50 mL	1518.5
J2-525-Mat-21	Magic Carpet	blue ciliate mat, *Folliculinopsis* sp. (slurp)	1 mL	1524
J2-525-Mat-22	Magic Carpet	blue ciliate mat, *Folliculinopsis* sp. (grab, large rock)	–	1525
J2-525-Mat-25	El Antiguo	orange microbial mat (large syringe)	100 mL	1521.9

Cultivation of Deep-Sea Vent Actinobacteria

Cultivation of microorganisms was central to methods used in early studies of microbial communities to determine community diversity, biomass and production rates (Karl, 1995). However, most hydrothermal vent microorganisms are extremely resistant to cultivation, which might be expected considering the extreme environments they inhabit (Jørgensen & Boetius, 2007). Cultivation strategies utilizing various *in situ* colonization devices including vent cap chambers (Reysenbach et al., 2000), pumice filled stainless-steel pipes (Takai et al., 2003), titanium-mesh catheters (Higashi et al., 2004) and titanium-sheathed thermocouple arrays (Page et al., 2008) showed moderate success in culturing some of these microbes in their natural environment for the study of *in situ* physiological expression (see Table 5.2 for example studies; Postec et al., 2007). Advances in laboratory cultivation have allowed fairly accurate replications of temperature, nutrient composition and pressure, which have greatly increased the diversity of cultured microbes from previously "uncultivated" microorganisms (Baross & Deming, 1995; Jannasch et al., 1996; Postec et al., 2007). It should be noted that the current upper limit for hyperthermophiles isolated in culture is 115 °C (Holden & Daniel, 2004), although Baross and Deming have reported (unreplicated) evidence for a consortium of growing "superthermophiles" in fluids collected from black smokers (the hottest vents) and maintained in culture at 150-250 °C under 265 atm (Baross & Deming, 1995).

Considerable effort has been applied to the large-scale cultivation of hyperthermophilic anaerobes to investigate their potential biotechnological applications (Holden & Daniel, 2004). Numerous biotechnology companies are actively involved in product development from thermophilic vent organisms. These biotechnological interests have focused mainly on the use of whole cells, for example, sulfate-reducing bacteria in waste management processes (Muyzer & Stams, 2008) and also the development of new enzymes (NEB, 2013; Verenium, 2013) and exo-polysaccharides (Nichols et al., 2005) to improve agriculture, biotechnology,

cosmetics, pharmaceutics and even bone healing (Zanchetta et al., 2003). There is also a focus on laboratory cultivation of deep vent microbes at the Center for Marine Biotechnology at Rutgers University, where they have developed laboratory techniques to culture tubeworms together with their symbiotic bacteria (Lutz, 2008). Other successes in laboratory culture of potential natural product producing microorganisms include the isolation of 38 actinomycetes from the Mariana Trench sediments (using marine agar and culture media selective for actinomycetes; Pathom-aree et al., 2006). These bacteria were assigned to the *Dermacoccus, Kocuria, Micromonospora, Streptomyces, Tsukamurella*, and *Williamsia* genera based on 16S rRNA analysis. Furthermore, nonribosomal peptide synthetase (NRPS) genes were detected in more than half of the isolates and type I polyketide synthases (PKS-I) were identified in five of the 38 strains. In contrast, there are few reported culture efforts of likely small molecule NPs-producing microbes (e.g., Actinobacteria) from deep-sea hydrothermal vents.

Alternately, national culture collections are a source of microbial vent samples. For example, JAMSTEC promotes collaborative efforts with industry through their Cooperative Research Project for Extremophiles program (JAMSTEC, 2013). Similarly, the Brittany Microbe Culture Collection (BMCC) allows academic and industrial access to over 1,300 microorganisms isolated from deep-sea hydrothermal vents by Ifremer (2013). In the United States, only the American Type Culture Collection (ATCC) publicly lists over 750 extremophile microorganisms available for purchase that include archaea, sulfur oxidizers, methylotrophs, alkaliphiles, sulfate reducers, thermophiles, psychrophiles, halophiles and acidophiles. However, only a small portion (< 20) are from hydrothermal vents (ATCC, 2013). This may be a reflection of the difficulties in obtaining pure cultures of these extremophiles consistent with ATCC standards, or the result of undisclosed collections due to agreements between researchers and private corporations.

Based on the reports of actinomycetes isolated from deep ocean sediments and hydrothermal vent environments, we performed a series of selective cultivation methods to recover actinomycetes from microbial mats and sediments collected from Axial Seamount. Several recent reports document the successful isolation and culture of deep-sea actinomycetes in low-nutrient media (Gontang et al., 2007; Pathom-aree et al., 2006). Furthermore, many common strains of marine microbes, identified either microscopically or genetically, are not adapted for growth in media containing high concentrations of nutrients (Connon & Giovannoni, 2002; Zengler et al., 2002) or only produce secondary metabolites in source-deficient media (Tormo et al., 2003). Thus, media (see Supporting Information, Table S-5.2) and sample processing methods (Jensen et al., 2005) that have resulted in the high recovery of actinomycetes from deep ocean and tropical marine sediments were used for the on-site culturing of deep-vent actinomycetes.

Biological Screening of Deep-Sea Vent Organisms

Extract Library Preparation and Bioassay Development

Prior to biological screening, a fractionation library was prepared from aqueous (MeOH–H_2O) and organic (MeOH–CH_2Cl_2 1:1) extracts obtained for several of the "bulk" collections (~50 mL) of deep-vent invertebrates and microbial mats collected during NeMO 2009 and 2010 expeditions to Axial Seamount (Tables 5.3 and 5.4). In addition, a number of small samples (15-50 mL) of deep-sea vent organisms were provided by Verena Tunnicliffe (UBC) and Craig Moyer (WWU) from collections made during expeditions (1991–2002) to various hydrothermal vent sites in the Pacific Ocean. Importantly, these latter samples were used to develop the extraction, analytical and screening methods used to evaluate the more recent Axial Seamount collections (2009, 2010). A typical fraction scheme, as used for cyanobacterial extracts, utilizes normal phase vacuum liquid chromatography (NP-VLC) using a

stepped solvent gradient of hexanes to EtOAc to MeOH to create a first-tier fractionation series (Figure 5.9). This scheme works well to separate highly lipophilic compounds from more hydrophilic material, the latter of which generally contains secondary metabolites of interest. However, in the deep-vent extracts, many of the first-tier VLC fractions also contained a high degree of elemental sulfur (5-10 % of dry mass of organism). Surprisingly, the sulfur compounds did not affect our biological assays, which is similar to the lack of feeding deterrent effects of H_2S reported by Hay et al. (1996). Nonetheless, to more accurately assess the biological activity of a fractionation library, it is imperative to remove nuisance compounds that may alter the final concentration, solubility or integrity of test compounds. A majority of the sulfur from the organic extracts was therefore removed by solvating the extract in 100 % dichloromethane (CH_2Cl_2) and reducing the temperature (-20 to -80 °C) until crystals of sulfur precipitated out of solution. Importantly, this extract pre-treatment resulted in a significant reduction in the amount of sulfur observed throughout the

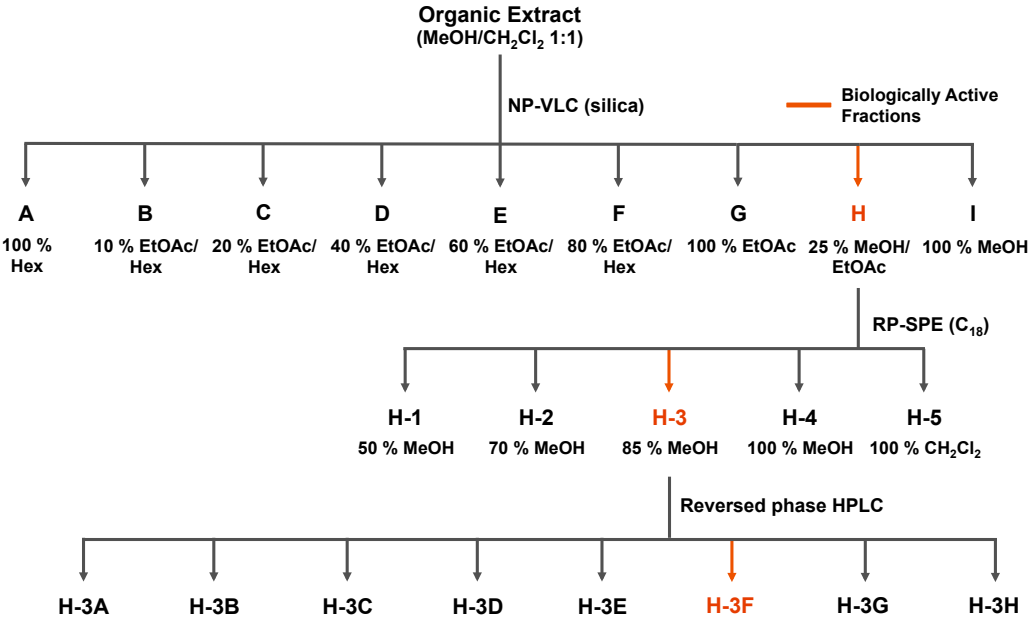

Figure 5.9. General bioassay-guided fractionation scheme for organic extracts showing the typical number of fractions collected at each chromatographic separation step and their corresponding eluting solvent.

fractionation scheme, and reduced the amount of *in vacuo* bumping (often resulting in sample loss) during the concentration steps of each sample. In several instances, a small sample/extract mass made it essential to conserve these limited materials by minimizing the number of chromatography steps. Thus, these crude extracts were directly processed over reversed phase C_{18} reversed-phase (RP_{18}) solid-phase extraction (SPE) cartridges to generate first-tier fractions (Figure 5.9).

A high throughput microtiter-plate (96-well format) antimicrobial assay was developed according to Casey et al. (2004), Smith et al. (2008) and the Clinical Laboratory Standards Institute's methods for dilution susceptibility testing (2009) as a primary screen to evaluate the deep-vent fractionation library and identify potential antimicrobial compounds. This assay has several advantages over the disk diffusion method in that it requires less sample material, allows high throughput screening of HPLC or LC-MS peak libraries in a relatively short amount of time, and replaces subjectivity associated with visual assessments of zones of inhibition (e.g. irregular zones due to in-growth and poor sample diffusion) with a quantitative measure of efficacy (e.g. optical density). Furthermore, this assay allows the generation of dose-response curves for test organisms exposed to a bioactive compound, which can be used to extrapolate the minimal inhibitory concentration (MIC): "the lowest concentration of an antimicrobial agent that prevents visible growth of a microorganism in an agar or broth dilution susceptibility test" (CLSI, 2009), for the bioactive compound. It is important to note that our initial antimicrobial screening strategy, which was used to assess the collections described here, tested against standard (non-resistant) strains of *Escherichia coli* (Gram-negative bacterium) and *Staphylococcus aureus* (Gram-positive bacterium). However, in collaboration with Dr. Aleksandra Sikora (Oregon State University) this assay has recently evolved to include a panel of clinically-relevant multi-drug resistant human pathogens including methicillin-resistant *Staphylococcus aureus* (MRSA; ATCC® BAA-1720™), gentamycin and vancomycin-resistant *Enterococcus faecalis* (ATCC® BAA-1720™),

Escherichia coli O157:H7 (Sikora et al., 2009), *Vibrio cholerae* O1 El Tor (N16961, ATCC® 39315D-5™) and *Pseudomonas aeruginosa* PAO. These more robust strains are currently being used to screen extract libraries of deep-vent microorganisms collected during NeMO 2011 and 2012, and NE Lau Basin expeditions, which are the subject of a separate, ongoing project in the McPhail laboratory.

Screening of Deep-Sea Vent Invertebrates and Microbial Mats

Preliminary screening in our microtiter plate-based antimicrobial assay against *Escherichia coli*, *Staphylococcus aureus,* and in a biofilm adherence assay using *Mycobacterium avum* A5, identified several possible antimicrobial and/or biofilm inhibitor leads (Table 5.5). In particular, multiple VLC fractions of a filamentous mat (DSV-09-14) collected from tubeworm casings (*Ridgeia piscesae*) showed promising activity profiles against both *E. coli* and *S. aureus* (256 μg/mL, < 50% cell viability) and reduced the biofilm formation of *M. avum* (250 μg/mL, > 20% reduction). Fractions E (60% EtOAc–hexanes) and F (80% EtOAc–hexanes) were the most active and were therefore subjected to RP_{18} SPE and RP-HPLC to yield four minor compounds (0.3, 0,4, 0.6, and 0.7 mg), and one major compound (**15**, 3.3 mg). ^{1}H and ^{13}C NMR data (Figure 5.10) coupled with a $[M]^+$ peak at *m/z* 386.3 in the EIMS of **15** suggested a molecular formula of $C_{27}H_{46}O$, and identified this compound as cholesterol (**15**). Analysis of the ^{13}C NMR spectra for each of the minor compounds revealed a close resemblance to the major sterol. Interestingly, analysis of the active fractions of DSV-09-15, a peach colored microbial mat, also resulted in the isolation of **15**, and several sterol-like compounds. However, in subsequent antimicrobial assays none of these compounds were active. In an attempt to identify any minor metabolites that may account for the observed parent fraction bioactivity, a trace HPLC peak observed throughout each active sample that displayed a matching retention time and UV signature was targeted for analysis. Collectively, these peaks resulted in the isolation of several putative phthalates (plasticizers). Further testing of these

Table 5.5. Antimicrobial activity of organic extracts and VLC fractions from deep-sea hydrothermal vent invertebrates and microbial mat collections.

Sample ID (collection date, dive #)[a]	Extract / Fraction ID[b]	% Cell Viability[c]		% Biofilm Formation[d]
		E. coli	*S. aureus*	*Mycobacterium avium*
small tubeworms (07-26-1994, AD-2805)	DSV-Eve-7a	100	100	**-21**
	DSV-Eve-7b	100	**10**	**-30**
	DSV-Eve-7c	100	100	100
	DSV-Eve-7d	100	100	100
palm worms (07-27-1991, AD-2420)	DSV-F27-8a	100	100	13
	DSV-F27-8b	100	100	100
	DSV-F27-8c	100	100	100
	DSV-F27-8d	100	100	100
sulphide worms (07-15-1991, AD-2408)	DSV-F8/9-9a	100	100	100
	DSV-F8/9-9b	100	100	**-22**
	DSV-F8/9-9c	100	100	47
	DSV-F8/9-9d	100	100	100
giant clams, *Calyptogena* sp. (06-27-1992, R-787-14-01)	DSV-MV-10	100	100	6
	DSV-MV-10 aq	100	100	–
hairy vent snail, *Alvinoconcha* sp. (04-02-2004, R-192-F2)	DSV-BB-11	100	100	100
	DSV-BB-11 aq	100	100	–
palm worms (06-21-2009, AD-4522)	DSV-09-12A	96	92	100
	DSV-09-12B	89	93	-2
	DSV-09-12C	64	100	100
	DSV-09-12D	100	89	100
	DSV-09-12E	90	90	-8
	DSV-09-12F	91	78	100
	DSV-09-12G	100	100	100
	DSV-09-12H	71	100	1
	DSV-09-12I	100	82	76
tubeworms, *Ridgeia piscesae*; white filamentous mat; scale worms; snails; and palm worms, *Paralvinella palmiformis* (06-16-2009, AD-4517)	DSV-09-13a	81	98	100
	DSV-09-13b	100	83	9.3
white filamentous mat from tubeworms, *Ridgeia piscesae* (6-21-2009, AD-4522)	DSV-09-14A	75	92	-10
	DSV-09-14B	**49**	88	**-55**
	DSV-09-14C	**51**	85	**-38**
	DSV-09-14D	72	77	**-38**
	DSV-09-14E	**50**	**39**	**-36**
	DSV-09-14F	**23**	**6**	**-21**
	DSV-09-14G	83	78	**-44**
	DSV-09-14H	80	100	**-53**
	DSV-09-14I	74	92	59

Table 5.5 (continued). Antimicrobial activity of organic extracts and VLC fractions from deep-sea hydrothermal vent invertebrates and microbial mat collections.

Sample ID (collection date, dive #)[a]	Extract / Fraction ID[b]	% Cell Viability[c]		% Biofilm Formation[d]
		E. coli	*S. aureus*	*Mycobacterium avium*
peach colored microbial mat	DSV-09-15	88	**10**	–
from rock substrate	DSV-09-15A	**0**	**0**	–
(06-19-2009, AD-4520)	DSV-09-15B	**42**	**0**	–
	DSV-09-15C	62	**0**	–
	DSV-09-15D	**0**	**10**	–
	DSV-09-15E	100	71	–
	DSV-09-15F	100	79	–
	DSV-09-15G	100	78	–
	DSV-09-15H	100	85	–
	DSV-09-15I	100	100	–
blue ciliate mat,	DSV-09-16	53	**12**	–
Folliculinopsis sp.	DSV-09-16A	**0**	**0**	–
(6-21-2009, AD-4522)	DSV-09-16B	65	92	–
	DSV-09-16C	**25**	**0**	–
	DSV-09-16D	100	**22**	–
	DSV-09-16E	**40**	62	–
	DSV-09-16F	**36**	100	–
	DSV-09-16G	100	80	–
	DSV-09-16H	93	91	–
	DSV-09-16I	88	91	–
blue ciliate mat,	DSV-10-17B3	93	**0**	–
Folliculinopsis sp.	DSV-10-17C	78	**44**	–
(09-05-2010, J2-525)	DSV-10-17D1	65	**0**	–
	DSV-10-17E	100	**0**	–
	DSV-10-17F	100	100	–
	DSV-10-17G	100	86	–
	DSV-10-17H	100	65	–
	DSV-10-17I	100	100	–

[a]Deep-sea submersible designations: AD, Alvin Dive; J2, Jason II; R, Ropos.

[b]Fractionation level designated by letter following sample number (e.g. A–I represents VLC fractionation scheme; a–d represents RP_{18} SPE; no letter represents organic parent extract and aq = aqueous parent extract).

[c]Cell viability was determined after 16 hours (256 μg/mL) in a microtitier plate-based antimicrobial assay using non resistant *Escherichia coli* (*E. coli*) and *Staphylococcus aureus* (*S. aureus*) cells and is reported as the percentage of viable cells relative to the vehicle control.

[d]Percent biofilm formation represents the percent of biofilm coverage for *Mycobacterium avium* A5 in treated wells (250 μg/mL) relative to the vehicle control. A reduction (reported as a negative value) in biofilm coverage of > 20% represents the inhibition of *M. avium* biofilm formation. Assay performed by Sasha Rose and Luiz Bermudez at Oregon State University as previously described (Carter et al., 2003).

compounds revealed that *S. aureus* (32 μg/mL, 2% cell viability) and *E. coli* (32 μg/mL, 60% cell viability) were highly sensitive to these nuisance compounds. These compounds may have been introduced into each sample during the pre-fractionation process to remove sulfur, which involved several filtration steps using glass-fiber filters that may have contained trace amounts of phthalates. Importantly, a Büchner funnel with a sintered glass disc was used in place of these filters during all subsequent pre-fractionation steps, and resulted in fewer instances of phthalate contamination.

The 25% MeOH–EtOAc VLC fraction (H) of DSV-09-14 (white filamentous mat) was the largest fraction (946 mg) and initially did not show antimicrobial activity at 256 μg/mL, but did inhibit the biofilm formation of *M. avium*. The selective inhibition of biofilm formation, without an antimicrobial effect, is generally preferred in the screening of biofilm inhibitors. However, after RP_{18} SPE using a gradient from 50% MeOH-H_2O to 100% MeOH, the 100% MeOH fraction (82.6 mg) showed significant activity against *S. aureus* (MIC = 64 μg/mL). Interestingly, the ^{13}C NMR spectrum matched the sterol fingerprint of **15** (Figure 5.10), although the latter was shown to be inactive. Thus, it is likely that the presence of a minor compound may account for the observed activity of this sample.

Fractions from 2009 (DSV-09-16) and 2010 (DSV-10-17) collections of a blue carpet-like mat identified as a folliculinid ciliate (*Folliculinopsis* sp.; Kouris et al., 2007) were subjected to bioassay-guided fractionation following microtiter plate-based antimicrobial assays against *S. aureus* and *E. coli.* Interestingly, DSV-09-16 fractions A–F showed activity against both Gram-positive and Gram-negative bacteria, while DSV-10-17 fractions B–E were active only against *S. aureus* (Table 5.5). The major difference between these two samples was the presence of small gastropods (limpets and snails) in the 2009 collection, which were removed from the 2010 collection prior to extraction. This suggests that the gastropods Gram-negative active metabloite or that folliculinid ciliates may produce different natural products in

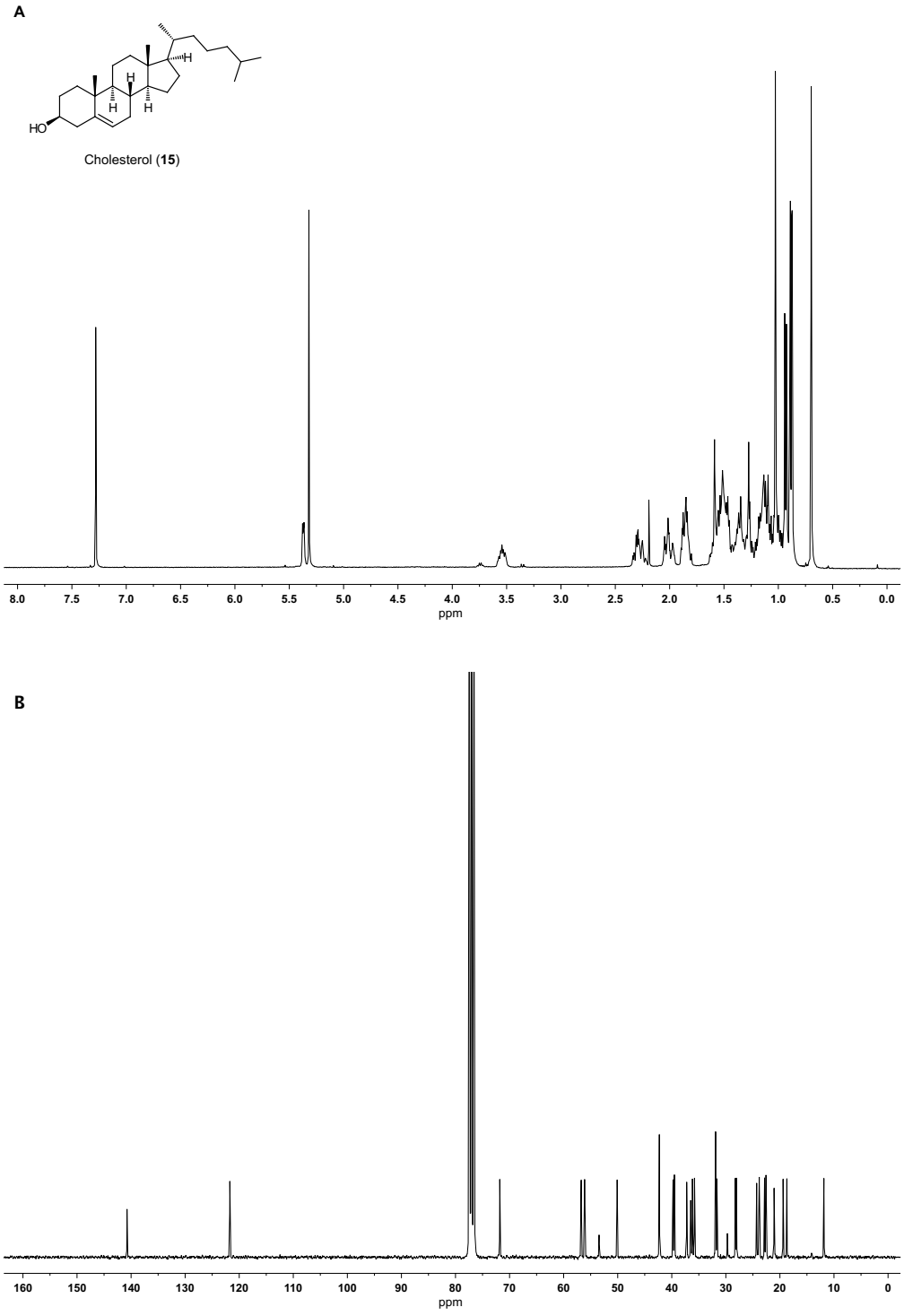

Figure 5.10. (A) ^{1}H (700 MHz) and (B) ^{13}C (175 MHz) NMR spectra for cholesterol (**15**) obtained from a white filamentous microbial mat (DSV-09-14E/F).

response to the gastropods and any associated microbial consortia. However, ^{1}H and ^{13}C NMR profiling of these lipophilic fractions (2009 and 2010) revealed the presence of a majority of sterols in these fractions. In order to avoid further isolation of cholesterol (**15**), the more polar fractions G and H, which did not show antimicrobial activity, were further fractionated and profiled by NMR and HPLC and individual peaks were collected and subjected to additional bioassays in conjunction with LC-MS/MS profiling to identify and de-replicate active components within each fraction. In particular, fractions F (80% EtOAc–hexanes) and G (100% EtOAc) of the 2009 extract lead to the isolation of several oxysterols in sub-milligram quantities. Notably, the ESIMS spectrum of the major component DSV-09-16F2/G2 (0.9 mg) showed major ions at *m*/z 439 $[M + Na]^+$ and *m*/*z* 855 $[2M + Na]^+$. Additional analysis by HRTOFMS suggested a molecular formula of $C_{27}H_{44}O_3$ (*m*/*z* 439.3183 $[M + Na]^+$) or $C_{54}H_{88}O_6$ (*m*/*z* 855.6473 $[2M + Na]^+$) for the 2M ion series. Analysis of the ^{13}C NMR spectrum (Figure 5.11 B) showed twice the number of carbon atoms (C_{54}) expected for the putative $[M + Na]^+$ molecular formula (C_{27}), suggesting that DSV-09-16F2/G2 may be a non-symmetrical dimer. The terpenoid nature of this sample was evident in the ^{1}H NMR spectrum (Figure 5.11 A), which showed 10 methyls (δ_H 0.60–1.17), four oxygenated methine protons (δ_H 3.18–4.46), and numerous overlapped aliphatic protons. Importantly, integration of the ^{1}H NMR spectrum showed that the sample comprised two sterol-like compounds present in a 2:3 ratio (Figure 5.11 A). Given the small amount of material available for structural elucidation, no further attempts to separate these compounds were made. Instead, analysis of the 2D NMR spectra (HSQC, HMBC, COSY) for DSV-09-16F2/G2 allowed the assignment of each component. Interestingly, a literature search of the individual structures show that **16** is melithasterol A isolated from a gorgonian coral *Melithaea ocracea* collected near the Okinawa Islands (Kobayashi & Kanda, 1991), and that **17** is a known sterol 5α,6α-epoxy-3*β*,7α-dihydroxycholest-8(14)-ene isolated from the sponge *Ircinia fasciculata* Pallas in the Indian Ocean (Venkateswarlu et al., 1996). Thus, the isolation of epoxy

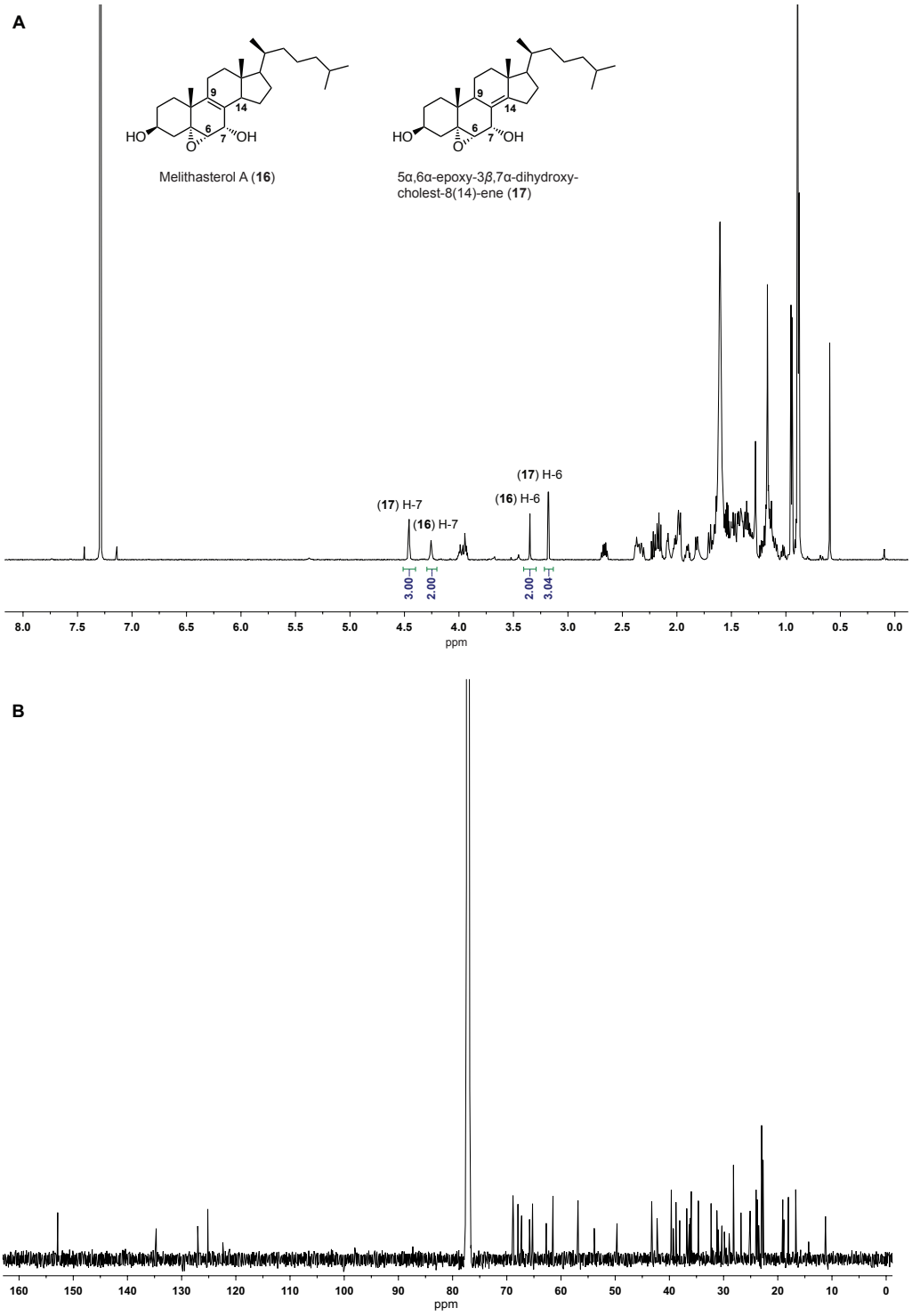

Figure 5.11. (A) ^{1}H (700 MHz) NMR spectrum of DSV-09-16F2/G2 with key integrals labeled to show a 2:3 ratio of **16** to **17**. (B) ^{13}C (175 MHz) NMR spectrum for **16**/**17**.

sterols from this heterogeneous microbial assemblage poses additional questions as to the biogenetic origin of these metabolites, which were also detected in the 2010 collection that did not contain gastropods.

Scanning electron microscopy images (Kouris et al., 2007) of the recently described deep-vent *Folliculinopsis* ciliate species reveal a close epibiotic association of densely packed short-rod and coccoid-shaped bacteria (~0.9 μm in length) present on the ciliate body (zooid) and peristomal lobes (arm-like extensions) protruding from the mouth of the lorica (tube). Folliculinids, like other ciliates, are known bacterivores that use their peristomal lobes to collect bacteria or other food sources from their surrounding environment, which are then "packaged" into vacuoles in the cytostome and transported to the cytoplasm for ingestion by phagocytosis. However, Kouris et al. (2007) also report an even distribution of vacuolated, intact bacteria among the *Folliculinopsis* sp. ciliate cortex, which is typically devoid of digestive enzymes. This, they suggest is evidence of an endosymbiotic relationship between the ciliate and intracellular bacteria. The bacteria were subsequently confirmed to be sulfide-oxidizing autotrophic symbionts that are likely the primary source of carbon for the ciliates (Kouris et al., 2010). Furthermore, the latter study found that a recurrent assemblage of invertebrates was associated with these sessile, colonial forming folliculinid ciliates. Notably, juvenile *Lepetodrilus fucensis* limpets were among the dominant macrofaunal species observed in these mats, which typically form at areas of diffuse flow, while adult *L. fucensis* limpets only occupied areas of intense vent flow that did not contain blue mats (Kouris et al., 2010). Thus, juvenile limpets may use the folliculinid mats as a safehaven from its predators and/or sequester secondary metabolites as a feeding deterrent, similar to the defense strategy of many shallow water marine gastropods (e.g. sea hares and nudibranchs) and tunicates (Fontana et al., 2012). Interestingly, Bergquist et al. (2007) identified 39 macrofaunal and 9 meiofaunal taxa associated with a single aggregation of the tubeworm *Ridgeia piscesae* that was collected from the Main Endeavor segment of the Juan de Fuca

Ridge. Of these, a *Clypeosectus curvus* snail (gastropod) was found to feed selectively on an unidentified blue pigmented ciliate also present in the tubeworm aggregation. Although *C. curvus* was not detected in any of the Axial Seamount blue mats, Kouris et al. (2010) do report the major presence of the snail *Depressigyra globulus*. Furthermore, stable isotope analysis, coupled with microscopic observations of "bluish pigmentation" in the tissues of this snail and *L. fucensis* limpets, suggested that these gastropods were feeding to some extent on the blue mats. These reports contrast starkly with our observations of *Folliculinopsis* sp. mats at the Marker N3 (Magic Carpet) vent site, where a clear boundary was typically observed between white filamentous bacteria inhabiting numerous species of macrofauna and substratum surfaces and the blue carpet-like mats of *Folliculinopsis* sp. (Figure 5.7 A and B). Importantly, limpets, snails and scale worms appeared to graze only on the white bacterial mats at these boundaries. Furthermore, the blue mats have occupied more than 70% of the substratum within an area of 10 to 20 m^2 at this site for more than 10 years (Kouris et al., 2007), suggesting minimal grazing occurs on this *Folliculinopsis* species. Based on these observations and putative defensive roles of pigments derived from marine invertebrates (Bandaranayake, 2006), the dark purple-teal fractions of DSV-09-16 and DSV-10-17 were pooled and investigated further.

Initial HPLC profiles of the pigment-containing peaks displayed broad, irregular peak shapes that were not readily reproducible. These properties coupled with preliminary LC-MS data suggested that the pigmented compounds were related to the pyrroloiminoquinone class of alkaloids. Importantly, the highly cytotoxic (L1210 mouse lymphocytic leukemia cells, ED_{50} < 100 ng/mL) pryrroloiminoquinone-related discorhabdin C (**18**) from a red-brown *Latrunculia* sponge collected in New Zealand (Perry et al., 1986) has been reported as a dark purple formate salt in pure form (Na et al., 2009). In addition, the marine ascidian *Clavelina* sp. collected from shallow water reefs off Wakaya Island in Fiji (Copp et al., 1991) produces a cytotoxic (HCT116 human colon carcinoma cells, IC_{50} = 0.5 μg/mL) dark blue (trifluoroacetate salt, TFA)

pyrroloiminoquinone derivative, wakayin (**19**). A common theme reported throughout the isolation of pyrroloiminoquinone-related alkaloids is their isolation as an acid salt derivative due to the positive charge maintained on the imine moiety in solution. This likely explains the broad chromatographic peaks that were observed without the use of an acid modifier in the HPLC mobile phase.

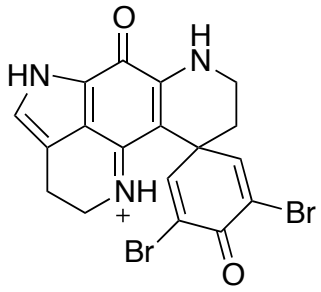

Discorhabdin C (**18**)

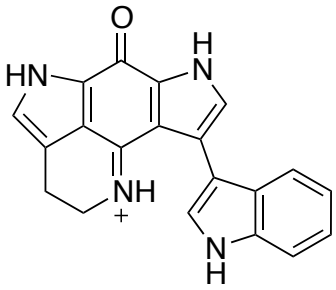

Wakayin (**19**)

Prior to using acid to aid in the isolation of these compounds, a small aliquot of the DSV-09/10 pigments was treated with 0.1N TFA to assess whether or not acid would affect the sample's integrity. Immediately following the dropwise addition of a catalytic amount of TFA, the solution transitioned from dark purple-teal, to dark brown-green and finally to a red-brown solution. Interestingly, the addition of base (1N NaOH) to the latter solution resulted in the transition back to the original color, followed by the precipitation of a dark green "fluffy" precipitate. Several pyrroloiminoquinone-related acid salts have been reported as dark brown-green (Na et al., 2009) or red-brown solids (E. W. Schmidt et al., 1995), suggesting that the observed pH-dependent color change in the *Folliculinopsis* extract corresponds to a free base (pH > 8, purple) or acid salt (pH < 6, red) of the major compound(s). Unfortunately, attempts to dissolve an appreciable amount of the "fluffy" precipitate were unsuccessful using numerous solvent combinations with and without acid or base, which prevented the acquisition of spectroscopic and biological data. It should be noted, that a relatively small percentage of the dark green precipitate was solvated

in dimethyl sulfoxide (DMSO) and was moderately cytotoxic to NCI-H460 human lung cancer cells (55% cell viability at ~30 μg/mL). However, given that the concentration of individual test solutions are based on their dry mass and assume 100% solubility in the test solvent, the true activity of this pigment is significantly underestimated in this assay.

A portion of the remaining colored fraction (0.48 g) was subjected to Sephadex LH-20 (280 mL; 9:1 MeOH–CH_2Cl_2) to yield two minimally separated bands: a dark purple band (fractions 50–54, 12.6 mg) and a teal-green band (fractions 55–60, 63.7 mg). The latter fraction was subsequently fractionated on Sephadex LH-20 (45 mL; 100% MeOH). However, the sample degraded to a tan-brown color midway through the elution process, and could not be eluted from the column, and thus was not recoverable from the column bed material. To avoid degradation of the purple pigment (50–54) on LH-20, these fractions were subsequently filtered over RP_{18} SPE cartridges and profiled by HPLC with and without the use of TFA (0.05%) in the mobile phase. Unfortunately, this sample also degraded, and attempts to recollect this organism from the July 2011 NeMO expedition at Marker N3 (Magic Carpet) were thwarted by the discovery that this site is now buried by nearly 4 m of new volcanic basalt from an underwater volcanic eruption that occurred at Axial Seamount in April 2011 (Chadwick et al., 2012).

Screening of Deep-Sea Vent Actinobacteria from Culture

From a total of 22 sediment and microbial mat samples (Table 5.4) collected from Axial Seamount during the NeMO 2010 expedition, 77 unique bacterial strains were identified based on their colony color and morphology. Of these, 64 strains gave positive results for partial 16S rRNA gene sequences (see Supporting Information, Table S-5.1) and, based on NCBI nucleotide BLAST analysis, 8 strains (12.5%) were identified as members of the *Actinomycetales* (Figure 5.12). These actinomycetes are

closely related to seawater-requiring actinomycetes of the genus *Dietzia* (strains RJ004, RJ043, RJ051, RJ053 and RJ056) and *Rhodococcus* (strains RJ040 and RJ054; Figure 5.12). The remaining strain, RJ076, was identified as *Microbacterium* sp. and clustered with several actinomycetes reported from deep-sea vents and thermal sediments. However, several of these strains are closely associated with the actinomycete *Propionibacterium acnes*, a bacterium normally associated with human skin. Thus, the previously reported clones likely represent contaminants from the handling of these samples. Remarkably, the relationship of these clones (Figure 5.12, clones LC1022b39, a2b011 and SC-NB05) with *P. acnes* was not addressed, and these strains continue to be reported as deep-vent associated actinomycetes in the major databases. Although RJ076 is not closely associated with this group, *Microbacterium* spp. are common clinical isolates (Gneiding et al., 2008). Given that this sample, a relatively large chimney spire, was handled quite extensively during its removal from the submersible collection platform, it is likely that this strain is also a skin-associated bacterium. Thus, the final number of deep-sea hydrothermal actinomycetes isolated from the 2010 sampling is seven, representing only two genera. Of these, two *Dietzia* strains (RJ053 and RJ056) share identical 16S rRNA sequences and were isolated from the same collection.

Prior to large-scale fermentation studies for natural products production, each of the unique strains (six total) were analyzed for genes representative of the biosynthetic enzymes of type I polyketide synthases (PKS-I) and non-ribosomal peptide synthetases (NRPS). Notably, a *Dietzia* sp. (RJ004), isolated from the bore of a chimney spire collected near the Escargot vent, and a *Rhodococcus* sp. (RJ054), isolated from a tubeworm-associated orange mat at Marker 113 (Figure 5.8), were both positive for putative NRPS genes, while the *Dietzia* sp. also contained putative PKS-I genes. These positive strains, along with those that were negative for NRPS and PKS-I genes, were cultivated using a variety of different culture conditions according the "OSMAC (One Strain MAny Compounds)" approach described by Zeeck and co-

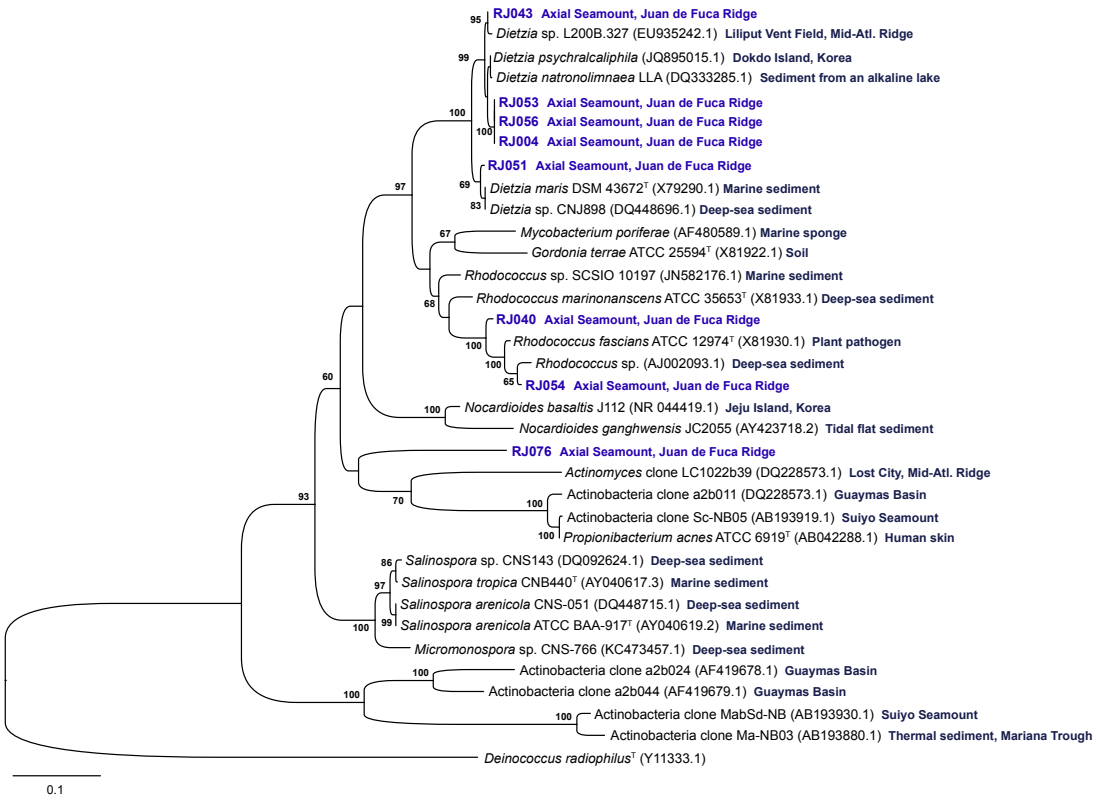

Figure 5.12. Phylogenetic tree showing the relationship between the cultured Axial Seamount actinomycetes and nearest type strains (^{T}) based on Maximum-likelihood (PhyML) analysis of SSU (16S) rRNA gene sequences. *Deinococcus radiophilus* (Deinococcus-Thermus phylum) is included as an outgroup. Labels on the terminal nodes indicate the taxa, strain, GenBank accession numbers in parenthesis, and collection sites for relevant strains. Bootstrap values (in percent) calculated from 1,000 resamplings using the maximum-likelihood method are shown at the nodes for values ≥ 60 %. The scale bar indicates 0.1 expected nucleotide substitutions per site.

workers (Bode et al., 2002). In this approach, minimal and random changes to the cultivation parameters such as media composition, aeration, light, temperature or shape and volume of the culture flask have resulted in the elicitation of secondary metabolites in a number of fungal and bacterial strains. Unfortunately, this process, as well as many traditional cultivation methods, has not resulted in the production of any bioactive natural products from our isolated *Dietzia* and *Rhodococcus* strains to date.

This is consistent with a lack of natural products reported for actinomycetes of these two genera, despite their isolation in a number of marine natural product studies.

To assess the microbial diversity of the tubeworm-associated orange mat that yielded the cultured *Rhodococcus* sp. (RJ054) actinomycete, we used a pyrosequencing strategy similar to that described in the seminal work of Sogin et al. (2006). We obtained 120,378 high-quality sequence reads (69.2% of all reads) spanning the V3 to V6 hypervariable region of 16S rRNA gene present in the genomic DNA pool of this sample. Of these, 84.7% were of the genus *Thioploca* (gammaproteobacteria) and 4.4% were members of the *Desulfonema* genus (deltaproteobacteria), while Actinomycetales comprised only 0.137% (165 reads) of the sequenced community. Furthermore, a majority of actinomycetes in this dataset belonged to the mineral-sulfide-oxidizing acidophiles of the Acidimicrobineae subclass (147 reads), with *Saxeibacter* sp. (7), *Planosporangium* sp. (5), *Kutzneria* sp. (2), *Actinospica* sp. (1), *Conexibacter* sp. (1) and unclassified PeM15 (1) comprising the remaining reads. Interestingly, 16S rRNA gene sequences for *Dietzia* and *Rhodococcus* members were not detected in this genomic DNA sample, suggesting an incomplete sampling of the community. This is possibly due to the complexity of the sample (e.g. tubeworms and other invertebrates, orange and white filamentous bacteria, sediment and seawater), which required the generation of several sub-samples for storage and further processing, where each sub-sample likely comprised a different subset of the community. Thus, to estimate the species richness for the tubeworm-associated orange mat, rarefaction curves were generated for the number of Operational Taxonomic Units (OTUs) present at a 3% divergent level in the genomic DNA sequence dataset (Figure 5.13). In general, greater than 97% identity between ribosomal RNA sequences defines membership in the same microbial species (Schloss & Handelsman, 2005). Although this distinction is not without controversy (Stackebrandt & Goebel, 1994), we chose a 3% divergent level because it allows our work to be compared to other deep-vent microbial diversity studies. The rarefaction

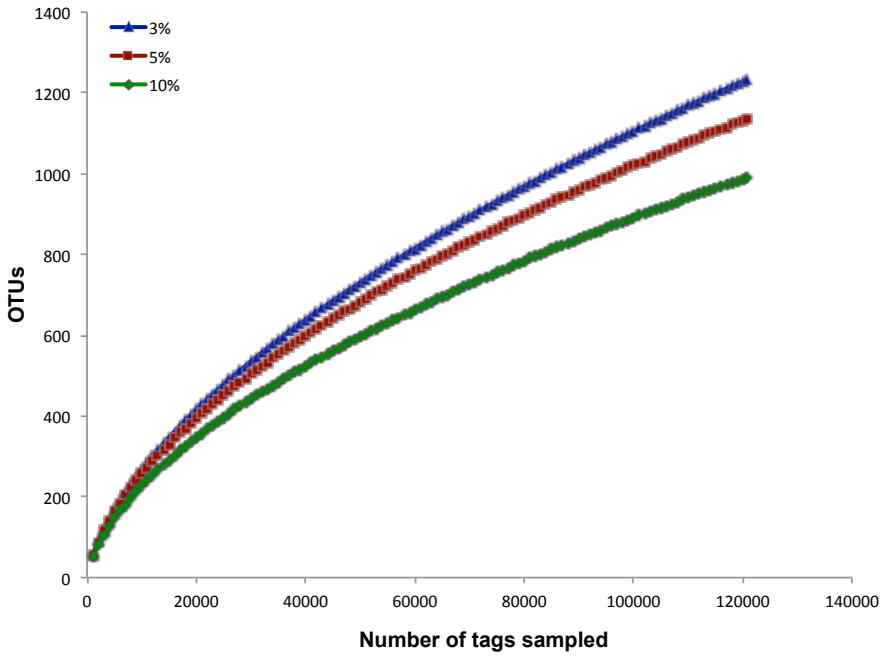

Figure 5.13. Rarefaction analysis for the number of OTUs present at 3%, 5% and 10% divergent levels within the ribosomal RNA dataset obtained from an orange microbial mat (J2-520 T07) collected from Axial Seamount at Marker 113.

curve generated for the 1233 OTUs defined by this method does not approach asymptotic shape at the 3% divergent level (Figure 5.13). Furthermore, similarity groups defined at relatively large genetic distances (5% and 10%) show a similar slope in the rarefaction analysis (Figure 5.13), indicating that additional sampling will likely lead to increased coverage of the community diversity within this sample.

Conclusion

No assessment of the potential for discovery of new chemical templates can be made based on the results obtained here and the sole reports to date of the loihichelins and ammonificins from deep-sea vent organisms. New, more advanced deep-sea research technology and molecular techniques similar to those already employed at Verenium (2013) and other research institutions are aimed at screening a more inclusive genetic assembly and may permit a molecular genomics approach to accelerate natural product discoveries from deep-sea vent environments. Thus, biodiscovery within these environments appears still to be in its infancy, as the full extent of the biological diversity present has yet to be realized. This may, in part, be due to the costs of sampling in the deep ocean (e.g., a 30 day expedition cruise costs roughly US $1 million with average daily operating costs of about US $30,000; Ruth 2006) versus terrestrial and shallow marine sampling costs. Notably, decreasing numbers of microorganisms with depth to almost undetectable levels are observed in deep ocean cold sediment cores (Parkes et al., 1994), which have been the major focus of most deep ocean natural products investigations. In contrast, 16S rRNA analysis of hydrothermally active sediments from the Guaymas Basin (Gulf of California) show high abundance and diversity of bacteria and archaea (Teske et al., 2002). However, Sogin and colleagues have shown that new molecular approaches aimed at defining the “rare biosphere,” which is typically masked by conventional molecular techniques, show an even greater diversity than previously estimated by 16S rRNA analysis (Huber et al., 2007; Sogin et al., 2006). This diversity is mirrored in our pyrosequencing efforts for only one sample. Furthermore, as the cost of pyrosequencing becomes more manageable, analyses such as these can be used to drive the selection of sampling sites and cultivation media that may afford higher yields of culturable microorganisms or the selective isolation of minor community members for natural products investigations. Thus, a more successful sampling

strategy, in terms of increasing the likelihood of collecting a larger biomass and potentially more diverse community, may be to target hydrothermal vent communities of the deep-sea. However, as with any potential natural products source, the logistics of collecting organisms, extracting metabolites from complex sample matrices, assessing bioactivities and culturing natural-product producing microorganisms must be addressed. Several of these logistics were addressed in this work, providing key methodologies that may accelerate natural product investigations from deep-sea hydrothermal vent organisms in our laboratory.

Experimental

General Experimental Procedures. NMR data was acquired in $CDCl_3$ and referenced to residual $CHCl_3$ chemical shifts (δ_C 77.2, δ_H 7.26) on a Bruker Avance III 700 MHz spectrometer equipped with a 5mm ^{13}C cryogenic probe. High-resolution mass spectrometry for each compound was performed in positive ion mode on an AB SCIEX Triple TOF 5600 mass spectrometer. LC-ESIMS data were obtained on an AB SCIEX 3200 Q TRAP mass spectrometer. HPLC was performed using a Shimadzu dual LC-20AD solvent delivery system with a Shimadzu SPD-M20A UV/VIS photodiode array detector.

Collection of Deep-Sea Vent Samples. Using the HOV Alvin and ROV Jason II, samples were collected during NeMO 2009 (HOV Alvin) and 2010 (ROV Jason II) expeditions from hydrothermal vent fields throughout the Axial Seamount caldera, located on the Juan de Fuca Ridge. Microbial mats and loose sediment were collected using the syringe samplers described in this study or with the pump-operated suction sampler on the submersible. Larger organisms, rocks and chimney spires were collected using the submersible manipulator arm and stowed in a closed biological box. Sediment cores (~20 to 30 cm) were obtained using a hollow coring device operated by the submersible.

DNA Extraction, PCR Gene Amplification, and 454 Pyrosequencing. For genetic screening (16S rRNA, NRPS and PKS-1) and pyrosequencing studies, genomic or community DNA was extracted using the Wizard Genomic DNA purification kit (Promega Inc., A1120), following the manufacturer's protocol. DNA concentration and purity was measured using a NanoDrop® spectrophotometer.

The 16S rRNA bacterial gene sequence of each cultured deep-vent bacterium was amplified from genomic DNA using the eubacterial primers 27F and 1492R (Lane, 1991). Sequences were amplified from approximately 50 ng of gDNA using GoTaq® Hot Start polymerase (0.5 μL, Promega) according to the manufacturer's

specifications. Polymerase chain reactions (PCR) were performed in an Eppendorf Mastercycler® gradient thermal cycler (Eppendorf, Hauppauge, NY, USA) as follows: initial denaturation at 96 °C for 4 min; 35 cycles of 96 °C for 1 min, 55 °C for 1 min, 72 °C for 1 min; and a final elongation at 72 °C for 10 min. PCR products were gel-purified, cleaned with the QIAquick® Gel Extraction kit (cat. no. 28704, Promega) and directly sequenced on an ABI 3730 capillary sequencer by the Oregon State University Center for Genome Research and Biocomputing (CGRB) DNA Sequencing Core Facility. The 16S rRNA partial gene sequences were inspected visually and assembled using CAP3 (X. Huang & Madan, 1999). The resulting contigs were analyzed for chimeric sequences using Pintail (Ashelford et al., 2005) and compared to sequences in the Ribosomal Database Project database (http://rdp.cme.msu.edu) and GenBank (http://www.ncbi.nlm.nih.gov).

Degenerate primers targeting adenylation domain sequences (NRPS): A3F (5′-GCSTACSYSATSTACACSTCSGG-3′), A7R (5′-SASGTCVCCSGTSCGGTAS-3′) and ketosynthase to methyl-malonyl-CoA trasferase domains (PKS-I): K1F (5′-TSAAGTCSAACATCGGBCA-3′), M6R (5′-CGCAGGTTSCSGTACCAGTA-3′) were used to interrogate the genomic DNA from each cultured actinomycete (Ayuso-Sacido & Genilloud, 2005). Sequences were amplified from approximately 50 ng of gDNA using GoTaq® Hot Start polymerase (0.5 μL, Promega) according to manufacturer's specifications. PCR was performed as follows: initial denaturation at 95 °C for 5 min; 35 cycles of 95 °C for 30 s, 55 °C (K1F/M6R) or 59 °C (A3F/A7R) for 2 min, 72 °C for 4 min; and a final elongation at 72 °C for 10 min. PCR products were purified and sequenced as described for 16S rRNA.

For 454 pyrosequencing of community DNA, primers flanking the V3 to V6 hypervariable region of bacterial 16S rRNAs (*Escherichia coli* positions 341-1046) were designed to include the Roche 454 A or B sequencing adaptor (shown in lowercase) fused to the 5′ end of primer A-341F (5′-gcctccctcgcgccatcag-CCTACGGGAGGCAGCAG-3′; Sogin et al., 2006) and B-1046R (5′-

gccttgccagcccgctcag-CGACAGCCATGCANCACCT; Yu & Morrison, 2004). PCR amplicon libraries were generated from genomic DNA (3-10 ng) using GoTaq Hot Start polymerase (0.5 μL, Promega), 5X Reaction Buffer (10 μL), 10 mM dNTPs (1 μL), 25 mM $MgCl_2$ (3 μL), and a 0.4 μM concentration of each primer in a reaction volume of 50 μL. Polymerase chain reactions (PCR) were performed in an Eppendorf Mastercycler gradient thermal cycler (Eppendorf, Hauppauge, NY, USA) as follows: initial denaturation at 96 °C for 2.5 min; 25 cycles of 96 °C for 30 s, 64 °C for 50 s, 72 °C for 1 min; and a final elongation at 72 °C for 10 min. PCR reaction products were gel purified and cleaned using the QIAEX II gel extraction kit (Qiagen, Valencia, CA), following the manufacturer's protocol. The quality of the PCR product was assessed on a Bioanalyzer 2100 (Agilent, Palo Alto, CA) prior to 454 sequencing. Emulsion PCR and 454 sequencing (Roche 454 GS Junior) were performed by the Oregon State University Center for Genome Research and Biocomputing DNA Sequencing Core Facility. 454 tag sequences were trimmed to remove primers and low-quality data, and analyzed using the mothur software package (Schloss et al., 2009).

Phylogenetic Analysis. The 16S rRNA gene sequences from Axial Seamount cultured isolates were compared to sequences within the NCBI GenBank database (http://www.ncbi.nlm.nih.gov), and the nearest type strains were imported into Geneious 5.6 (Drummond et al., 2010), screened for chimeric sequences using the computer program Mallard (Ashelford et al., 2006) and aligned using the ClustalW feature in Geneious. The resulting alignment was edited to exclude gaps and missing data, except for partial 16S rRNA sequences. The evolutionary relationship of the Axial Seamount Actinobacteria was compared with other strains of Actinobacteria using the phylogenetic maximum likelihood (PhyML v3.0; Guindon & Gascuel, 2003) algorithm in Geneious, performed with 500 bootstrap replicates using the GTR model with the number of rate categories set to 4.

Extraction and Isolation Procedures. Field-collected samples of deep-sea vent invertebrates and microbial mats were stored at -80 °C until their processing. Samples

were lyophilized before sequential, exhaustive extractions in 50% aqueous methanol (MeOH) and 50% MeOH in dichloromethane (CH_2Cl_2) to produce aqueous and organic extracts, respectively. All organic extracts were subjected to bioassay-guided fractionation via NP-VLC using a stepped solvent gradient of hexanes to EtOAc to MeOH to produce nine fractions (A, B, C, D, E, F, G, H and I). All biologically active fractions were subjected to additional bioassay-guided fractionation via RP_{18} SPE using a stepped solvent gradient of MeOH–H_2O from 50% MeOH–H_2O to 100% MeOH, followed by 100% CH_2Cl_2. For DSV-09-14, the RP_{18} SPE fractions eluting in 100% MeOH from the active VLC parent fractions (E = 60% EtOAc–hexanes and F = 80% EtOAc–hexanes) were subjected to RP-HPLC using a linear gradient of 90% to 100% MeOH over 30 min, followed by 100% MeOH for 10 min (column: Synergi Fusion-RP, 10 x 250 mm, 3.0 mL/min) to yield cholesterol (6.7 mg, t_R = 31.1 min). For DSV-09-16, fraction F (80% EtOAc–hexanes) was selectively active against *E. coli* (36% cell viability at 256 μg/mL) and, given a limited sample mass (4.2 mg), filtered over a RP_{18} SPE cartridge in 100% MeOH before proceeding directly to RP-HPLC. Isocratic RP-HPLC (column: Synergi Fusion-RP, 10 x 250 mm, 92% MeOH–H_2O, 3.0 mL/min) of the SPE-filtered fraction yielded a single major chromatographic peak that was collected (0.2 mg, t_R = 14.0 min) and pooled with a corresponding peak from fraction G (0.7 mg, t_R = 14.0 min) using the same HPLC conditions. This pooled sample (0.9 mg) comprised a 2:3 mix of melithasterol A and 5α,6α-epoxy-3β,7α-dihydroxycholest-8(14)-ene as determined by NMR spectroscopic methods. Subsequent LC-MS profiling (Synergi Fusion-RP, 2 x 100 mm, 0.2 mL/min, linear gradient of 60 to 100% MeOH in 0.1% [v/v] aqueous TFA) of fraction G from DSV-10-17 yielded *m/z* 439.3 and 855.6 (**16** and **17**, $[M + Na]^+$ and $[2M + Na]^+$, respectively) at the same retention times as **16** and **17** purified from the DSV-09-16 collection.

Following collection, deep-vent sediment and microbial mat samples were dried overnight under ambient conditions in a sterile petri dish. A polyester fiber-tipped

sterile swab was pressed into the dried sample once and then onto the agar surface in a radial, clockwise pattern from the outermost edge to the center of the culture plate approximately 25 to 30 times, creating a serial-dilution effect. Cultures of deep-vent actinomycetes were grown using a variety of different growth conditions including different mediums (see Supporting Information, Table S-5.2), various culture flask sizes and shapes, different temperatures, with or without shaking and/or light. Cultures were also harvested at different time points, at which time an absorbent resin (either Amberlite XAD-16 or HP-20, 20 mg/mL) was added to each flask and agitated gently for 2h. The resin was recovered and washed with deionized water and eluted exhaustively with either acetone or MeOH. Alternatively, cultures were harvested via centrifugation at 12,000 rpm (0 °C) in 250 mL centrifuge bottles. The supernatant was extracted with EtOAc and the bacterial pellet was resuspended in 100% MeOH and heated to 40 °C for 2 h to lyse the cells, before evaporation to dryness. The dried extract, containing the lysed cells, was resuspended in 100% CH_2Cl_2 and partitioned with deionized water to remove cellular debris (generally located at the CH_2Cl_2/H_2O solvent interface). Organic extracts from the cultured material were subjected to bioassay-guided fractionation as described previously. For small scale cultures, where minimal quantities were afforded, extracts were filtered over RP_{18} SPE cartridges and analyzed directly by LC-MS and RP-HPLC, with peak libraries generated in 96-well plates for biological testing.

Cholesterol (15): white, amorphous solid; ^{1}H and ^{13}C NMR data, see Figure 5.10 and Spectral Database for Organic Compounds, Number 887 (SDBSWeb, 2013); LREIMS *m/z* 386.3 $[M]^+$.

Melithasterol A (16): white, amorphous solid; ^{1}H and ^{13}C NMR data, see Figure 5.11 and Kobayashi & Kanda (1991); HRTOFMS *m/z* 439.3183 $[M + Na]^+$ (calcd for $C_{27}H_{44}O_3Na$, 439.3188), m/*z* 855.6473 $[2M + Na]^+$ (calcd for $C_{54}H_{88}O_6Na$, 855.6479).

5*α*,6*α*-epoxy-3*β*,7*α*-dihydroxycholest-8(14)-ene (17): white, amorphous solid; ^{1}H and ^{13}C NMR data, see Figure 5.11 and Venkateswarlu et al. (1996). HRTOFMS

m/*z* 439.3183 $[M + Na]^+$ (calcd for $C_{27}H_{44}O_3Na$, 439.3188), m/*z* 855.6473 $[2M + Na]^+$ (calcd for $C_{54}H_{88}O_6Na$, 855.6479).

Antibacterial Assay. Antibacterial activity was determined using a microtiter dilution method (96-well plate) based on several methods: Casey et al. (2004), Smith et al. (2008) and the Clinical Laboratory Standards Institute's methods for dilution susceptibility testing (2009). Crude extracts were tested at 500, 250, 125, and 62.5 μg/mL against *Escherichia coli* and *Staphylococcus aureus*. Bacterial strains were cultured as follows: *S. aureus* in tryptic soy broth (Becton, Dickinson and Co.) and *E. coli*. in Luria-Bertani liquid medium (Becton, Dickinson and Co.). On the day of the assay, the test organisms were grown in 5 mL aliquots of their respective medium with shaking (200 rpm) at 37 °C until the broth reached an optical density (OD_{600}) of 0.1 (usually 4 to 6 hours). A stock suspension (1:800) of each strain was generated in sterile media from the respective 0.1 absorbance culture for approximately 5×10^5 cells/mL, determined by direct microscopic count using a Petroff-Hausser (Hausser Scientific) counting chamber. For all experiments, 200 μL of this stock suspension was added to 96-well tissue culture-treated microtiter plates (Greiner Bio-One) containing lyophilized test compounds, and incubated without shaking at 37 °C for 16 h. Optical densities (600 nm) were measured on a SpectraMax190 (Molecular Devices) plate reader before and after incubation to calculate the final OD_{600} values ($OD_{Final} = T_{16} - T_0$). Each microtiter plate also contained a serially diluted positive control (ampicillin or kanamycin at final concentrations ranging from 0 to 256 μg/mL), negative controls (vehicle-treated cells and untreated cells), and a contamination control (medium only). Percentage growth inhibition was determined relative to the vehicle control OD_{600} values, with the viability of vehicle-treated control cells defined as 100% in all experiments.

Biofilm assay. The inhibition of *Mycobacterium avium* A5 biofilm formation was performed by Sasha Rose and Luiz Bermudez at Oregon State University as previously described (Carter et al., 2003).

Cell Viability Assays. Cytotoxicity of the organic extract and crude fractions of DSV-09-16 and DSV-10-17 was evaluated in human NCI-H460 lung cancer cells (ATCC, Manassas, VA) as previously described (Thornburg et al., 2011), with minor modifications. Cells were seeded into 96-well plates (5,000 cells per well) in 50 μL of medium 16 h before treatment. Approximately 2 h before treatment, test samples were generated from a stock solution (6 mg/mL, 100% DMSO) that was serially diluted in serum-free medium. Following aspiration of seed growth medium, test samples (50 μL) were added to seeded cells at final concentrations ranging from 0.01 nM to 10.0 μM. Each 96-well plate also contained untreated and vehicle-treated control cells. Cell viability was determined after 48 h treatment using a standard 3-(4,5-dimethylthiazol-2-yl)-2,5,diphenyly tetrazolium bromide (MTT) assay as previously described (Thornburg et al., 2011). The cytotoxicity of each purified compound was assessed in at least three independent cultures with the viability of vehicle-treated control cells defined as 100% in all experiments. Dose response curves were plotted using GraphPad Prism® (v5.0) and IC_{50} values were derived from nonlinear regression analysis.

Acknowledgement

We gratefully acknowledge the crew of the *R/V Thompson* and *R/V Atlantis*, and the ROV Jason and Alvin crews for their support and assistance with collecting samples. We thank Jeff Morré of the Environmental Health Sciences Center at OSU for MS data acquisition (NIEHS P30 ES00210). The National Science Foundation (CHE-0722319) and the Murdock Charitable Trust (2005265) are acknowledged for their support of the OSU Natural Products and Small Molecule Nuclear Magnetic Resonance. This work is supported by NIH/NIAID R21 AI085540-01, Oregon Sea Grant under award number NA10OAR4170059 (project number R/BT-48) and NOAA Ocean and Human Health Initiative.

Supporting Information

Table S-5.1. Information on the deep-sea hydrothermal vent bacterial isolates including collection site, depth, isolation medium, colony morphology and nearest strain ID determined by BLAST analysis of representative 16S rRNA gene sequences.

Isolate ID	Collection ID	Location/Vent	Depth (m)	[a]Media	[b]Morphology Color/Form/Surface/Elevation/Margin					Genetic ID
RJ001	J2-523-Chimney-15	Escargot	1519.6	A1, A4	P	C	S	R	E	*Halomonas* sp. (γ-Proteobacteria)
RJ002	J2-523-Chimney-15	Escargot	1519.6	A1, A4	O	C	S, G	R	E	*Erythrobacter* sp. (α-Proteobacteria)
RJ003	J2-523-Chimney-15	Escargot	1519.6	A1, A4	O	C	S	R	E	*Halomonas* sp. (γ-Proteobacteria)
RJ004	J2-523-Chimney-15	Escargot	1519.6	A1, A4	O, P	C	S	R	E	*Dietzia* sp. (Actinobacteria)
RJ005	J2-521-MAT-17 (Wet)	Gollum	1541.2	A1–4	O	C	S	R	E	*Erythrobacter* sp. (α-Proteobacteria)
RJ006	J2-521-MAT-17 (Wet)	Gollum	1541.2	A1–4	Y, O	C	S	R	E	*Sufflavibacter* sp. (Bacteroidetes)
RJ007	J2-521-MAT-17 (Wet)	Gollum	1541.2	A1–4	Y	C	S, G	R	E	*Sufflavibacter* sp. (Bacteroidetes)
RJ008	J2-521-MAT-17 (Wet)	Gollum	1541.2	A1–4	O, T	C	S	R	E	*Sphingomonas* sp. (α-Proteobacteria)
RJ009	J2-525-MAT-21	Magic Carpet	1524	A1–4	W	C	S	F	E	*Halomonas* sp. (γ-Proteobacteria)
RJ010	J2-522-03	Marker 33	1520	A1–4	W	C	S, G	R	E	*Pseudoalteromonas* sp. (γ-Proteobacteria)
RJ011	J2-522-03	Marker 33	1520	A1–4	W	F	R	F	F	*Penicillium* sp. (Fungi)
RJ012	J2-523-MAT-10	9 Meter	1518.5	A1–4	W	C	S	R	U	*Pseudoalteromonas* sp. (γ-Proteobacteria)
RJ013	J2-523-MAT-10	9 Meter	1518.5	A1–4	W	C	S	R	E	*Halomonas* sp. (γ-Proteobacteria)
RJ014	J2-523-MAT-10	9 Meter	1518.5	A1–4	W	C	S, G	R	E	*Halomonas* sp. (γ-Proteobacteria)
RJ015	J2-523-MAT-10	9 Meter	1518.5	A3, A4	Y	I	S	R	C	*Pseudomonas* sp. (γ-Proteobacteria)
RJ018	J2-522-02	Marker 33	1520	A1–4	P	C	S	R	E	*Shewanella* sp. (γ-Proteobacteria)
RJ019	J2-522-02	Marker 33	1520	A1–4	O, T	I	R	F	C	*Pseudomonas* sp. (γ-Proteobacteria)
RJ020	J2-522-02	Marker 33	1520	A1–4	O	C	S	R	E	*Chromohalobacter* sp. (γ-Proteobacteria)
RJ021	J2-522-02	Marker 33	1520	A1–4	W	C	S	R	E	*Chromohalobacter* sp. (γ-Proteobacteria)
RJ022	J2-520-T07-SED	Marker 113	1522.9	A1–4	Cr	C	S	R	E	*Halomonas* sp. (γ-Proteobacteria)
RJ023	J2-520-T07-SED	Marker 113	1522.9	A1–4	Cl	C, P	S	R	E	*Alcanivorax* sp. (γ-Proteobacteria)
RJ024	J2-520-T07-MAT	Marker 113	1522.9	A1–4	P	C, P	S	R	E	*Rhodobacterales* sp. (α-Proteobacteria)
RJ025	J2-520-T07-MAT	Marker 113	1522.9	A1–4	Cr	C	S	R	E	*Cobetia* sp. (γ-Proteobacteria)
RJ026	J2-520-T07-MAT	Marker 113	1522.9	A1–4	Y	C, P	S	R	E	*Erythrobacter* sp. (α-Proteobacteria)
RJ027	J2-520-T07-MAT	Marker 113	1522.9	A1–4	P	C	S	R	E	*Rhodobacterales* sp. (α-Proteobacteria)
RJ028	J2-521-SED-03 (2cm)	Ashes Rim	1415	A1, A4	Y	C, P	S	R	E	*Paenibacillus* sp. (Firmicutes)
RJ029	J2-520-T07-MAT	Marker 113	1522.9	A4	Y, T	C	S	R	E	*Salegentibacter* sp. (Bacteroidetes)

Table S-5.1 (continued). Information on the deep-sea hydrothermal vent bacterial isolates including collection site, depth, isolation medium, colony morphology and nearest strain ID determined by BLAST analysis of representative 16S rRNA gene sequences.

Isolate ID	Collection ID	Location/Vent	Depth (m)	[a]Media	[b]Morphology Color/Form/Surface/Elevation/Margin					Genetic ID
RJ030	J2-520-T07-MAT	Marker 113	1522.9	A3, A4	O	C, P	S	R	E	*Erythrobacter* sp. (α-Proteobacteria)
RJ031	J2-520-T07-MAT	Marker 113	1522.9	A3, A4	O, T	C	S	R	E	*Pseudoalteromonas* sp. (γ-Proteobacteria)
RJ032	J2-520-T07-MAT	Marker 113	1522.9	A1–4	W	C	S	R	E	*Pseudoalteromonas* sp. (γ-Proteobacteria)
RJ033	J2-521-SED-03 (1cm)	Ashes Rim	1415	A4	O	C	S	R	E	*Erythrobacter* sp. (α-Proteobacteria)
RJ034	J2-521-SED-03 (1cm)	Ashes Rim	1415	A1–4	Cr	C	S	R	E	*Cobetia* sp. (γ-Proteobacteria)
RJ035	J2-521-SED-03 (1cm)	Ashes Rim	1415	A1–4	Cr	C	S	R	E	*Cobetia* sp. (γ-Proteobacteria)
RJ036	J2-521-SED-01	Ashes Rim	1415	A4	O, T	C	S	R	E	*Erythrobacter* sp. (α-Proteobacteria)
RJ037	J2-521-SED-01	Ashes Rim	1415	A1–4	Pc, T	C	S	R	E	*Halomonas* sp. (γ-Proteobacteria)
RJ038	J2-521-MAT-17 (Wet)	Gollum	1541.2	A2, A4	Y, O	C	S	R	E	*Erythrobacter* sp. (α-Proteobacteria)
RJ039	J2-521-MAT-17 (Wet)	Gollum	1541.2	A1, A3	Cl	C	S	R	E	*Neptuniibacter* sp. (γ-Proteobacteria)
RJ040	J2-521-MAT-17 (Wet)	Gollum	1541.2	A2, A4	Y	C	S, M	R	E	*Rhodococcus* sp. (Actinobacteria)
RJ041	J2-521-MAT-17 (Dry)	Gollum	1541.2	A2, A4	O, T	C	S	R	E	*Erythrobacter* sp. (α-Proteobacteria)
RJ042	J2-521-MAT-17 (Dry)	Gollum	1541.2	A1–4	Cr, T	C	S	F	E	*Alteromonas* sp. (γ-Proteobacteria)
RJ043	J2-521-MAT-17 (Dry)	Gollum	1541.2	A4	P	C, P	S	R	E	*Dietzia* sp. (Actinobacteria)
RJ044	J2-521-MAT-17 (Dry)	Gollum	1541.2	A3, A4	Cr, T	C	S	F	E	*Pseudoalteromonas* sp. (γ-Proteobacteria)
RJ045	J2-523-Chimney-15	Escargot	1519.6	A4	P	C, P	S	R	E	*Paenibacillus* sp. (Firmicutes)
RJ046	J2-523-Chimney-15	Escargot	1519.6	A1, A4	Y	C	S	R	E	*Paenibacillus* sp. (Firmicutes)
RJ048	J525-Rock-05	Spanish Steps	1520	A3	Y, W	I	S	R	C	*Pseudomonas* sp. (γ-Proteobacteria)
RJ049	J2-521-MAT-37(Wet)	Mushroom	1542	A1, A2, A4	Cr, T	C, P	S	R	E	*Sphingomonas* sp. (α-Proteobacteria)
RJ050	J2-521-MAT-37(Wet)	Mushroom	1542	A1, A2, A4	Y	C, P	S	R	E	*Sphingobium* sp. (α-Proteobacteria)
RJ051	J2-521-SED-03 (1cm)	Ashes Rim	1415	A4	O	C, P	S	R	E	*Dietzia* sp. (Actinobacteria)
RJ052	J2-520-T07-MAT	Marker 113	1522.9	A3, A4	Cr	C	S, G	R	E	*Halomonas* sp. (γ-Proteobacteria)
RJ053	J2-520-T07-SED	Marker 113	1522.9	A2, A4	O, P	C	S	R	E	*Dietzia* sp. (Actinobacteria)
RJ054	J2-520-T07-SED	Marker 113	1522.9	A2, A4	Y	C	S	R	E	*Rhodococcus* sp. (Actinobacteria)
RJ056	J2-520-T07-SED	Marker 113	1522.9	A2, A4	O	C	S	R	E	*Dietzia* sp. (Actinobacteria)
RJ057	J2-520-T07-SED	Marker 113	1522.9	A1–4	W	C	S	R	E	*Oceanibulbus* sp. (α-Proteobacteria)
RJ058	J2-520-T07-MAT	Marker 113	1522.9	A3, A4	W	C	S	R	E	*Oceanibulbus* sp. (α-Proteobacteria)

Table S-5.1 (continued). Information on the deep-sea hydrothermal vent bacterial isolates including collection site, depth, isolation medium, colony morphology and nearest strain ID determined by BLAST analysis of representative 16S rRNA gene sequences.

Isolate ID	Collection ID	Location/Vent	Depth (m)	[a]Media	[b]Morphology Color/Form/Surface/Elevation/Margin					Genetic ID
RJ061	J2-521-SED-03 (2cm)	Ashes Rim	1415	A1, A4	W	C	S	R	E	*Paenibacillus* sp. (Firmicutes)
RJ063	J2-523-MAT-05	Marker 151	1521.8	A1, A4	Pc, T	C	S	R	E	*Pseudoalteromonas* sp. (γ-Proteobacteria)
RJ064	J2-523-MAT-05	Marker 151	1521.8	A1, A3	W	C	S	R	E	*Psychrobacter* sp. (γ-Proteobacteria)
RJ065	J2-525-SED-01	East Caldera	1518.5	A1, A4	Pr, T	I	R	R	E	*Alteromonas* sp. (γ-Proteobacteria)
RJ069	J2-520-MAT-19	Marker 36	1531	A1, A4	O, W	C	S	R	E	*Pseudoalteromonas* sp. (γ-Proteobacteria)
RJ073	J2-525-SED-01	East Caldera	1518.5	A1, A4	Y	C	S	R	E	*Erythrobacter* sp. (α-Proteobacteria)
RJ076	J2-523-Chimney-15	Escargot	1519.6	A1, A4	Y	C	S	R	E	*Microbacterium* sp. (Actinobacteria
RJ077	J2-523-Chimney-15	Escargot	1519.6	A1, A4	O	C, P	S	R	E	*Erythrobacter* sp. (α-Proteobacteria)

[a]See Table A-5.2 for media components.
[b]Color: Cl (clear), Cr (cream), P (pink), Pc (peach), Pr (purple), O (orange), Y (yellow), T (translucent); Form: C (circular), I (irregular), F (filamentous), P (punctiform); Surface: S (smooth), R (rough), G (glossy); Elevation: F (flat), R (raised); Margin: C (curled), E (entire), F (filiform/ filamentous), U (undulate).

Table S-5.2. List of isolation and growth mediums used to culture deep-sea hydrothermal vent microorganisms.

Media	Constituents
A1 (HV)	18 g agar, 100 mg humic acid sodium salt in 0.2 N NaCl, 1 liter natural seawater and cyclohexamide (100 μg/mL)
A2 (SMP)	8 g noble agar, 0.5 g mannitol, 0.1 g peptone, 800 mL natural seawater and 200 mL DI water, cyclohexamide (100 μg/mL) and rifampicin (5 μg/mL)
A3 (SNC)	18 g agar, 800 mL natural seawater and 200 mL DI water, cyclohexamide (100 μg/mL) and novobiocin (25 μg/mL)
A4 (SPC)	18 g agar, 800 mL natural seawater and 200 mL DI water, cyclohexamide (100 µg/mL) and polymixin B sulfate (5 µg/mL)
CAM	5 g glucose, 5 g NaCl, 3 g $NaNO_3$, 2 g sodium acetate, 1 g sodium propionate, 1 g casamino acids, 1 mL trace metals, 950 mL DI water and 50 mL DI water containing 50 mg K_2HPO_4
STM	10 g starch, 4 g peptone, 4 g yeast extract, 1g $CaCO_3$, 100 mg KBr, 40 mg $Fe_2(SO_4)_3$ and 1 liter Instant Ocean (30 g/L)
SWYE	23.4 g NaCl, 10 g peptone, 6.9 g $MgSO_4 \cdot 7H_2O$, 3g yeast extract, 0.75g KCl and 1 liter DI water
TCG	5 g caseine digest, 4 g glucose, 3 g tryptone and 1 liter Instant Ocean (30 g/L)
Trace Metals	520 mg Na_2EDTA, 178 mg $FeSO_4 \cdot 7H_2O$, 23.2 mg $Co(NO_3)_2 \cdot 6H_2O$, 14.8 mg $ZnSO_4 \cdot 7H_2O$, 10 mg $MnCl_2$, 6.2 mg H_3BO_3, 3.6 mg $NaMoO_4 \cdot 2H_2O$, 2.7 mg $NiSO_4 \cdot 6H_2O$, 1.7 mg $CuCl_2 \cdot 2H_2O$ and 100 mL DI water

References

Alain, K., Olagnon, M., Desbruyeres, D., Page, A., Barbier, G., Juniper, S. K., Querellou, J., & Cambon-Bonavita, M.-A. (2002). Phylogenetic characterization of the bacterial assemblage associated with mucous secretions of the hydrothermal vent polychaete *Paralvinella palmiformis*. *FEMS Microbiol. Ecol., 42*(3), 463-476.

Alain, K., Zbinden, M., Le Bris, N., Lesongeur, F., Querellou, J., Gaill, F., & Cambon-Bonavita, M.-A. (2004). Early steps in microbial colonization processes at deep-sea hydrothermal vents. *Environ. Microbiol., 6*(3), 227-241.

Amann, R., Ludwig, W., & Schleifer, K. (1995). Phylogenetic identification and *in situ* detection of individual microbial cells without cultivation. *Microbiol. Rev., 59*, 143-169.

Andrianasolo, E. H., Haramaty, L., McPhail, K. L., White, E., Vetriani, C., Falkowski, P., & Lutz, R. (2011). Bathymodiolamides A and B, Ceramide Derivatives from a Deep-Sea Hydrothermal Vent Invertebrate Mussel, *Bathymodiolus thermophilus*. *J. Nat. Prod., 74*(4), 842-846.

Andrianasolo, E. H., Haramaty, L., Rosario-Passapera, R., Bidle, K., White, E., Vetriani, C., Falkowski, P., & Lutz, R. (2009). Ammonificins A and B, Hydroxyethylamine Chroman Derivatives from a Cultured Marine Hydrothermal Vent Bacterium, *Thermovibrio ammonificans*. *J. Nat. Prod., 72*(6), 1216-1219.

Andrianasolo, E. H., Haramaty, L., Rosario-Passapera, R., Vetriani, C., Falkowski, P., White, E., & Lutz, R. (2012). Ammonificins C and D, hydroxyethylamine chromene derivatives from a cultured marine hydrothermal vent bacterium, *Thermovibrio ammonificans*. *Mar. Drugs, 10*(10), 2300-2311.

Ashelford, K. E., Chuzhanova, N. A., Fry, J. C., Jones, A. J., & Weightman, A. J. (2005). At Least 1 in 20 16S rRNA Sequence Records Currently Held in Public Repositories Is Estimated To Contain Substantial Anomalies. *Appl. Environ. Microbiol., 71*(12), 7724-7736.

Ashelford, K. E., Chuzhanova, N. A., Fry, J. C., Jones, A. J., & Weightman, A. J. (2006). New Screening Software Shows that Most Recent Large 16S rRNA Gene Clone Libraries Contain Chimeras. *Appl. Environ. Microbiol., 72*(9), 5734-5741.

ATCC. (2013). Home Page for the American Type Culture Collection: ATCC. Retrieved February 27, 2013, from http://www.atcc.org

Atkins, M. S., Anderson, O. R., & Wirsen, C. O. (1998). Effect of hydrostatic pressure on the growth rates and encystment of flagellated protozoa isolated from a deep-sea hydrothermal vent and a deep shelf region. *Mar. Ecol. Prog. Ser., 171*, 85-95.

Ayuso-Sacido, A., & Genilloud, O. (2005). New PCR primers for the screening of NRPS and PKS-I systems in actinomycetes: detection and distribution of these biosynthetic gene sequences in major taxonomic groups. *Microb. Ecol., 49*(1), 10-24.

Baker, E. T., Fox, C. G., & Cowen, J. P. (1999). In situ observations of the onset of hydrothermal discharge during the 1998 Submarine Eruption of Axial Volcano, Juan de Fuca Ridge. *Geophys. Res. Lett., 26*(23), 3445-3448.

Bandaranayake, W. M. (2006). The nature and role of pigments of marine invertebrates. *Nat. Prod. Rep., 23*(2), 223-255.

Baross, J. A., & Deming, J. W. (1995). Growth at High Temperatures: Isolation and Taxonomy, Physiology, and Ecology. In D. M. Karl (Ed.), *The Microbiology of Deep-Sea Hydrothermal Vents* (pp. 169-217). Boca Raton: CRC Press.

Bérdy, J. (2005). Bioactive Microbial Metabolites. *J. Antibiot., 58*(1), 1-26.

Bergquist, D. C., Eckner, J. T., Urcuyo, I. A., Cordes, E. E., Hourdez, S., Macko, S. A., & Fisher, C. R. (2007). Using stable isotopes and quantitative community characteristics to determine a local hydrothermal vent food web. *Marine Ecology Progress Series, 330*, 49-65.

Bode, H. B., Bethe, B., Höfs, R., & Zeeck, A. (2002). Big Effects from Small Changes: Possible Ways to Explore Nature's Chemical Diversity. *ChemBioChem, 3*(7), 619-627.

Brazelton, W. J., Schrenk, M. O., Kelley, D. S., & Baross, J. A. (2006). Methane- and Sulfur-Metabolizing Microbial Communities Dominate the Lost City Hydrothermal Field Ecosystem. *Appl. Environ. Microbiol., 72*(9), 6257-6270.

Burgess, E. A., Wagner, I. D., & Wiegel, J. (2007). Thermal environments and biodiversity. In C. Gerday & Glansdorff (Eds.), *Physiology and Biochemistry of Extremophiles* (pp. 13-29). Washington, DC: ASM Press.

Carter, G., Wu, M., Drummond, D. C., & Bermudez, L. E. (2003). Characterization of biofilm formation by clinical isolates of *Mycobacterium avium*. *J. Med. Microbiol., 52*(Pt 9), 747-752.

Cary, S. C., Cottrell, M. T., Stein, J. L., Camacho, F., & Desbruyeres, D. (1997). Molecular Identification and Localization of Filamentous Symbiotic Bacteria Associated with the Hydrothermal Vent Annelid *Alvinella pompejana*. *Appl. Environ. Microbiol., 63*(3), 1124-1130.

Casey, J. T., O'Cleirigh, C., Walsh, P. K., & O'Shea, D. G. (2004). Development of a robust microtiter plate-based assay method for assessment of bioactivity. *J. Microbiol. Methods, 58*(3), 327-334.

Cavanaugh, C. M., Gardiner, S. L., Jones, M. L., Jannasch, H. W., & Waterbury, J. B. (1981). Prokaryotic Cells in the Hydrothermal Vent Tube Worm *Riftia pachyptila* Jones: Possible Chemoautotrophic Symbionts. *Science, 213*(4505), 340-342.

Chadwick, W. W., Butterfield, D. A., Embley, R. W., Tunnicliffe, V., Huber, J. A., Nooner, S. L., & Clague, D. A. (2010). Spotlight 1: Axial Seamount. *Oceanography, 23*(1), 38-39.

Chadwick, W. W., Nooner, S. L., Butterfield, D. A., & Lilley, M. D. (2012). Seafloor deformation and forecasts of the April 2011 eruption at Axial Seamount. *Nature Geosci., 5*(7), 474-477.

Chao, L. S. L., Davis, R. E., & Moyer, C. L. (2007). Characterization of bacterial community structure in vestimentiferan tubeworm *Ridgeia piscesae* trophosomes. *Mar. Ecol., 28*(1), 72-85.

Childress, J. J., & Fisher, C. R. (1992). The biology of hydrothermal vent animals: physiology, biochemistry, and autotrophic symbiosis. In M. Barnes, A. D. Ansell & R. N. Gibson (Eds.), *Oceanography and Marine Biology an Annual Review* (Vol. 30, pp. 337-441). London: UCL Press Limited.

CLSI. (2009). Methods for dilution antimicrobial susceptibility tests for bacteria that grow aerobicllay; 8th editon. (Vol. 29, pp. 84). Wayne, Pennsylvania 19087, USA: Clinical Laboratory Standards Institute.

Cole, J. R., Chai, B., Farris, R. J., Wang, Q., Kulam-Syed-Mohideen, A. S., McGarrell, D. M., Bandela, A. M., Cardenas, E., Garrity, G. M., & Tiedje, J. M. (2007). The ribosomal database project (RDP-II): introducing myRDP space and quality controlled public data. *Nucl. Acids Res., 35*(suppl_1), D169-172.

Cole, J. R., Wang, Q., Cardenas, E., Fish, J., Chai, B., Farris, R. J., Kulam-Syed-Mohideen, A. S., McGarrell, D. M., Marsh, T., Garrity, G. M., & Tiedje, J. M. (2009). The Ribosomal Database Project: improved alignments and new tools for rRNA analysis. *Nucl. Acids Res., 37*(suppl_1), D141-145.

Comita, P. B., Gagosian, R. B., Pang, H., & Costello, C. E. (1984). Structural elucidation of a unique macrocyclic membrane lipid from a new, extremely thermophilic, deep-sea hydrothermal vent archaebacterium, *Methanococcus jannaschii*. *J. Biol. Chem., 259*(24), 15234-15241.

CoML. (2013). Census of Marine Life. Retrieved February 26, 2013, from http://www.coml.org

Connon, S. A., & Giovannoni, S. J. (2002). High-Throughput Methods for Culturing Microorganisms in Very-Low-Nutrient Media Yield Diverse New Marine Isolates. *Appl. Environ. Microbiol., 68*(8), 3878-3885.

Copp, B. R., Ireland, C. M., & Barrows, L. R. (1991). Wakayin: a novel cytotoxic pyrroloiminoquinone alkaloid from the ascidian *Clavelina* species. *J. Org. Chem., 56*(15), 4596-4597.

Corliss, J. B., Dymond, J., Gordon, L. I., Edmond, J. M., Richard, P. v. H., Ballard, R. D., Green, K., Williams, D., Bainbridge, A., Crane, K., & Andel, T. H. v. (1979). Submarine Thermal Springs on the Galápagos Rift. *Science, 203*(4385), 1073-1083.

Corre, E., Reysenbach, A.-L., & Prieur, D. (2001). ε-Proteobacterial diversity from a deep-sea hydrothermal vent on the Mid-Atlantic Ridge. *FEMS Microbiol. Lett., 205*(2), 329-335.

Cragg, G. M., Boyd, M. R., Khanna, R., Kneller, R., Mays, T. D., Mazan, K. D., Newman, D. J., & Sausville, E. A. (1999). International collaboration in drug discovery and development: the NCI experience. *Pure Appl. Chem., 71*(9), 1619-1633.

Desbruyères, D., Segonzac, M., & Bright, M. (Eds.). (2006). *Handbook of Deep-Sea Hydrothermal Vent Fauna*. Linz, Australia: Denisia 18.

Drummond, A., Ashton, B., Buxton, S., Cheung, M., Cooper, A., Duran, C., Field, M., Heled , J., Kearse, M., Markowitz, S., Moir, R., Stones-Havas, S., Sturrock, S., Thierer, T., & Wilson, A. (2010). Geneious v5.3. from http:// www.geneious.com

Dubilier, N., Bergin, C., & Lott, C. (2008). Symbiotic diversity in marine animals: the art of harnessing chemosynthesis. *Nat. Rev. Microbiol., 6*, 725-740.

Dunlap, W. C., Battershill, C. N., Liptrot, C. H., Cobb, R. E., Bourne, D. G., Jaspars, M., Long, P. F., & Newman, D. J. (2007). Biomedicinals from the phytosymbionts of marine invertebrates: a molecular approach. *Methods, 42*(4), 358-376.

Dziak, R. P., Haxel, J. H., Bohnenstiehl, D. R., Chadwick, W. W., Nooner, S. L., Fowler, M. J., Matsumoto, H., & Butterfield, D. A. (2012). Seismic precursors and magma ascent before the April 2011 eruption at Axial Seamount. *Nature Geosci., 5*(7), 478-482.

Edgcomb, V. P., Kysela, D. T., Teske, A., de Vera Gomez, A., & Sogin, M. L. (2002). Benthic eukaryotic diversity in the Guaymas Basin hydrothermal vent environment. *Proc. Natl. Acad. Sci., 99*(11), 7658-7662.

Edmond, J. M., Von Damm, K. L., McDuff, R. E., & Measures, C. I. (1982). Chemistry of hot springs on the East Pacific Rise and their effluent dispersal. *Nature, 297*(5863), 187-191.

Felbeck, H. (1981). Chemoautotrophic Potential of the Hydrothermal Vent Tube Worm, *Riftia pachyptila* Jones (Vestimentifera). *Science, 213*(4505), 336-338.

Fisher, C. R., Childress, J. J., Arp, A. J., Brooks, J. M., Distel, D., Favuzzi, J. A., Felbeck, H., Hessler, R., Johnson, K. S., Kennicutt II, M. C., Macko, S. A., Newton, A., Powell, M. A., Somero, G. N., & Soto, T. (1988). Microhabitat variation in the hydrothermal vent mussel, *Bathymodiolusthermophilus*, at the Rose Garden vent on the Galapagos Rift. *Deep-Sea Research, 35*, 1769-1791.

Fontana, A., Manzo, E., Ciavatta, M. L., Cutignano, A., Gavagnin, M., & Cimino, G. (2012). Biosynthetic Studies Through Feeding Experiments in Marine Organisms. 895-946.

Gage, J. D., & Tyler, P. A. (1991). *Deep-Sea Biology: A Natural History of Organisms at the Deep-Sea Floor*. Cambridge: Cambridge University Press.

Gneiding, K., Frodl, R., & Funke, G. (2008). Identities of Microbacterium spp. encountered in human clinical specimens. *J. Clin. Microbiol., 46*(11), 3646-3652.

Goffredi, S. K., Waren, A., Orphan, V. J., Van Dover, C. L., & Vrijenhoek, R. C. (2004). Novel Forms of Structural Integration between Microbes and a Hydrothermal Vent Gastropod from the Indian Ocean. *Appl. Environ. Microbiol., 70*(5), 3082-3090.

Gontang, E. A., Fenical, W., & Jensen, P. R. (2007). Phylogenetic Diversity of Gram-Positive Bacteria Cultured from Marine Sediments. *Appl. Environ. Microbiol., 73*(10), 3272-3282.

Gonthier, I., Rager, M.-N., Metzger, P., Guezennec, J., & Largeau, C. (2001). A di-O-dihydrogeranylgeranyl glycerol from *Thermococcus* S 557, a novel ether lipid, and likely intermediate in the biosynthesis of diethers in Archaea. *Tetrahedron Lett., 42*(15), 2795-2797.

Guindon, S., & Gascuel, O. (2003). A Simple, Fast, and Accurate Algorithm to Estimate Large Phylogenies by Maximum Likelihood. *Syst. Biol., 52*(5), 696-704.

Haddad, A., Camacho, F., Durand, P., & Cary, S. C. (1995). Phylogenetic characterization of the epibiotic bacteria associated with the hydrothermal vent polychaete Alvinella pompejana. *Appl. Environ. Microbiol., 61*(5), 1679-1687.

Harmer, T. L., Rotjan, R. D., Nussbaumer, A. D., Bright, M., Ng, A. W., DeChaine, E. G., & Cavanaugh, C. M. (2008). Free-living tubeworm endosymbionts found at deep-sea vents. *Appl. Environ. Microbiol.*, *74*(12): 3895–3898.

Harmsen, H. J. M., Prieur, D., & Jeanthon, C. (1997). Distribution of Microorganisms in Deep-Sea Hydrothermal Vent Chimneys Investigated by Whole-Cell Hybridization and Enrichment Culture of Thermophilic Subpopulations. *Appl. Environ. Microbiol., 63*(7), 2876-2883.

Hay, M. E. (1996). Marine chemical ecology: what's known and what's next? *J. Exp. Mar. Biol. Ecol., 200*(1–2), 103-134.

Haymon, R. M. (1983). Growth history of hydrothermal black smoker chimneys. *Nature, 301*(5902), 695-698.

Higashi, Y., Sunamura, M., Kitamura, K., Nakamura, K.-i., Kurusu, Y., Ishibashi, J.-i., Urabe, T., & Maruyama, A. (2004). Microbial diversity in hydrothermal surface to subsurface environments of Suiyo Seamount, Izu-Bonin Arc, using a catheter-type in situ growth chamber. *FEMS Microbiol. Ecol., 47*(3), 327-336.

Holden, J. F., & Daniel, R. M. (2004). The upper temperature limit for life based on hyperthermophile culture experiments and field observations *The Subseafloor Biosphere at Mid-Ocean Ridges* (Vol. 144, pp. 13-24). Washington, DC: AGU.

Homann, V. V., Sandy, M., Tincu, J. A., Templeton, A. S., Tebo, B. M., & Butler, A. (2009). Loihichelins A−F, a Suite of Amphiphilic Siderophores Produced by the Marine Bacterium *Halomonas* LOB-5. *J. Nat. Prod., 72*(5), 884-888.

Huang, X., & Madan, A. (1999). CAP3: A DNA Sequence Assembly Program. *Genome Res., 9*(9), 868-877.

Huber, J. A., Butterfield, D. A., & Baross, J. A. (2002). Temporal Changes in Archaeal Diversity and Chemistry in a Mid-Ocean Ridge Subseafloor Habitat. *Appl. Environ. Microbiol., 68*(4), 1585-1594.

Huber, J. A., Butterfield, D. A., & Baross, J. A. (2003). Bacterial diversity in a subseafloor habitat following a deep-sea volcanic eruption. *FEMS Microbiol. Ecol., 43*(3), 393-409.

Huber, J. A., Mark Welch, D. B., Morrison, H. G., Huse, S. M., Neal, P. R., Butterfield, D. A., & Sogin, M. L. (2007). Microbial Population Structures in the Deep Marine Biosphere. *Science, 318*(5847), 97-100.

Ifremer. (2013). Ifremer: Brittany Culture Collection. Retrieved February 27, 2013, from http://www.ifremer.fr/souchotheque/internet/htdocs/generique.php?lang=uk

JAMSTEC. (2013). JAMSTEC (Japan Agency for Marine-Earth Science and Technology): Cooperative Research Project for Extremophiles. Retrieved February 27, 2013, from http://www.jamstec.go.jp/e/index.html

Jannasch, H. W., & Wirsen, C. O. (1979). Chemosynthetic primary production at East Pacific sea floor spreading centers. *Bioscience, 29*(10), 592-598.

Jannasch, H. W., & Wirsen, C. O. (1981). Morphological Survey of Microbial Mats Near Deep-Sea Thermal Vents. *Appl. Environ. Microbiol., 41*(2), 528-538.

Jannasch, H. W., Wirsen, C. O., & Doherty, K. W. (1996). A Pressurized Chemostat for the Study of Marine Barophilic and Oligotrophic Bacteria. *Appl. Environ. Microbiol., 62*(5), 1593-1596.

Jensen, P. R., Gontang, E., Mafnas, C., Mincer, T. J., & Fenical, W. (2005). Culturable marine actinomycete diversity from tropical Pacific Ocean sediments. *Environ. Microbiol., 7*(7), 1039-1048.

Jørgensen, B. B., & Boetius, A. (2007). Feast and famine – microbial life in the deep-sea bed. *Nat Rev Micro, 5*(10), 770-781.

Juniper, K. S., Bird, D. F., Summit, M., Vong, M. P., & Baker, E. T. (1998). Bacterial and viral abundances in hydrothermal event plumes over northern Gorda Ridge. *Deep Sea Research Part II: Topical Studies in Oceanography, 45*(12), 2739-2749.

Karl, D. M. (1995). Ecology of Free-Living, Hydrothermal Vent Microbial Communities. In R. H. Vreeland (Ed.), *The Microbiology of Deep-Sea Hydrothermal Vents* (pp. 35-124). Boca Raton: CRC Press, Inc.

Kelley, D. S., Baross, J. A., & Delaney, J. R. (2002). Volcanoes, fluids, and life at mid-ocean ridge spreading centers. *Annual Review of Earth & Planetary Sciences, 30*(1), 385.

Kicklighter, C. E., Fisher, C. R., & Hay, M. E. (2004). Chemical defense of hydrothermal vent and hydrocarbon seep organisms: a preliminary assessment using shallow-water consumers. *Mar. Ecol. Prog. Ser., 275*, 11-19.

Kobayashi, M., & Kanda, F. (1991). Marine sterols. 18. Isolation and structure of four novel oxygeneted sterols from a gorgonian coral *Melithaea ocracea*. *J. Chem. Soc., Perkin Trans., 1*(5), 1177.

Konstantinidis, K. T., Braff, J., Karl, D. M., & DeLong, E. F. (2009). Comparative Metagenomic Analysis of a Microbial Community Residing at a Depth of 4,000 Meters at Station ALOHA in the North Pacific Subtropical Gyre. *Appl. Environ. Microbiol., 75*(16), 5345-5355.

Konstantinidis, K. T., & Tiedje, J. M. (2004). Trends between gene content and genome size in prokaryotic species with larger genomes. *Proc. Natl. Acad. Sci., USA, 101*(9), 3160-3165.

Kormas, K. A., Tivey, M. K., Von Damm, K., & Teske, A. (2006). Bacterial and archaeal phylotypes associated with distinct mineralogical layers of a white smoker spire from a deep-sea hydrothermal vent site (9°N, East Pacific Rise). *Environ. Microbiol., 8*(5), 909-920.

Kouris, A., Juniper, S. K., Frébourg, G., & Françoise, G. (2007). Protozoan-bacterial symbiosis in a deep-sea hydrothermal vent folliculinid ciliate (*Folliculinopsis* sp.) from the Juan de Fuca Ridge. *Mar. Ecol., 28*(1), 63-71.

Kouris, A., Limén, H., Stevens, C. J., & Juniper, S. K. (2010). Blue mats: faunal composition and food web structure in colonial ciliate (*Folliculinopsis* sp.) mats at Northeast Pacific hydrothermal vents. *Mar. Ecol. Prog. Ser., 412*, 93-101.

Kysela, D. T., Palacios, C., & Sogin, M. L. (2005). Serial analysis of V6 ribosomal sequence tags (SARST-V6): a method for efficient, high-throughput analysis of microbial community composition. *Environ. Microbiol., 7*(3), 356-364.

Lane, D. J. (1991). 16S/23S rRNA sequencing. In E. Stackebrandt & M. Goodfellow (Eds.), *Nucleic acid techniques in bacterial systematics* (pp. 115-175). New York, NY: John Wiley and Sons.

Lonsdale, P. (1977). Clustering of suspension-feeding macrobenthos near abyssal hydrothermal vents at oceanic spreading centers. *Deep-Sea Research, 24*, 857-863.

Lopez-Garcia, P., Duperron, S., Philippot, P., Foriel, J., Susini, J., & Moreira, D. (2003). Bacterial diversity in hydrothermal sediment and epsilon-proteobacterial dominance in experimental microcolonizers at the Mid-Atlantic Ridge. *Environ. Microbiol., 5*(10), 961-976.

Lopez-Garcia, P., Gaill, F., & Moreira, D. (2002). Wide bacterial diversity associated with tubes of the vent worm *Riftia pachyptila*. *Environ. Microbiol., 4*(4), 204-215.

Lutz, R. A. (2008). *AGRO-034 Abstract Title: Bioprospecting in extreme, deep-sea environments*. Paper presented at the 236th ACS National Meeting, Philadelphia, PA, August 17-21, 2008; American Chemical Society: Washington, DC.

Lutz, R. A., Shank, T. M., & Evans, R. (2001). Life after death in the deep sea: Following immolation by volcanic eruption, the community around a hydrothermal vent recovers spectacularly. *Am. Sci., 89*, 422-431.

Marcus, J., Tunnicliffe, V., & Butterfield, D. A. (2009). Post-eruption succession of macrofaunal communities at diffuse flow hydrothermal vents on Axial Volcano, Juan de Fuca Ridge, Northeast Pacific. *Deep Sea Research Part II: Topical Studies in Oceanography, 56*(19-20), 1586-1598.

Moyer, C. L., Dobbs, F. C., & Karl, D. M. (1994). Estimation of diversity and community structure through restriction fragment length polymorphism distribution analysis of bacterial 16S rRNA genes from a microbial mat at an active, hydrothermal vent system, Loihi Seamount, Hawaii. *Appl. Environ. Microbiol., 60*(3), 871-879.

Moyer, C. L., Dobbs, F. C., & Karl, D. M. (1995). Phylogenetic diversity of the bacterial community from a microbial mat at an active, hydrothermal vent system, Loihi Seamount, Hawaii. *Appl. Environ. Microbiol., 61*(4), 1555-1562.

Muyzer, G., & Stams, A. J. M. (2008). The ecology and biotechnology of sulphate-reducing bacteria. *Nat. Rev. Micro., 6*(6), 441-454.

Na, M., Ding, Y., Wang, B., Tekwani, B. L., Schinazi, R. F., Franzblau, S., Kelly, M., Stone, R., Li, X.-C., Ferreira, D., & Hamann, M. T. (2009). Anti-infective Discorhabdins from a Deep-Water Alaskan Sponge of the Genus *Latrunculia*. *J. Nat. Prod., 73*(3), 383-387.

Nagahama, T., Hamamoto, M., Nakase, T., & Horikoshi, K. (2001). Rhodotorula lamellibrachii sp. nov., a new yeast species from a tubeworm collected at the deep-sea floor in Sagami Bay and its phylogenetic analysis. *Antonie Van Leeuwenhoek, 80*(3), 317-323.

Nagahama, T., Hamamoto, M., Nakase, T., & Horikoshi, K. (2003). Rhodotorula benthica sp. nov. and Rhodotorula calyptogenae sp. nov., novel yeast species from animals collected from the deep-sea floor, and *Rhodotorula lysiniphila* sp. nov., which is related phylogenetically. *Int. J. Syst. Evol. Microbiol., 53*(3), 897-903.

Nakagawa, S., Takai, K., Inagaki, F., Chiba, H., Ishibashi, J.-i., Kataoka, S., Hirayama, H., Nunoura, T., Horikoshi, K., & Sako, Y. (2005). Variability in microbial community and venting chemistry in a sediment-hosted backarc hydrothermal

system: Impacts of subseafloor phase-separation. *FEMS Microbiol. Ecol., 54*(1), 141-155.

Nakagawa, S., Takaki, Y., Shimamura, S., Reysenbach, A.-L., Takai, K., & Horikoshi, K. (2007). Deep-sea vent ε-proteobacterial genomes provide insights into emergence of pathogens. *Proc. Natl. Acad. Sci., 104*(29), 12146-12150.

NEB. (2013). New England BioLabs, Inc.: Thermophilic DNA Polymerases. Retrieved February 27, 2013, from http://www.neb.com

Nelson, D. C., & Fisher, C. R. (1995). Chemoautotrophic and methanotrophic endosymbiotic bacteria at deep-sea vents and seeps. In D. M. Karl (Ed.), *Microbiology of Deep Sea Hydrothermal Vents* (pp. 125-167). Boca Raton, FL: CRC Press Inc.

NeMO. (2013). NeMO: New Millennium Observatory. A seafloor observatory at an active underwater volcano. Retrieved March 3, 2013, from http:// www.pmel.noaa.gov/vents/nemo/index.html

Nett, M., & Konig, G. M. (2007). The chemistry of gliding bacteria. *Nat. Prod. Rep., 24*(6), 1245-1261.

Nichols, C. A. M., Guezennec, J., & Bowman, J. P. (2005). Bacterial Exopolysaccharides from Extreme Marine Environments with Special Consideration of the Southern Ocean, Sea Ice, and Deep-Sea Hydrothermal Vents: A Review. *Mar. Biotechnol., 7*(4), 253-271.

Pace, N. R. (1997). A Molecular View of Microbial Diversity and the Biosphere. *Science, 276*(5313), 734-740.

Page, A., Tivey, M. K., Stakes, D. S., & Reysenbach, A.-L. (2008). Temporal and spatial archaeal colonization of hydrothermal vent deposits. *Environ. Microbiol., 10*(4), 874-884.

Parkes, R. J., Cragg, B. A., Bale, S. J., Getlifff, J. M., Goodman, K., Rochelle, P. A., Fry, J. C., Weightman, A. J., & Harvey, S. M. (1994). Deep bacterial biosphere in Pacific Ocean sediments. *Nature, 371*(6496), 410-413.

Pathom-aree, W., Stach, J., Ward, A., Horikoshi, K., Bull, A., & Goodfellow, M. (2006). Diversity of actinomycetes isolated from Challenger Deep sediment (10,898 m) from the Mariana Trench. *Extremophiles, 10*(3), 181-189.

Perry, N. B., Blunt, J. W., McCombs, J. D., & Munro, M. H. G. (1986). Discorhabdin C, a highly cytotoxic pigment from a sponge of the genus Latrunculia. *J. Org. Chem., 51*(26), 5476-5478.

Polz, M. F., Robinson, J. J., Cavanaugh, C. M., & Dover, C. L. v. (1998). Trophic Ecology of Massive Shrimp Aggregations at a Mid-Atlantic Ridge Hydrothermal Vent Site. *Limnol. Oceanogr., 43*(7), 1631-1638.

Postec, A., Lesongeur, F., Pignet, P., Ollivier, B., Querellou, J., & Godfroy, A. (2007). Continuous enrichment cultures: insights into prokaryotic diversity and

metabolic interactions in deep-sea vent chimneys. *Extremophiles, 11*(6), 747-757.

Postec, A., Urios, L., Lesongeur, F., Ollivier, B., Querellou, J., & Godfroy, A. (2005). Continuous enrichment culture and molecular monitoring to investigate the microbial diversity of thermophiles inhabiting deep-sea hydrothermal ecosystems. *Curr. Microbiol., 50*(3), 138-144.

Reysenbach, A.-L., Longnecker, K., & Kirshtein, J. (2000). Novel Bacterial and Archaeal Lineages from an In Situ Growth Chamber Deployed at a Mid-Atlantic Ridge Hydrothermal Vent. *Appl. Environ. Microbiol., 66*(9), 3798-3806.

Robigou, V., Delaney, J. R., & Stakes, D. S. (1993). Large massive sulfide deposits in a newly discovered active hydrothermal system, the High-Rise field, Endeavour Segment, Juan de Fuca Ridge. *Geophys. Res. Lett., 20*(17), 1887-1890.

Ruth, L. (2006). Gambling in the deep sea. *EMBO reports, 7*(1), 17-21.

Sanders, H. L., & Hessler, R. R. (1969). Ecology of the Deep-Sea Benthos. *Science, 163*, 1419-1424.

Santelli, C. M., Orcutt, B. N., Banning, E., Bach, W., Moyer, C. L., Sogin, M. L., Staudigel, H., & Edwards, K. J. (2008). Abundance and diversity of microbial life in ocean crust. *Nature, 453*(7195), 653-656.

Schloss, P. D., & Handelsman, J. (2005). Introducing DOTUR, a Computer Program for Defining Operational Taxonomic Units and Estimating Species Richness. *Appl. Environ. Microbiol., 71*(3), 1501-1506.

Schloss, P. D., Westcott, S. L., Ryabin, T., Hall, J. R., Hartmann, M., Hollister, E. B., Lesniewski, R. A., Oakley, B. B., Parks, D. H., Robinson, C. J., Sahl, J. W., Stres, B., Thallinger, G. G., Van Horn, D. J., & Weber, C. F. (2009). Introducing mothur: open-source, platform-independent, community-supported software for describing and comparing microbial communities. *Appl. Environ. Microbiol., 75*(23), 7537-7541.

Schmidt, C., Vuillemin, R., Le Gall, C., Gaill, F., & Le Bris, N. (2008). Geochemical energy sources for microbial primary production in the environment of hydrothermal vent shrimps. *Mar. Chem., 108*(1-2), 18-31.

Schmidt, E. W., Harper, M. K., & Faulkner, D. J. (1995). Makaluvamines H-M and Damirone C from the Pohnpeian Sponge *Zyzzya fuliginosa*. *J. Nat. Prod., 58*(12), 1861-1867.

Schrenk, M. O., Kelley, D. S., Delaney, J. R., & Baross, J. A. (2003). Incidence and Diversity of Microorganisms within the Walls of an Active Deep-Sea Sulfide Chimney. *Appl. Environ. Microbiol., 69*(6), 3580-3592.

SDBSWeb. (2013). National Institute of Advanced Industrial Science and Technology. Retrieved March 10, 2013, from http://sdbs.riodb.aist.go.jp

Seyfried, W. E., Jr., & Mottl, M. J. (1995). Geologic Setting and Chemistry of Deep-Sea Hydrothermal Vents. In D. M. Karl (Ed.), *The Microbiology of Deep-Sea Hydrothermal Vents* (pp. 1-34). Boca Raton: CRC Press, Inc.

Sikora, A. E., Beyhan, S., Bagdasarian, M., Yildiz, F. H., & Sandkvist, M. (2009). Cell envelope perturbation induces oxidative stress and changes in iron homeostasis in *Vibrio cholerae*. *Journal of bacteriology, 191*(17), 5398-5408.

Skropeta, D. (2008). Deep-Sea natural products. *Nat. Prod. Rep., 25*(6), 1131-1166.

Smith, S. M., Beattie, A. J., Gillings, M. R., Holley, M. P., Stow, A. J., Turnbull, C. L., Wilson, P. D., & Briscoe, D. A. (2008). An enhanced miniaturized assay for antimicrobial prospecting. *J. Microbiol. Methods, 72*(1), 103-106.

Sogin, M. L., Morrison, H. G., Huber, J. A., Welch, D. M., Huse, S. M., Neal, P. R., Arrieta, J. M., & Herndl, G. J. (2006). Microbial diversity in the deep sea and the underexplored "rare biosphere". *Proc. Natl. Acad. Sci., 103*(32), 12115-12120.

Stackebrandt, E., & Goebel, B. M. (1994). Taxonomic Note: A Place for DNA-DNA Reassociation and 16S rRNA Sequence Analysis in the Present Species Definition in Bacteriology. *Int. J. Syst. Bacteriol., 44*(4), 846-849.

Sunamura, M., Higashi, Y., Miyako, C., Ishibashi, J.-i., & Maruyama, A. (2004). Two Bacteria Phylotypes Are Predominant in the Suiyo Seamount Hydrothermal Plume. *Appl. Environ. Microbiol., 70*(2), 1190-1198.

Takai, K., & Horikoshi, K. (1999). Genetic Diversity of Archaea in Deep-Sea Hydrothermal Vent Environments. *Genetics, 152*(4), 1285-1297.

Takai, K., Inagaki, F., Nakagawa, S., Hirayama, H., Nunoura, T., Sako, Y., Nealson, K. H., & Horikoshi, K. (2003). Isolation and phylogenetic diversity of members of previously uncultivated ε-Proteobacteria in deep-sea hydrothermal fields. *FEMS Microbiol. Lett., 218*(1), 167-174.

Takai, K., Komatsu, T., Inagaki, F., & Horikoshi, K. (2001). Distribution of Archaea in a Black Smoker Chimney Structure. *Appl. Environ. Microbiol., 67*(8), 3618-3629.

Takai, K., Nakagawa, S., Reysenbach, A. L., & Hoek, J. (2006). Microbial ecology of mid-ocean ridges and back-arc basins *Back-Arc Spreading Systems: Geological, Biological, Chemical, and Physical Interactions* (Vol. 166, pp. 185-213). Washington, DC: AGU.

Takai, K., Oida, H., Suzuki, Y., Hirayama, H., Nakagawa, S., Nunoura, T., Inagaki, F., Nealson, K. H., & Horikoshi, K. (2004). Spatial Distribution of Marine Crenarchaeota Group I in the Vicinity of Deep-Sea Hydrothermal Systems. *Appl. Environ. Microbiol., 70*(4), 2404-2413.

Tarasov, V. G., Gebruk, A. V., Mironov, A. N., & Moskalev, L. I. (2005). Deep-sea and shallow-water hydrothermal vent communities: Two different phenomena? *Chem. Geol., 224*(1-3), 5-39.

Teske, A., Hinrichs, K.-U., Edgcomb, V., de Vera Gomez, A., Kysela, D., Sylva, S. P., Sogin, M. L., & Jannasch, H. W. (2002). Microbial Diversity of Hydrothermal Sediments in the Guaymas Basin: Evidence for Anaerobic Methanotrophic Communities. *Appl. Environ. Microbiol., 68*(4), 1994-2007.

Thornburg, C. C., Thimmaiah, M., Shaala, L. A., Hau, A. M., Malmo, J. M., Ishmael, J. E., Youssef, D. T. A., & McPhail, K. L. (2011). Cyclic Depsipeptides, Grassypeptolides D and E and Ibu-epidemethoxylyngbyastatin 3, from a Red Sea *Leptolyngbya* Cyanobacterium. *J. Nat. Prod., 74*(8), 1677-1685.

Tivey, M. K. (1991). Hydrothermal Vent Systems. *Oceanus, 34*(4), 68-74.

Tormo, J. R., García, J. B., DeAntonio, M., Feliz, J., Mira, A., Díez, M. T., Hernández, P., & Peláez, F. (2003). A method for the selection of production media for actinomycete strains based on their metabolite HPLC profiles. *J. Ind. Microbiol. Biotechnol., 30*(10), 582-588.

Tsurumi, M., & Tunnicliffe, V. (2001). Characteristics of a hydrothermal vent assemblage on a volcanically active segment of Juan de Fuca Ridge, northeast Pacific. *Can. J. Fish. Aquat. Sci., 58*, 530-542.

Tunnicliffe, V., & Fowler, C. M. R. (1996). Influence of sea-floor spreading on the global hydrothermal vent fauna. *Nature, 379*, 531-533.

Van Dover, C. L. (2000). *The Ecology of Deep-Sea Hydrothermal Vents*. Princeton, New Jersey: Princeton University Press.

Van Dover, C. L., & Fry, B. (1994). Microorganisms as food resources at deep-sea hydrothermal vents. *Limnol. Oceanogr., 39*(1), 51-57.

Van Dover, C. L., German, C. R., Speer, K. G., Parson, L. M., & Vrijenhoek, R. C. (2002). Evolution and Biogeography of Deep-Sea Vent and Seep Invertebrates. *Science, 295*(5558), 1253-1257.

Van Dover, C. L., Humphris, S. E., Fornari, D., Cavanaugh, C. M., Collier, R., Goffredi, S. K., Hashimoto, J., Lilley, M. D., Reysenbach, A. L., Shank, T. M., Von Damm, K. L., Banta, A., Gallant, R. M., Gotz, D., Green, D., Hall, J., Harmer, T. L., Hurtado, L. A., Johnson, P., McKiness, Z. P., Meredith, C., Olson, E., Pan, I. L., Turnipseed, M., Won, Y., Young, C. R., III, & Vrijenhoek, R. C. (2001). Biogeography and Ecological Setting of Indian Ocean Hydrothermal Vents. *Science, 294*(5543), 818-823.

Venkateswarlu, Y., Venkata Rami Reddy, M., & Rama Rao, M. (1996). A New Epoxy Sterol from the Sponge *Ircinia fasciculata*. *J. Nat. Prod., 59*(9), 876-877.

Venter, J. C., Remington, K., Heidelberg, J. F., Halpern, A. L., Rusch, D., Eisen, J. A., Wu, D., Paulsen, I., Nelson, K. E., Nelson, W., Fouts, D. E., Levy, S., Knap, A. H., Lomas, M. W., Nealson, K., White, O., Peterson, J., Hoffman, J., Parsons, R., Baden-Tillson, H., Pfannkoch, C., Rogers, Y.-H., & Smith, H. O. (2004). Environmental Genome Shotgun Sequencing of the Sargasso Sea. *Science, 304*(5667), 66-74.

Verenium. (2013). Home Page for Verenium Corporation. Retrieved February 26, 2013, from http://www.verenium.com

Vraspir, J. M., & Butler, A. (2009). Chemistry of Marine Ligands and Siderophores. *Ann. Rev. Mar. Sci., 1*(1), 43-63.

Walsh, J. J., Rowe, G. T., Iverson, R. L., & McRoy, C. P. (1981). Biological export of shelf carbon is a sink of the global CO2 cycle. *Nature, 291*(5812), 196-201.

Winn, C. D., Karl, D. M., & Massoth, G. J. (1986). Microorganisms in deep-sea hydrothermal plumes. *Nature, 320*(6064), 744-746.

Woese, C. R. (2004). A New Biology for a New Century. *Microbiol. Mol. Biol. Rev., 68*(2), 173-186.

Yu, Z., & Morrison, M. (2004). Comparisons of Different Hypervariable Regions of rrs Genes for Use in Fingerprinting of Microbial Communities by PCR-Denaturing Gradient Gel Electrophoresis. *Appl. Environ. Microbiol., 70*(8), 4800-4806.

Zanchetta, P., Lagarde, N., & Guezennec, J. (2003). A New Bone-Healing Material: A Hyaluronic Acid-Like Bacterial Exopolysaccharide. *Calcif. Tissue Int., 72*(1), 74-79.

Zengler, K., Toledo, G., Rappe, M., Elkins, J., Mathur, E. J., Short, J. M., & Keller, M. (2002). Cultivating the uncultured. *Proc. Natl. Acad. Sci. U S A, 99*(24), 15681-15686.

Chapter Six

General Conclusions

Christopher C. Thornburg

Marine natural product compounds, like their terrestrial counterparts, display a remarkable chemical diversity that occupies biologically relevant chemical space (Clardy & Walsh, 2004; Dobson, 2004). This is evidenced by the nearly 45% of approved drugs from 1981–2010 that owe their origins to natural products (Newman & Cragg, 2012). Remarkably, anticancer and anti-infective agents (99 and 104, respectively; excluding biologicals and vaccines) were almost exclusively derived from natural products during this time period (79.7% and 75.0%, respectively). Somewhat surprising is that only four marine-derived drugs have been approved (1981–2011): brentuximab vedotin (Adcetris®; "Seattle Genetics," 2013), eribulin mesylate (Halaven®; "Eisai Oncology," 2013), trabectedin (Yondelis®; "PharmaMar," 2013b), and ziconotide (Prialt®; Bingham et al., 2010). However, the history of marine natural products is relatively short compared to that of terrestrial natural products, which is further exemplified by the more than 175,000 unique natural products characterized to date, with about 22,000 derived from marine sources (Blunt et al., 2012), suggesting that an enormous potential for natural products discovery still exists in the marine environment. Thus, the challenge is to discover new chemical scaffolds from the many unexplored repositories of the marine environment.

The focus of this research was to investigate the natural products potential of phylogenetically diverse organisms from rare or extreme ecosystems, such as the Red Sea and deep-sea hydrothermal vents, respectively. It is hypothesized that the 'extreme' environmental conditions of deep-sea vents, coupled with the high biodiversity and dense microbial communities found within these environments, drives the development of unique secondary metabolites involved in their chemical defense or communication. Furthermore, a fundamental problem, especially in marine natural products isolation, is a limited/inaccessible supply of the source organism as well as the impracticality of a synthetic supply given the complexity of natural products (Koehn & Carter, 2005). Thus, our sampling strategy involved the cultivation of microorganisms from the Red Sea and deep-sea vents to circumvent the potential

supply bottleneck, and to survey the culture-dependent diversity within these environments.

In general, primary productivity in the Red Sea is low, with a pronounced South to North decrease due to a lack of winter upwelling and higher evaporation rate to the North (Fenton et al., 2000). This likely explains the disproportionate number of biologically active natural products from marine organisms in this challenging environment. Notably, the chemistry of Red Sea cyanobacteria is unreported in the literature, although a wealth of unusual specimens growing in low abundance were observed and recently collected for laboratory cultivation in this study. Importantly, five new culturable strains of cyanobacteria (see Appendix) were characterized based on their morphology and 16S rRNA gene sequence, and deposited in the NCBI GenBank database (http://www.ncbi.nlm.nih.gov). These include three *Leptolyngbya* strains (accession numbers JX470180, JX481735 and JF518829), a *Moorea* strain (JX470179) and a *Symploca* sp. (JX481736). Of these, three strains were found to produce new metabolites with nanomolar cytotoxicity to cancer cells. These include grassypeptolides D and E (HeLa cervical carcinoma cells, IC_{50} = 335 and 192 nM, respectively), apratoxin H (H460 human lung cancer cells, IC_{50} = 3.4 nM), and leptochelin (H460 human lung cancer cells, IC_{50} = 153 nM).

Although the cyanobacterial strains documented here were collected from a relatively isolated and unique habitat, the compounds reported mostly show structural motifs comparable to cyanobacteria collected pantropically, which poses additional questions as to the biogenetic origin of these metabolites, and further exemplifies the ability of marine cyanobacteria to adapt to a wide range of habitats (Whitton, 2012). These investigations did not translate to the production of chemical scaffolds unique to Red Sea cyanobacteria. However, it should be noted that additional strains that we isolated from the Red Sea collection have been resistant to large-scale cultivation, or do not provide sufficient biomass, even after years of culture harvests (e.g. *Symploca* sp. RS04; JX481736). Further characterization of these strains, as well as attempts to

optimize culture conditions, may provide new, exciting chemical entities. Additionally, each of the natural product-producing strains expresses at least two biosynthetic pathways, as evidenced by the isolation of biosynthetically distinct metabolites. There biosynthetic potential may be further exploited with the "OSMAC (One Strain MAny Compounds)" cultivation methods described in Chapter Five (Bode et al., 2002). In addition, characterization of the biosynthetic genes within the grassypeptolide-producing Red Sea *Leptolyngbya* sp. RS03 (JF518829), which is currently the only known producer of grassypeptolides in laboratory culture, and the leptochelin-producing *Leptolyngbya* sp. RS02, would shed light on their biosynthetic origins as well as aid in the production of an increased supply of these metabolites or additional analogues for mechanism of action and structure-activity relationship studies, respectively. Notably, the apratoxin A biosynthetic gene cluster was recently identified from a single cyanobacterial cell using a genome sequencing technique that relies on 454 pyrosequencing (Grindberg et al., 2011).

Despite the extreme conditions of deep-sea hydrothermal vents, and in contrast to the Red Sea, deep-vent organisms exist as islands of highly dense and diverse communities. Although this diversity has not yet correlated to new/unprecedented natural products isolation in our laboratory, the putative identification of nonribosomal peptide synthetase (NRPS) and type I polyketide synthase (PKS) genes in several of the isolated actinomycetes and α- and γ-proteobacteria suggests that these genetic loci may be silent or "cryptic." Thus, further attempts to induce the biosynthesis of the putative metabolites could include co-culturing of these isolates with other deep-vent microbes, antibiotic-resistant strains, or entirely different taxa (e.g. fungi). A co-cultivation strategy has been employed in several recent studies and has resulted in the activation of silent gene clusters and production of new natural products (reviewed in Scherlach and Hertweck, 2009; Brakhage and Schroeckh, 2011; Onaka et al., 2011). Furthermore, the Clardy and Lewis groups have isolated previously uncultured bacteria in the presence of "helper strains", which had originated from the same

environment (D'Onofrio et al., 2010). Remarkably, subsequent investigations revealed that the newly cultured strains were dependent on the presence of siderophores produced by the helper strain. This strategy, coupled with additional tailoring of the isolation medium to match the suspected environmental conditions, may expand the culturable range of deep-vent bacteria for natural products investigation.

Of the reported compounds from deep-vent organisms to date, only the ammonificins, and loihichelins are likely true secondary metabolites. The loihichelins are known siderophores that chelate Fe(III), while the ammonificins contain functional groups that have been shown to coordinate the binding of metals ions in other marine metabolites (Michael & Pattenden, 1993; Vraspir & Butler, 2009). Given the geochemical complexity of hydrothermal vent environments, coupled with the chemosynthetic nature of vent primary productivity, it is likely that many if not all deep-vent bacteria produce compounds capable of binding reduced metals. Thus, these compounds may serve a role in the metabolism of metals for energy generation, or the acquisition of a trace nutrient, or may serve to reduce the toxicity of metal-enriched hydrothermal fluids. A similar functionality may be attributed to cyanobacterial metabolites isolated in this research, which include the grassypeptolides, as described by Kwan et al. (2010), and leptochelin (Chapter Four). As reviewed in Chapter Four, many metal-complexing secondary metabolites are also cytotoxic to mammalian cells, suggesting a dual functionality for these compounds in the producing organism. Furthermore, metal-binding natural products may also affect multiple cellular targets and/or biochemical pathways. This ‘one-two punch’ typically leads to unprecedented cytotoxic potency in cancer cells. Thus, the challenge for future natural products investigations is to develop methods for the production (e.g. metal-free culture medium) and recovery of intact metal complexes or potential chelators, which are often degraded under reverse-phase chromatographic conditions, from marine invertebrates and microorganisms inhabiting these unique environments. Methods similar to those recently developed by Jaspars and colleagues (Wright et al., 2008),

which rely upon size-exclusion chromatography (SEC-HPLC column) and inductively coupled plasma mass spectrometry (ICP-MS), an elemental mass spectrometric technique, should be very productive for the screening and isolation of metabolites complexed to transition metals.

References

Blunt, J. W., Munro, M. H., & Upjohn, M. (2012). The Role of Databases in Marine Natural Products Research. In E. Fattorusso, W. H. Gerwick & O. Taglialatela-Scafati (Eds.), *Handbook of Marine Natural Products* (pp. 389-421): Springer Netherlands.

Bode, H. B., Bethe, B., Höfs, R., & Zeeck, A. (2002). Big Effects from Small Changes: Possible Ways to Explore Nature's Chemical Diversity. *ChemBioChem, 3*(7), 619-627.

Brakhage, A. A., & Schroeckh, V. (2011). Fungal secondary metabolites - strategies to activate silent gene clusters. *Fungal Genet. Biol., 48*(1), 15-22.

Clardy, J., & Walsh, C. (2004). Lessons from natural molecules. *Nature, 432*(7019), 829-837.

D'Onofrio, A., Crawford, J. M., Stewart, E. J., Witt, K., Gavrish, E., Epstein, S., Clardy, J., & Lewis, K. (2010). Siderophores from neighboring organisms promote the growth of uncultured bacteria. *Chem. Biol., 17*(3), 254-264.

Dobson, C. M. (2004). Chemical space and biology. *Nature, 432*(7019), 824-828.

Eisai Oncology. (2013). Retrieved February 24, 2013, from www.halaven.com

Fenton, M., Geiselhart, S., Rohling, E. J., & Hemleben, C. (2000). Aplanktonic zones in the Red Sea. *Mar. Micropaleontol., 40*(3), 277-294.

Grindberg, R. V., Ishoey, T., Brinza, D., Esquenazi, E., Coates, R. C., Liu, W.-t., Gerwick, L., Dorrestein, P. C., Pevzner, P., Lasken, R., & Gerwick, W. H. (2011). Single Cell Genome Amplification Accelerates Identification of the Apratoxin Biosynthetic Pathway from a Complex Microbial Assemblage. *PLoS ONE, 6*(4), e18565.

Koehn, F. E., & Carter, G. T. (2005). The evolving role of natural products in drug discovery. *Nat. Rev. Drug Discov., 4*(3), 206-220.

Kwan, J. C., Ratnayake, R., Abboud, K. A., Paul, V. J., & Luesch, H. (2010). Grassypeptolides A-C, Cytotoxic Bis-thiazoline Containing Marine Cyclodepsipeptides. *J. Org. Chem., 75*(23), 8012-8023.

Michael, J. P., & Pattenden, G. (1993). Marine Metabolites and Metal Ion Chelation: The Facts and the Fantasies. *Angew. Chem. Int. Ed. Engl., 32*(1), 1-23.

Newman, D. J., & Cragg, G. M. (2012). Natural products as sources of new drugs over the 30 years from 1981 to 2010. *J. Nat. Prod., 75*(3), 311-335.

Onaka, H., Mori, Y., Igarashi, Y., & Furumai, T. (2011). Mycolic acid-containing bacteria induce natural-product biosynthesis in *Streptomyces* species. *Appl. Environ. Microbiol., 77*(2), 400-406.

PharmaMar. (2013b). *PharmaMar, Zeltia Group. Yondelis® (trabectedin)*. Retrieved February 24, 2013, from http://www.pharmamar.com/yondelis.aspx

Scherlach, K., & Hertweck, C. (2009). Triggering cryptic natural product biosynthesis in microorganisms. *Org. Biomol. Chem., 7*(9), 1753-1760.

Seattle Genetics. (2013). *CD30-Directed Adcetris® (brentuximab vedotin).* Retrieved January 21, 2013, from www.seattlegenetics.com/adcetris

Vraspir, J. M., & Butler, A. (2009). Chemistry of Marine Ligands and Siderophores. *Ann. Rev. Mar. Sci., 1*(1), 43-63.

Whitton, B. A. (2012). *Ecology of Cyanobacteria II: Their Diversity in Space in Time*: Springer Netherlands.

Wright, S. H., Raab, A., Tabudravu, J. N., Feldmann, J., Long, P. F., Battershill, C. N., Dunlap, W. C., Milne, B. F., & Jaspars, M. (2008). Marine metabolites and metal ion chelation: intact recovery and identification of an iron(II) complex in the extract of the ascidian Eudistoma gilboviride. *Angew. Chem. Int. Ed. Engl., 47*(42), 8090-8092.

APPENDIX

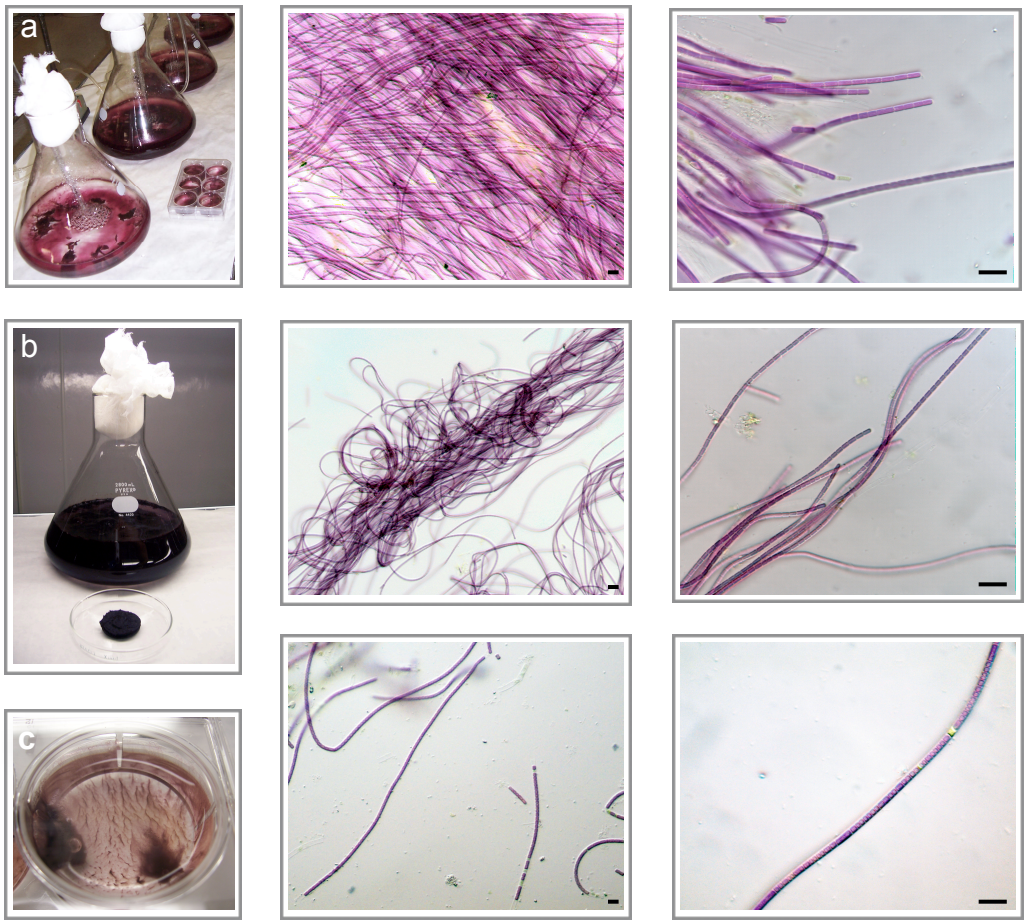

Figure A-1. Laboratory cultures and their corresponding photomicrographs (x400 and x1000, respectively) for filamentous marine cyanobacteria isolated from the Red Sea. (a) *Leptolyngbya* sp. RS01 (JX470180); (b) *Leptolyngbya* sp. RS02 (JX481735); (c) *Leptolyngbya* sp. RS03 (JF518829). Scale bar = 10 μm.

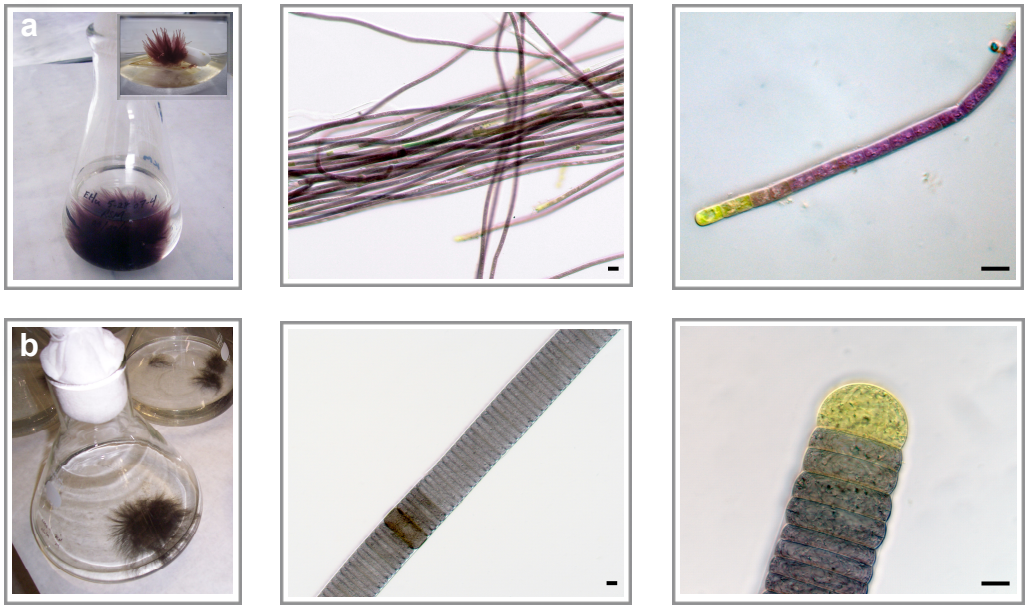

Figure A-2. Laboratory cultures and their corresponding photomicrographs (x400 and x1000, respectively) for filamentous marine cyanobacteria isolated from the Red Sea. (a) *Symploca* sp. RS04 (JX481736); (b) *Moorea* sp. RS05 (JX470179). Scale bar = 10 μm.